PHYSICAL CHARACTERISTICS OF CAPROCK FORMATIONS USED FOR GEOLOGICAL STORAGE OF CO_2 AND THE IMPACT OF UNCERTAINTY IN FRACTURE PROPERTIES ON CO_2 TRANSPORT THROUGH FRACTURED CAPROCKS

Submitted in partial fulfillment of the requirements for

the degree of

Doctor of Philosophy

in

Civil and Environmental Engineering

CRAIG ALEXANDER GRIFFITH

MChE, Chemical Engineering, Carnegie Mellon University, Pittsburgh, PA (2006)
B.S., Chemical Engineering, University of Virginia, Charlottesville, VA (2002)

Carnegie Mellon University
Pittsburgh, PA

May, 2012

ABSTRACT

Capture and geological sequestration of CO_2 from energy production is proposed to help mitigate climate change caused by anthropogenic emissions of CO_2 and other greenhouse gases. Performance goals set by the US Department of Energy for CO_2 storage permanence include retention of at least 99% of injected CO_2 mass. Part of meeting these goals will be detailed assessments of each potential storage site's geologic environment, especially properties of the storage reservoir(s) and caprock(s) that may affect permanence of CO_2 storage.

The overall goals of this research were to examine the physical and lithologic characteristics of caprock formations considered for saline CO_2 sequestration, and to investigate the impact of uncertainty in hydraulic properties of a fractured caprock on the ability to meet long-term CO_2 storage goals. To accomplish these goals three specific objectives were pursued: 1) Review the current state of knowledge on the physical and lithologic characteristics of caprocks in areas considered for CO_2 sequestration, and identify common features that may impact long-term CO_2 storage. 2) Develop an integrated analytical model to investigate the influence of fracture hydraulic properties on the transport of CO_2 through caprocks. 3) Investigate the impact of uncertainty in fracture aperture and density on predicting CO_2 loss and caprock hydraulic fracture properties associated with meeting long-term storage goals.

Review of the caprock properties revealed that they were generally thick and exhibited low permeability. However, they were not continuous or uniform in lithology throughout the regions examined. Caprocks exhibited lateral facies changes, fractures, and spatial variability in thickness, permeability, porosity, and other physical properties that could affect CO_2 storage. Fractures reported in caprock formations were not fully characterized and had unknown regional extent and interconnectivity.

An integrated analytical model was developed to estimate the limits of hydraulic fracture properties within a caprock that are consistent with storage performance criteria, and with observed ranges for aperture size and density within field studies on fracture networks. Results showed hydraulic fracture properties, consistent with performance objectives, to be low in comparison to reported measurements. In particular, 1) microfractures (e.g. 10^{-7} to 10^{-6} m range) yielded CO_2 loss rates of concern given certain conditions. (2) Fracture permeability was in the nano- to micro-Darcy (μD) range (i.e. 10^{-21} – 10^{-18} m^2), and 3) Fracture porosities were below 0.02 %.

For the third objective, a stochastic framework was applied to the integrated analytical model to examine the impact of uncertainty in caprock fracture aperture and density on predicting CO_2 loss and hydraulic fracture properties meeting CO_2 storage criteria. Major findings include: 1) combinations of parameters meeting the CO_2 loss criteria were rare events and more data would be needed to characterize caprock fractures. 2) Fracture porosity was identified as a good diagnostic parameter for caprock screening. (3) Fracture permeability had the strongest association with CO_2 loss, with a high probability (>90%) that caprocks which met performance goals had values < 10^{-17} m^2. (4) Correlations between reservoir parameters and caprock fracture properties became stronger as the CO_2 loss from the system became more constrained.

Overall, the results of this study showed that selected caprocks in the U.S, currently investigated for CO_2 storage, exhibit significant variability in their structural, lithologic, and fluid transport characteristics. Pre-existing fractures can occur in caprocks, which is of interest for impact on long-term CO_2 storage. Modeling results suggest a low tolerance for microfractures in overlying caprocks, where acceptable hydraulic fracture properties were low in comparison to reported measurements. In addition, the interdependence of the transport parameters showed that the storage reservoir and caprock fracture properties needed to be modeled together in order to assess the potential to meet CO_2 storage criteria.

THIS WORK IS DEDICATED TO:

My Lord and Savior Jesus Christ

[*In partial fulfillment of my earthly duties*]

ACKNOWLEDGEMENTS

TABLE OF CONTENTS

LIST OF TABLES

xiv

List of Figures and Illustrations

CHAPTER 1

INTRODUCTION

There is concern for the accumulation of greenhouse gases in the atmosphere and their adverse impact on global climate, particularly from anthropogenic sources of CO_2 (Solomon et al. 2007). Global CO_2 emissions in 2011 were estimated to be 31.6 Gigatonnes (Gt) and are projected to increase to 43.2 Gt in the year 2035 (EIA 2011). In the United States (U.S.) alone, CO_2 emissions were estimated to reach 5.6 Gt in 2011 with a projected increase to 6.3 Gt in 2035 (EIA 2011). Fossil fuel conversion systems like electricity production are major point sources for anthropogenic emissions of CO_2 in the atmosphere. Development of technologies and strategies to abate projected CO_2 emissions from these point sources are currently explored (IPCC 2005).

Carbon capture and storage (CCS) is a promising technological option to mitigate this increase of atmospheric CO_2 and other greenhouse gases (Pacala and Socolow 2004). CCS, in general, encompasses the capture and separation of CO_2 at its source, transport, and injection of CO_2 into suitable geological formation(s) to be stored for long periods of time (IPCC 2005). In the U.S., carbon capture and storage is being developed with the goal of having fossil fuel conversion systems achieve 90% CO_2 capture with 99% storage permanence at less than 10% increase in cost of energy services (NETL 2007). This approach is aimed at developing a foundation for the commercialization of CCS technologies for reduction of atmospheric CO_2 concentrations while at the same time imposing little or no negative impacts on energy availability and economic growth (NETL 2008, 2009, 2011).

Part of reaching the goal of 99% CO_2 storage permanence is related to characterizing potential geological storage and confining formations to assess the risk of unplanned migration from the storage zones (NETL 2007; 2011). Analyzing the risk associated with each CCS project is a process that primarily involves three aspects: risk source assessment, risk characterization, and risk management (IEAGHG 2009; Rechard 1999).

Risk source assessment involves the identification of project risks and specific features, events, and processes (FEPs) that could contribute to, or prevent, unplanned CO_2 migration from the storage zone (NETL 2011). Examples of FEPs could include: presence of conductive fractures in caprock (feature), unexpected overpressure in storage formation (event), or lateral migration of CO_2 plume in other resources (process). A registry of FEPs is generated for each potential CCS site. During the risk source assessment, potential receptors are identified and consequences are associated with the FEPs.

Once a risk source assessment has been completed, a risk characterization is undertaken where the probability and impact of an FEP occurrence is determined. At this stage, the examined risks are categorized and ranked in terms of likelihood and magnitude of consequence (IEAGHG 2009; Rechard 1999). The ranking allows high-priority risks to be identified, where plans for mitigation or control of these risks can be undertaken, and lower-priority risks to be slated for monitoring or undergo further investigation (NETL 2011). For a potential CCS site, the priorities of identified risks can be updated as more information is garnered from site characterization or trial operations.

Risk management takes the project risks and priority ranking results of the risk characterization to develop mitigation and control plans to address potential consequences. Risk mitigation plans generally address two primary aspects: (1) programmatic risks – including resource and management risks which can affect progress or cost, and (2) technical risks which may affect the achievement of scientific and engineering objectives of

a storage project (NETL 2009, 2011). Currently, CCS risk management is largely focused on the technical aspects of deployment, and mitigation plans are based primarily on monitoring data.

Uncertainty is a critical factor in risk characterization for potential CCS operations (NETL 2011). For example, deep saline formations have the largest potential capacity among the various geological options (others include unmineable coal seams, and oil and gas reservoirs) for CO_2 storage, with estimates for their storage potential ranging from 3,300 – 12,600 Gt in North America alone (NETL 2008). However, saline formations and their associated caprocks are the least characterized of the geological storage options (NETL 2009, 2011; Chapter 2).

Higher risks are currently associated with CO_2 storage in saline formations because, unlike oil and gas reservoirs, the properties and effectiveness of their caprock (or confining zones) are not sufficiently understood or proven (NETL 2011). The inherent variability and heterogeneity of the saline formations may result in considerable uncertainty when quantifying the probability and impacts of potential FEPs present at site. Therefore, model simulations are heavily relied upon in the early stages of risk analysis to assess the probabilities and impact of the different FEPs that may be at a potential site (NETL 2011a,b).

This work was aimed at addressing, in part, the uncertainty in risk source and risk characterization associated with caprock formations considered for CO_2 storage in saline formations in the U.S.

1.1 PREVIOUS STUDIES

In the United States, the Department of Energy (DOE) initiated Regional Carbon Sequestration Partnership programs (RCSPs) to determine the operational and technical feasibility for geologically sequestering CO_2 in various regions of the United States (Litynski

et al. 2009; NETL 2009). Each of the regional partnerships is engaged in assessing project and technical risks associated with demonstrating pilot and large-scale projects, particularly in saline reservoirs. One the technical challenges encountered in demonstrating CCS is verifying the integrity of the geological sealing units for long-term containment of injected CO_2. Of concern is the transport of CO_2 through the secondary porosity of caprock rock (NETL 2009; Bruant et al. 2002).

CO_2 leakage across a caprock generally fall under three basic types: 1) leakage through poorly sealed or failed injection well casing, or improperly abandoned wells (Bruant et al. 2002; Gasda et al. 2004); 2) leakage through pre-existing dissolution channels (Bruant et al. 2002; NASCENT 2005); and 3) lateral or vertical migration of CO_2 along faults or fractures (Bruant et al. 2002; Streit and Hillis 2004). Relatively few studies have examined the role of fracture properties on CO_2 transport across a fractured caprock, and fewer still have considered how the uncertainty in the caprock hydraulic fracture properties might influence CCS risk assessment or caprock performance (Chapter 3; Chapter 4; Oldenburg et al., 2009; Smith et al., 2011; Zhang et al., 2010).

Most studies focus on assessing the potential for geomechanical failure of a seal due to pressure buildup in a reservoir upon injection of a fluid, or wellbore leakage (Rohmer and Bouc, 2010; Rutqvist et al., 2007; Rutqvist et al., 2008; Smith et al., 2011; Celia et al., 2011; Kopp et al., 2010; Nordbotten et al., 2005; Nordbotten et al., 2009). When numerous wells exist in a field for potential CO_2 storage, poorly completed wells offer direct pathways to the surface that can compromise the integrity of the sealing unit(s) and capacity of a storage unit (NETL 2009, Nordbotten et al., 2009). In regards to geomechanical failure, intact caprocks generally have low permeability where, in an enclosed geologic structure, the potential exists for reservoir overpressure and subsequent mechanical failure of caprock (Chapter 2; Economides 2009; Rutqvist et al., 2007; Rutqvist et al., 2008).

Other numerical and semi-analytical studies that have modeled transport of CO_2 through a storage reservoir and a continuous fracture in the overlying caprock have noticed several features: (1) CO_2 loss may be a self-enhancing process (Pruess and Garcia 2002; Rutqvist and Tsang 2002). (2) As fluid pressure within the reservoir enters the fracture, the relative permeability of CO_2 fluid flow increases as the entire fracture becomes saturated with CO_2 (Rutqvist and Tsang 2002). (3) CO_2 transport can be described by steady-state, rather than fully time-dependent calculations under idealized conditions (Pritchard 2007; Neufeld et al. 2009). (4) CO_2 storage efficiency of a reservoir with a fractured caprock can decay with time (Neufeld et al. 2011; Vella et al. 2011), and be significantly influenced by small, pre-existing cracks in the caprock (Saripalli and McGrail 2002).

1.2 OBJECTIVES

The overall goals of this research were to examine the physical characteristics of caprock formations overlying saline reservoirs considered for CO_2 storage and to investigate the impact of uncertainty in hydraulic properties of a fractured caprock on the ability to meet long-term CO_2 storage goals. To accomplish these goals three specific objectives were defined, as follows:

- Review the current state of knowledge on the physical and lithologic characteristics of caprocks in areas considered for CO_2 sequestration, and identify common features that may impact long-term CO_2 storage.

- Develop an integrated aalytical model for estimating fracture hydraulic properties of caprocks relied upon for long-term CO_2 storage.

- Investigate the impact of uncertainty in fracture aperture and density on predicting CO_2 loss and caprock hydraulic fracture properties associated with meeting long-term storage goals.

1.3 DISSERTATION OVERVIEW

This dissertation consists of five chapters and six appendices. The principal chapters of this thesis (Chapter 2 – 4) are organized as self-contained papers that address each of the three specific objectives of this research, and are either published (Chapter 2) or will be submitted for publication (Chapters 3 and 4) in peer-reviewed journals. Chapter 1 provides a general introduction to the dissertation, giving the background and context to the work pursued in this study, while Chapter 5 summarizes major conclusions and presents recommendations for follow-up research.

Chapter 2 reviews the available information on the physical and chemical characteristics of some geological caprock strata within candidate basins considered for CO_2 sequestration in the US, and identifies characteristics relevant to meeting CO_2 storage goals within the basins. Regions investigated in this study included the northern Gulf Coast, Cincinnati Arch, Colorado Plateau–north Arizona, and the Paradox, Illinois, Michigan, and Appalachian basins. Potential caprock(s) within the Gulf Coast, Illinois, and Paradox Basins were examined in detail for their structural, physical, and mineralogical features. This material, written by Craig Griffith and co-authored by David Dzombak and Gregory Lowry, is published in *Environmental Earth Sciences* journal with the reference:

> Griffith, C.A., Dzombak, D.A. and Lowry, G.V. (2011), "Physical and Chemical Characteristics of Potential Seal Strata in Regions Considered for Demonstrating Geological Saline CO_2 Sequestration," Environmental Earth Sciences, 64(4):925-948

Chapter 3 presents the development of an integrated analytical model intended for evaluating the effect of hydraulic properties of a fractured caprock on CO_2 transport through a caprock-reservoir system. The integrated model combines analytical models previously developed for CO_2 plume transport and pressure distribution within a storage reservoir, with a 'cubic' law Darcy equivalent transport equation for flow in fractured caprock. Using a deterministic approach, the integrated analytical transport model was employed to

determine the range of hydraulic fracture aperture, density, porosity, and permeability values of a fractured caprock suitable for meeting CCS performance criteria, given parameter constraints obtained from field studies.

Chapter 4 utilizes the model developed in Chapter 3 to evaluate the impact of uncertainty within the caprock and reservoir properties on predicting CO_2 loss and hydraulic parameter associated with meeting long-term CO_2 storage requirements. The integrated model is cast in a stochastic framework, using a generalized sensitivity analysis (GSA) and three case simulation experiments to evaluate the influence of uncertain caprock fracture and reservoir properties on CO_2 leakage.

Chapter 5 summarizes the major findings and conclusions of this dissertation, and the original contributions of the work. Chapter 5 also provides suggestions for future work in the ongoing research areas of fracture characterization and flow modeling for CCS.

Appendix A provides supporting geological and geochemistry information for CCS candidate sites examined in Chapter 2. Appendix B provides supporting derivations of key pressure and fracture percolation equations used in Chapters 3 and 4. Appendices C – D provide background information into the direct, importance sampling, and kernel density estimation procedures used in the Monte Carlo method of Chapter 4. Appendices E – F give the resulting descriptive statistics and spearman correlation coefficient matrices for the three case experiments of Chapter 4.

1.4 REFERENCES

Bruant RG, Guswa AJ, Celia MA, Peters CA (2002), Safe storage of CO_2 in deep saline aquifers. Environmental Science & Technology 36(11):240A-245A

Celia, M.A., Nordbotten, J.M., Court, B., Dobossy, M. and Bachu, S., 2011. Field-scale application of a semi-analytical model for estimation cif CO2 and brine leakage along old wells. International Journal of Greenhouse Gas Control, 5(2): 257-269.

Economides, C.E. and Economides M.J., 2010. Sequestering carbon dioxide in a closed underground volume. Journal of Petroleum Science and Engineering 70: 123–130

EIA (2011) International Energy Outlook 2009. Energy Information Administration DOE/EIA-0484(2011), Washington, DC

IEAGHG (2009) A review of the international state of the art in risk assessment guidelines and proposed terminology for use in CO_2 geological storage. International Energy Agency Greenhouse Gas R&D Programme, 2009/TRP, Gloucestershire, UK

Kopp, A., Binning, P.J., Johannsen, K., Helmig, R. and Class, H., 2010. A contribution to risk analysis for leakage through abandoned wells in geological CO2 storage. Advances in Water Resources, 33: 867-879.

Litynski J, Plasynski S, Spangler L, Finley R, Steadman E, Ball D, Nemeth KJ, McPherson B, Myer L (2009), U.S. Department of Energy's Regional Carbon Sequestration Partnership Program: Overview. Energy Procedia 1(1):3959-3967

NETL (2007) Carbon Sequestration Technology Roadmap and Program Plan 2007. US Department of Energy, National Energy Technology Laboratory, Morgantown, West Virginia

NETL (2008) Carbon Sequestration Atlas of the United States and Canada. US Department of Energy, National Energy Technology Laboratory, Morgantown, West Virginia

NETL (2009) Best Practices for: Monitoring, Verification, and Accounting of CO_2 Stored in Deep Geological Formations. US Department of Energy, National Energy Technology Laboratory, Morgantown, West Virginia

NETL (2011) Best Practices for: Risk Analysis and Simulation for Geologic Storage of CO_2. US Department of Energy, National Energy Technology Laboratory, Morgantown, West Virginia

Neufeld, J.A., Vella, D. and Huppert, H.E., 2009. The effect of a fissure on storage in a porous media. Journal of Fluid Mechanics, 639: 239-259.

Nordbotten, J.M., Celia, M.A., Bachu, S. and Dahle, H.K., 2005. Semianalytical solution for CO_2 leakage through an abandoned well. Environmental science & technology, 39(2): 602-611.

Nordbotten, J.M., Kavetski, D., Celia, M.A. and Bachu, S., 2009. Model for CO_2 leakage including multiple geological layers and multiple leaky wells. Environmental science & technology, 43(3): 743-749.

Oldenburg, C.M., Bryant, S.L. and Nicot, J.P., 2009. Certification framework based on effective trapping for geologic carbon sequestration. International Journal of Greenhouse Gas Control, 3(4): 444-457.

Pacala,S, Socolow R (2004) Stabilization Wedges: Solving the Climate Problem for the Next 50 Years with Current Technologies. Science 305(5686): 968-972

Pritchard, D., 2007. Gravity currents over fractured substrates in a porous media. Journal of Fluid Mechanics, 584: 415-431.

Pruess, K. and Garcia, J., 2002. Multiphase flow dynamics durign CO_2 disposal into salne aquifers. Environmental Geology, 42: 282-295.

Rechard, RP (1999) Historical Relationship Between Performance Assessment for Radioactive Waste Disposal and other types of Risk Assessment. Risk Analysis 19: 763 -807

Rohmer, J. and Bouc, O., 2010. A response surface methodology to address uncertainties in cap rock failure assessment for CO_2 geological storage in deep aquifers. International Journal of Greenhouse Gas Control, 4(2): 198-208.

Rutqvist, J. and Tsang, C.-F., 2002. A study of caprock hydromechanical changes associated with CO_2-injection into a brine formation. Environmental Geology, 42: 296-305.

Rutqvist, J., Birkholzer, J., Cappa, F. and Tsang, C.F., 2007. Estimating maximum sustainable injection pressure during geological sequestration of CO_2 using coupled fluid flow and geomechanical fault-slip analysis. Energy Conversion and Management, 48(6): 1798-1807.

Rutqvist, J., Birkholzer, J. and Tsang, C.F., 2008. Coupled reservoir-geomechanical analysis of the potential for tensile and shear failure associated with CO_2 injection in multilayered reservoir-caprock systems. International Journal of Rock Mechanics and Mining Sciences, 45: 132-143.

Saripalli, P. and McGrail, P., 2002. Semi-analytical approaches to modeling deep well injection of CO_2 for geological sequestration. Energy Conversion and Management, 43: 185-198.

Smith, J., Durucan, S., Korre, A. and Shi, J.Q., 2011. Carbon dioxide storage risk assessment: Analysis of caprock fracture network connectivity. International Journal of Greenhouse Gas Control, 5(2): 226-240.

Solomon S, Qin D, Manning M, Marquis M, Averyt K, Tignor M, Miller HL, Chen Z (2007) Climate Change 2007: the physical science basis. Contribution of Working Group I to the Fourth Assessment Report of the Intergovernmental Panel on Climate Change. Cambridge University Press, New York

Vella, D., Neufeld, J.A., Huppert, H.E. and Lister, J.R., 2011. Leakage from gravity currents in a porous medium. Part 2. A line sink. Journal of Fluid Mechanics, 666: 414-427.

Zhang, Y.Q., Oldenburg, C.M. and Finsterle, S., 2010. Percolation-theory and fuzzy rule-based probability estimation of fault leakage at geologic carbon sequestration sites. Environmental Earth Sciences, 59(7): 1447-1459.

CHAPTER 2

REVIEW OF PHYSICAL AND LITHOLOGIC CHARACTERISTICS OF POTENTIAL CAPROCKS IN REGIONS CONSIDERED FOR DEMONSTRATION OF GEOLOGICAL SALINE CO$_2$ SEQUESTRATION[1]

ABSTRACT

Capture and geological sequestration of CO$_2$ from energy production is proposed to help mitigate climate change caused by anthropogenic emissions of CO$_2$ and other greenhouse gases. Performance goals set by the US Department of Energy for CO$_2$ storage permanence include retention of at least 99% of injected CO$_2$, which requires detailed assessments of each potential storage site's geologic system, including reservoir(s) and caprock(s). The objective of this study was to review relevant basinwide physical and chemical characteristics of geological caprocks considered for saline reservoir CO$_2$ sequestration in the United States. Results showed that the caprock strata can exhibit substantial heterogeneity in the composition, structural and fluid transport characteristics on a basin scale. Analysis of available field and wellbore core data reveal several common inter-basin features of the caprocks, including the occurrence of quartz, dolomite, illite, calcite, and glauconite minerals along with structural features containing fractures, faults, and salt structures. In certain localities within the examined basins, some caprock strata also serve as source rock for oil and gas production and can be subject to salt intrusions. The regional features identified in this study can help guide modeling, laboratory, and field studies needed to assess local caprock performances within the examined basins.

2.1 INTRODUCTION

There exists a concern for the growing accumulation of atmospheric greenhouse gases levels adversely impacting the global climate, particularly from anthropogenic sources of CO_2 (Solomon et al. 2007). Most of the anthropogenic sources of CO_2 stem from energy-related emissions, with estimates of global emissions reaching 28 Gigatonnes (Gt) in 2005 and projected to reach 40.4 Gt in the year 2030 (McArdle and Lindstrom 2008; Doman et al. 2009). Carbon capture and sequestration (CCS) is a viable mitigation option to abate this increase of atmospheric CO_2, and has emerged as the most promising storage option (Metz et al. 2005).

Deep saline formations appear to have the largest potential capacity among the various geological options, with estimates for their storage potential ranging from 3,300 – 12,600 Gt in North America alone (NETL 2008). CO_2 storage in deep saline formations also has the potential for stable, permanent chemical sequestration of at least some of the injected CO_2 due to mineral precipitation from chemical interactions of the injected CO_2 with the brine and reservoir rock (Benson et al. 2005; NETL 2007).

In 2003, the U.S Department of Energy (U.S. DOE) initiated the Regional Carbon Sequestration Partnership programs (RCSPs) to determine the operational and technical issues faced in geologically sequestering CO_2 in various regions of the United States (Litynski et al. 2009; NETL 2009). Each of the regional partnerships is exploring the demonstration of CO_2 sequestration in saline reservoirs. Some potential large and pilot-scale projects are located within the Gulf Coast, Cincinnati Arch, Colorado Plateau – north Arizona, Wyoming Thrust Belt, and in the San Joaquin, Unita, Paradox, Williston, Illinois, Michigan, and Appalachian Basins (Figure 2.1) (Litynski et al. 2009, 2008).

These RCSP demonstration projects are being developed to meet the goal of 99% storage permanence by selecting the demonstration sites following detailed site assessments coupled with comprehensive site-specific risk assessments (NETL 2007; NETL

11

2009). Containment of the CO_2, along with potential the co – contaminant H_2S, at each of these sites relies on both the storage reservoir units as well as the overlying caprock rock strata within the geological system (Smith 2009a, 2009b). These storage and caprock strata can occur broadly throughout the basins, and hence can represent potential units for storage beyond the specific sites that have been assessed. A better understanding of the physical and chemical properties of the storage and caprock formation can reduce the risk, uncertainty, and financial costs of future commercial CCS projects (Eccles 2009).

The objective of this study was to review available information on the physical and chemical characteristics of some geological caprock strata within candidate basins considered for CO_2 sequestration in the U.S., and to identify characteristics that could be relevant to CO_2 storage within the basins. Regions investigated in this study included the northern Gulf Coast, Cincinnati Arch, Colorado Plateau – north Arizona, and the Paradox, Illinois, Michigan, and Appalachian basins. Potential caprock(s) within the Gulf Coast, Illinois, and Paradox basins were examined in detail for their structural, physical, and mineralogical features (Figure 2.1).

2.2   CAPROCK CHARACTERISTICS FOR GEOLOGICAL CO_2 STORAGE

The ability for a geological caprock to retard fluid flow depends on its intrinsic transport properties, which include flow through its primary and secondary porosity. Primary and secondary porosity account for fluid transport through the rock matrix and fracture networks, respectively. The effectiveness of caprock rocks in trapping CO_2 depends on how the combination of these intrinsic properties, along with geomechanical and geochemical factors associated with CO_2 injection, affect the overall integrity of the caprock (Benson et al. 2005).

Transport of supercritical CO_2 or CO_2-saturated brine through the primary porosity of caprock rock depends on: capillary entry pressure, permeability, relative CO_2-brine

permeability, porosity, and effective diffusion rate through fluid saturated pore space (Schlomer and Krooss 1997; Hildenbrand et al. 2002). Capillary forces determine the capacity of a caprock to inhibit flow of a non-wetting phase through the caprock until the pressure of the underlying phase (such as supercritical CO_2) exceeds the capillary entry pressure. Once capillary entry pressure is exceeded, permeability and relative permeability will control fluid transport. The rate of fluid transport through the primary porosity of the caprock rock will depend on the formation's permeability and thickness, and the fluid pressure in the storage zone and overlying stratum (Schlomer and Krooss 1997).

Transport of CO_2 through the secondary porosity of caprock rock is generally considered to be of three basic types (Bruant et al. 2002): 1) leakage through poorly sealed or failed injection well casing, or improperly abandoned wells (Bruant et al. 2002; Gasda et al. 2004); 2) leakage through pre-existing dissolution channels (Bruant et al. 2002; NASCENT 2005); and 3) lateral or vertical migration of CO_2 along faults or fractures (Bruant et al. 2002; Streit and Hillis 2004). With respect to the last point, fluid movement along faults or fractures depend on several factors. These factors include: geometry, fluid pressures within faulted areas, state of stress on pre-existing faults, connectivity of faults or fractures, and hydraulic communication between stratigraphic units (Watts 1987; Aydin 2000; Jones and Hillis 2003). Faults can act as a potential barrier or be transmissive due to damage surrounding the fault area or to increased permeability from interlaid sediments (Aydin 2000). The state of stress on pre-existing faults in caprock along with the degree of connectivity and hydraulic communication determines if the rock strength may be susceptible to mechanical failure due to CO_2 injection, resulting in re-activation of pre-existing faults or generation of new fractures (Jones and Hillis 2003; Streit and Hillis 2004).

Mineralogy of the caprock is important because of the potential for alteration of the rock matrix or fault-interlaid-sediments due to exposure to supercritical CO_2 or CO_2-saturated brine. Of concern would be the presence of minerals susceptible to dissolution by

an acidic CO_2-saturated brine that lead to CO_2 transport through creation of permeable zones or lenses (Benson et al. 2005), and/or fluid flow along fractures and faults present in the caprock (Schlomer and Krooss 1997; Aydin 2000; Fisher and Knipe 2001; Bailey et al. 2006). CO_2 transport and the overall physical properties of a caprock may be affected by the presence of soluble mineral phases occurring in clusters, fractures, faults, or within the cement of the caprock strata (Aydin 2000; Li et al. 2006, 2007; Cunningham 2007)

2.3 METHODS

In several regions of the U.S. being considered for saline CO_2 sequestration, the primary, secondary, and tertiary geological caprocks within the candidate basins (or geologic structures) were investigated for their mineral characteristics. The dominant mineralogy of the candidate geological caprocks is described in stratigraphic order in Table 2.1, along with the corresponding storage reservoirs, basin, and geographical location. Based on available data, six caprock formations were examined in detail with respect to their mineralogy, physical, and structural features. The geological caprock strata studied include the formations immediately overlying the storage reservoirs, as well as some of the secondary and tertiary confining units.

Caprock formations examined in detail included: the Gothic and Chimney Rock shales within the Paradox basin in Utah; the Tuscaloosa Marine Shale and Selma Group within the northern region of the Gulf Coast, particularly in Mississippi; the Eau Claire and Mount Simon shale interbeds within the Illinois basin in Illinois. The mineral and physical characteristics of these six caprocks are presented in Table 2.1 and 2.3, respectively. In addition, structural features and other elements within the regions were also examined for their potential influence on the integrity of the geological seals.

The data collected for the depth, thickness, lithology, mineralogy, permeability, porosity, organic content, geomechanical properties, and structural features of the rock

seals were primarily drawn from U.S. DOE regional partnership reports, peer reviewed journals, state and federal geological survey open reports, and university theses containing geological data for the regions of the proposed demonstration sites. There were limited data available to describe the subsurface mineral and physical composition of the caprocks. When subsurface data were not available, data from related outcrop units were used to describe the geological strata. The abundance of each mineral among the caprock units was not quantified since some of the sources only provided uncalibrated or relative amounts. However, the presence or absence of minerals in the caprock units was documented in a profile, based on available information (Figure 2.2). The mineralogical profile identified minerals most likely to be involved with rock-brine-CO_2 interactions,

Plan view maps of the Northern Gulf Coast Province and Illinois Basin (including surrounding states) were generated with GIS shapefiles given from the respective state geological surveys, the SECARB, and MGSC regional partnerships (see Figure 2.3, 2.5 and 2.7). The plan view map of the Paradox Basin was redrawn and spatially geo-referenced from literature sources.

Site – specific data obtained and used by the U.S DOE regional partnerships for determining the expected performance of each caprock at their respective localities were not addressed as site-specific analysis was beyond the scope of this study. More detail is given in Appendix A on the geology, lithology, mineralogy, structural and physical features of both potential storage reservoirs and their associated geological seals. Discussed in this chapter are the physical and chemical characteristics relating only to potential geological seals.

2.4   RESULTS AND DISCUSSION

The lithology and dominant mineral characteristics of several potential caprock formations are presented in Table 2.1. The minerals listed were identified by petrographic

and X-ray diffraction (qualitative and quantitative) analysis. Storage reservoirs are listed on the left-most columns of Table 2.1 and correspond to their overlying caprocks in the right columns. The formations are listed in stratigraphic order at each proposed site with the overlying caprock rock adjacent to the storage reservoir(s) and the subsequent caprocks positioned above. Detailed mineral and physical data of six potential caprocks within the Gulf Coast, Paradox, and Illinois basins are presented in Tables 2.2 and 2.3, respectively. The mineral data presented in Table 2.2 are divided into major and minor mineral components. Here we define major minerals as those present in more than 20 weight % of the rock, and minor minerals as those present in less than 20 weight % of the rock. Figure 2.2 presents a profile of the minerals found within the seal strata.

2.4.1 COMMON MINERALOGY

Table 2.1 and Figure 2.2 reveal that calcite, quartz, dolomite, illite, feldspar (potassium or sodium), glauconite, and kaolinite were among the most common minerals reported for the geological seal formations in the regions of the sites evaluated. Due to the variation in reporting methods, mixed layer clays, though documented with less frequency, are likely to have higher occurrence among the caprocks – particularly illite. The thermodynamic and kinetic reaction characteristics of these common minerals, especially the clay minerals, under reservoir conditions of high salinity, high pressure of CO_2, and high temperature are not well understood (Marini 2007). Based on the current literature of the weathering behavior of these common minerals, including a few experiments at elevated pressures of CO_2, the carbonates are more susceptible to CO_2 attack than the clay or silica minerals. The reactions depend on the formation water chemistry, temperature, and pressure ranges (Marini 2007). However, a few experiments with glauconite show that its rate of dissolution, in the presence of acidic and alkaline mediums, is faster than a generalized illite and comparable to some carbonates (Fernandez-Bastero et al. 2005; Marini 2007). The lack of thermodynamic and kinetic data on the reactions of the common

caprock mineral phases with injected CO_2, under reservoir conditions, implies the need for the dissolution rates of these identified minerals to be examined under such conditions.

The characteristics of candidate caprock rocks for saline CO_2 sequestration throughout the Gulf Coast, Paradox, and Illinois basins are examined in detail in the next section.

2.4.2 PARADOX BASIN – UTAH

The Paradox basin near the 'four corners' (Utah, Arizona, Colorado, and New Mexico) is being considered by the Southwest Regional Partnership for potential saline CO_2 sequestration demonstration (Figure 2.3). One potential demonstration site is near Bluff, Utah in San Juan County, within the southern 'Blanding sub-basin' of the Paradox basin. It is primarily an enhanced oil recovery (EOR) operation, that would involve the injection of 450,000 – 750,000 tons of CO_2 into the Ismay and Desert Creek zones within the Paradox formation, located at depths of 1,707 to 1,768 m, with an additional 20,000 tons into a saline reservoir formation beneath the oil reservoirs (McPherson 2006; Litynski et al. 2008).

GEOLOGY

The target reservoir and geological caprocks for CO_2 saline sequestration lie within the Upper Pennsylvanian sediments of the Paradox formation, in the Paradox Basin. The Paradox Basin is a large elongate, northwest-southeast trending structural depression developed during the Middle to Upper Pennsylvanian (Desmoinesian) period. It covers an area of approximately 28,500 km^2; its boundaries are defined by the limit of the halite deposits in the Paradox formation, which can thicken up to 4,300 m (Figure 2.3) (Hite 1968; Raup and Hite 1992). The Paradox formation is part of the Hermosa Group and contains 29 to 33 "cycles" or beds of halite separated by a sequence of clastic and penesaline interbeds (Hite 1960). The EOR and proposed saline CO_2 sequestration operation both use the Gothic and Chimney Rock shales for geological seals, though it is unclear how the Gothic shale

17

serves as a geological seal for the Ismay reservoir zone. The Ismay, Desert Creek, Gothic, and Chimney Rock cycles within the Paradox formation are contained within the traditionally named 'Ismay-Desert Creek Interval,' which comprise the first five of these cycles (Hite 1960; Tuttle et al. 1996). The Gothic and Chimney Rock shales are cycles 3 and 5, respectively, within the 'Ismay-Desert Creek Interval', with the shale beds occurring near the center of each cycle (Raup and Hite 1992; Tuttle et al. 1996) (see Figure 2.4).

FOLDS AND FAULTS

The Paradox Basin has extensive and numerous folds and faults that can affect the structure of the caprock and reservoir formations in certain geographical locations. Major structural features of the Paradox Basin include the Middle Pennsylvanian Age evaporite-cored anticlines collectively known as the Paradox 'Fold and Fault Belt' to the north and the 'Blanding sub-basin' to the south-southwest (Figure 2.3) (Grout and Verbeek 1998; McClure et al. 2003). The anticlines in the Fold and Fault Belt trend N40° - 55°W and are cut by approximately nine regional sets of extension joints, extending from Middle Pennsylvanian to Cretaceous ages sediments (Grout and Verbeek 1997). The joints extend over 250 km within the region with widths up to 1,000 m (Grout and Verbeek 1997). Joints typically run parallel or sub-parallel to the graben-bounding normal faults present in the Fold and Fault Belt and are nearly perpendicular to bedding throughout the basin, regardless of bedding inclination (Grout and Verbeek 1997). Faults around Lisbon Valley have a N60° – 65°W orientation with a dip of 88°NW and strike angles of N21°E and N35°E (Grout and Verbeek 1997). Fault zone sediment displacement affecting geological caprocks can range from 1,200 – 1,500 m (Grout and Verbeek 1997). The Blanding sub-basin, however, is relatively un-deformed (McClure et al. 2003).

CAPROCK LITHOLOGY

The Gothic and Chimney Rock shale cycles, as well other evaporitic cycles of the Paradox formation, undergo lateral as well as vertical lithologic facies changes across the

Paradox Basin (Hite 1960; Hite and Lohman 1973; Tuttle et al. 1996). In the Blanding sub-basin, near the basin margins and shelf, the Gothic and Chimney Rock shale cycles contain a sequence of dominantly marine limestone with a succession of argillaceous and calcareous black shale (Hite 1960; Tuttle et al. 1996). The Gothic and Chimney Rock shale cycles near Bluff, Utah grade laterally into beds of halite with successive interbeds of anhydrite, silty dolomite, black shale, dolomite, and anhydrite in the northern regions of the basin (Hite and Lohman 1973; Hite and Buckner 1981; Raup and Hite 1992; Tuttle et al. 1996) (Figure 2.4). The black shales within the Gothic and Chimney Rock cycles are persistent throughout the Paradox basin whereas the halite beds can reach up to 70-80 weight % of the cycle rock composition (Hite and Lohman 1973).

The mineral characteristics of the Gothic and Chimney Rock black shales are described in Tables 2.1 and 2.2. Whole rock petrographic analysis show that the Gothic and Chimney Rock shales in the Paradox Basin are approximately 1/3 silt and clay-sized quartz, 1/3 carbonates, and 1/3 clay minerals and organic material (Tromp 1995). X-ray diffraction (XRD) analyses of sample cores from San Juan County show quartz, illite, dolomite, calcite, pyrite, chlorite, siderite, and plagioclase (sodium feldspar) to be major minerals in the caprocks near the Utah demonstration site (Tromp 1995; Tuttle et al. 1996). Throughout the Paradox Basin, vein-filling minerals in fractures and mico-fractures of the caprocks include: calcite, anhydrite, pyrite, halite, and rare halides like sylvite, sinjarite, and tachyhydrite (Tromp 1995; Tuttle et al. 1996). The carbonates are 15 - 40% by weight, and are divided equally between dolomite and calcite, with the Gothic shale being more calcareous in the vicinity of the test site and the Chimney Rock shale more dolomitic (Hite et al. 1984; Tromp 1995). The carbonates also act as cementing agents between clay minerals in the shales (Tromp 1995; Tuttle et al. 1996). XRD analyses of the clay minerals in the vicinity of the demonstration site show the mixed layer illite-smectite and chlorite-

smectite to be predominant in the Chimney Rock shale and Gothic shale, respectively (Tromp 1995) (See Table 2.2).

CAPROCK PHYSICAL PROPERTIES

There are limited data on the physical properties of the Gothic and Chimney Rock shales, where most of the physical data lies in the northern regions of the Paradox basin (Table 2.3). Porosity values range from 1.61 – 4.05% with horizontal permeability ranging from 5.6 – 6.9 x 10^{-20} m^2 at depths of 1,800 – 1,838 m (Bereskin and Mclennan 2008). Table 2.3 also includes geomechanical properties and modeled values used for simulation of the vertical and horizontal permeability (White et al. 2002; Bereskin and Mclennan 2008). At depths of 1,791 – 1,840 m, compressive stress ranged from 166.37 – 310.90 MPa, with a Young's modulus range of 38,562 – 56,613 MPa, and a Poisson's ratio range of 0.24 – 0.33 (Bereskin and Mclennan 2008).

The caprock strata are generally characterized by high porosity and low permeability, except where fracturing exists (Hite and Lohman 1973; White et al. 2002; Bereskin and Mclennan 2008). To the north in the 'Fold and Fault Belt', fractures in the caprocks are numerous and widespread with geometrically complex network patterns and can range from hairline (0.01) to 3.6 cm in width, with strike angles of N21°E (Hite and Lohman 1973; Grout and Verbeek 1997).

The black Gothic and Chimney Rock shales are relatively uniform (i.e. no folds or unconformities) in the Blanding sub – basin, but contain fractures in some locations within the sub-basin (Tuttle et al. 1996; McClure et al. 2003). For example, a description from a core sample of the Gothic shale (cycle 3) from the West Water Creek well No.1 in San Juan County, Utah (about 25 km from the test site) reported "massive fractures or veins filled with sulfides and sulfate minerals" (Tuttle et al. 1996). Elsewhere in the Blanding sub-basin,

the fractures are also described as having veins filled with sulfate or carbonate minerals near the limestone contact (Tuttle et al. 1996).

The Gothic and Chimney Rock shales have been assessed as good source rocks for potential oil and natural gas production in Utah and Colorado (Nuccio and Condon 1996; Schamel 2006). Characteristics that make them potentially good source rocks include: total organic carbon (TOC) values ranging from < 0.5 – 13%, hydrocarbon – yielding potential (S1 + S2) values >2.0 mg-hydrocarbon/g-sample, organic matter of Type II and III kerogen, and sufficient thermal maturity, i.e. production index (PI) and vitrinite values, throughout most of the basin (Hite et al. 1984; Nuccio and Condon 1996). There is also strong lateral variability in organic matter within the two shales, apparently associated with the lateral facies changes of the formations (Van Buchem et al. 2000). Regions within the Paradox basin where the Gothic and Chimney Rock black shales are enclosed by thick beds of halite are thought to entrap potentially more natural gas versus oil (Schamel 2006).

In summary, the Gothic and Chimney Rock shales undergo significant physical and chemical changes across the Paradox basin. Features relevant to CO_2 storage include: regionally extensive units with high porosity and low permeability; variation in lithology, mineralogy, and thickness (9 – 61 m); and the presence of filled fractures throughout the basin. The lithology of the Gothic and Chimney Rock shales across the basin changes from primarily carbonates in the south, to salt and anhydrite cycles in the north. Naturally occurring fractures in the caprocks are documented mostly in the northern, with some in the southern, regions of the basin, ranging from "hairline" to "massive" (Hite and Lohman 1973; Tuttle et al. 1996). The fractures are filled with carbonates, halides, anhydrite, and pyrite (Tromp 1995; Tuttle et al. 1996). Numerous faults transect the Paradox formation in the northern region and are mainly associated with the anticlines within the 'Fold and Fault Belt' (Grout and Verbeek 1997).

2.4.3 Gulf Coast Province of North America – Mississippi

The northern region of the Gulf Coast is being studied by the Southeast Regional Carbon Sequestration Partnership (SECARB) for possible demonstration of saline CO_2 sequestration. Two field demonstration sites are being investigated in Mississippi: one at Plant Daniel in Jackson County, the other within Cranfield oil field in Adams County (Figure 2.5). Both sites share the same CO_2 storage reservoir and caprock units where the proposed storage formation is the Lower Tuscaloosa Massive Sand formation (LTMS) with the Tuscaloosa Marine Shale (TMS) as the caprock and the Selma Group and Midway shale serving as secondary and tertiary caprocks, respectively (Litynski et al. 2008; Nemeth 2008). The LTMS is proposed to store up to 3,000 short tons at Plant Daniel in Jackson County and up to 2.25 Mt over 1.5 years of natural and anthropogenic CO_2 at Cranfield, in Adams County, at depths exceeding 2,200 and 3,000 m respectively (Rhudy 2006; Hill 2007). In this study, only the TMS and Selma Group caprocks are examined in detail.

Geology

The target reservoir and geological seals for CO_2 saline sequestration lie within the Upper Cretaceous Gulfian sediments of the northern region of the Gulf Coast Province of North America (Figure 2.5). The northern region of the Gulf Coast Province of North America covers a total area of approximately 750,000 km^2 with the LTMS and associated caprocks covering 120,000 km^2 (Ryder and Ardis 2002; Rhudy 2006; Nemeth and Hovorka 2007). The northern Gulf Coast includes parts of Florida, Alabama, Mississippi, Louisiana, Texas, Arkansas, Tennessee, Kentucky, Missouri, and Illinois (Murray 1961; Ryder and Ardis 2002). Broadly speaking, the Upper Cretaceous System of the coastal province form a syncline filled with vast amounts of sediment accompanied by folding, faulting, intrusions of igneous rock, and with regional uplifts along the axis of the trough. The overall dip of the sediments within the syncline are seaward, where the degree and slope are being modified by vertical

warping, fault and fracture systems of varying magnitude, and by igneous and salt emplacements (Murray 1961).

FOLDS AND FAULTS

Folds and uplifts, in certain localities across the northern Gulf Coast region, may alter caprock and storage strata. In southern Mississippi, major features include: the Wiggins Uplift, Monroe Uplift, Jackson Dome, and La Salle Arch (Figure 2.5). The folds generally trend northwest – southeast with the Wiggins Uplift having bifurcating lobes – the Wiggins anticline to the northwest and the Hancock ridge to the south (Murray 1961). The Wiggins Uplift is associated with complex and pronounced faults of thick early Quaternary – Tertiary age sediments. It is not clear if the faults influence Cretaceous age sediments, which contain the storage reservoir and caprock units (Murray 1961). Both the Monroe Uplift and the Jackson Dome are known to affect the storage and caprock sedimentary strata (Murray 1961). The Monroe Uplift is offset by emplacement of relatively large igneous masses with pronounced angular unconformities (Murray 1961). The Jackson Dome is an uplift that has thick, tilted, and truncated strata overlain with an angular unconformity (Murray 1961). The La Salle Arch is a gently dipping structure affecting all Tertiary strata, with Gulfian and Comanchean strata to a possibly lesser extent. The La Salle arch is generally not associated with any appreciable faulting (Murray 1961).

The major fault system in Mississippi is the Pickens-Gilbertown graben fault system. The Pickens-Gilbertown penetrates and displaces surface to subsurface strata, including the Cretaceous LTMS, TMS, and Selma Group sediments. It is a gulfward trending concave system of normal faults extending 1,610 km relatively uninterrupted through the Northern Gulf Coast Province, having faults 8,000 – 12,900 km wide running parallel or sub-parallel to the regional strike (see Figure 2.5). The regional strike ranges from NW30° to 40°SE, with dip angles ranging from 35° to 70° gulfward (Murray 1961). Sediment displacement associated with the Pickens-Gilbertown can range from 150 – 300 m (Murray 1961). The

Jackson-Mobile graben is another fault zone in the surrounding region affecting Cretaceous sediments (see Figure 2.5). Both the Pickens-Gilbertown and the Jackson-Mobile have similar characteristics, with varying degrees of sediment displacement and associated strata, possibly complexly warped and faulted (Murray 1961).

OTHER STRUCTURAL FEATURES

Numerous salt structures exist along the Northern Province of the Gulf Coast (Murray 1961) (see Figure 2.5). The salt structures can occur as piercements (spikes) or large elongated masses in which the enclosing sedimentary strata can exhibit upwarping and thinning of beds adjacent to the salt rock (Murray 1961). Normal faulting is typically associated with salt piercements, but can have multiple offset faults and fractures penetrating adjacent sediment strata. This is the case for the Tuscaloosa formation in the Jasper and Lincoln counties of Mississippi (Murray 1961).

CAPROCK LITHOLOGY

Figure 2.6 shows the lateral facies changes of the Tuscaloosa Marine Shale (TMS) and Selma Group as they grade upward and inland across Mississippi and the Northern Gulf Coast Province towards Arkansas and Tennessee.

The TMS is a fissile, fine-grained, dark-gray micaceous shale with minor interbeds of calcareous, glauconitic sandstone with some argillaceous limestone lentils, laminated claystone, mudstones, and calcareous siltstone (Braunstein 1950). Table 2.1 and 2.2 lists petrographic data taken from thin-sections and cores in Alabama near the outcrop of the equivalent Coker-Eoline formation, and from the shales of the "Stringer" member of the Lower Tuscaloosa (see Figure 2.6). The TMS is predominantly composed of quartz, kaolinite, illite, hematite, and siderite based on point-counts of thin-section and qualitative X-ray diffraction (XRD) (Pryor and Glass 1961; Bergenback 1964; Watkins 1985).

The Selma Group contains chalks, chalky marl, and limestone members. Tables 2.1 and 2.2 show manganese, ferrous, and magnesium carbonates within the limestone members and kaolinite, montmorillonite, illite, and glauconite within the marl members. Mineralogy of the Selma Group was compiled from semi-quantitative XRD data on samples near the surface in Alabama, Tennessee, Kentucky, Illinois, Missouri, and Arkansas, and qualitative XRD, thin-section, and insoluble residue analyses on equivalent formation core samples from central to east Texas (Pryor and Glass 1961; Bergenback 1964; Scholle 1977; Freed 1980; Czerniakowski et al. 1984).

CAPROCK PHYSICAL PROPERTIES

Few data were available on the permeability and porosity of the TMS in southern Mississippi. Table 2.3 lists the thickness, porosity, and permeability available for the TMS within the northern Gulf Coast Province. Porosity ranged from 2.3 – 8.0% based on a report in the Gillsburgh Oil field adjacent to Adams County (John et al. 1997). Vertical permeability in one area was estimated to range from 3.6 – 36 x 10^{-19} m^2, based on well testing of confining beds within the Gordo and Coker formations in Alabama (Planert and Sparkes 1985). The Gordo and Coker formation are the surface-equivalent to the subsurface Upper Tuscaloosa and TMS (Planert and Sparkes 1985; Stromm and Mallory 1995) (see Figure 2.6). Horizontal permeability of the TMS at depths greater than 3,220 m range from 9.87 – 59.2 x 10^{-18} m^2 in southeast Louisiana (John et al. 1997). In northern Mississippi at shallower depths, the horizontal permeability of the TMS ranges from 7.19 – 540 x 10^{-13} m^2, based on the Gordo and Coker formations (Slack and Darden 1991). The thickness of the TMS varies from 114 – 244 m across southwest Mississippi and central Louisianna, and from 137 – 145 m in the Jackson County, Mississippi area (John et al. 1997; Hovorka et al. 2007; Rhudy 2007).

Few data were available for permeability and porosity of the Selma Group in southern Mississippi. Table 2.3 has the vertical permeability estimated to range from 3.24 x

10^{-22} – 3.24 x 10^{-16} m^2 (Brahana and Mesko 1988). Horizontal permeability range from <4.93 – 987 x 10^{-17} m^2, in Texas, where the Austin Group is the Selma Group equivalent (Scholle 1977), In northern Mississippi, the horizontal permeability ranges from 2.52 – 97.1 x 10^{-13} m^2 (Slack and Darden 1991). The porosity of the Selma Group ranged from 9 – 45% in Texas and Alabama, with 31 – 35% in some areas in Alabama, and is depth dependent (Scholle 1977; Holston et al. 1989).

The TMS and Selma Group are oil and gas source formations within certain localities in Mississippi and other regions along the Gulf Coast (Beebe and Curtis 1968; Scholle 1977; John et al. 1997; Condon and Dyman 2006). The TMS contains significant amounts of thermally mature total organic carbon (> 0.5%) and has reports of oil production in southwest Mississippi (Miranda 1988; Miranda and Walters 1992; John et al. 1997; Mancini 2005) (see Table 2.3). Fractures are noted in TMS core samples from Lincoln, and Amite County and were associated with oil production (John et al. 1997). The Selma Group has significant gas production in certain horizons in south central Mississippi, and in east Texas (Beebe and Curtis 1968; Scholle 1977; Condon and Dyman 2006).

In summary, the TMS and Selma Group undergo significant physical and chemical changes across the northern Gulf Coast region. In particular to Mississippi (and adjacent states), changes that could be relevant to saline reservoir CO_2 storage include: Thick (114 – 305 m), regionally extensive units with variations in lithology, permeability, and porosity; the presence of fractures and salt piercements; and, oil and gas production from the caprocks in the southwest areas of Mississippi. Permeability of the TMS and Selma Group varies significantly along the Gulf Coast. Between south and north Mississippi, the horizontal permeability of the TMS and Selma Group can increase up to 6 orders of magnitude with up to 10 orders of magnitude difference between their vertical and horizontal permeabilites. Lithology of the TMS and Selma Group changes from predominantly shale and chalk,

respectively, in southern Mississippi to sandstone in northern regions of Mississippi, Alabama, and Tennessee.

2.4.4 ILLINOIS BASIN – ILLINOIS

The Illinois Basin is being studied by the Midwest Geological Sequestration Consortium (MGSC) for possible saline CO_2 sequestration demonstration projects. In Illinois, three potential sites are being investigated: the Louden and Mattoon oil fields, and the Archer Daniels Midland Company (ADM) ethanol plant (Litynski et al. 2008; Litynski et al. 2009). They are located in Fayette, Coles, and Macon County respectively. All of these sites proposed to inject CO_2 into the Mount Simon sandstone reservoir and use the overlying Eau Claire formation, of the Knox group, as the primary caprock with the shale interbeds of the Mount Simon modeled to further restrict flow of CO_2 (Finley 2005; Finley and Leetaru 2006; Finley 2008). The Mount Simon sandstone is capable of storing 10,000 – 1,000,000 t of CO_2 in Illinois, at depths ranging from 2,130 – 2,290 m (Finley and Leetaru 2006; Finley 2008; Litynski et al. 2008; Litynski et al. 2009). Additional geological caprocks include the Maquoketa formation and the New Albany Shale, 910 – 1,130 m above the Eau Claire, respectively (Finley 2005). In this study, only the upper member of the Mount Simon and the lower members of the Knox group (the Eau Claire and the Ironton – Galesville sandstone) were examined in detail.

GEOLOGY

The proposed sites, storage reservoir, and geological seals for CO_2 saline sequestration in Illinois lie within the Cambrian age sediments of the Illinois Basin (Figure 2.7 and 2.8). The Illinois Basin is a spoon-shaped, asymmetrical shallow structural depression that trends northwest-southeast and covers an area of 155,000 km^2, with the deepest part of the basin (4,570 m) near the intersection of Illinois, Indiana, and Kentucky (McBride 1998; Finley 2005). Regional slopes reverse direction at the borders of the arches and domes, and the basin's sediments are overlapped by the Mississippi Embayment to the

south where it is complexly faulted, and subjected to seismic reactivation, as it approaches the New Madrid Rift System and the Rough Creek Graben (Willman et al. 1975; McBride and Nelson 1999) (see Figure 2.7).

FOLDS AND FAULTS

There are numerous folds in Illinois basin. In Illinois, Major features include the late Mississippian – early Pennsylvanian Du Quoin monocline, Louden, La Salle 'Anticlinorium' (LSA) and Clay City anticlines (see Figure 2.7). These folds extend over 400 km in the region and are north-trending, asymmetrical anticlines and monoclines that are elongated and branched (McBride 1998). Their folding, particularly the Clay City anticline, can affect the entire Paleozoic sediments – including the storage and caprock(s) (McBride and Nelson 1999).

Associated faults beneath several anticlines and monoclines within the Fairfield sub-basin have normal, high-angle reverse, and antithetic faults with dip angles ranging from 60° – 75° (McBride 1998; McBride and Nelson 1999). Sediment displacement associated with faults along the Du Quoin monocline range from 30 – 50 m (McBride and Nelson 1999). The Cottage grove fault system is a major fault system in the Fairfield sub-basin that contain a series of transgressional reverse faults that form a strike-slip zone that affects the entire Paleozoic strata and Precambrian basement (McBride and Nelson 1999) (see Figure 2.7). High resolution seismic studies show that these faults transect primary, secondary, and tertiary seals (which are thousands of feet apart), along with the indication of having strike-slip components that could provide a structural fabric capable of seismic reactivation (McBride 1998; McBride and Nelson 1999).

OTHER STRUCTURAL FEATURES

Seismic activity exists within the New Madrid Seismic Zone (NMSZ), located in the southern region of Illinois at the border of Kentucky and Wisconsin (see Figure 2.7). The

NMSZ is a structurally complex zone of faults associated with a long history of reactivation (McBride 1998; McBride and Nelson 1999). Earthquakes are spatially associated with the extension of the NMSZ to the La Salle Anticlinorium (LSA) and Wasbash Valley Fault System (WVFS) in the Fairfield sub-basin of the Illinois Basin (McBride 1998; McBride and Nelson 1999).

CAPROCK LITHOLOGY

The Eau Claire formation undergoes significant lateral lithologic facies changes in the Illinois Basin. Figure 2.8 shows that the Eau Claire trends from a sandstone or sandy dolomite in northern Illinois to a siltstone or shale in central Illinois, to a mixture of dolomite and limestone near the Missouri border, where it is a relatively pure dolomite (Willman et al. 1975; Finley 2005). In Macon County, regional cross-sections show the Eau Claire to have a persistent shale interval above the Mount Simon sandstone. The siltstone facies contain clay seams and laminae and is commonly interbedded with very dark green to black shale (Willman et al. 1975; Finley 2005). Table 2.8 list qualitative and quantitative X-ray diffraction (XRD) data from two locations in Illinois that shows that the Eau Claire, by volume percent, is dominantly illite, quartz, and dolomite, with glauconite or chlorite also being a major component in some reports (Finley 2005; KunleDare 2005).

The shale interbeds in the upper segments of the Mount Simon formation are present at the sites considered for storage, and are considered a confining unit for groundwater movement in northern Illinois (Nicholas et al. 1987; Finley 2005). The shale interbeds are lithologically described as red and green micaceous shales with illite, quartz, and potassium feldspar as dominant minerals (see Table 2.8)(Finley 2005).

CAPROCK PHYSICAL PROPERTIES

Few data are available on the permeability and porosity of the Eau Claire in southern Illinois. The thickness, porosity, vertical and horizontal permeability of the Eau Claire are

reported in Table 2.3. Vertical permeability ranged from $9.87 \times 10^{-19} - 4.78 \times 10^{-16}$ m^2 and porosity from 0.4 – 15.4% (KunleDare 2005). Data were gathered from core samples in Henderson County, Illinois. Horizontal permeabilities were based on two reports in northern Illinois (Nicholas et al. 1987; Mills et al. 2002). Thickness of the Eau Claire ranges from 60 – 300 m throughout Illinois, and 150 – 210 m near potential demonstration localities (Willman et al. 1975; Finley 2005).

No permeability or porosity data for the Mount Simon shale interbed layers were available in southern Illinois. However in northern Illinois, the shale interbed layers were tested to give a permeability of 4.68×10^{-13} m^2, in Table 2.3, where the shaley interbeds behave effectively as a hydraulic confining unit for water movement from the Mt Simon aquifer (Visocky et al., 1985; Nicholas et al. 1987). Initial modeling done by the MGSC has indicated that the shaley interbeds of the upper segment of the Mount Simon could inhibit CO_2 migration in southern Illinois but are not likely to be used as a separate, effective caprock (Finley 2005). The thicknesses of the Mount Simon shale intervals are reported to be 150 m with individual shale beds as thin as 4.6 m thick (Nicholas et al. 1987; Willman et al. 1975). The areal extent and continuity of the Mount Simon shale intervals are not known (Nicholas et al. 1987; Finley 2005).

In the Illinois basin, the Eau Claire is generally described as being an effective caprock for successful natural gas storage projects in the Mount Simon (Finley 2005). However there is evidence of gas migration into overlying formations in certain localities where the Mount Simon is cut by at least four faults (Finley 2005).

Possibly relevant to CO_2 storage in the northern areas of Illinois, is the observation of saline water movement into the Ironton – Galesville aquifer from adjacent aquifers, including the Mount Simon (Visocky et al., 1985; Nicholas et al. 1987). The movement of water into the Ironton – Galesville from the Mount Simon through the Eau Claire confining

unit, as well as other adjacent aquifers, was documented via well tests and measurements of conductivity, temperature, and chloride. The influx of water appears to have been induced by excessive pumping of Ironton – Galesville aquifer around the Chicago area in northern Illinois (Visocky et al., 1985; Nicholas et al. 1987).

In summary, the physical and chemical characteristics of the Eau Claire vary across the Illinois basin. Features relevant to saline CO_2 sequestration include its use for current, successful natural gas storage projects; regionally extensive units with variations in thickness and lithology; existence of faults throughout the southern region of the basin; seismic activity in the NMSZ; and, brine movement through the caprock in localities near Chicago. The characteristic behavior of the Mount Simon shale interbeds across the Illinois basin is unclear. However, within northern Illinois, available reports indicate that the shale interbeds behave as an effective hydraulic confining unit (Nicholas et al. 1987).

2.5 SUMMARY AND CONCLUSIONS

The goal of this study was to review available information on the physical and chemical features of geological seal strata within some candidate basins considered for saline CO_2 sequestration in the U.S. and present characteristics that could be relevant to CO_2 storage. Several caprocks were examined for their dominant mineral phases in their lithology. Based on available data, a subset of these caprocks were also examined for their structural features and physical properties.

The main conclusions are: 1) caprock formations are regionally extensive, and are generally thick with low permeability; 2) common minerals in the caprock formations are quartz, illite, dolomite, calcite, and glauconite; 3) there is substantial spatial variability in the composition, thickness, and fluid transport properties of the caprock formations within the basins; 4) fractures and faults penetrate caprock strata throughout the basins examined, highlighting the importance of site – specific evaluations in the selection of a

storage reservoir; 5) some of the caprock rock strata are oil and gas sources; and 6) each basin has unique regional features that could be relevant to CO_2 storage, such as the presence of salt piercements, previous seismic activity and water resource aquifers in certain localities. The significance of these features with regards to site – specific caprock integrity is currently the focus of investigations conducted by the U.S. DOE regional partnerships.

Understanding the reactive behavior of minerals in rock cements and matrices with CO_2 and brine, under relevant temperatures, pressures, and salinities, is necessary to understand the extent of chemical alterations within candidate caprocks. The data compiled in Tables 1, 2, and 3 are useful for determining the kinds of minerals that merit special attention in the lab and field investigations.

Caprock strata examined are generally thick, ranging from 9 – 352 m in the areas examined, and generally exhibit low permeability. The caprocks are not continuous or uniform in lithology throughout the regions examined, having lateral facies changes, fractures, and spatial variability in thickness, permeability, porosity, and other physical properties that could impact caprock performance within certain areas of the candidate basins. Fractures reported in caprock strata are not fully characterized and have unknown regional extent and interconnectivity. Detailed site – specific data are needed to assess the influence of fractures, lithologic changes, and variable permeability and porosity at any particular site with the basin.

Faults and fault zones are common within each of the regions examined. The influence of fault proximity, extent of deformation, and fluid conductivity on caprock strata performance at a potential site within the Gulf Coast, Paradox or Illinois basin merits investigation.

Proposed caprock formations in Mississippi and Utah are considered source rocks for oil and gas production in some areas within the two regions. The potential effects of recovery operations on the performance of the caprocks used for potential CO_2 storage, in those localities, need to be investigated. Related efforts on enhanced oil recovery could provide insight into the integrity of the caprocks that previously served as oil and gas source formations.

There exist other regional features that could be relevant to CO_2 storage. For instance, the salt piercements and domes found within the Gulf Coast and Paradox basin could affect caprock integrity due to the offset faulting and fractures frequently associated with them. In the Illinois basin, excessive pumping of overlying aquifers near metropolitan areas may affect CO_2 transport at shallower depths. Knowing where these features exist can aid in determining the most favorable site(s) for demonstrating CO_2 sequestration, where the extent and manner in which these geological phenomena influence caprock performance would be determined by site – specific studies.

This review of physical and chemical characteristics of the seal rock formations overlying candidate saline reservoirs has highlighted features that merit focused attention when investigating candidate sites for long-term CO_2 storage within these selected basins. The common characteristics identified in this study regarding heterogeneity in caprock composition, physical attributes, and regional structural features can help guide the development of laboratory and field studies for site – specific assessments.

Acknowledgments

Partnerships (RCSPs), and with geologists at state agencies. The authors are also grateful to

Dann Burton for drawing the cross-sectional views.

2.6 REFERENCES

Aydin A (2000), Fractures, faults, and hydrocarbon entrapment, migration and flow. Marine and Petroleum Geology 17:797-814

Bailey WR, Underschultz J, Dewhurst DN, Kovack G, Mildren S, Raven M (2006), Multi-disciplinary approach to fault and top seal appraisal; Pyrenees-Macedon oil and gas fields, Exmouth Sub-basin, Australian Northwest Shelf. Marine and Petroleum Geology 23(2):241-259

Beebe BW, Curtis BF (eds) (1968), Natural Gas in Post-Paleozoic Rocks in Mississippi, American Association of Petroleum Geologist, Tulsa, Oklahoma, 2 volumes, v. 1: 1176-1226 pp.

Benson S, Cook P, Anderson J, Bachu S, Nimir HB, Basu B, Bradshaw J, Deguchi G, Gale J, Goerne GV, Heidug W, Holloway S, Kamal R, Keith D, Lloyd P, Rocha P, Senior B, Thomson J, Torp T, Wildenborg T, Wilson M, Zarlenga F, Zhou D (2005) Underground geological storage. In: Metz B, Davidson O, Coninck HD, Loos M, Meyer L (eds) Carbon Dioxide Capture and Storage: Special Report of the Intergovernmental Panel on Climate Change. Cambridge University Press, pp 195-276

Bereskin SR, McLennan J (2008) Hydrocarbon Potential of Pennsylvanian Black Shale Reservoirs, Paradox Basin, Southeastern Utah, Utah Geological Survey Open File Report 534. Salt Lake City, Utah

Bergenback RE (1964) Petrology of pre-Selma strata from core holes in western Alabama, U. S. Geological Survey Bulletin 1160-B. United States Government Printing Office, Washington, D.C.

Bingham PS, Savrda CE (2006) Paleoenvironmental context of the Ingersoll Shale, an Upper Cretaceous Konservat-Lagerstaette, Eutaw Formation, eastern Alabama. Paper presented at Geological Society of America, Southeastern Section, 55th annual meeting, Knoxville, Tennesse, 23-24 March 2006

Bond DC (1972) Hydrodynamics in deep aquifer of the Illinois Basin, Illinois State Geological Survey Circular 470. Urbana, Illinois

Brahana JV, Mesko TO (1988) Hydrogeology and preliminary assessment of regional flow in the Upper Cretaceous and adjacent aquifers in the northern Mississippi embayment U.S. Geological Survey Water Resources Investigations Report 87-4000. Nashville, Tennessee

Braunstein J (1950) Subsurface stratigraphy of the Upper Cretaceous in Mississippi. Mississippi Geological Society, pp 13-21

Brett CE, Tepper DH, Goodman WM, LoDuca ST, Eckert B-Y (1995) Revised Stratigraphy and Correlations of the Niagaran Provincial Series (Medina, Clinton, and Lockport Groups) in the Type Area of Western New York, U.S. Geological Survey Bulletin 2086

Bruant RG, Guswa AJ, Celia MA, Peters CA (2002), Safe storage of CO_2 in deep saline aquifers. Environmental Science & Technology 36(11):240A-245A

Cadigan RA (1971) Geochemical Distribution of Some Metals in the Moenkopi Formation and Related Strata, Colorado Plateau Region, U.S. Geological Survey Bulletin 1344. United States Government Printing Office, Washington, D.C.

Cadigan RA, Stewart JH (1971) Petrology of the Triassic Moenkopi Formation and Related Strata in the Colorado Plateau Region, U.S. Geological Survey Professional Paper 692. United States Government Printing Office, Washington, D.C.

Condon SM, Dyman TS (2006) 2003 geologic assessment of undiscovered conventional oil and gas resources in the Upper Cretaceous Navarro and Taylor Groups, Western Gulf Province, Texas, U.S. Geological Survey Digital Data Series DDS-69-H. Reston, Virginia

Cunningham JA, Fadel ZJ (2007) Contaminant degradation in physically and chemically heterogeneous aquifers. Journal of Contaminant Hydrology 94:293-304

Cushing EM, Boswell EH, Hosman RL (1964) General Geology of the Mississippi Embayment, U.S. Geological Survey Professional Paper 448-B. United States Government Printing Office, Washington, D.C.

Czerniakowski LA, Lohmann KC, Wilson JL (1984), Closed-system marine burial diagenesis: isotopic data from the Austin Chalk and its components. Sedimentology 31:863-877

Doman LE, Smith K, Lindstrom P, Mayne L, Staub J, Yucel E, Barden J, Fawzi A, Martin P, Mellish M, Kearney D, Kette S, Murphy B, LaRiviere M, Vincent K, Kapilow-Cohen B (2009) International Energy Outlook 2009, Energy Information Administration Report DOE/EIA-0484(2009). Washington, D.C.

Eccles JK, Pratson L, Newell RG, Jackson RB (2009), Physical and Economical Potential of Geological CO2 Storage in Saline Aquifers. Environmental Science & Technology 43(6): 1962-1969

Farmerie RL, Coogan AH (1995), Silurian Salina salt strata terminations in northeastern Ohio. Northeastern Geology and Environmental Sciences 17(4):383-393

Fernandez-Bastero S, Garcia T, Santos A, Gago-Duport L (2005), Geochemical potentiality of glauconitic shelf sediments for sequestering atmospheric CO2 of anthropogenic origin. Ciencias Marinas 31(4):593-615

Finley R (2005) An Assessment of Geological Carbon Sequestration Options in the Illinois Basin, Illinois State Geological Survey Final Report U.S. DOE Contract: DE-FC26-03NT41994. Champaign, Illinois

Finley R (2007) Update on Regional Characterization Activites and Large Scale Storage Projects, Demonstrating CO_2 storage in the Mount Simon Sandstone of the Illinois

Basin. In: Proceedings of the Regional Carbon Sequestration Partnerships Annual Review Meeting. Pittsburgh, PA

Finley R (2008) An Assessment of Geological Carbon Sequestration in the Illinois Basin - A Research Update. In: Proceedings of the Regional Carbon Sequestration Partnerships Annual Review Meeting. Pittsburgh, PA

Finley R, Leetaru H (2006) Pilot Tests Fact Sheets: CO_2 Sequestration in Saline Formations - II, Illinois Basin, MGSC. In: Proceedings of the Regional Carbon Sequestration Partnerships Initiative Review Meeting. Pittsburgh, PA

Fisher QJ, Knipe RJ (2001), The permeability of faults within siliciclastic petroleum reservoirs of the North Sea and Norwegian Continental Shelf. Marine and Petroleum Geology(18):1063-1081

Freed RL (1980), X-ray study of the bulk mineralogy and clay content of six samples from the Austin Formation, Bexar and Medina counties, Texas. Bulletin of the South Texas Geological Society 20(5):7-9

Freeman ML, Naftz DL, Snyder T, Johnson G (2008) Assessment of Nonpoint Source Chemical Loading Potential to Watersheds Containing Uranium Waste Dumps Associated with Uranium Exploration and Mining, San Rafael Swell, Utah, U.S. Geological Survey Scientific Investigations Report 2008-5110, Figure 1. Reston, Virginia

Gasda SE, Bachu S, Celia MA (2004), Spatial characterization of the location of potentially leaky wells penetrating a deep saline aquifer in a mature sedimentary basin. Environmental Geology 46(6-7):707-720

Grout MA, Verbeek ER (1997) Tectonic and Paleostress Significance of the Regional Joint Network of the Central Paradox Basin, Utah and Colorado, U.S. Geological Survey bulletin 2158. United States Government Printing Office, Washington, DC

Gupta N (2008) Appalachian Basin, R.E. Burger Plant, Cincinnati Arch, East Bend Plant. In: Proceedings of the Regional Carbon Sequestration Partnerships Initiative Annual Review Meeting. Pittsburgh, PA

Gupta N, Ball D (2006) Pilot Project Fact Sheets: CO_2 Sequestration in Saline Formations - I, Michigan Basin, MRCSP. In: Proceedings of the Regional Carbon Sequestration Partnerships Initiative Review Meeting. Pittsburgh, PA

Gupta N, Ball D (2008a) Project Fact Sheets: Phase II CO_2 Sequestration in Saine Formations, Appalachian Basin- MRCSP. In: Proceedings of the Regional Carbon Sequestration Partnerships Initiative Annual Review Meeting. Pittsburgh, PA

Gupta N, Ball D (2008b) Project Fact Sheets: Phase II CO_2 Sequestration in Saine Formations, Cincinnati Arch Geologic Test- MRCSP. In: Proceedings of the Regional Carbon Sequestration Partnerships Initiative Annual Review Meeting. Pittsburgh, PA

Gupta N, Ball D (2008c) Project Fact Sheets: Phase II CO_2 Sequestration in Saine Formations, Michigan Basin - MRCSP. In: Proceedings of the Regional Carbon Sequestration Partnerships Initiative Annual Review Meeting. Pittsburgh, PA

Hepple RP, Benson SM (2005), Geologic storage of carbon dioxide as a climate change mitigation strategy: Performance requirements and the implications of surface seepage. Environmental Geology 47(4):576-585

Hildenbrand A, Schlomer S, Krooss BM (2002), Gas breakthrough experiments on fine-grained sedimentary rocks. Geofluids 2:3-23

Hill GR (2007) SECARB - Large Scale CO_2 Storage in the Lower Tuscaloosa Massive Sand Formation. In: Proceedings of the Regional Carbon Sequestration Partnerships Annual Project Review Meeting. Pittsburgh, PA

Hite RJ (1960) Stratigraphy of the saline facies of the Paradox Member of the Hermosa Formation of southeastern Utah and southwestern Colorado, U.S. Geological Survey Open-File Report 60-70. Salt Lake City, Utah

Hite RJ (1968) Salt deposits of the Paradox basin, southeast Utah and southwest Colorado. In: Mattox RB (ed) Saline deposits: Geological Society of America Special Paper 88. Geological Society of America, pp 319-330

Hite RJ, Anders DE, Ging TG (1984) Organic-rich source rocks of Pennsylvanian age in the Paradox basin of Utah and Colorado. In: Woodward J, Meissner FF, Clayton JL (eds) Hydrocarbon Source Rocks of the Greater Rocky Mountain Region. Rocky Mountain Association of Geologists Guidebook, pp 255-274

Hite RJ, Buckner DH (1981), Stratigraphic correlations, facies concepts and cyclicity in Pennsylvanian rocks of the Paradox Basin. Field Conference - Rocky Mountain Association of Geologists 1981:147-159

Hite RJ, Lohman SW (1973) Geological Appraisal of Paradox Basin Salt Deposits for Waste Emplacement, U.S. Geological Survey Open File Report 73-114. Denver, Colorado

Hluchy MM, Reynolds RC (1989), Clay-mineral assemblages associated with Salina Group rocks in New York State. Geological Society of America, Northeastern Section, 24th annual meeting; abstracts with programs Abstracts with Programs - Geological Society of America 21(2):23

Holston I, King DT, Jr., Bittner E (1989), Porosity and cementation in Upper Cretaceous Mooreville and Demopolis chalks, central Alabama. AAPG Bull 73(9):1184

Hosterman JW, Whitlow SI (1983) Clay Mineralogy of Devonian Shales in the Appalachian Basin, U.S Geological Survey Professional Paper 1298. United States Government Printing Office, Washington, D.C.

Hovorka S, Meckel T, Nicot JP, Wang F, Paine J (2007) Gulf Coast Stacked Storage SECARB Phase II Test No.1. In: Proceedings of the Regional Carbon Sequestration Partnerships Annual Project Review Meeting. Pittsburgh, PA

Huffman AC, Condon SM (1993) Stratigraphy, Structure, and Paleogeography of Pennsylvanian and Permian Rocks, San Juan Basin and Adjacent Areas, Utah, Colorado, Arizona, and New Mexico, U.S. Geological Survey Bulletin 1808-O. United States Government Printing Office, Washington, D.C.

Huntoon PW (1988) Late Cenozoic gravity tectonic deformation related to the Paradox salts in the Canyonlands area of Utah. In: Doelling HH., Oviatt CG, Huntoon PW (eds) Salt deformation in the Paradox Basin. Utah Geological and Mineral Survey Bulletin 122: 81-93

John CJ, Jones BL, Moncrief JE, Bourgeois R, Harder BJ (1997), An Unproven Unconventional Seven Billion Barrel Oil Resource - the Tuscaloosa Marine Shale. The Basin Research Institute Bulletin 7:3-24

Johnson HS (1959) Uranium Resources of the Green River and Henry Mountains Districts, Utah A Regional Synthesis, U.S. Geological Survey Bulletin 1087-C, Plate 9. United States Government Printing Office, Washington, D.C.

Johnson RC, Nuccio VF (1993) Surface Vitrinite Reflectance Study of the Uinta and Piceance Basins and Adjacent Areas, Eastern Utah and Western Colorado - Implications for the development of the Laramide Basins and Uplifts, U.S. Geological Survey Bulletin 1787-DD. United States Government Printing Office, Washington D.C.

Jones RM, Hillis RR (2003), An integrated, quantitative approach to assessing fault-seal risk. American Association of Petroleum Geologists Bulletin 87:507-524

Kelly VC (1958a) Tectonics of the region of the Paradox Basin. In: Sanborn AF (ed) Guidebook to the Geology of the Paradox Basin. Intermountain Association of Petroleum Geologists, pp 31-38

Kelly VC (1958b) Tectonics of the Black Mesa region of Arizona. In: Anderson RY, Harshbarger JW (eds) Guidebook of the Black Mesa Basin, Northeastern Arizona. New Mexico Geological Society, pp 137-144

KunleDare MA (2005) Petrographic investigation into the development of secondary porosity in sandstones: A case study of the Cambrian Mount Simon and Galesville Sandstones, Illinois Basin. PhD, Department of Geological Sciences & Engineering, University of Missouri-Rolla, Rolla, Missouri

Landes KK (1951) Detroit River group in the Michigan Basin, Geological Survey Circular 133. Washington, D.C.

Lewis RQ, Trimble DE (1959) Geology and Uranium Deposits of Monument Valley San Juan County, Utah, U.S. Geological Survey Bulletin 1087-D. United States Government Printing Office, Washington, D.C.

Li L, Peters CA, Celia MA (2007) Effects of mineral spatial distribution on reaction rates in porous media. Water Resources Research 43(1): 1-17

Li L, Peters CA, Celia MA (2006) Upscaling geochemical reaction rates using pore-scale network modeling. Advances in Water Resources 29: 1351-1370

Litynski J, Plasynski S, Spangler L, Finley R, Steadman E, Ball D, Nemeth KJ, McPherson B, Myer L (2009), U.S. Department of Energy's Regional Carbon Sequestration Partnership Program: Overview. Energy Procedia 1(1):3959-3967

Litynski JT, Plasynski S, McIIvried HG, Mahoney C, Srivastava RR (2008), The United States Department of Energy's Regional Carbon Sequestration Partnerships Program Validation Phase. Environmental International 34:127-138

Mancini EA (2005) Resource Assessment of the In-Place and Potential Recoverable Deep Natural Gas Resource of the Onshore Interior Salt Basins, North Central and Northeastern Gulf of Mexico, University of Alabama Annual Progress Report for Year 2. Tuscaloosa, AL

Marini L (2007) Geological Sequestration of Carbon Dioxide - Thermodynamics, Kinetics, and Reaction Path Modeling (First ed.). Elsevier B.V., Amsterdam, The Netherlands, pp 453

Martin DL (1985) Depositional systems and ichnology of the Bright Angel Shale (Cambrian), eastern Grand Canyon, Arizona. Master's, Department of Geology, Northern Arizona University Flagstaff

McArdle P, Lindstrom P (2008) Emissions of Greenhouse Gases in the United States 2007, Energy Information Administration Report DOE/EIA-0573(2007). Washington, D.C.

McBride JH (1998), Understanding basement tectonics of an interior cratonic basin: southern Illinois Basin, USA. Tectonophysics 293:1-20

McBride JH, Nelson WJ (1999), Style and origin of Mid-Carboniferous deformation in the Illinois Basin, USA - Ancestral Rockies deformation? Tectonophysics 305(1/3):249-273

McClure K, Morgan CD, Chidsey TC, Eby DE (2003) Deliverable 1.1.1 Regional Paradox Formation Structure and Isochore Maps, Blanding Sub-Basin, Utah, Utah Geological Survey Contract No. DE-2600BC15128. Salt Lake City, Utah

McKee ED (1982) The Supai Group of Grand Canyon, U.S. Geological Survey Professional Paper 1173. United States Government Printing Office, Washington, D.C.

McPherson B (2006) Project Fact Sheets: CO_2 Sequestration in Saline Formations - II, Paradox Basin, Aneth Field - Saline and Oil, SWRPCS. In: Proceedings of the Regional Carbon Sequestration Partnerships Initiative Annual Review Meeting. Pittsburgh, PA

McPherson B, Grigg R (2008) Project Fact Sheets: Phase II CO_2 Sequestration in Oil Fields, Aneth Field EOR and Sequestration Test, Paradox Basin, Utah - SWP. In: Proceedings of the Regional Carbon Sequestration Partnerships Initiative Annual Review Meeting. Pittsburgh, PA

Metz B, Davidson O, Coninck Hd, Loos M, Meyer L (eds) (2005), IPCC Special Report on Carbon Dioxide Capture and Storage. Prepared by Working Group III of the Intergovernmental Panel on Climate Change, Cambridge University Press, Cambridge, United Kingdom and New York, NY, USA: 442 pp.

Milici RC, Swezey CS (2006) Assessment of Appalachian Basin Oil and Gas Resources: Devonian Shale - Middle and Upper Paleozoic Total Petroleum System, U.S. Geological Survey Open-File Report Series 2006-1237. Reston, Virginia

Mills PC, Nazimek JE, Halford KJ, Yeskis DJ (2002) Hydrogeology and Simulation of Ground-Water Flow in the Aquifers Underlying Belvidere, Illinois, U.S. Geological Survey Water-Resources Investigations Report 01-4100. Urbana, Illinois

Miranda RM (1988) Geochemical variations in sedimentary organic matter within a one hundred meter shale core of uniform lithology and thermal history (middle Tuscaloosa, Upper Cretaceous). Master's., University of Texas at Dallas, Dallas, Texas

Miranda RM, Walters CC (1992), Geochemical variations in sedimentary organic matter within a "homogeneous" shale core (Tuscaloosa Formation, Upper Cretaceous, Mississippi, USA). Organic Geochemistry 18(6):899-911

Murray GE (1961) Geology of the Atlantic and Gulf Coastal Province of North America. Harper & Brothers, New York, pp 21-451

Myer LR, Benson SM (2006) Pilot Tests Fact Sheets: CO2 Sequestration in Saline Formations - I, Kaiparowits Basin, WESTCARB. In: Proceedings of the Regional Carbon Sequestration Partnerships Initiative Review Meeting. Pittsburgh, PA

Naftz DL, Peterman ZE, Spangler LE (1997), Using del 87 Sr values to identify sources of salinity to a freshwater aquifer, Greater Aneth Oil Field, Utah, USA. Chem Geol 141(3-4):195-209

Nakicenovic N, Swart R (eds) (2000), Special Report on Emissions Scenarios: A Special Report of Working Group III of the Intergovernmental Panel on Climate Change (1st ed.), Cambridge University Press, Cambridge, United Kingdom and New York, NY USA: 612 pp.

NASCENT (2005) Natural Analogues for the Geological Storage of CO_2, IEA Greenhouse Gas R&D Programme Report 2005/6 March

Nemeth KJ (2008) Project Fact Sheets: Phase III Early and Anthropogenic CO_2 Injection Field Tests. In: Proceedings of the Regional Carbon Sequestration Partnerships Initiative Annual Review Meeting. Pittsburgh, PA

Nemeth KJ, Hovorka S (2007) Project Fact Sheets: CO_2 Sequestration in Saline Formations - I, Gulf Coast Stacked Storage SECARB Phase II Test #1. In: Proceedings of the Regional Carbon Sequestration Partnerships Annual Review Meeting. Pittsburgh, PA

NETL (2007) Carbon Sequestration Technology Roadmap and Program Plan 2007. U.S. Department of Energy, Office of Fossil Energy, National Energy Technology Laboratory, Morgantown, West Virginia, pp 86

NETL (2008) Carbon Sequestration Atlas of the United States and Canada (2nd ed.). U.S. Department of Energy, Office of Fossil Energy, National Energy Technology Laboratory, Morgantown, West Virginia, pp 140

NETL (2009) Best Practices for: Monitoring, Verification, and Accounting of CO_2 Stored in Deep Geological Formations, U.S. Department of Energy, National Energy Technology Laboratory Report DOE/NETL-311/081508

Nicholas JR, Sherrill MG, Young HL (1987) Hydrogeology of the Cambrian-Ordovician Aquifer System at a test well in northeastern Illinois, U.S. Geological Survey Water Resources Investigations Report 84-4165. Urbana, Illinois

Nuccio VF, Condon SM (1996) Burial and thermal history of the Paradox Basin, Utah and Colorado, and petroleum potential of the Middle Pennsylvanian Paradox Basin, U.S. Geological Survey Open-File Report 2000-O. United States Government Printing Office, Washington, D.C.

Oinonen RL (1965) A study of selected Salina salt beds in northeastern Ohio, Master's, Ohio University at Athens, Athens, Ohio

Ozol MA (1963) Alkali Reactivity of Cherts and Stratigraphy of Petrology of Cherts and Associated Limestones of the Onondaga Formation of Central and Western New York. PhD, Department of Geology, Rensselaer Polytechnic Institute, Troy, New York

Park SG (1987) Deposition, diagenesis, and porosity development of the Middle Devonian, Lucas Formation in the West Branch Oil Field, Ogemaw County, Michigan. Master's, Department of Geology, Western Michigan University, Kalamazoo

Planert M, Sparkes SL (1985) Estimation of vertical hydraulic conductivity of the clay layer between the Eutaw and Gordo aquifers in the vicinity of Faunsdale, Marengo County, Alabama, U.S. Geological Survey Water Resources Investigations Report 90-4155. Tuscaloosa, Alabama

Pryor WA, Glass HD (1961), Cretaceous-Tertiary Clay Mineralogy of the Upper Mississippi Embayment. Journal of Sedimentary Petrology 31(1):38-51

Raup OB, Hite RJ (1992) Lithology of evaporite cycles and cycle boundaries in the upper part of the Paradox Formation of the Hermosa Group of Pennsylvanian age in the Paradox Basin, Utah and Colorado, U.S. Geological Survey bulletin 2000-B. United States Government Printing Office, Washington, DC

Raup OB, Hite RJ (1996) Bromine geochemistry of chloride rocks of the Middle Pennsylvanian Paradox Formation of the Hermosa Group, Paradox Basin, Utah and Colorado, U.S. Geological Survey Bulletin 2000-M. United States Government Printing Office, Washington, D.C.

Reeves DK (1991) Clay Mineralogy and Early Diagenesis in the Yazoo Formation (Upper Eocene) and Undifferentiated Midway Group (Paleocene). Master's, University of Tennessee, Knoxville

Repenning CA, Cooley ME, Akers JP (1969) Stratigraphy of the Chinle and Moenkopi formations, Navajo and Hopi Indian reservations; Arizona, New Mexico, and Utah, U. S. Geological Survey Professional Paper 521-B. United States Government Printing Office, Washington, D.C.

Repetski JE, Ryder RT, Avary KL, Trippi MH (2005) Thermal maturity patterns (CAI and %Ro) in the Ordovician and Devonian rocks of the Appalachian basin in West Virginia, U.S. Geological Survey Open-File Report 2005-1078. Reston, Virginia and Morgantown, West Virginia

Rhudy R (2006) Pilot Tests Fact Sheets: CO2 Sequestration in Saline Formations - I, Mississippi Salt Basin, SECARB. In: Proceedings of the Regional Carbon Sequestration Partnerships Initiative Review Meeting. Pittsburgh, PA

Rhudy R (2007) CO2 Sequestration in Saline Formations - II, The SECARB Mississippi Test Site Project Update. In: Proceedings of the Regional Carbon Sequestration Partnerships Annual Project Meeting. Pittsburgh, PA

Rudd LP (2005) Using AVIRIS hyperspectral imagery to study the role of clay mineralogy in Colorado Plateau debris-flow initiation. PhD, Department of Geosciences, University of Arizona, Tucson

Ryder PD, Ardis AF (2002) Hydrology of the Texas Gulf Coast aquifer systems, U.S. Geological Survey Professional Paper 1416-E. Denver, Colorado

Ryder RT, Swezey CS, Trippi MH, Lentz EE, Avary KL, Harper JA, Kappel WM, Rea RG (2007) In search of a Silurian Total Petroleum System in the Appalachian basin of New York, Ohio, Pennsylvania, and West Virginia, U.S. Geological Survey Open-File Report 2007-1003

Schamel S (2006) Shale Gas Resources of Utah: Assessment of Previously Undeveloped Gas Discoveries, Utah Department of Natural Resources, Utah Geological Survey

Schlomer S, Krooss BM (1997), Experimental characterisation of the hydrocarbon sealing efficiency of cap rocks. Marine and Petroleum Geology 14(5):565-580

Scholle PA (1977) Current oil and gas production from North American Upper Cretaceous chalks, U.S. Geological Survey Circular 767. Arlington, Virginia

Schultz LG (1963) Clay Minerals in Triassic Rocks of the Colorado Plateau, U.S. Geological Survey Bulletin 1147-C. United States Government Printing Office, Washington, D.C.

Slack LJ, Darden D (1991) Summary of aquifer tests in Mississippi, June 1942 through May 1988, U.S. Geological Survey Water-Resources Investigations Report 90-4155. Jackson, Mississippi

Smith SA, Sorensen JA, Steadman EN, Harju JA (2009a). Acid gas injection and monitoring at the Zama oil field in Alberta, Canada: a case study in demonstration-scale carbon dioxide sequestration. Energy Procedia 1(1): 1981-1988

Smith SA, McLellan P, Hawkes C, Steadman EN, Harju JA (2009b). Geomechanical testing and modeling of reservoir and cap rock integrity in an acid gas EOR/sequestration project, Zama, Alberta, Canada. Energy Procedia 1(1): 2169-2176

Smosna R, Patchen DG, Warshauer SM, Perry WJ, Jr. (1977) Relationships between depositional environments, Tonoloway Limestone, and distribution of evaporites in the Salina Formation, West Virginia. SG 5: Reefs and Evaporites--Concepts and Depositional Models. American Association of Petroleum Geologists, Tulsa, OK, pp 125-143

Solana-Acosta W, Greb S, Rupp J, Drahovzal J, Wickstrom L, Sminchak J (2006) Preliminary Assessment of Potential CO2 Storage Reservoirs and Caprocks at the Cincinnati Arch

Site, Indiana, Kentucky, and Ohio Geological Surveys, Battelle Memorial Institute, Midwest Regional Carbon Sequestration Partnership Report (Second Draft)

Solomon S, Qin D, Manning M, Marquis M, Averyt K, Tignor M, Miller HL, Chen Z (eds) (2007), Climate Change 2007: The Physical Science Basis. Contribution of Working Group I to the Fourth Assessment Report of the Intergovernmental Panel on Climate Change, Cambridge University Press, United Kingdom and New York, NY, USA: 996 pp.

Spangler LE, Naftz DL, Peterman ZE (1996) Hydrology, Chemical Quality, and Characterization of Salinity in the Navajo Aquifer in and near The Greater Aneth Oil Field, San Juan County, Utah, U.S. Geological Survey Water-Resources Investigations Report 96-4155. Salt Lake City, Utah

Streit JE, Hillis RR (2004), Estimating fault stability and sustainable fluid pressures for underground storage of CO2 in porous rock. Energy 29(9-10):1445-1456

Stromm EW, Mallory MJ (1995) Hydrogeology and simulation of ground-water flow in the Eutaw-McShan aquifer and in the Tuscaloosa aquifer system in northeastern Mississippi, U.S. Geological Survey Water-Resources Investigations Report 94-4223. Jackson, Mississippi

Sullivan KJ (1986) Petrography, diagenetic history, and development of porosity in the Richfield Member of the Lower Middle Devonian Lucas Formation, northeast Isabella County, central Michigan Basin. Master's, Department of Geology, Western Michigan University, Kalamazoo

Tarbutton RJ (1979) Petrography of some selected Upper Cretaceous Selma Group sediments in parts of Humphreys, Sharkey, and Yazoo counties, Mississippi. Master's, University of Southern Mississippi, Hattiesburg

Tetra Tech Inc. (2007) Final Risk Assessment Report for the FutureGen Project Environmental Impact Statement, Tetra Tech, Inc. Report Contract No. DE-AT26-06NT42921

Tomastik TE (1997), The Sedimentology of the Bass Islands and Salina Groups in Ohio and its effect on Salt-Solution Mining and Underground Storage, USA Carbonates and Evaporites 12(2):236-253

Tromp DE (1995) Clays as indicators of depositional and diagenetic conditions in Pennsylvanian black shales, Paradox Basin, Utah and Colorado. Master's, Department of Geology, Colorado School of Mines, Golden

Tuttle ML, Klett TR, Richardson M, Breit GN (1996) Geochemistry of two interbeds in the Pennsylvanian Paradox Formation, Utah and Colorado: a record of deposition and diagenesis of repetitive cycles in a marine basin, U.S. Geological Survey bulletin 2000-N. United States Government Printing Office, Washington, D.C.

Van Buchem FSP, Houzay J-P, Peniguel G (2000) Variations in distribution and quality of organic matter in Middle Pennsylvanian source rock levels of the Paradox Basin (Utah, USA). In: Homewood PW, Eberli GP (eds) Genetic stratigraphy on the

exploration and production scales : case studies from the Upper Devonian of Alberta and the Pennsylvanian of the Paradox Basin. Elf EP Editions, pp 131-137

Visocky AP, Sherrill MG, Cartwright K (1985) Geology, hydrology, and water quality of the Cambrian and Ordovician systems in northern Illinois, Illinois State Geological Survey and Illinois State Water Survey Cooperative Groundwater Report 10. Champaign, Illinois

Watkins HH (1985) The petrology and diagenesis of the lower Tuscaloosa, Fayette Field, Jefferson County, Mississippi. Master's, Graduate School, University of Southern Mississippi, Hattiesburg

Watts NL (1987), Theoretical aspects of cap-rock and fault seals for single- and two-phase hydrocarbon columns. Marine and Petroleum Geology 4(11):274-307

White SP, Allis RG, Moore J, T.Chidsey, C.Morgan, Gwynn W, Adams M (2002) Natural CO2 Reservoirs on the Colorado Plateau and Southern Rocky Mountains, USA, A Numerical Model. Paper presented at Proc. Greenhouse Gas Control Technologies 6th Conference, Kyoto, Japan October 2002

White SP, Allis RG, Moore J, T.Chidsey, C.Morgan, Gwynn W, Adams M (2003) Injection of CO2 into an Unconfined Aquifer Located beneath the Colorado, Central Utah, USA. Paper presented at Second Annual Conference on Carbon Sequestration, Alexandria, Virginia, 5-8 May 2003

Wickstrom LH, Venteris ER, Harper JA, McDonald J, Slucher ER, Carter KM, Greb SF, Wells JG, III WBH, Nuttall BC, Riley RA, Drahovzal JA, Rupp JA, Avary KL, Lanham S, Barnes DA, Gupta N, Baranoski MA, Radhakkrishnan P, Solis MP, Baum GR, Powers D, Hohn ME, Parris MP, McCoy K, G.M. G, Pool S, Luckhardt C, Kish P (2005) Characterization of Geologic Sequestration Opportunities in the MRCSP Region Phase I Task Report Period of Performance: October 2003 – September 2005, U.S. Department of Energy DOE Cooperative Agreement No. DE-PS26-05NT42255

Wigley T, Richels R, Edmonds JA (1996), Economic and environmental choices in the stabilization of atmospheric CO2 concentrations. Nature 379:240-243

Willman HB, Atherton E, Buschback TC, Collinson C, Frye JC, Hopkins ME, Lineback JA, Simon JA (1975) Handbook of Illinois Stratigraphy. Illinois State Geological Survey Bulletin 95, Urbana, Illinois, pp 34-46

Witkind IJ, Thaden RE, Malde HE, Johnson DH (1963) Geology and uranium-vanadium deposits of the Monument Valley area, Apache and Navajo counties, Arizona, U.S. Geological Survey Bulletin 1103. United States Government Printing Office, Washington, D.C.

TABLE 2.1: Basins, localities and generalized lithology, depth, thickness, and dominant mineralogy of geological seals considered by the U.S. DOE for saline CO_2 sequestration (in Figure 2.1).

Geologic Structure (state), County	Geological Storage Reservoir			Geological Seal				
	Formation	Depth (m)	Thickness (m)	Formation	Depth (m)	Thickness (m)	Lithology	Dominant minerals
Colorado Plateau (Northern Arizona)	Kaibab Limestone	512[1]	4.6[1]	Chinle-Moenkopi	160[1]	352[1] 30–400[2]	Reddish brown siltstone, course sandstone, swelling claystone, silty limestone[3-6]	Matrix of quartz, feldspar, illite with chlorite for Moenkopi with cements of quartz, calcite, dolomite, hematite; Montmorillonitic clay for Chinle[3, 6]
	Coconino Sandstone	517[1]	169[1] 100–300[2]					
	Cedar Mesa Sandstone	824[1]	401[1] 20–200[2]	Organ-Rock Shale	686[1]	139[1] 30–300[2]	Red, poorly sorted, fine-grained sandstone, siltstone, mudstone, and claystone with upper contact a fine-grained sandstone and lower contact micaceous siltstone[7, 8]	Clays with kaolinite-illite, kaolinite, illite[9]; Cements of calcite and iron oxide[8];Outcrops vary in smectite concentration[7]
	Redwall Limestone	1,398[1]	166[1] 150–300[2]					
1 Coconno County	Tapeats Sandstone	1,978[1]	101[1] 50–80[2]	Muav Limestone/ Bright Angel Shale	1,791[1]	187[1] 100–250[2]	Dolomitic siltstone, glauconitic mudshale, hematitic sandstone, aphanitic limestone[10, 11]	Framework of quartz, glauconite, orthoclase (feldspar), hematite. Cement of silica, hematite, calcite, and dolomite. Matrix negligible. Clays include illite, kaolinite, and chlorite[11]
2 Apache County								

Table 2.1:   Cont'd

Geologic Structure (state), County		Geological Storage Reservoir			Geological Seal				
		Formation	Depth (m)	Thickness (m)	Formation	Depth (m)	Thickness (m)	Lithology	Dominant minerals
Gulf Coast (Mississippi)					Midway Shale Formation	1,463-2,073[12]	244–305[12] (Jackson Co.)	Argillaceous with grey calcareous, and bentonitc shales; with chalk, marl marine clay, siltstones and limestone beds[12-15]	Quartz, calcite, pyrite, montmorillonite, mixed layer illite/smectite[15,16]
						-	305[15] (Adams Co.)		
					Selma Group (Selma Chalk)	1,676–2,377[12]	305[12] (Jackson Co.)	Chalky marl containing thin beds of glauconitic sand and sandstone, sandy clay[13,14]	Framework of conglomerate calcareous fragments of quartz, calcite/ aragonite. Matrix of quartz, glauconite[14].Clays include equal amounts of kaolinite, illite, montmorillonite[16]
						-	107–251[14,17] (Adams Co.)		
3	Jackson County	Lower Tusca-loosa (Massive sand)	2,621[12]	58[12]	Tuscaloosa Marine Shale	2,339 - 2,484[18]	137–145[18]	Fine-grained shales and mud-stones[12]	Mineral composition unknown but similar to "Stringer" sand member of the Massive Sand. Shale composition of quartz, kaolinite, illite, hematite, and siderite[19]. Equivalent to unnamed upper member of Coker formation composed of quartz, calcite, hematite, kaolinite, muscovite, montmorillonite[20]
4	Adams County		3,109[21]	15–27[21,22]		3,005–3124[21]	114[21]		

Table 2.1: Cont'd

Geologic Structure (state), County		Geological Storage Reservoir			Geological Seal				
		Formation	Depth (m)	Thickness (m)	Formation	Depth (m)	Thickness (m)	Lithology	Dominant minerals
Michigan Basin (Michigan)					Lucas Formation	670–897[23]	229-244[23, 24]	Dolomite with interbedded anhydrite and salt, limestone, minor sandstone beds. Richfield member has porous dolomite[24]	Dolomite with cementation of anhydrite[25, 26]. Dolomite, calcium sulfate (anhydrite), halite, calcite [24]
5	Otsego County	Bois Blanc-Sylvania Sandstone[27]; Bass Island Dolomite[23]	853-975[27]; 1,049–1,071[23]	107[27]; 22[23]	Amherstberg group	897–972[23]	76[23]	Dark-brown to black limestone or dolomite with nodules of anhydrite and chert[23, 24].	Calcite, dolomite, anhydrite[24]
Paradox Basin (Utah)		Ismay	1,707-1,768[28]	40–61[28]	Gothic Shale	1,707-1,768[28]	61[29]	Hard black shales with dolomitic claystone with small varying amounts of organic matter[30]	Cements of calcite, dolomite, plagioclase feldspar, siderite, pyrite;clay size quartz, illite-smectite, chlorite, chlorite-smectite, muscovite, illite[30]. Fracture filling anhydrite and halite[29]
6	San Juan County	Desert Creek			Chimney Rock Shale		9–12[29]		

Table 2.1:   Cont'd

Geologic Structure (state), County		Geological Storage Reservoir			Geological Seal				
		Formation	Depth (m)	Thickness (m)	Formation	Depth (m)	Thickness (m)	Lithology	Dominant minerals
Appalachian Basin (Ohio)					Hamilton Group/ Marcellus shale[31,32]	1,617–2,017[33]‡	6–41[33]‡ < 15[34]	Limy black shales interbedded with gray – green shales and siltstone[34, 35]	Illite, chlorite, kaolinite, illite-smectite, illite-chlorite, calcite, quartz[35]
		Oriskany Sandstone	1,805–1,815[32]	10[32]	Onondaga/ Huntersville Chert formation[31,32]	1,701–1,719[33]†	18[33]†	Limestone and chert containing zones of quartz sandstone and siltstone with phosphatic and glauconitic zones at base[34, 36]	Quartz, calcite, dolomite, pyrite, glauconite[33,34,36]
		Middle Saline Carbonate (C-Unit)	2,053–2,148[32]	95[32]	Salina Group/ Tonoloway foramation[32,37]	1,951–2,256[32]	305[32] 213–244[37]	Salina Group relatively continuous with halite, anhydrite/ gypsum, dolomite and gray-green-brown shale units[38, 39]. Grades to Tonoloway in West Virginia with more limestone members[37]	Halite, anhydrite/ gypsum, dolomite, illite/ smectite,and chlorite/ smectite in dolomite and anhydrite[38, 40]
7	Belmont County	Medina Group ("Clinton")	2,501-2,522[32]	21[32]	Lockport Dolomite	2,256–2,377[32]	122[32] 62–144[41]	Argillaceous dolomite, limestone, and shale[42]	Dolomite[42]

Table 2.1: Cont'd

Geologic Structure (state), County		Geological Storage Reservoir			Geological Seal				
		Formation	Depth (m)	Thickness (m)	Formation	Depth (m)	Thickness (m)	Lithology	Dominant minerals
Cincinnati Arch (Kentucky)		Mt. Simon Sandstone	975–1,067[43]	91[43]	Eau Claire	823–975[43]	152[43]; 86–190[44,45]	In the Cincinnati Arch region, it consists of green, grey and red shales with minor finely crystalline dolomite, micaceous and glauconitic siltstones, and thin limestone beds[45, 46]	Quartz, dolomite, calcite, potassium feldspar, albite, anorthite (?), glauconite, other clay minerals (?)[47,48]
8	Boone County								
Illinois Basin (Illinois)					Eau Claire	1,982–1,753[49**]	91–152[50]; 152–213[50,51]	In the Illinois Basin it consists of silty, argillaceous dolomitic sandstone northward, shale eastward, dolomite westward[51-53]. Siltstones, shales interbedded with dolomite. Shale interval is regionally persistent near sites[53]	Quartz, dolomite, potassium feldspar with glauconite and illite main clay minerals in shale subfacies[52, 53]
9	Fayette County	Mt. Simon Sandstone	2,134-2,286[49]	396–533[49,54]	Mt. Simon Shale Interbeds*	2,134-2,286[49]	<152[55]	Beds of red and green micaceous shale[51]	Illite, quartz, and potassium feldspar[53]
10	Coles County								
11	Macon County								

Table 2.1:   Cont'd

‡ Depth and thickness estimated from core sample intervals in Marshal and Wetzel County, West Virginia
† Depth and thickness estimated from core sample intervals in Marshall County, West Virginia
? – Unsure mineral type
*within the top 152 m of Mt. Simon formation
 **Inferred from description in Partnership report

1. (U.S. Department of Energy et al. 2006a) **2.** (Shirley et al. 2006) **3.** (Cadigan and Stewart 1971) **4.** (Repenning et al. 1969) **5.** ((Cadigan 1971) **6.** (Schultz 1963) **7.** (Lewis and Trimble 1959) **8.** (Witkind et al. 1963) **9.** (Rudd 2005) **10.** (McKee 1982) **11.** (Martin 1985) **12.** (U.S. Department of Energy et al. 2006c) **13.** (Cushing et al. 1964) **14.** (Tarbutton 1979) **15.** (Reeves 1991) **16.** (Pryor and Glass 1961) **17.** (Braunstein 1950) **18.** (U.S. Department of Energy et al. 2007c) **19.** (Watkins 1985) **20.** (Bergenback 1964) **21.** (U.S. Department of Energy et al. 2007e) **22.** (Beebe and Curtis 1968) **23.** (U.S. Department of Energy et al. 2008e) **24.** (Landes 1951) **25.** (Park 1987) **26.** (Sullivan 1986) **27.** (U.S. Department of Energy et al. 2006b) **28.** (U.S. Department of Energy et al. 2008b) **29.** (Tuttle et al. 1996) **30.** (Tromp 1995) **31.** (Ryder et al. 2007) **32.** (U.S. Department of Energy et al. 2008c) **33.** (Repetski et al. 2005) **34.** (Milici and Swezey 2006) **35.** (Hosterman and Whitlow 1983) **36.** (Ozol 1963) **37.** (Smosna et al. 1977) **38.** (Oinonen 1965) **39.** (Tomastik 1997) **40.** (Hluchy and Reynolds 1989) **41.** (Farmerie and Coogan 1995) **42.** (Brett et al. 1995) **43.** (U.S. Department of Energy et al. 2008d) **44.**(Rupp et al. 2006) **45.** (Drahovzal et al. 1992) **46.** (Becker et al. 1978) **47.** (Wickstrom et al. 2005) **48.** (Harris et al. 2004) **49.** (U.S. Department of Energy et al. 2006d) **50.** (Tetra Tech 2007) **51.** (Willman et al. 1975) **52.** (KunleDare 2005) **53.** (Finley 2005) **54.** (U.S. Department of Energy et al. 2007d) **55.** (Nicholas et al. 1987)

TABLE 2.2: Mineral data of geological seals considered for saline CO2 sequestration in the Paradox Basin, Gulf Coast, and Illinois Basin.

Characteristic	Paradox Basin	Gulf Coast		Illinois Basin	
	Gothic & Chimney Rock Shale	Tuscaloosa Marine Shale	Selma Group	Mt. Simon Shale Interbeds	Eau Claire
Major Mineral Components (> 20 wt%)					
Quartz	20 – 40%[1,2]	2 – 33%[3] > 20%[4]	-	18 – 24%[5]	10 – 33%[5] > 20%[6]
Carbonates:	20 – 30%[2,7] 15 – 37 %,[8]	-	-	-	-
- Crystalline carbonate cement	-	39 – 45%[3]	8 – 58%[3]	-	-
- Calcite	> 20%[7]	-	-	-	-
- Low-Magnesium calcite	-	-	> 20%[9]	-	-
- Manganese calcite	-	-	> 20%[10]	-	-
- Ferrous calcite	-	-	> 20%[10]	-	-
- Argillaceous calcilluite	-	-	14 – 87%[3]	-	-
- Dolomite	> 20%[7]	-	-	-	3.6 – 26%[5] > 20%[6]
K-feldspar	-	-	-	19 – 20%[5]	20 – 37 %[5]
Na-feldspar/Plagioclase	> 20%[7]	-	-	-	-
Siderite	> 20%[7]	> 20%[4]	-	-	-
Hematite	-	> 20%[4]	-	-	-
Pyrite	> 20%[7]	-	-	-	-
Gypsum	-	-	> 20%[9]	-	-

Table 2.2:   Cont'd

Characteristic	Paradox Basin	Gulf Coast		Illinois Basin	
	Gothic & Chimney Rock Shale	Tuscaloosa Marine Shale	Selma Group	Mt. Simon Shale Interbeds	Eau Claire
Major Mineral Components (> 20 wt%)					
Clays:	~ 33 wt%[7]	1 – 68%[3]	-	-	-
- Kaolinite	-	19 – 100%[12] (av:57%,n:12)[12,b] > 20%[4]	1 – 96%[12] (av:37%,n:111)[12,b]	-	-
- Illite	> 20%[7]	0 – 81%[12] (av:34%,n:12)[12,b] > 20%[4]	1 – 85%[12] (av:23%,n:111)[12,b]	36 – 41%[5] 82 – 83%[5,a]	5.5 – 51%[5] 57 – 91%[5,a] > 20%[6]
- Illite/smectite	> 20%[7]	-	-	-	-
- Glauconite	-	-	8 – 28%[3]	-	> 20%[6]
- Montmorillonite	-	0 – 28%[12] (av:9%,n:12)[12,b]	0 – 92% (av:40%,n:111)[12,b]	-	-
- Muscovite	-	1 – 22%[3]	-	-	-
- Chlorite	> 20%[7]	-	-	-	0.5 – 3.4%[5] 6.4 – 39%[5,a]
- Chorite/smectite	> 20%[7]	-	-	-	-
Minor Mineral Components (< 20 wt%)					
Quartz	-	-	1 – 9%[3]	-	-
Feldspar	-	1 – 8%[3]	< 20%[9]	-	-
K-feldspar	< 20 wt%[7,13]	-	-	-	< 20%[6]
Na-feldspar/Plagioclase	< 20 wt%[7,13]	-	-	1.2 – 2.5%[5]	0.8 – 3.3%[5]
Calcite	-	-	-	0.7 – 2.4%[5]	0.7 – 2.0%[5]
Dolomite	-	-	-	1.2 – 3.4%[5]	-
Halite	< 20 wt%[7,13,c]	-	-	-	-
Sylvite	< 20 wt%[7,c]	-	-	-	-
Sinjarite	< 20 wt%[7,c]	-	-	-	-
Tachyhydrite	< 20 wt%[7,c]	-	-	-	-
Anhydrite	< 20 wt%[13,c]	-	-	-	-
Gypsum	< 20 wt%[13]	-	-	-	-
Apatite (fluorapatite)	< 20 wt%[13]	-	-	-	-
Hornblende	-	-	-	0.4 – 0.5%[5]	0.2 – 0.4%[5]

Table 2.2:   Cont'd

Characteristic	Geological seal formations				
	Paradox Basin	**Gulf Coast**		**Illinois Basin**	
	Gothic & Chimney Rock Shale	Tuscaloosa Marine Shale	Selma Group	Mt. Simon Shale Interbeds	Eau Claire
Minor Mineral Components (< 20 wt%)					
Pyrite	< 20 wt%[7,13,c]	-	-	0.1 – 0.5%[5]	0 – 1.7%[5]
Marcasite	-	-		0.1 – 0.5%[5]	0.6 – 3.2%[5]
Mixed lattice clay	-	-	< 20%[12]	-	-
Expandable clays	-	-		1 – 1.4%[5] 1.1 – 1.6%[5,a]	0.3 – 3.2%[5] 1.1 – 2.6%[5,a]
Kaolinite	-	-	< 20%[9]	5 – 7.4%[5] 10%[5,a]	0.3 – 1.5%[5] 1.5 – 3%[5,a] < 20%[6]
Chlorite	-	1 – 10%[3] < 20%[4]	< 20%[12]	2 – 4.1%[5] 5.2 – 6.6%[5,a]	< 20%[6]
Glauconite	-	1 – 15%[3]	-	-	-
Organic Content					
Oil (%vol)	-	0.7 – 4.3[14]	-	-	-
Total Organic Carbon (TOC)	0.5 - 11%[2] 0.5 – 13%[1]	0.2 – 1.1%[15]	1.2 – 1.8%[16]	-	-
Total Inorganic Carbon (TIC)	-	0.1 – 3.2%[15]	-	-	-

[a]Amounts present in clay size fraction
[b]Average of several formations comprising the outcrop equivalent of the Tuscaloosa Marine Shale and Selma Group in Mississippi, Tennessee, Kentucky, Illinois, Missouri, and Arkansas
[c]Also vein and fracture filling minerals
av – average of dataset
n – number of samples analyzed
"-" Data not available

1. (Raup and Hite 1992) **2.** (Nuccio and Condon 1996) **3.** (Bergenback 1964) **4.** (Watkins 1985) **5.** (Finley 2005) **6.** (KunleDare 2005) **7.** (Tromp 1995) **8.** (Hite and Lohman 1973) **9.** (Freed 1980) **10.** (Czerniakowski et al. 1984) **11.** (Scholle 1977) **12.** (Pryor and Glass 1961) **13.** (Tuttle et al. 1996) **14.** (John et al. 1997) **15.** (Miranda and Walters 1992) **16.** (Bingham and Savrda 2006)

TABLE 2.3: Physical data of geological seals considered for saline CO2 sequestration in the Paradox Basin, Gulf Coast, and Illinois Basin with statistical data given when available

Characteristic	Geological seal formations				
	Paradox Basin	**Gulf Coast**		**Illinois Basin**	
	Gothic & Chimney Rock Shale	Tuscaloosa Marine Shale	Selma Group	Mt. Simon Shale Interbeds	Eau Claire
Depth (m)	1,707 – 1,768[1]	2,339 – 2,484[3,a] ; 3,005 – 3124[4b]	1,676 – 2,377[5]	2,134 – 2,286[6,7]	1,982 –1,753[6,7,e]
Thickness (m)	61[1]; 9 – 12[8]	137 – 145[3,a]; 114[3,b]; 152 – 244[4,c]	305[5] ; 107 – 251[9,10]	< 152[11]	91 – 152[12] ; 152 – 213[12,13]
Porosity (%)	10[14]; 1.6 – 4.1[15]	2.3 – 8.0[4]	9 – 45[16] ; 31 – 41[17]	-	0.4 – 15[18] (av:7.7±2.9, n:119)[18]
Vertical permeability, $-\ln[k_v]$ (m^2)	39.16 – 36.86[14,f]	42.51 – 40.21[19,g]	42.62 – 40.21 [20,f,g]	41.00[21,h]	41.00[21,h] ; 41.46 – 35.28[18] (av:39.8±1.94,n:37)[18]
Horizontal permeability, $-\ln[k_h]$ (m^2)	39.16 – 36.86[14,f] ; 44.32 – 44.12[15] (av:44.21±0.09, n:4)[15]	39.16 – 37.37[4] (av: -, n:110)[4] ; 28.00 – 23.69[22,g] (av:25.24±1.08, n:33)[22,g]	<37.55 – 32.50[16] ; 36.59 – 34.66[17] ; 26.40 – 24.40[27,g] ; 29.05 – 25.40[22,g] (av:26.87±1.28,n:7)[22,g]	28.32[11,h]	28.17[11,h] ; 28.92 – 25.26[23,h,i] (av:27.16±0.84,n:46)[23,h,i]
Compressive strength, σ (MPa)[d]	166 – 311[15] (av:246.58±54.74,n:7)[15]	-		-	
Poission's Ratio, v[d]	0.24 – 0.33[15] (av:0.27±0.04,n:7)[15]	-		-	
Young's Modulus, E (MPa)[d]	38,562 – 56,613[15] (av:47,315±6,447,n:7)[15]	-		-	
Basin areal extent (km^2)	28,490[24]	15,281 – 119,139[4,25]		155,000[26]	

Table 2.3: Cont'd

av average of dataset, *n* number of samples analyzed, - Data not available
[a]Jackson County, Mississippi
[b]Adams County, Mississippi
[c]Pike County, Mississippi to Washington Parrish, Louisiana
[d]Static mechanical properties determined on 7 sample cores under 24.31 −24.97 MPa effective confining pressure, cores from depths of 1,791 − 1,840 m
[e]Inferred from description in Partnership report
[f]Modeled values for groundwater transport simulation
[g] Permeability calculated with water kinematic viscosity, 1.0×10^{-6} m^2/s (T = 22 °C, P =0.1 MPa)
[h] Permeability calculated with water kinematic viscosity, 1.1×10^{-6} m^2/s, from test well (T = 16.8 °C, P = 5.8 MPa)
[i] Estimated from Eau Claire transmissivity data using Eau Claire isopach data of Willman et al. (1975)

1. (U.S. Department of Energy et al. 2008b) **2.** (U.S. Department of Energy et al. 2007c) **3.** (U.S. Department of Energy et al. 2007e) **4.** (John et al. 1997) **5.** (U.S. Department of Energy et al. 2006c) **6.** (U.S. Department of Energy et al. 2006d) **7.** (U.S. Department of Energy et al. 2007d) **8.** (Tuttle et al. 1996) **9.** (Tarbutton 1979) **10.** (Braunstein 1950) **11.** (Nicholas et al. 1987) **12.** (Tetra Tech 2007) **13.** (Willman et al. 1975) **14.** (White et al. 2002) **15.** (Bereskin and McLennan 2008) **16.** (Scholle 1977) **17.** (Holston et al. 1989) **18.** (KunleDare 2005) **19.** (Planert and Sparkes 1985) **20.** (Brahana and Mesko 1988) **21.** Schicht et al. (1976) **22.** (Slack and Darden 1991) **23.** Visocky et al. (1985) **24.** (Raup and Hite 1996) **25.** (U.S. Department of Energy et al. 2007b) **26.** (McBride and Nelson 1999) **27**. Boswell et al. (1965)
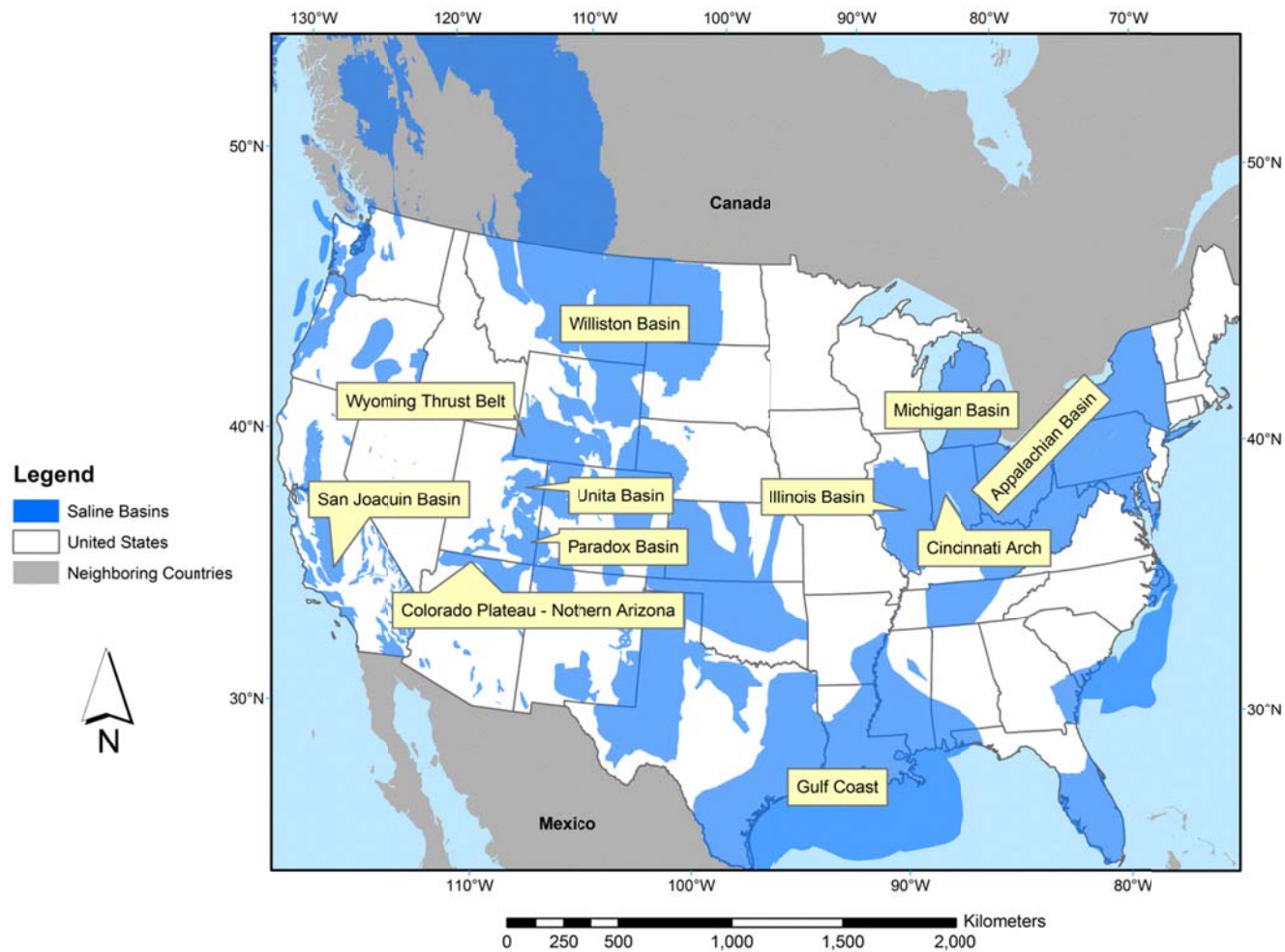
FIGURE 2.1: Map showing some of the saline basins explored for CO_2 sequestration in the U.S. and Canada, with highlighted geological basins and tectonic structures explored in this study.
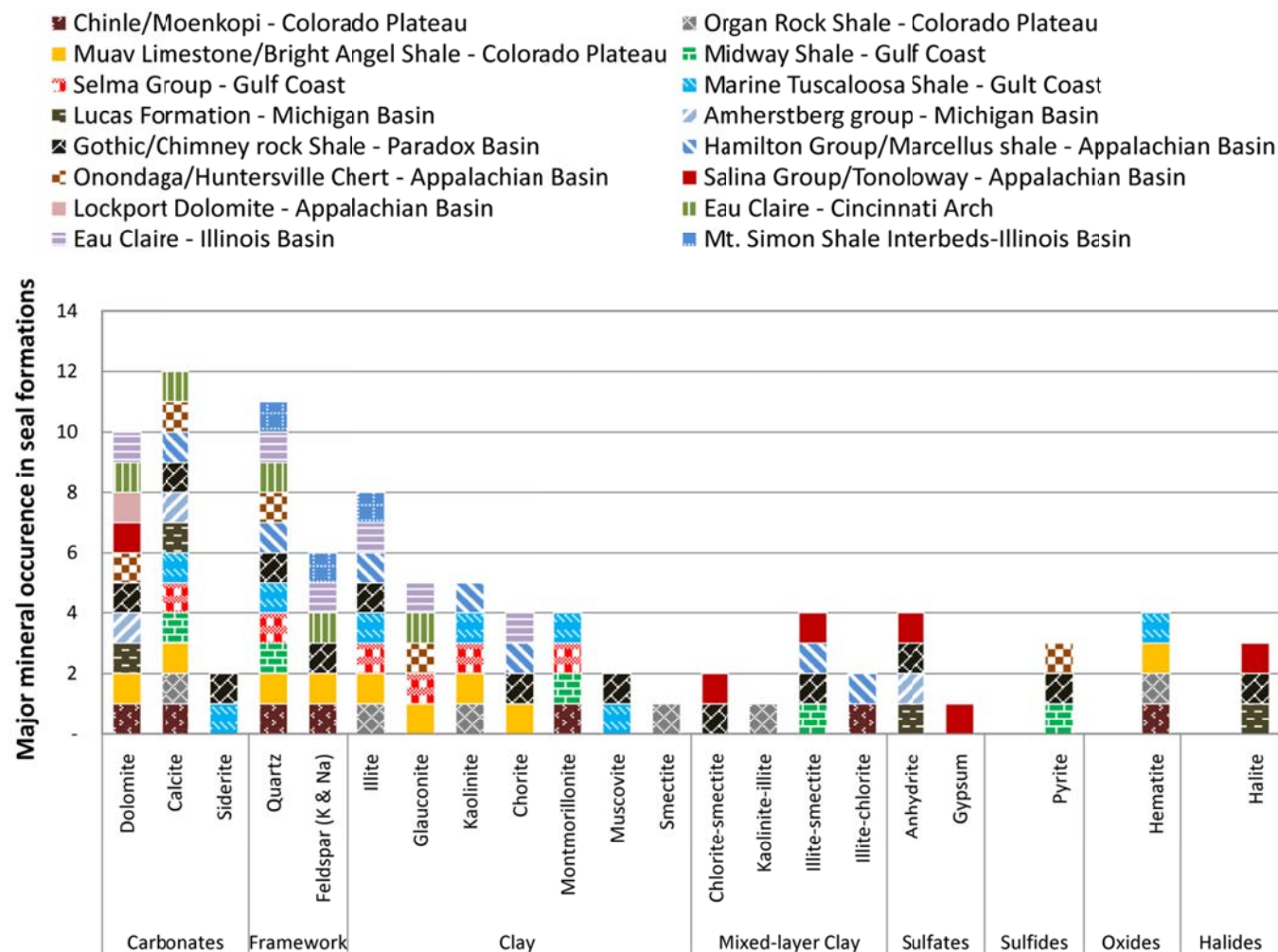
FIGURE 2.2: Frequency of predominant minerals reported among candidate geological seals for saline CO$_2$ sequestration in the U.S.
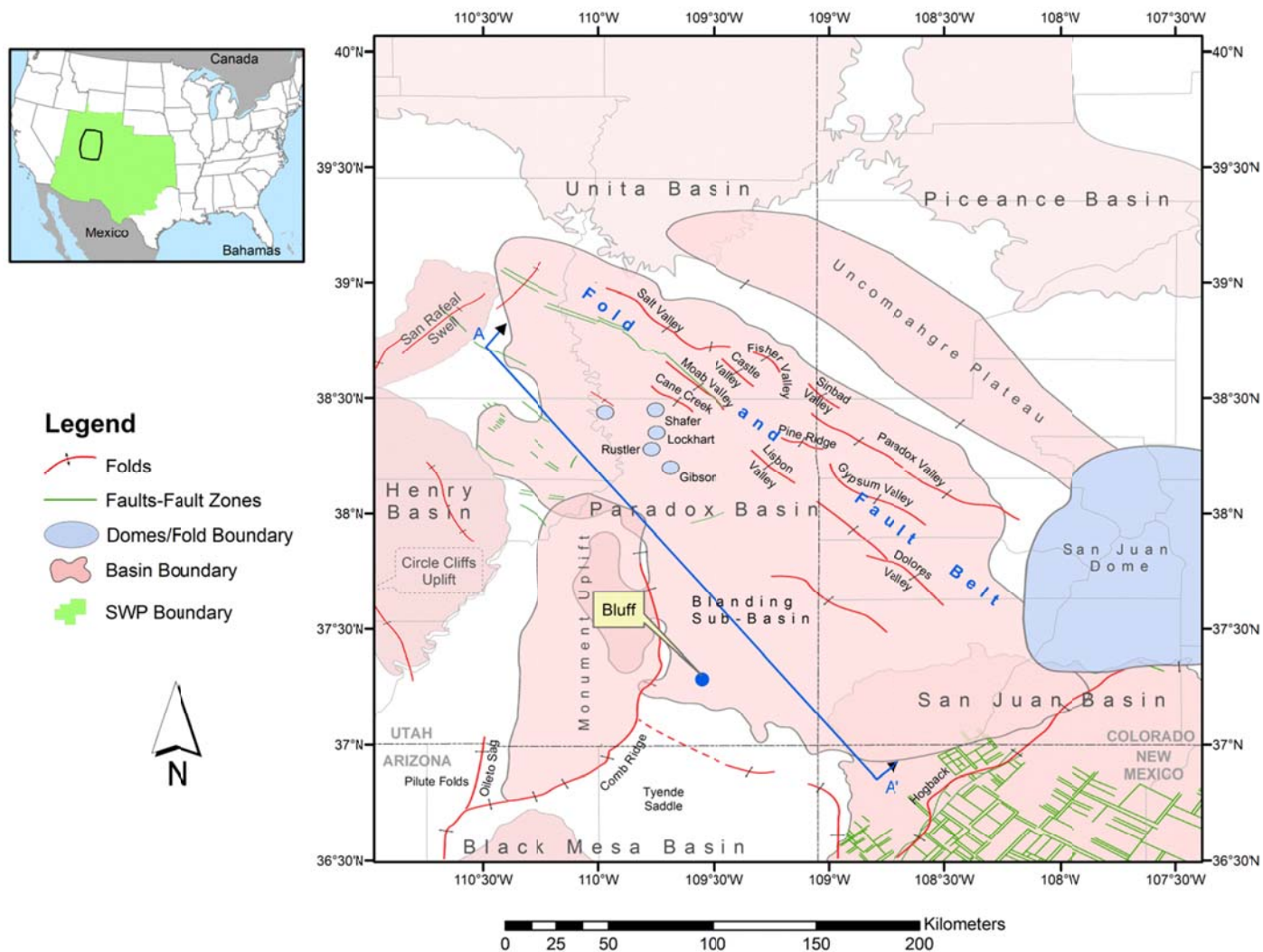
Figure 2.3: Plan view map showing the major folds and faults in and around the Paradox Basin with the demonstration site location called out. Modified from Nuccio and Condon (1996) with additions from Freeman et al. (2008); Huffman and Condon (1993); Johnson (1959); Johnson and Nuccio (1993).
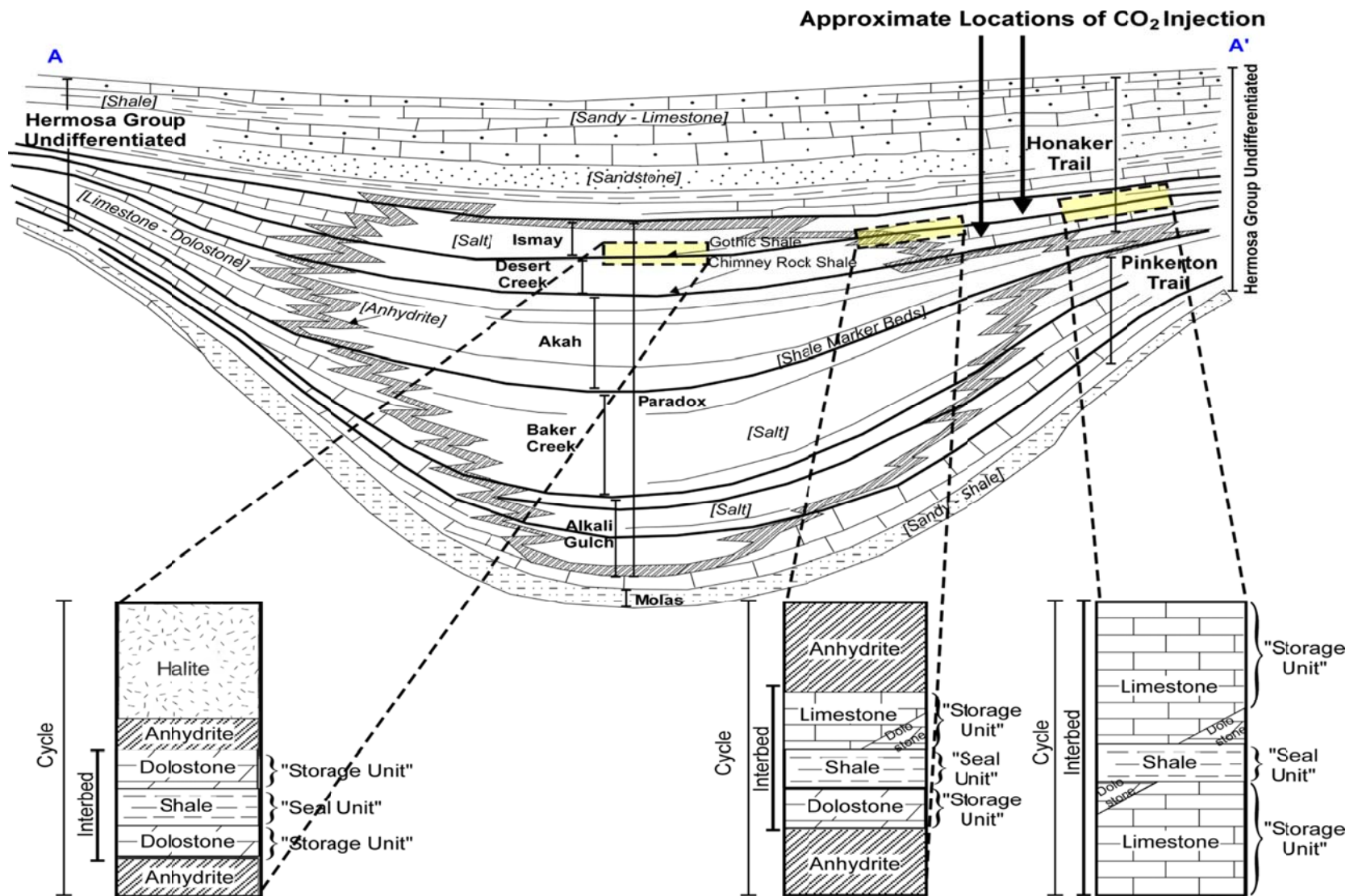
FIGURE 2.4: Cross section (AA') of Figure 2.3 depicting the lithofacies of the Pennsylvanian age sediments throughout the Paradox Basin in relation to CO_2 injection. Modified after Huntoon (1988) and Tuttle et al. (1996).
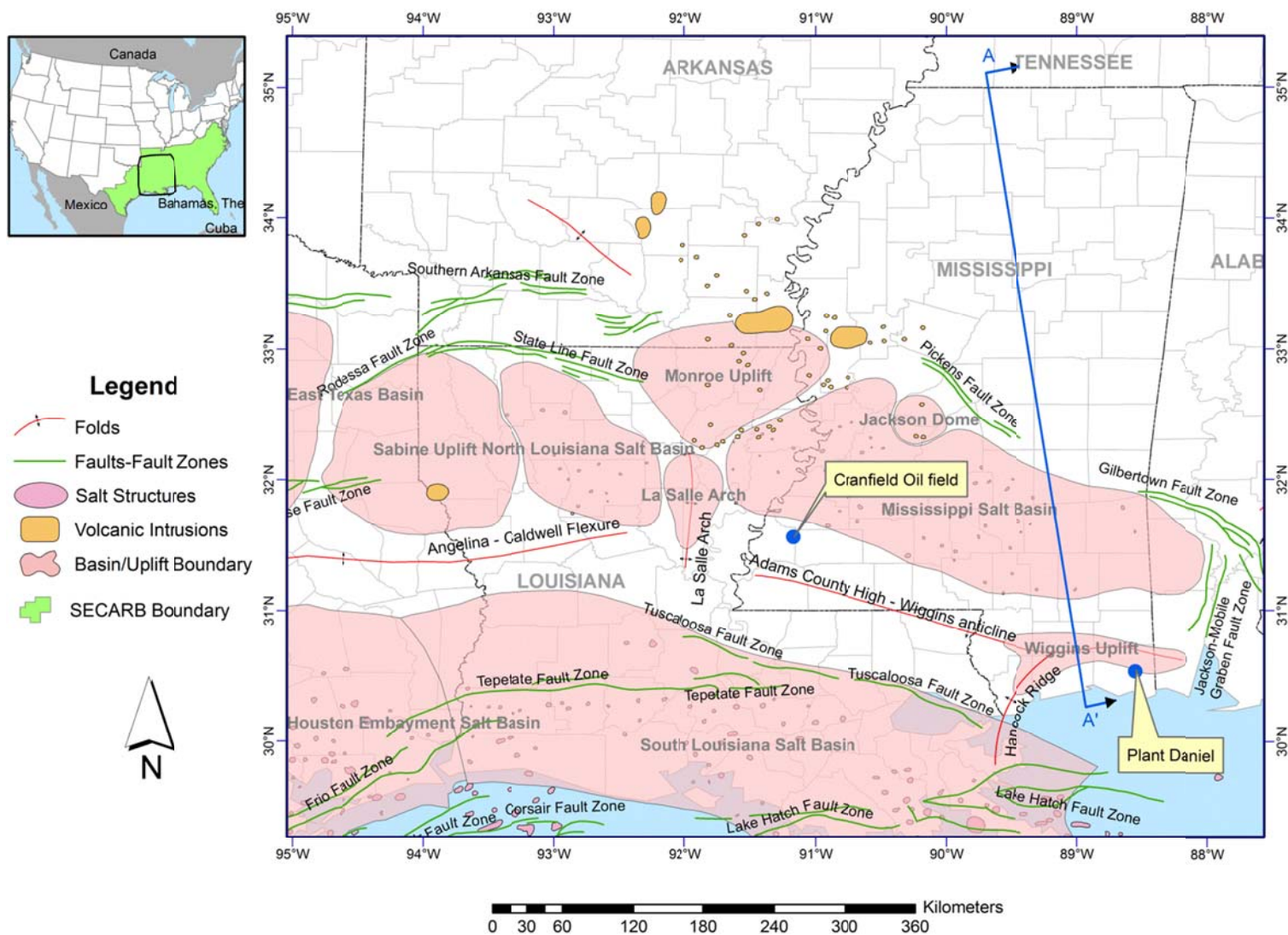
FIGURE 2.5: Plan view map showing the major folds and faults within the Northern Gulf Coast Province, with potential saline CO_2 sequestration demonstration sites called out.
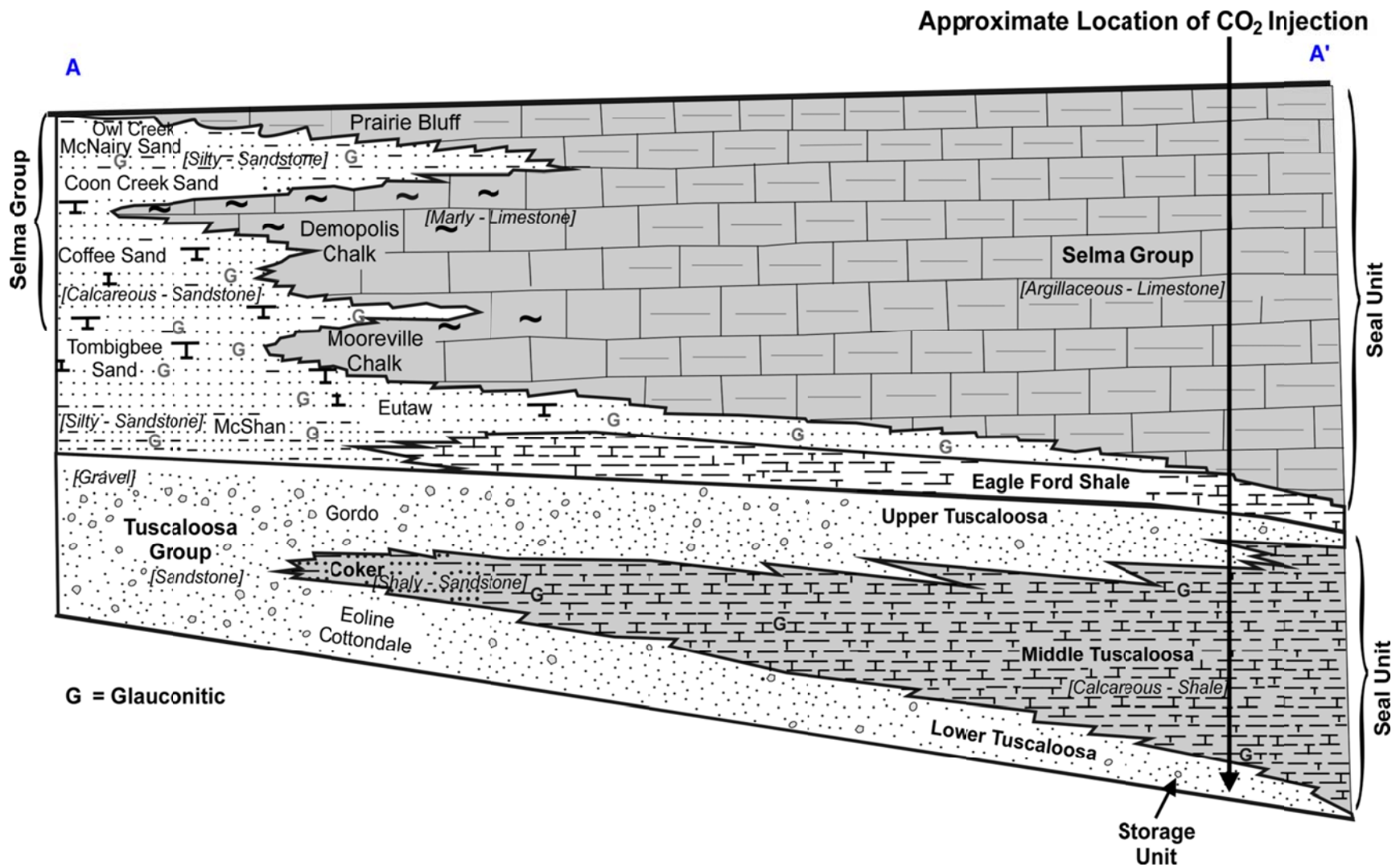
FIGURE 2.6: Cross section (AA') of Figure 2.5 depicting the lithofacies of the Upper Cretaceous, Gulfian sediments throughout the eastern region of Northern Gulf Coast province in relation to CO_2 injection. Modified from Murray (1961) and Tarbutton (1979).
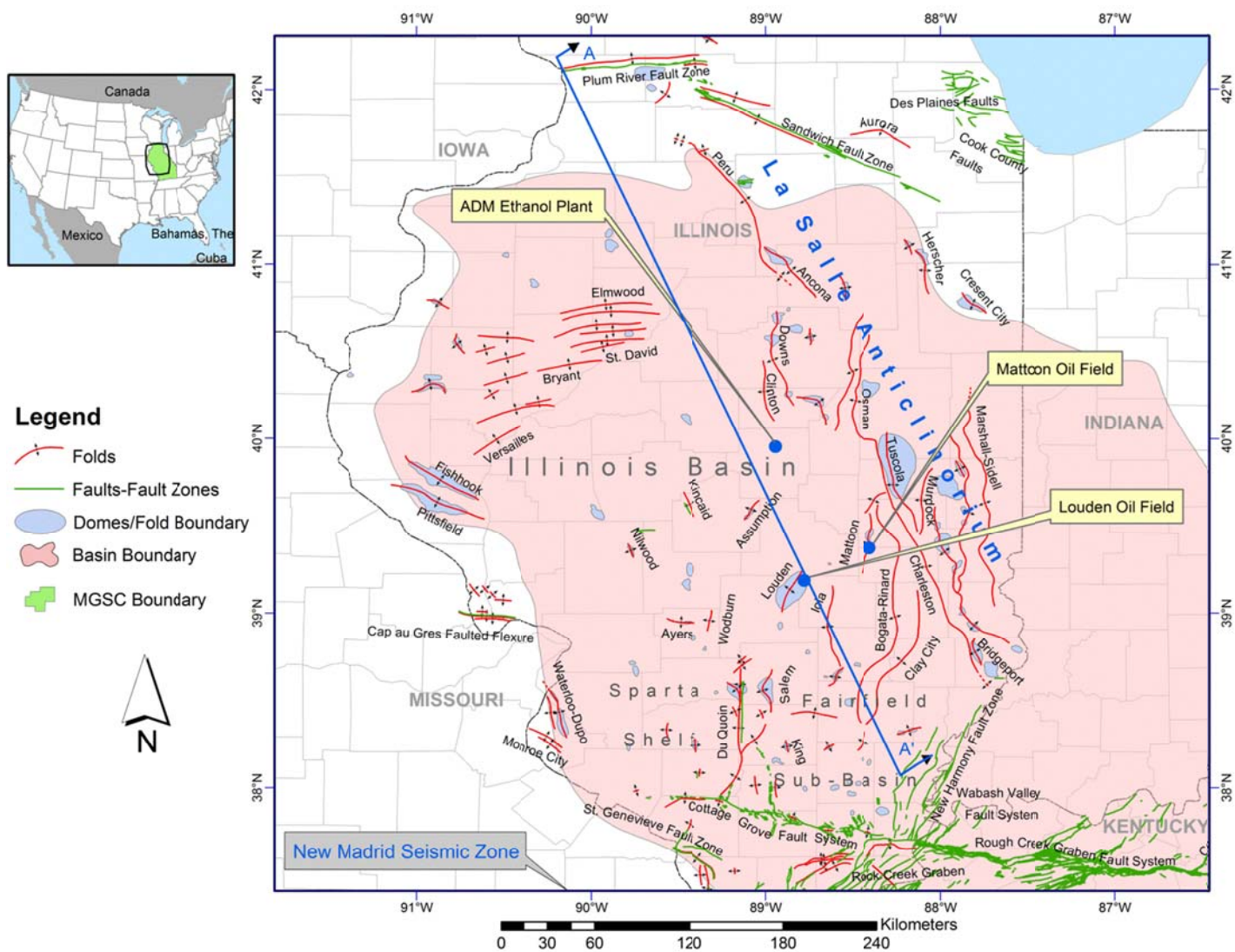
FIGURE 2.7: Plan view map showing the major folds and faults within the Illinois Basin, with potential saline CO_2 sequestration demonstration sites called out.
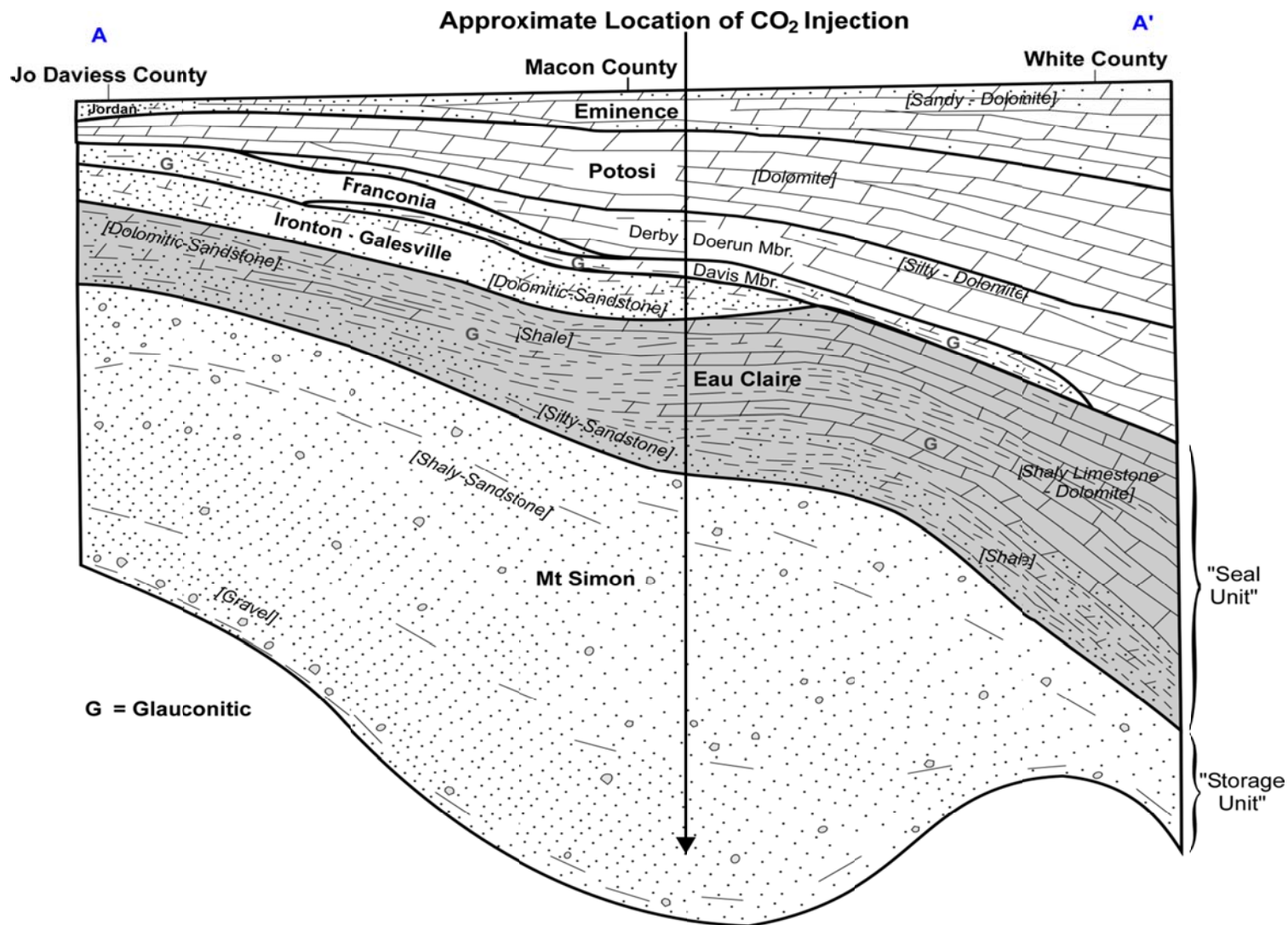
FIGURE 2.8: Cross section (AA') of Figure 2.7 depicting the lithofacies of the Cambrian age sediments throughout Illinois in relation to CO_2 injection. Modified from Willman et al. (1975).

CHAPTER 3

AN INTEGRATED ANALYTICAL MODEL FOR ESTIMATING FRACTURE HYDRAULIC PROPERTIES OF CAPROCKS RELIED UPON FOR LONG-TERM CO$_2$ STORAGE[2]

ABSTRACT

Proposed performance goals for geological storage of CO$_2$ have included either surface leakage rates of 0.01 – 0.1% of CO$_2$ inventory per year or achieving 99% storage permanence within storage reservoirs. Permanence of injected CO$_2$ is primarily dependent on the hydraulic conductivity of the overlying caprock, which can be influenced by a pre-existing fracture network. The goal of this study was to evaluate the influence of fracture hydraulic properties on the performance of caprocks with respect to CO$_2$ leakage criteria, and in particular to assess under what kinds of conditions, if any, that microfractures may be of concern. An integrated analytical transport model was constructed to examine the influence of caprock fracture properties (e.g. fracture aperture, fracture density) and connectivity on effective CO$_2$ transport through an idealized reservoir – caprock system. Effective fracture hydraulic properties examined included fracture aperture (e), fracture density (N/L), fracture porosity (ϕ_f), and fracture permeability (k_f). The modeling results suggest that (1) microfractures (e.g. 10^{-7} to 10^{-6} m range) could yield CO$_2$ loss rates of concern under certain conditions; (2) fracture permeability was the key parameter governing CO$_2$ loss and apart from fracture density, its constitutive parameters could only vary within a limited range; (3) suitable fracture permeability lied in the nano- to micro-

---

Darcy (μD) range (i.e. $10^{-21} - 10^{-17}$ m^2) which is indistinguishable from caprock matrix permeability; (4) fracture porosities were low ($\leq$ 0.02 %) with only a narrow range of observed values meeting the target for 99% CO_2 storage permanence; (5) apart from fracture permeability, no other single fracture parameter (e.g. fracture porosity, aperture, density) uniquely predicted CO_2 transport in caprock. The observations noted in this study highlighted the range and uncertainty of variables governing fracture flow in a CO_2 constrained environment. The conservative approach taken in this modeling study could provide first-order estimates for hydraulic properties within fractured caprocks that are suitable for CCS.

3.1   INTRODUCTION

Geological storage of CO_2 has emerged as a leading option for large-scale sequestration of CO_2, owing to its relatively high potential for storage capacity and extensive operational experience in the oil and gas industry (Pacala and Socolow, 2004). Proposed performance goals for Carbon Capture and Storage (CCS) projects have included achieving 99% storage permanence in storage reservoirs or a maximum CO_2 surface leakage rate of 0.01 – 0.1% of CO_2 inventory per year (NETL 2011, Hepple and Benson 2005). Recent reviews of caprocks used for CO_2 storage revealed that important factors in meeting these goals are the structural and transport properties of the overlying caprock formations, where transmissive pre-existing fractures or reactivated faults are considered fast paths for fluid flow and CO_2 loss (Berkowitz 2002; Shukla et al. 2010; Tsang et al. 2008). In addition, some caprocks used at geological sequestration demonstration sites can exhibit significant lithological and physical variability, with faults and fractures occurring commonly within the regions (Griffith et al. 2011).

Fractures are structural joints, shear bands, or faults that begin at a given point in a formation and propagate into the rock mass (Nelson 2003). They can be systematic,

occurring in sets of parallel fractures, or randomly distributed. Fracture systems that inter-connect can form a fracture network. Quantitative evaluation of the hydraulic behavior of a fracture network within a formation requires the determination of three main fracture system characteristics: 1) fracture spacing or density, 2) fracture plane morphology and width, and 3) fracture and matrix connectivity or interaction (Nelson 2003; Van Golf-Racht 1982; Lemonnier and Bourbiaux 2010a,b). Consideration of these fracture characteristics is important in the evaluation and prediction of CO_2 storage performance at geological sequestration sites with fractured caprock.

3.1.1 PREVIOUS STUDIES

Previous studies that have examined the influence of a caprock fracture network on CO_2 storage consider the probability of a CO_2 plume encountering an intersecting conductive fault (Zhang et al. 2010; Jordan et al. 2008) or assess if sufficient connectivity or channeling exists within the caprock to impact CO_2 leakage (Smith et al. 2011; Grimstad et al. 2009). In fracture networks, the fluid path is a small portion of the total fracture network where fracture connectivity is an important geometric parameter because it links the global physical properties (e.g. fracture permeability) to an average measure of the network geometric properties (Bour and Davy 1997; de Dreuzy 2001). What is useful for evaluation and prediction of CO_2 storage is that patterns of faults and fracture systems can appear qualitatively similar at different scales of investigation, whereby fractures at the surface can provide analogues of subsurface flow in lieu of limited in – situ data on the fracture system within the subsurface formation (Odling et al. 1999; Odling 1997).

Other numerical and semi-analytical studies that have modeled transport of CO_2 through a storage reservoir and a continuous fracture in the overlying caprock have noticed several features. (1) CO_2 loss may be a self-enhancing process, where the pressure associated with injection can accelerate the flowrate of CO_2 across the fracture as it escapes

(Pruess and Garcia 2002; Rutqvist and Tsang 2002). (2) As fluid pressure within the reservoir penetrates the fracture, the relative permeability of CO_2 fluid flow increases as the entire fracture becomes saturated with CO_2 (Rutqvist and Tsang 2002). (3) Principal features of CO_2 transport in the reservoir and through a fractured caprock can be described by steady-state, rather than fully time-dependent, calculations under idealized conditions (Pritchard 2007; Neufeld et al. 2009). (4) CO_2 storage efficiency of a reservoir with a fractured caprock can decay with time (Neufeld et al. 2011; Vella et al. 2011), and be significantly influenced by small, pre-existing cracks in the caprock (Saripalli and McGrail 2002).

3.1.2 INVERSE MODELING FOR PERFORMANCE ASSESSMENT

Modeling fracture permeability, and its associated fracture geometry, to meet expected performance requires inverse modeling. Inverse modeling is commonly carried out in hydrological studies and refers to the process of gathering info about the model from measurements of what is being modeled (Carrera 2005). Inverse modeling is often incorporated into to risk assessment studies with the goal of characterizing the hydraulic properties of the aquifer (or reservoir) that predict contaminant transport and the uncertainty associated with parameter estimation, all conditioned on available data (Carrera 2005; Zimmerman et al. 1998).

Modeling of this type requires model identification and parameter estimation. Typically, it involves optimizing an objective function that incorporates parameter correlations and conditioning of sample data (Zimmerman et al. 1998). Describing the results of inverse modeling is often skewed by the presence of non-uniqueness and ill-posedness (Zimmerman et al. 1998). Errors in the conceptual model or the constraints placed on the parameters can lead to non-unique solutions. However, a properly designed

67

parameterization should transform the original ill-posed problem into a well-posed problem with a unique solution (Zimmerman et al. 1998).

For this study, model identification was not performed and point estimates for hydraulic parameters were not sought for investigate caprock efficacy for CCS. Rather, an analytical model was developed to identify the parameter space of hydraulic properties within a fracture network of overlying caprock used for long-term CO_2 storage, where field and laboratory data were used to condition the parameter space.

The goal of this study was to evaluate the influence of fracture hydraulic properties on the performance of caprocks with respect to CO_2 leakage, and in particular to assess under what conditions, if any, that microfractures may be of concern. This study drew upon the approaches of Saripalli and McGrail (2002), Zhang et al. (2010), and Viswanathan et al. (2008) to construct an integrated analytical transport model to examine the impact of observed fracture geometry on the effective hydraulic properties needed to meet performance criteria for long-term CO_2 storage. Specifically, we determined the limits of the fracture aperture and density on fracture permeability and porosity within the caprock fracture network that would be consistent with performance goals for CO_2 storage. The caprock fracture permeability and fracture porosity ranges identified were then compared to those measured in field studies. A benchmark geological environment for studying CO_2 storage (Class et al. 2009; Ebigo et al. 2007) was used as the basis for developing the analytical model to evaluate the effects of fracture aperture, density, and connectivity within the fractured caprock on supercritical CO_2 transport.

3.2   MODEL DEVELOPMENT

Figure 3.1 depicts the physical scenario for the integrated model framework used to evaluate effects of caprock fracture properties. The model is based on an idealized reservoir – caprock system of Class et al. (2009) where supercritical CO_2 (scCO_2) is continuously

injected into a homogeneous saline reservoir and radially expands over time under a fractured caprock with variable fracture network properties. In the reservoir, $scCO_2$ displaces the brine uniformly and is transported across the caprock through a set of smooth and parallel vertical fractures that are uniformly distributed and continuous throughout the entire caprock. In this study, the $scCO_2$ was assumed to fully saturate the fractures of a constant aperture size with no capillary effects over the timeframe for estimating $scCO_2$ loss from the system. This assumption therefore neglects the complexity of the transient behavior of $scCO_2$ transport through the caprock fractures and the time required to fill the fracture space prior to the onset of leakage. However, the void space of the fractures is relatively small, compared to the caprock's matrix porosity and its fluid flow can be approximated with steady – state solutions (Pritchard 2007, Van Golf-Racht 1982). This study, provides conservative bounds for the fracture properties that would govern leakage after $scCO_2$ saturates the caprock fracture – a worst case scenario (e.g. Rutqvist and Tsang 2002) – and it provides a means to compare those bounds with properties observed in caprock found in nature. Also, acceptable fracture hydraulic properties were examined in light of fracture geometries that satisfied the system size required for a 'percolating' fracture network. This is further discussed in Section 3.2.4.

Values of the fracture aperture, porosity, and permeability of the caprock fracture network consistent with acceptable amounts of $scCO_2$ loss from the reservoir were determined by constraining fracture to a fixed range and $scCO_2$ loss in the system to 10% or 1%.

A continuum transport modeling approach was used in which $scCO_2$ flow was calculated through vertical fractures within the caprock, and not through the primary porosity of the rock matrix. Vertical fracture flow was modeled with the assumption of parallel plate geometry for uniformly distributed fractures using a "cubic law" equivalent Darcy flow equation (de Marsily 1986):

$$Q_f = \frac{k_f A}{\mu_c} \nabla p \qquad (3.1)$$

where Q_f (m³ s⁻¹) is the steady – state Darcy flow of scCO$_2$ in the fractures; A (m²) the plan–view area of the scCO$_2$ plume in the reservoir in contact with the caprock; k_f (m²) the intrinsic fracture permeability of the caprock in contact with the scCO$_2$ plume; μ_c (kg m⁻¹ s⁻¹) the viscosity of scCO$_2$ in fractures; and ∇p (Pa/m) the vertical pressure gradient driving scCO$_2$ across the caprock.

The plan-view area (A) of the scCO$_2$ plume in the reservoir in equation 3.1 was determined with a reservoir model, presented later, that predicts the maximum radial extent of an ideal scCO$_2$ plume in the reservoir, r_{max}, as a function of injection time.

$$A = \pi r_{max}^2 (t) \qquad (3.2)$$

The vertical pressure gradient in equation 3.1 can be represented by

$$\nabla p = \left(\frac{\overline{p_1}(r) - p_2}{b_{cap}} - \rho_c g \right) \qquad (3.3)$$

where $\overline{p_1}(r)$ (Pa) is the volume-averaged reservoir pressure that coincides with the scCO$_2$ plume radial extent over time; p_2 (Pa) the hydrostatic pressure above caprock; b_{cap} (m) the thickness of caprock; ρ_c (kg m⁻³) the density of scCO$_2$; and g (m s⁻²) the gravitational acceleration constant. Calculation of the average reservoir pressure is discussed in more detail later.

The intrinsic fracture permeability in equation 3.1 is a combination of two hydraulic fracture properties: the fracture porosity, ϕ_f (dimensionless), and fracture aperture, e (m).

$$k_f = \frac{\phi_f e^2}{12} \qquad \qquad (3.4)$$

The fracture porosity is also a function of e and the fracture density N/L (m^{-1}), which is the number of fractures per cross-sectional length of exposed caprock (see Fig.1).

$$\phi_f = \frac{N}{L} e \qquad \qquad (3.5)$$

Given that a continuum modeling approach is employed, where the transport properties are treated as averages within the representative elementary volume for the system, the fracture properties used in the model framework should be considered as 'effective' properties for scCO$_2$ transport.

3.2.1 RESERVOIR SCCO$_2$ PLUME MODEL

A volumetric fluid displacement model was chosen to simulate the maximum radial extent of CO$_2$ migration over time. The model is based on the semi-analytical approach of Nordbotten et al. (2005) and accounts for the presence of brine, scCO$_2$,and residual water saturation in the reservoir (Okwen et al. 2010).

$$r_{max} = \sqrt{\frac{MQ_{in}t}{\pi b_{res}\phi_m(1-s_{wr})}} \qquad \qquad (3.6)$$

r_{max} (m) is the effective maximum radius of the reservoir needed to hold the amount of scCO$_2$ injected over time, Q_{in} (m^{3}s^{-1}) the volumetric flow rate of injected scCO$_2$; M (dimensionless) the fluid mobility ratio; t (s) the maximum time for scCO$_2$ injection; b_{res} (m) the reservoir thickness; ϕ_m (dimensionless) the reservoir matrix porosity; and s_{wr} (dimensionless) the residual brine saturation.

The volumetric injection rate is determined from the specified constant mass injection rate ($\dot{m}_{in}$) of CO_2 (kg s^{-1}) and the scCO$_2$ density, ρ_c (kg m^{-3}), at a specified reservoir temperature and pressure.

$$Q_{in} = \frac{\dot{m}_{in}}{\rho_c} \qquad (3.7)$$

The fluid mobility ratio is defined as the ratio of the relative fluid mobility of invading fluid (CO$_2$) to the *relative* fluid mobility of the displaced fluid (brine) in reservoir:

$$M = \frac{\lambda_{rc}}{\lambda_{rw}} \qquad (3.8)$$

where $\lambda_{r\alpha}$ (m s kg^{-1}) is the individual relative fluid mobility of brine or scCO$_2$ with fluid phases c and w representing scCO$_2$ and brine, respectively. The individual fluid mobilities are defined as:

$$\lambda_{r,\alpha} = \frac{k_{r\alpha}}{\mu_\alpha} \qquad (3.9)$$

with $k_{r\alpha}$ (dimensionless) as the relative permeability of each fluid phase, and μ_α the individual fluid phase viscosity.

Equation 3.6 is valid only when the flow of scCO$_2$ in the reservoir is dominated by the injection rate rather than by buoyancy forces, which is brought about by the density differences between the scCO$_2$ and brine (Nordbotten et al. 2005; Okwen et al. 2010). A dimensionless gravity factor, Γ, is used to weight the relative importance of gravity to viscous and pressure forces (Nordbotten et al. 2005):

$$\Gamma = \frac{2\pi\Delta\rho g \lambda_w k b_{res}^2}{Q_{in}} \qquad (3.10)$$

where $\Delta\rho$ is the density difference between the scCO$_2$ and brine and k is the intrinsic permeability of the storage reservoir. Equation 3.6 is constrained to values that yield $\Gamma <$ 0.5, where the analytical solution is valid.

3.2.2 PRESSURE DISTRIBUTION

The vertical pressure gradient (equation 3.1) driving scCO$_2$ transport across the fractured caprock is assumed to be uniform across the entire caprock thickness. The pressure gradient assumes normal hydrostatic pressure at the top of the caprock and an average reservoir pressure at the bottom. In the conceptual model used for this study, the storage reservoir is assumed to be infinitely large and filled with a supply of saline water much greater than the scCO$_2$ pumped into it over time. With this in mind, the reservoir pressure sought is the pressure zone around the injection well that is associated with the radial extent of the growing scCO$_2$ plume (see figure 3.1). Typically for multiple fluid phases within an infinite-acting reservoir, the transient response of the pressure distribution can be described with (Lee et al. 2003; Dake 1979):

$$p(r,t) = p_i + \frac{Q_{in}}{4\pi\lambda_t b_{res}} Ei(u) \tag{3.11}$$

$$u = \frac{\phi_m c_t r^2}{4\lambda_t t} \tag{3.12}$$

where $p(r,t)$ is a 'Theis' type solution for the pressure in the reservoir at location r and time t; p_i the initial reservoir pressure - taken to be hydrostatic; λ_t the total fluid mobility; $Ei(u)$ is the exponential integral, also known as the "well" function; c_t the fluid saturation weighted compressibility; and λ_t the total fluid mobility.

However, if t is large, the transient pressure response within a radial 'zone of action' around the well can be approximated with a logarithmic solution (de Marsily 1986). In our

73

model, this 'zone of action' is represented by the radial extent of the scCO$_2$ plume movement in the reservoir (equation 3.6). For our model, the pressure within this 'zone of action' takes the form of a peusdo-steady state volumetric average within an injection domain that has an expanding outer boundary (Nordbotten et al. 2004; Lee et al. 2003; Dake 1979):

$$\overline{p_1}(r_e,t) = p_i + \frac{Q_{in}}{2\pi\lambda_t b_{res}} \ln\left[\frac{r_e = r_{max}(t)}{r_w} - \frac{3}{4}\right]$$ (3.13)

where $\overline{p_1}(r,t)$ represents the volumetric average reservoir pressure build-up to the 'zone of action' boundary extent r_e, represented by the scCO$_2$ plume r_{max}(t); r_w (m) is the injection well radius - assumed to be 17.8 cm diameter. The total fluid mobility λ_t is given by (Lee et al. 2003):

$$\lambda_t = \lambda_w + \lambda_c = \frac{k_w}{\mu_w} + \frac{k_c}{\mu_g} = k\left(\frac{k_{rw}}{\mu_w} + \frac{k_{rc}}{\mu_c}\right)$$ (3.14)

where λ_t represents the sum of the individual fluid mobilites, and k_g and k_w represent the individual effective permeabilites of the supercritical fluid and water phases, respectively. The individual fluid mobilities shown in equation 3.14 differ from the relative mobilities shown in equation 3.9 with the inclusion of absolute permeability, k.

Assuming that the reservoir is infinite and not recharged, r_e represents a moving pressure boundary whose location varies as $\sqrt{t}$; and if t is large, r_e varies very slowly where it seems as if steady-state has been obtained (Nordbotten et al. 2004; Nordbotten et al. 2005; de Marsily 1986). This approximation was shown to be suitable for most practical problems in CCS and water-flood applications (Nordbotten et al. 2004; Dake 1979).

Equation 3.13 is only valid after a long time of constant injection. This time, t_{min}, gives the criterion for the application of equation 3.13 (Lee et al. 2003).

$$t > t_{min} > \frac{\phi_m c_t r_{max}^2}{\lambda_t} \qquad (3.15)$$

where

$$c_t = s_w c_w + s_c c_c + c_f \qquad (3.16)$$

c_t represents the fluid saturation weighted compressibility of the reservoir; s_w and s_g, represent the water and supercritical fluid saturation fractions in the reservoir, respectively; and c_g, c_w, c_f represent gas, water and rock formation compressibility.

Additional assumptions for the reservoir pressure distribution include:

i)   Injection well is fully penetrating the reservoir to ensure radial flow

ii)   Darcy's law is valid within the reservoir, implying smooth laminar-type flow

iii)   The reservoir is isotropic with constant permeability, k

iv)   Isothermal conditions

v)   Fluid viscosity, μ, and compressibility, c_t, are constant

vi)   There are negligible gravity effects on the reservoir fluid

vii)   Small pressure and saturation gradient terms

viii)   Negligible capillary pressure

ix)   The initial pressure is uniform and constant

There are other models that are suitable for simulating the pressure distribution within 'leaky' reservoirs (Hantush and Jacob 1955; Hantush 1967; Boulton and Streltsova 1975; Neuman and Witherspoon 1969a,b; Neuman and Witherspoon 1972). However, the pressure build-up that would ensue from the use of these models would be less than those

predicted for a non-leaky reservoir. Therefore, the pressure predictions based on the 'Theis' type solution, implemented in this study, provide a conservative estimate for leaky systems (Freeze and Cherry 1979). Appendix B gives more detail on describing the pressure distribution of the conceptual model.

3.2.3 CAPILLARY ENTRY PRESSURE FOR CAPROCK

Two additional assumptions applied to the CO_2 loss model accounted for the capillary entry pressure and connectivity of fractures within the caprock. Capillary breakthrough of $scCO_2$ into the caprock fractures occurs when the overpressure in the reservoir, i.e. the pressure difference between the injected fluid ($scCO_2$) and formation brine (that imbibes the caprock), exceeds the maximum capillary entry pressure (Chiquet et al. 2007; Chalbaud et al. 2009). This pressure is expressed by:

$$\overline{p_1} - p_2 > p_{ce} = \frac{2\gamma}{e} \tag{3.17}$$

where p_{ce} represents the maximum capillary entry pressure predicted for the fractured caprock based on the aperture size e and brine – CO_2 surface tension γ (mPa). Surface tension γ between the CO_2 and brine is pressure and temperature dependent and has been shown to have an experimental range of 25 – 48 mPa (Chiquet et al. 2007; Chalbaud et al. 2009).

Capillary pressure plays an important role in fluid transport through low permeably media with small pore 'throats'. However, in our study, the fluid is assumed to be transported only along smooth, continuous, open-mode fracture planes, where the size of the 'throats' can be orders of magnitude greater than that the caprock's matrix.

3.2.4 FRACTURE CONNECTIVITY

Connectivity is a calculated measure of the extent to which the fracture geometry influences flow paths in the rock (Jaeger et al 2007; Stauffer and Aharony 1992). Fracture connectivity is a function of system size, fracture density, fracture length; and, is typically addressed in the context of "percolation theory" through the application of a dimensionless percolation parameter p_p (Stauffer and Aharony 1992; Bour and Davy 1997). The percolation parameter is measure (based on statistical theory) that links global physical properties (e.g. permeability) to geometric properties of fracture network. For a 2D system, the percolation parameter is defined as:

$$p_p = Nl^2 / L^2 \tag{3.18}$$

where N is the number of fractures in L^2 the plan-view surface area of system, and l the constant fracture length – equivalent b_{cap} in this conceptual system. Equation 3.18 was derived from the connection probability of fractures, proportional to mean surface surrounding each fracture l^2, and holds true fractures with random or non-random orientations (Bour and Davy 1997). There is a critical percolation threshold p_{pc} above which there exists a sufficient density of fractures in the caprock to allow fluid flow across the medium (on average). Bour and Davy (1997) showed that in the limit of an infinitely large system, $p_{pc} \sim 5.6$.

A range of estimated linear fracture densities calculated from data compiled in Bonnet et al. (2001) was used to examine the parameter space of caprock hydraulic properties. The vertical fractures depicted in our conceptual model (figure 3.1) represent the presence of an 'effective' density of fractures in caprock. When accounting for the effect of fracture geometry on hydraulic properties, the range of fracture densities had to be limited to those that gave, $p_{pc} \geq 5.6$ for our conceptual system.

3.2.5 scCO₂ LOSS AND PARAMETER ESTIMATION

The change in the percent $scCO_2$ stored over time was determined by calculating the fraction of accumulated mass leaving the system through the fractured caprock, given the amount of $scCO_2$ injected into the reservoir over the specified time period. Assuming that the fluid properties in the system are constant, accumulated mass is directly proportional to volumetric accumulation.

$$\text{scCO}_2 \text{ loss} = \xi_{CO_2} = \frac{V_{out}}{V_{in}} = \frac{\int Q_f dt}{\int Q_{in} dt} \tag{3.19}$$

Volumetric accumulation of $scCO_2$ in the reservoir (V_{in}) was determined by integrating the injection rate over the time period of interest. Volumetric loss of $scCO_2$ through the caprock (V_{out}) was determined by integrating the volumetric fracture flow with respect to time, accounting for all associated model equations for $scCO_2$ plume extent and pressure distribution.

The resulting equation for the volumetric percent loss of $scCO_2$ over time is:

$$\xi_{CO_2} = \frac{Mt}{2b_{res}\phi_m(1-s_{wr})} \cdot \frac{1}{\mu_c} \cdot \frac{e^3}{12} \cdot \frac{N}{L} \cdot \left[\frac{\overline{p_1}(r_{max},t)-p_2}{b_{cap}} - \rho_c g \right] \tag{3.20}$$

For simplicity, the equations for $scCO_2$ transport within the reservoir and caprock were not coupled in the volumetric loss estimation in equation 3.20, and accumulated $scCO_2$ mass in the reservoir was not adjusted for losses through caprock. In order to make a closed form solution, the average reservoir pressure $\overline{p_1}(r_e,t)$ was not treated as explicitly time dependent for $scCO_2$ loss, but rather was calculated separately as a function of r_{max}. To minimize the error associated with these assumptions, only predicted losses from the reservoir that were less than 10% of the total injected mass were considered. The 10% limit

also aligns with the proposed performance goals over a 100 year horizon (NETL 2011; Hepple and Benson 2005).

The scCO$_2$ loss model (equation 3.20) was evaluated with respect to fracture permeability, fracture porosity, and fracture aperture that met the 1% CO$_2$ loss CCS performance criterion and the 10% CO$_2$ loss limit for analytical validity. The fracture properties were also constrained to a range of fracture densities (e.g. no. of faults per linear system size – N/L) and aperture sizes from field studies compiled in Bonnet et al. (2001). A subset of these reported fracture densities were considered 'percolating' for the idealized case examined in this study, given equation 3.18. Based on the scCO$_2$ loss model, suitable intrinsic caprock fracture permeability and porosity followed:

$$ k_f = \frac{\phi_f e^2}{12} = \xi_{CO_2} \mu_c \left[\frac{Mt}{2b_{res}\phi_m(1-s_{wr})} \right]^{-1} \cdot \left[\frac{\overline{p_1}(r_{max},t)-p_2}{b_{cap}} - \rho_c g \right]^{-1} \tag{3.21} $$

and suitable fracture aperture sizes followed:

$$ e = \left[\xi_{CO_2} \mu_c \cdot \left[\frac{N}{12L} \right]^{-1} \cdot \left[\frac{Mt}{2b_{res}\phi_m(1-s_{wr})} \right]^{-1} \cdot \left[\frac{\overline{p_1}(r_{max},t)-p_2}{b_{cap}} - \rho_c g \right]^{-1} \right]^{\frac{1}{3}} \tag{3.22} $$

Inverse modeling of this type requires practical constraints on parameters investigated in order to reduce ill posedness and non-unique solutions. In order to minimize these issues, results also had to conform to the analytical constraints on bouyancy Γ, capillary entry pressure p_{ce}, minimum injection time t_{min}, and exceeding percolation threshold p_{pc}. Figures 3.2 - 3.5 presents the results of these analyses.

3.3   CASE STUDY

A hypothetical environment, based on a benchmark study on $scCO_2$ plume evolution and leakage, was used to examine the effects of fracture geometry on the hydraulic properties within a fractured caprock used for long-term CO_2 storage (Ebigbo et al. 2007; and Class et al. 2009). The caprock was considered to be 2,870 m deep, 100 m thick, with fractures uniformly spaced and fracture aperture constant in an otherwise impermeable formation (figure 3.1). The caprock was considered to overlie a porous saline reservoir 30 m thick. A constant $scCO_2$ injection rate into the reservoir of 0.28 MMT/yr from 0.1 – 100 years, under isothermal conditions, was assumed. The brine and $scCO_2$ fluid properties were assumed to be constant throughout the entire system. The reservoir and fluid properties are given in Table 3.1.

3.4   RESULTS AND DISCUSSION

The integrated analytical $scCO_2$ loss model (equation 3.20) was applied to the case study environment, where the resulting profiles of fracture aperture, porosity, and permeability were inversely determined from a range of fracture densities that met CCS storage criteria, which considered percolation, capillary entry pressure, and observed data. Table 3.2 compares the resulting maximum range of fracture properties simulated in this study to those reported in various field and laboratory studies.

3.4.1 scCO$_2$ PLUME EXTENT IN RESERVOIR

The reservoir $scCO_2$ plume model affects the predicted $scCO_2$ leakage from the reservoir by changing the plume area (A) of the caprock that is exposed to the $scCO_2$ in the reservoir (see equation 3.2). Figure 3.2 shows the results of using the Nordbotten et al. (2005) analytical model (see equation 3.6) for estimating the maximum extent (r_{max}) of the

scCO$_2$ plume. Given the conditions listed in Table 3.1, the predicted radial extent of the scCO$_2$ plume over 100 years was 2.2 km for a continuous injection of scCO$_2$.

For the idealized system with parameter values as given in Table 3.1, the fluid mobility ratio was close to 1 (~0.96) and had negligible buoyancy effects (Γ = 0.13 < 0.5). This means the scCO$_2$ displaced the brine over time with a sharp, piston-like interface where the viscous properties of the injected scCO$_2$ plume prevented it from bypassing the displaced brine (Dake 1979). This interface changes when the fluid mobility ratio is greater than 1.

3.4.2 VERTICAL PRESSURE GRADIENT ACROSS CAPROCK

Figure 3.2 shows the change in the vertical pressure gradient over time period of the case study. Given the conditions listed in Table 3.1, the predicted vertical pressure gradient did not exceed 0.07 MPa/m with a continuous injection of scCO$_2$. The simulated reservoir pressure ranged from 35.4 – 37.6 MPa with a corresponding vertical pressure gradient ranging from 0.05 – 0.07 MPa/m over 100 years (figure 3.2).

In this study, only the pressure within the scCO$_2$ plume radial zone of influence was of concern, and the small changes in the vertical pressure gradient came from the r_{max} in equation 3.13 which represented a moving boundary that was proportional to $\sqrt{t}$. As the scCO$_2$ plume expands over 100 years, the pressure in reservoir changes very little due to the correlation in equation 3.13. Over long times the pressure response in the reservoir is no longer dependent on the rock properties (e.g. porosity, compressibility) but mainly on the injection rate and the fluid properties of the CO$_2$ and brine. Changes in reservoir pressure encompassing the expanding scCO$_2$ plume did not significantly contribute to overall scCO$_2$ leakage. Therefore, in a large reservoir with a small scCO$_2$ injection rate over 100

years, one of the main contributors to CO_2 loss is predicting the aerial location of the $scCO_2$ plume not its associated overpressure.

The capillary entry pressure within the caprock fractures was always exceeded in our case study. Reservoir pressure starting time (t = 0.1 yrs.) gave an overpressure $\left(\overline{p_1}(r_{\max},t) - p_2\right)$ of 5.92 MPa, where the smallest aperture size e considered was $\sim 10^{-7}$ m. This gave a maximum $p_{ce} \sim 1$ MPa. Therefore, all subsequently constrained fracture apertures and densities represented those already exceeding capillary entry pressures.

3.4.3 FRACTURE PERMEABILITY AND POROSITY SENSITIVITY

Figure 3.3 presents the CO_2 % loss versus fracture permeability trend of the CO_2 loss model given the case study's constant $scCO_2$ injection rate of 0.28 MMT/yr over 100 yrs. Figure 3.3 shows the range of values that meet the 1% criteria (green shaded area "A") and the 10% loss criteria (blue shaded area "B") given the fracture properties of Table 3.2. The vertical double line and arrow represent the cut-off and direction for values above the percolation threshold, p_{pc} = 5.6. Vertical dashed lines and double pointed arrows represent the overlap of modeled values with observed ranges for fracture permeability and caprock matrix permeability k_m listed in Table 3.2. Intrinsic fracture permeability, as seen in equation 3.20 and 3.21, was directly correlated to predicted CO_2 loss and had a range of 10^{-23} – 10^{-17} m² that were modeled to fit the 1 – 10% CO_2 loss window. When considering percolation for the case study environment, a more narrow range of 10^{-19} – 10^{-17} m² emerged. The parameter space of modeled fracture permeability fell mostly within the measured range of intact caprock matrix permeability (horizontal and vertical). Only a small portion of the modeled values fell within the observed range of fracture permeability, with no values occurring within the 1% CO_2 loss range. However, the range of k_f that met percolation and CCS criteria indicate that caprocks need to be relatively impermeable over a

large area of review (AoR) (IPCC 2005). It is important to note that the observed range of fracture permeability, to which the model results were compared, were taken from sources that primarily examined fractured reservoirs not the overlying caprocks.

Fracture porosity, unlike fracture permeability, was a non-unique indicator for CO_2 loss. Instead of linear relationship to CO_2 loss, like with fracture permeability, a 'wedge' of values existed for fracture porosities that covered the window of CO_2 loss and percolation meeting the 1 – 10% CO_2 loss cut-off. Figure 3.4 shows this 'wedge' of fracture porosity values, based on Table 3.2 and 3.3, which was bound by minimum fracture aperture (10^{-7} m) on the right and minimum observed fracture density (i.e. 5 x 10^{-4} m^{-1}) on the left. The horizontal borders of the wedge at the 1 and 10% CO_2 loss consist of many porosities that could fit either CO_2 loss criteria but differ in the combination of aperture and density. As fracture density increases with porosity to the right in figure 3.4, the double line represents the point where sufficient fracture density was present to exceed the critical percolation threshold for the conceptual system. The wedge of values in figure 3.4 suggest that caprocks with fracture porosities greater than 0.02% could yield CO_2 losses greater than 10% and exceed percolation threshold. Only a small portion of the resulting parameter space fell within the observed range of fracture porosities, given 1% CO_2 loss and percolation fracture porosity. The majority of resulting ϕ_f values were within the lower limit of interpretation when compared to field studies (see Table 3.2).

3.4.4 FRACTURE APERTURE AND DENSITY SENSITIVITY

Figure 3.5 further examined the relationship between the constitutive parameters of the fracture permeability and – porosity the fracture aperture and density. Figure 3.5 showed a narrow range of fracture apertures 10^{-7} – 10^{-5} m that met the CO_2 loss limits and were within documented aperture sizes, given the range of fracture densities used in this study. Figure 3.5 also showed that only submicron to micron size apertures could meet the

CCS criteria, particularly when considering network percolation. This indicated that the parameter space of k_f and ϕ_f that met percolation and CSS criteria was dictated by this narrow submicron – micron aperture size range.

Figure 3.3 – 3.5 enable several important observations about the influence of the caprock fracture properties in meeting the 1% CO_2 loss criterion. First, the required fracture permeabilities were constantly low, $\leq 10^{-17}\,m^2$ compared to field measurement of fractured formations (Table 3.2). Secondly, though there is a "cubic" relationship between the aperture size and fracture permeability (equation 3.4), there was only a very narrow fracture aperture range ($10^{-7} – 10^{-6}$ m) that met the performance criteria and threshold for percolation that lied within observed field values. Thirdly, acceptable fracture porosities were low ($\leq 0.02\%$) with only a narrow range (0.001 – 0.002%) of observed values meeting the target for 99% CO_2 storage permanence. Fourthly, when accounting for fracture connectivity, the parameter space for fracture permeability yielded no values within observed limits for the 1% CO_2 loss performance criteria. Only a small range of modeled fracture porosities met this criterion.

Simulating the fluid flow behavior in naturally fractured formations is a challenge that requires the synthesis of many different data types to characterize the fracture system (Narr et al. 2006). Most data on formation fracture geometry are predominantly taken at the field scale, with fewer done in the laboratory (Narr et al. 2006; Bonnet et al. 2001). They include outcrop scan lines, aerial photography, seismic surveys, wellbore logs and imaging, or core and thin section analysis (Bonnet et al 2001; Laudbach et al. 2006). Each method has its detection limitations with thresholds for attaining reliable data sets.

To get perspective to the modeling results, thresholds cut-offs for reliable fracture aperture measurements are recommended at 0.2 – 0.5 mm for outcrop analysis, 0.05 mm for core – scale analysis, and 0.005 mm for thin-section analysis (Guerriero et al. 2011).

These recommended thresholds suggest that field scale measurements may not reliably capture aperture sizes that could affect long-term storage. However, as figure 3.5 suggests, larger fractures may exist within the caprock but may not be 'connected' enough to impact CO_2 storage.

Nonetheless, general parameter bounds based on CO_2 loss were identified through this modeling study. Fracture aperture size did not exceed 10^{-5} m for either CO_2 loss criteria, fracture permeability did not exceed 10^{-17} m^2, and fracture porosity did not exceed 0.02%. These hydraulic properties were significant when fracture densities $N/L > 0.28$ m^{-1} (e.g. approx. 3 fractures for every 10 meters), which was sufficient to establish flow connectivity between the microfractures in a 2.2 km radius from injection well, for the case study examined. Compared to field studies, the fracture permeability of this CO_2 constrained system are on the order of the nano- to micro Darcy permeability of the caprock matrix (Table 3.2). However, geomechanical deformation was not considered in this study, where changes in the stress field within the system could offset or reduce the conductivity of fractures present in a caprock (Rutqvist and Tsang 2002).

3.5   SUMMARY AND CONCLUSIONS

An integrated analytical model was developed to evaluate the effects of fracture aperture and density on estimating the hydraulic properties of a caprock fracture network that were consistent with proposed storage performance criteria for CCS. A benchmark geological environment was used as the basis to evaluate how fracture aperture, density, and connectivity affect transport $scCO_2$ through caprock.

Several observations were made in this study: (1) microfractures (e.g. 10^{-7} to 10^{-6} m range) can yield CO_2 loss rates of concern under certain conditions; (2) fracture permeability was the key parameter governing CO_2 loss and apart from fracture density, its constitutive parameters could only vary within a limited range; (3) fracture permeability

meeting the CO_2 loss criteria lied in the nano- to micro-Darcy (µD) range (i.e. $10^{-24} - 10^{-17}$ m^2) which may be indistinguishable from caprock matrix permeability; (4) fracture porosities were low ($10^{-9} - 0.02$ %), (5) apart from fracture permeability, no other single fracture parameter (e.g. fracture porosity, aperture, density) uniquely predicted CO_2 transport in caprock; and (6) compared to reported measurements of fracture systems, interpretation of hydraulic flow within a $1 - 10\%$ CO_2 loss window may be difficult depending on degree of fracture connectivity.

The conservative approach taken in this study can provide first-order estimates for constitutive fracture properties within caprock which are consistent with long-term CO_2 storage performance objectives. However, this study considers only losses through a single caprock formation and did not consider other factors – like geomechanical deformation that may lead to greater fracturing. The observations noted in this modeling study highlight the range and uncertainty of variables governing fracture flow in a CO_2 constrained environment. Future work should include a stochastic analysis to examine the inter-relationships of the transport parameters to better characterize the solution domain of the hydraulic fracture parameters over the long time scales of interest.

Acknowledgments

3.6 REFERENCES

Aguilera, R., 1980. Naturally fractured reservoirs. The Petroleum Publishing Company, Tulsa, Oklahoma, 703 pp.

Berkowitz, B., 2002. Characterizing flow and transport in fractured geological media: A review. Advances in Water Resources, 25(8-12): 861-884.

Bonnet, E. et al., 2001. Scaling of fracture systems in geological media. Reviews of Geophysics, 39(3): 347-383.

Bour, O. and Davy, P., 1997. Connectivity of random fault networks following a power law fault length distribution. Water Resources Research, 33(7): 1567-1583.

Carrera, J., Alcolea, A., Medina, A., Hidalgo, J. and Slooten, L.J., 2005. Inverse problem in hydrogeology. Hydrogeology Journal, 13: 206-222.

Chalbaud, C. et al., 2009. Interfacial tension measurements and wettability evaluation for geological CO2 storage. Advances in Water Resources, 32: 98-109.

Chiquet, P., Daridon, J.-L., Broseta, D. and Thibeau, S., 2007. CO2/water interfacial tensions under pressure and termperature conditions of CO2 geological storage. Energy Conversion and Management, 48: 736-744.

Class, H. et al., 2009. A benchmark study on problems related to CO2 storage in geologic formations. Computational Geosciences, 13(4): 409-434.

Dake, L.P., 1978. Fundamentals of reservoir engineering. Developments in petroleum science. Elsevier Scientific Publishing Company, Amsterdam, The Netherlands.

de Dreuzy, J.R., Davy, P. and Bour, O., 2001. Hydraulic properties of two-dimensional random fracture networks following a power law length distribution 1. Effective connectivity. Water Resources Research, 37(8): 2065-2078.

de Marsily, G., 1986. Quantitative Hydrogeology. Academic Press, Inc., Orlando, FL.

Ebigbo, A., Class, H. and Helmig, R., 2007. CO_2 leakage through an abandoned well: problem-oriented benchmarks. Computational Geosciences, 11(2): 103-115.

Freeze, R.A. and Cherry, J.A., 1979. Groundwater. Prentice-Hall, Inc.

Griffith, C.A., Dzombak, D.A. and Lowry, G.V., 2011. Physical and chemical characteristics of potential seal strata in regions considered for demonstrating geological saline CO_2 sequestration. Environmental Earth Sciences, 64(4): 925-948.

Grimstad, A.-A., Georgescu, S., Lindeberg, E. and Vuillaume, J.-F., 2009. Modelling and simulation of mechanisms for leakage of CO_2 from geological storage. Energy Procedia, 1: 2511-2518.

Guerriero, V., Vitale, S., Ciarcia, S. and Mazzoli, S., 2011. Improved statistical multi-scale analysis of fractured reservoir analogues. Tectonophysics, 504(1-4): 14-24.

Gutierreza, M., Øino, L.E. and Nygard, R., 2000. Stress-dependent permeability of a de-mineralised fracture in shale. Marine and Petroleum Geology, 17: 895–907.

Hantush, M.S., 1960. Modification of the theory of leaky aquifers. Journal of Geophysical Research, 65(11): 3713-3725.

Hantush, M.S. and Jacob, C.E., 1955. Nonsteady radial flow in an infinite leaky aquifer. Transactions American Geophysical Union, 36(1): 95-100.

Hepple, R.P. and Benson, S.M., 2005. Geologic storage of carbon dioxide as a climate change mitigation strategy: performance requirements and the implications of surface seepage. Environmental Geology, 47(4): 576-585.

Iding, M. and Ringrose, P., 2010. Evaluating the impact of fractures on the performance of the In Salah CO2 storage site. International Journal of Greenhouse Gas Control, 4(2): 242-248.

Jaeger, J.C., Cook, N.G.W. and Zimmerman, R.W., 2007. Fundamentals of rock mechanics. Blackwell Publishing, 488 pp.

Jordan, p., Oldenburg, C.M. and Nicot, J.-P., 2011. Estimating the probability of CO_2 plumes encountering faults. Greenhouse Gases: Science and Technology, 1(2): 160-174.

Laubach, S.E. and Ward, M.E., 2006. Diagenesis in porosity evolution of opening-mode fractures, Middle Triassic to Lower Jurassic La Boca Formation, NE Mexico. Tectonophysics, 419(1-4): 75-97.

Lee, J. and Wattenbarger, R.A., 1996. Gas reservoir engineering. SPE Textbook Series. Society of Petroleum Engineers, Richardson, TX.

Lemonnier, P. and Bourbiaux, B., 2010a. Simulation of Naturally Fractured Reservoirs. State of the Art Part 1 Physical Mechanisms and Simulator Formulation. Oil & Gas Science and Technology-Revue De L Institut Francais Du Petrole, 65(2): 239-262.

Lemonnier, P. and Bourbiaux, B., 2010b. Simulation of Naturally Fractured Reservoirs. State of the Art Part 2 Matrix-Fracture Transfers and Typical Features of Numerical Studies. Oil & Gas Science and Technology-Revue De L Institut Francais Du Petrole, 65(2): 263-286.

Nelson, R.A., 2001. Geological Analysis of Naturally Fractured Reservoirs. Gulf Professional Publishing, Woburn, Massachusetts.

NETL, 2011. Carbon Sequestration Program: Technology Program Plan - Enhancing the Success of Carbon Capture and Storage Technologies, Applied Research and Development from Lab- to Large-Field Scale, National Energy Technology Laboratory

Neufeld, J.A., Vella, D. and Huppert, H.E., 2009. The effect of a fissure on storage in a porous media. Journal of Fluid Mechanics, 639: 239-259.

Neufeld, J.A., Vella, D., Huppert, H.E. and Lister, J.R., 2011. Leakage from gravity currents in a porous medium. Part 1. A localized sink. Journal of Fluid Mechanics, 666: 391-413.

Neuman, S.P. and Witherspoon, P.A., 1969a. Applicability of current theories of flow in leaky aquifers. Water Resources Research, 5: 817-829.

Neuman, S.P. and Witherspoon, P.A., 1969b. Theory of flow in a confined two-aquifer system. Water Resources Research, 5: 803-816.

Nordbotten, J.M., Celia, M.A. and Bachu, S., 2004. Analytical solutions for leakage rates through abandoned wells. Water Resources Research, 40: W04204.

Nordbotten, J.M., Celia, M.A., Bachu, S. and Dahle, H.K., 2005. Semianalytical solution for CO_2 leakage through an abandoned well. Environmental science & technology, 39(2): 602-611.

Odling, N.E., 1997. Scaling and connectivity of joint systems in sandstones from western Norway. Journal of Structural Geology, 19(10): 1257-1271.

Odling, N.E. et al., 1999. Variations in fracture system geometry and their implications for fluid flow in fractured hydrocarbon reservoirs. Petroleum Geoscience, 5(4): 373-384.

Okwen, R.T., Stewart, M.T. and Cunningham, J.A., 2010. Analytical solution for estimating storage efficiency of geologic sequestration of CO2. International Journal of Greenhouse Gas Control, 4: 102-107.

Pacala, S. and Socolow, R., 2004. Stabilization wedges: solving the climate problem for the next 50 years with current technologies. Science (New York, N.Y.), 305(5686): 968-972.

Pritchard, D., 2007. Gravity currents over fractured substrates in a porous media. Journal of Fluid Mechanics, 584: 415-431.

Pruess, K. and Garcia, J., 2002. Multiphase flow dynamics durign CO_2 disposal into salne aquifers. Environmental Geology, 42: 282-295.

Rutqvist, J. and Tsang, C.-F., 2002. A study of caprock hydromechanical changes associated with CO_2-injection into a brine formation. Environmental Geology, 42: 296-305.

Saripalli, P. and McGrail, P., 2002. Semi-analytical approaches to modeling deep well injection of CO2 for geological sequestration. Energy Conversion and Management, 43: 185-198.

Shukla, R., Ranjith, P., Haque, A. and Choi, X., 2010. A review of studies on CO_2 sequestration and caprock integrity. FUEL, 89(10): 2651-2664.

Smith, J., Durucan, S., Korre, A. and Shi, J.Q., 2011. Carbon dioxide storage risk assessment: Analysis of caprock fracture network connectivity. International Journal of Greenhouse Gas Control, 5(2): 226-240.

Stauffer, D. and Aharony, A., 1992. Introduction to percolation theory. Taylor and Francis, Bristol, PA, 181 pp.

Tsang, C.F., Birkholzer, J. and Rutqvist, J., 2008. A comparative review of hydrologic issues involved in geologic storage of CO_2 and injection disposal of liquid waste. Environmental Geology, 54(8): 1723-1737.

Van Golf-Racht, T.D., 1982. Fundamentals of fractured reservoir engineeering. Developments in Petroleum Science. Elsevier Scientific Publishing Company, Amsterdam, The Netherlands, 710 pp.

Vella, D., Neufeld, J.A., Huppert, H.E. and Lister, J.R., 2011. Leakage from gravity currents in a porous medium. Part 2. A line sink. Journal of Fluid Mechanics, 666: 414-427.

Viswanathan, H.S. et al., 2008. Development of a hybrid process and system model for the assessment of wellbore leakage at a geologic CO_2 sequestration site. Environmental Science & Technology, 42: 7280-7286.

Wang, F.P. and Reed, R.M., 2009. Pore networks and fluid flow in gas shales, 2009 SPE Annual Technical Conference and Exhibition. Society of Petroleum Engineers, New Orleans, Louisiana, USA.

Wollenweber, J. et al., 2010. Experimental investigation of the CO2 sealing efficiency of caprocks. International Journal of Greenhouse Gas Control 4(2): 231-241.

Zhang, Y.Q., Oldenburg, C.M. and Finsterle, S., 2010. Percolation-theory and fuzzy rule-based probability estimation of fault leakage at geologic carbon sequestration sites. Environmental Earth Sciences, 59(7): 1447-1459.

Zimmerman, D.A. et al., 1998. A comparison of seven geostatistically based inverse approaches to estimate transmissivities for modeling advective transport by groundwater flow. Water Resources Research, 34(6): 1373-1413.

TABLE 3.1: Caprock, reservoir and fluid properties with parameter range for fracture aperture and fracture density

Input parameters	Unit	value
Caprock		
Depth, z_{Top}	m	2870
Thickness, b_{cap}	m	100
Reservoir		
Reservoir thickness, b_{res}	m	30
Reservoir porosity, ϕ_m	-	0.15
Reservoir water saturation, s_w	-	1
CO_2 gas saturation, s_q	-	-
Reservoir residual water saturation, s_{wr}	-	0.2
Reservoir permeability, k	m^2	2×10^{-14}
CO_2 relative permeability, k_{rq}	-	0.15
Reservoir brine relative permeability, k_{rw}	-	1
Hydrostatic pressure gradient, G_h	Pa m^{-1}	1.05×10^4
Reservoir initial pressure, p_i	Pa	$p_i \approx G_h(z_{Top} + L)$
Rock compressibility, c_f	Pa^{-1}	1×10^{-9}
Fluid		
CO_2 injection rate, Q_{in}	MMT/yr	0.28
CO_2 injection time, t	yr	0.1 – 100
CO_2 viscosity, μ_q	Pa-s	3.95×10^{-5}
CO_2 density, ρ_g	kg m^{-3}	479
Reservoir brine viscosity, μ_w	Pa-s	2.54×10^{-4}
Reservoir brine density, ρ_w	kg m^{-3}	1045
Brine compressibility, c_w	Pa^{-1}	4.4×10^{-10}

TABLE 3.2: Typical caprock fracture and matrix properties compared to the resulting fracture properties of this study.

Characteristic	Modeled range for suitable CO_2 loss	Documented range	Source
Fracture properties			
Fracture aperture, e (m)	10^{-7}–10^{-5}	10^{-7}–10^{-3}	Bonnet et. al (2001); Inding and Ringrose (2010);Nelson (2003)
*Fracture density, N/L (m^{-1})	10^{-4}–10^{2}	10^{-3}–10^{4}	
Fracture porosity, ϕ_f (%)	10^{-9}–10^{-2}	10^{-3}–3% ; 4×10^{-2}–5%	Van Golf-Racht (1982) Nelson (2003); Aguillera 1980
Fracture permeability, k_f (m^2)	10^{-24}–10^{-17}	2.6–7.2×10^{-10} 4×10^{-17}–3×10^{-12}	Gutierrez et al. (2000) Nelson (2003); Aguillera 1980
Matrix properties			
Matrix porosity, ϕ_m (%)	N/A	0.4–45 0–9 6–15	Griffith et al. (2011);Wang and Reed (2009); Wollenweber et al. (2010)
Vertical matrix permeability, k_v (m^2)	N/A	3.1×10^{-19}– 4.8×10^{-16}	Griffith et al. (2011)
Horizontal matrix permeability, k_h (m^2)	N/A	5.7×10^{-20}–2.5×10^{-11} 1×10^{-26}–1×10^{-17} 1×10^{-22}–1×10^{-21}	Griffith et al. (2011);Wang and Reed (2009); Wollenweber et al. (2010)

Fracture density was held constant during the simulation and was based on the compilation of field studies in Bonnet et al. (2001) listed in Table 3.3.

TABLE 3.3: Fracture densities derived from compiled sources in Bonnet et al. (2001) with associated percolation parameters given a constant caprock fracture length of 100 m.

No. of fractures	Area, L^2 (m²)	Est. system linear size, L (m)	Est. linear fracture density N/L (m⁻¹)	Percolation parameter, p_p	Source
201	3.00E-01	5.48E-01	366.97	6,700,000	Schlische et al. (1996)
873	3.40E+01	5.83E+00	149.72	256,765	Ackermann and Schlische (1997)
800	2.50E+01	5.00E+00	160.00	320,000	Reches (1986)
218	1.00E+00	1.00E+00	218.00	2,180,000	Knott et al. (1996)
121	2.50E+01	5.00E+00	24.20	48,400	Bahat (1987)
107	2.40E+01	4.90E+00	21.84	44,583	Bahat (1987)
470	1.17E+04	1.08E+02	4.35	402	Odling et al. (1999)
260	8.75E+03	9.35E+01	2.78	297	Segall and Pollard (1983)
380	3.43E+03	5.86E+01	6.49	1,107	Ouillon et al. (1996)
100	2.10E+03	4.58E+01	2.18	476	Segall and Pollard (1983)
40	2.00E+04	1.41E+02	0.28	20	Fossen and Hesthammer (1997)
Below critical percolation threshold					
417	6.00E+07	7.75E+03	0.054	0.06950	Pickering et al. (1997)
318	1.69E+08	1.30E+04	0.024	0.01882	Gauthier and Lake (1993)
291	1.69E+08	1.30E+04	0.022	0.01722	Gauthier and Lake (1993)
1034	8.70E+07	9.33E+03	0.111	0.11885	Clark et al. (1999)
1034	8.70E+07	9.33E+03	0.111	0.11885	Watterson et al. (1996)
400	1.20E+08	1.10E+04	0.037	0.03333	Scott and Castellanos (1984)
78	1.69E+08	1.30E+04	0.006	0.00462	Gauthier and Lake (1993)
1000	1.65E+10	1.28E+05	0.008	0.00061	Ouillon et al. (1996)
450	2.20E+08	1.48E+04	0.030	0.02045	Yielding et al. (1996)
1000	1.60E+09	4.00E+04	0.025	0.00625	Ouillon et al. (1996)
1700	1.00E+10	1.00E+05	0.017	0.00170	Scholz (1997)
350	1.26E+08	1.12E+04	0.031	0.02778	Ouillon et al. (1996)
3499	2.70E+11	5.20E+05	0.007	0.00013	Bour and Davy (1999)
50	2.90E+07	5.39E+03	0.009	0.01724	Krantz (1988)

320	2.07E+07	4.55E+03	0.070	0.15459	Belfield (1992)
180	2.80E+08	1.67E+04	0.011	0.00643	Kakimi (1980)
120	8.25E+07	9.08E+03	0.013	0.01455	Gudmundsson (1987a)
111	8.40E+07	9.17E+03	0.012	0.01321	Needham et al. (1996)
300	-	-	-	-	Yielding et al. (1996)
101	2.62E+07	5.12E+03	0.020	0.03855	Gudmundsson (1987b)
200	6.20E+09	7.87E+04	0.003	0.00032	Cladouhos and Marrett (1996)
400	2.90E+11	5.39E+05	0.001	0.00001	Stewart (1980)
350	1.50E+09	3.87E+04	0.009	0.00233	Yielding et al. (1996)
150	5.10E+09	7.14E+04	0.002	0.00029	Cladouhos and Marrett (1996)
250	2.50E+11	5.00E+05	0.001	0.00001	Blackstone (1988)
380	-	-	-	-	Scholz and Cowie (1990)
100	6.00E+08	2.45E+04	0.004	0.00167	Villemin and Sunwoo (1987)
70	3.60E+09	6.00E+04	0.001	0.00019	Cladouhos and Marrett (1996)
300	-	-	-	-	Hatton et al. (1993)
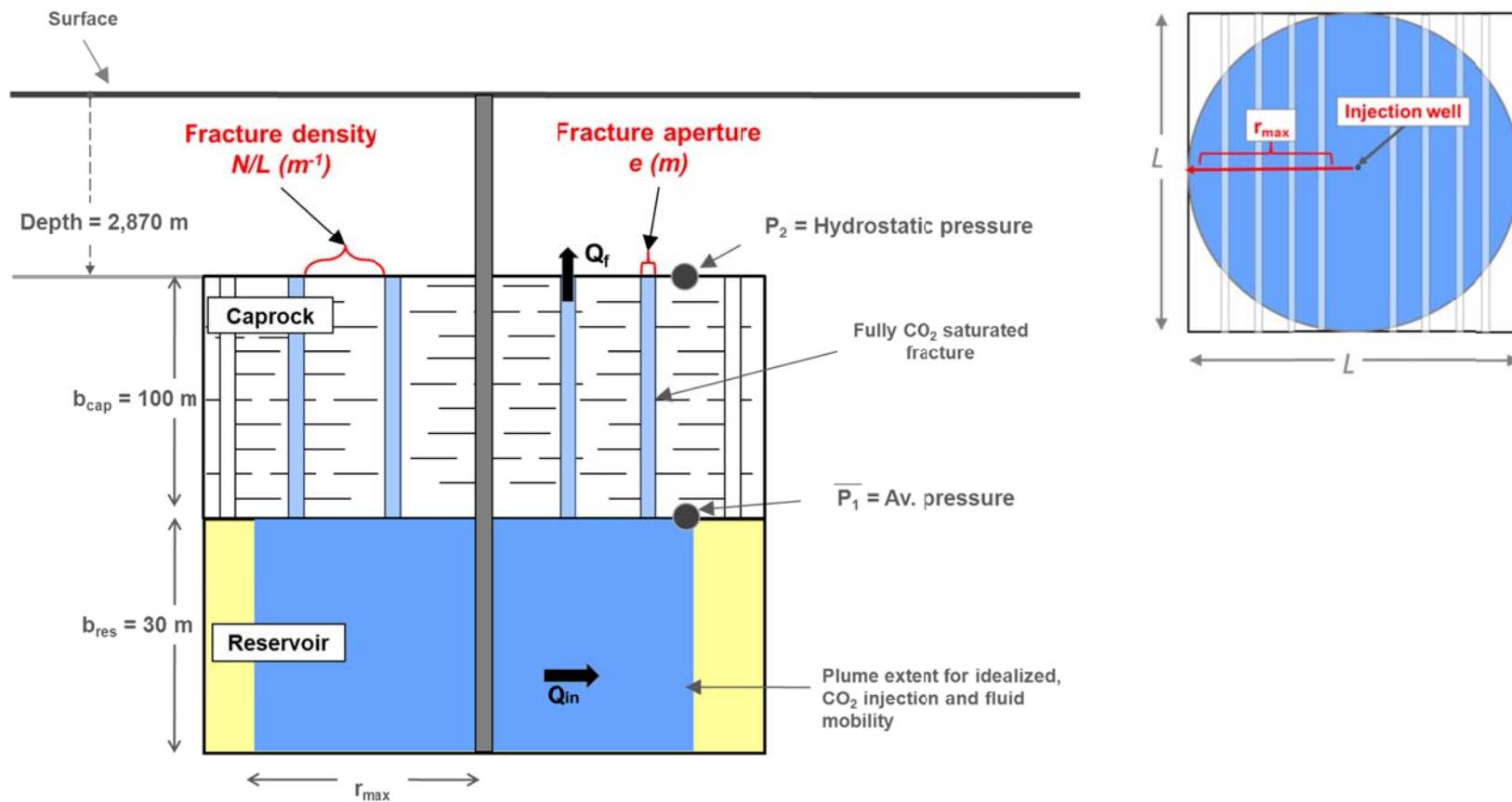
FIGURE 3.1: Conceptual model for an idealized geologic reservoir and caprock system. The integrated analytical model for flow through the reservoir and the overlying caprock has fixed transport properties, parameters, and a caprock with uncertain fracture geometry. Fractures are assumed open-mode with smooth, parallel plate geometry and completely saturated with $scCO_2$. Plan view map illustrates the 2D geometric coverage of fractures in caprock in contact with the $scCO_2$ plume in the reservoir.
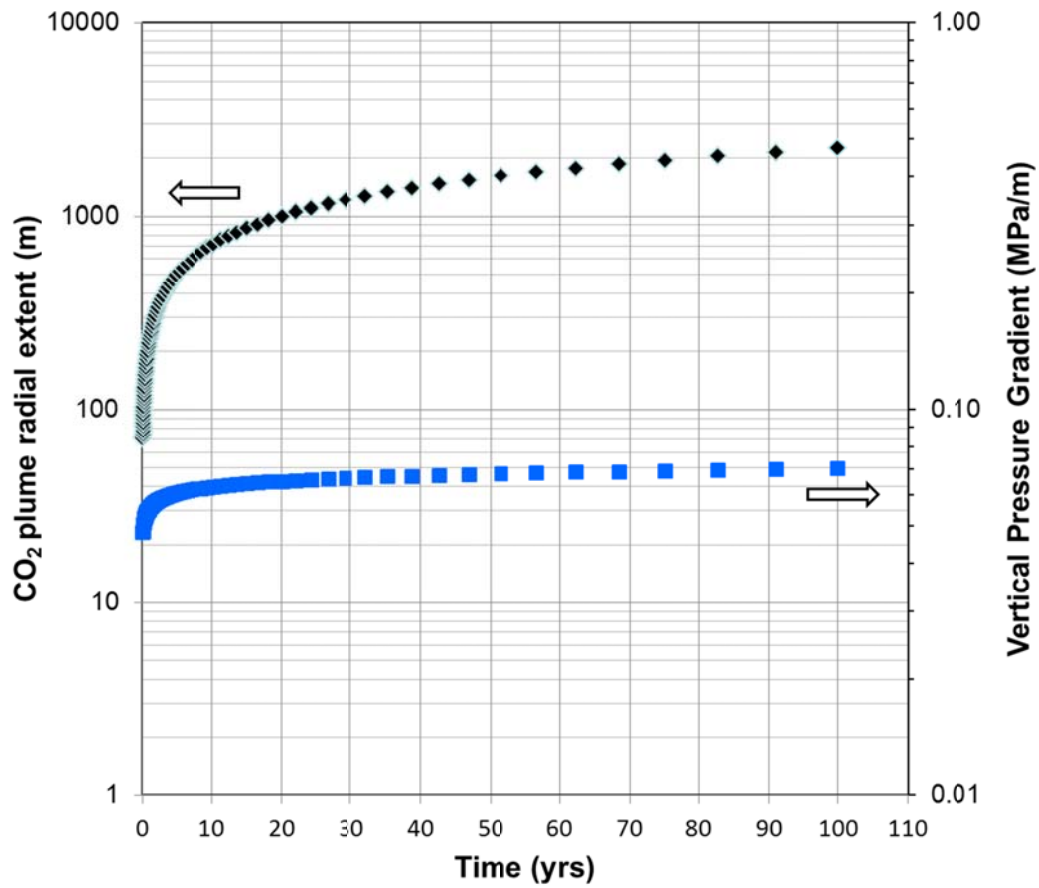
FIGURE 3.2: Predicted radial extent of CO_2 plume using the Nordbotten et al. (2005) model and vertical pressure gradient across the caprock over 100 years, given the conditions on Table 3.1.
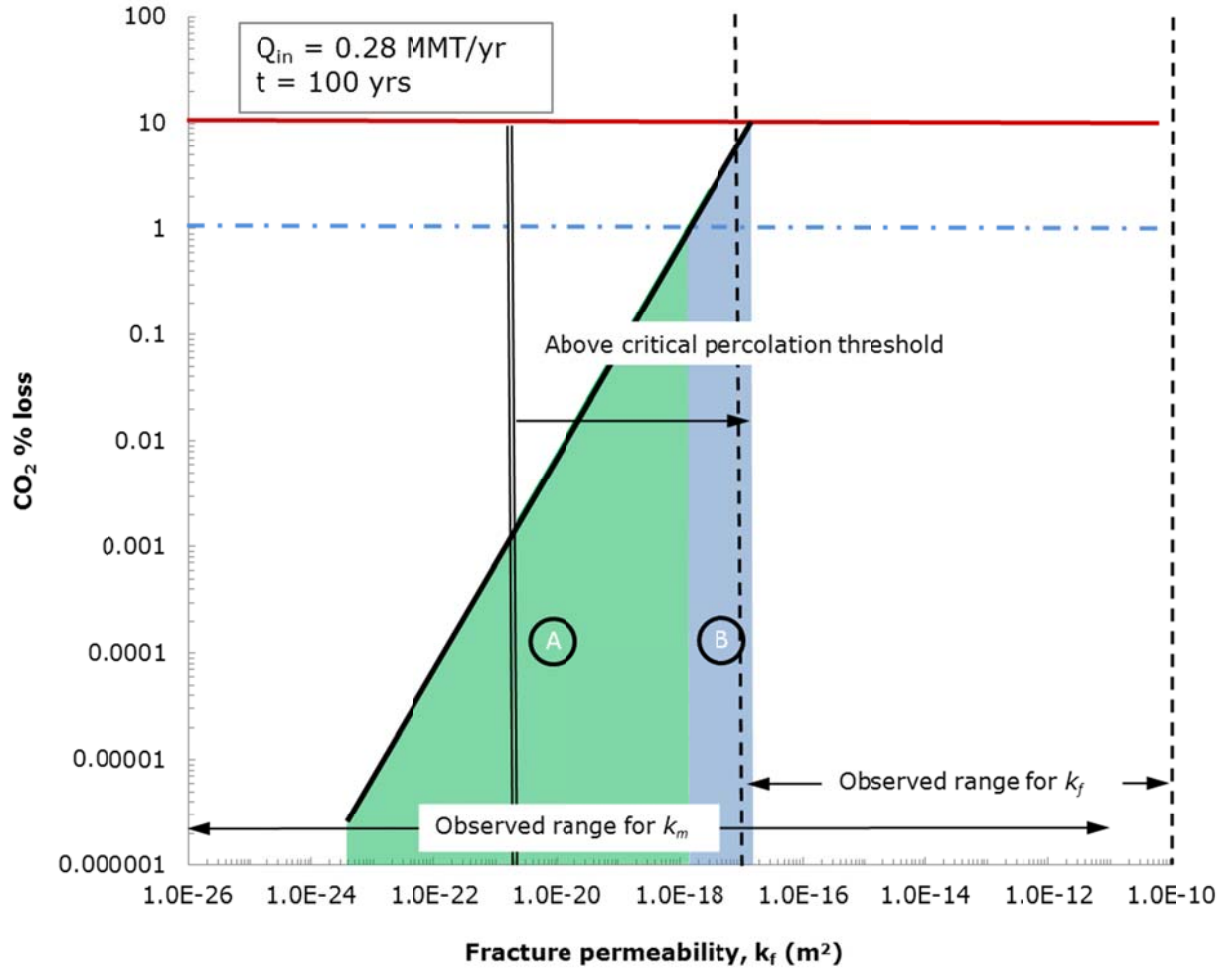
FIGURE 3.3: CO_2 loss vs. fracture permeability trend of the CO_2 loss model showing the range of values that meet the 1% criteria (green shaded area "A") and the 10% loss criteria (blue shaded area "B") given the fracture properties of Table 3.2 and 3.3. The vertical double line and arrow represent the cut-off and direction for values above the percolation threshold, $p_{pc} = 5.6$. Vertical dashed lines and double pointed arrows represent the overlap of modeled values with observed ranges for fracture permeability and caprock matrix permeability km listed in Table 3.2.
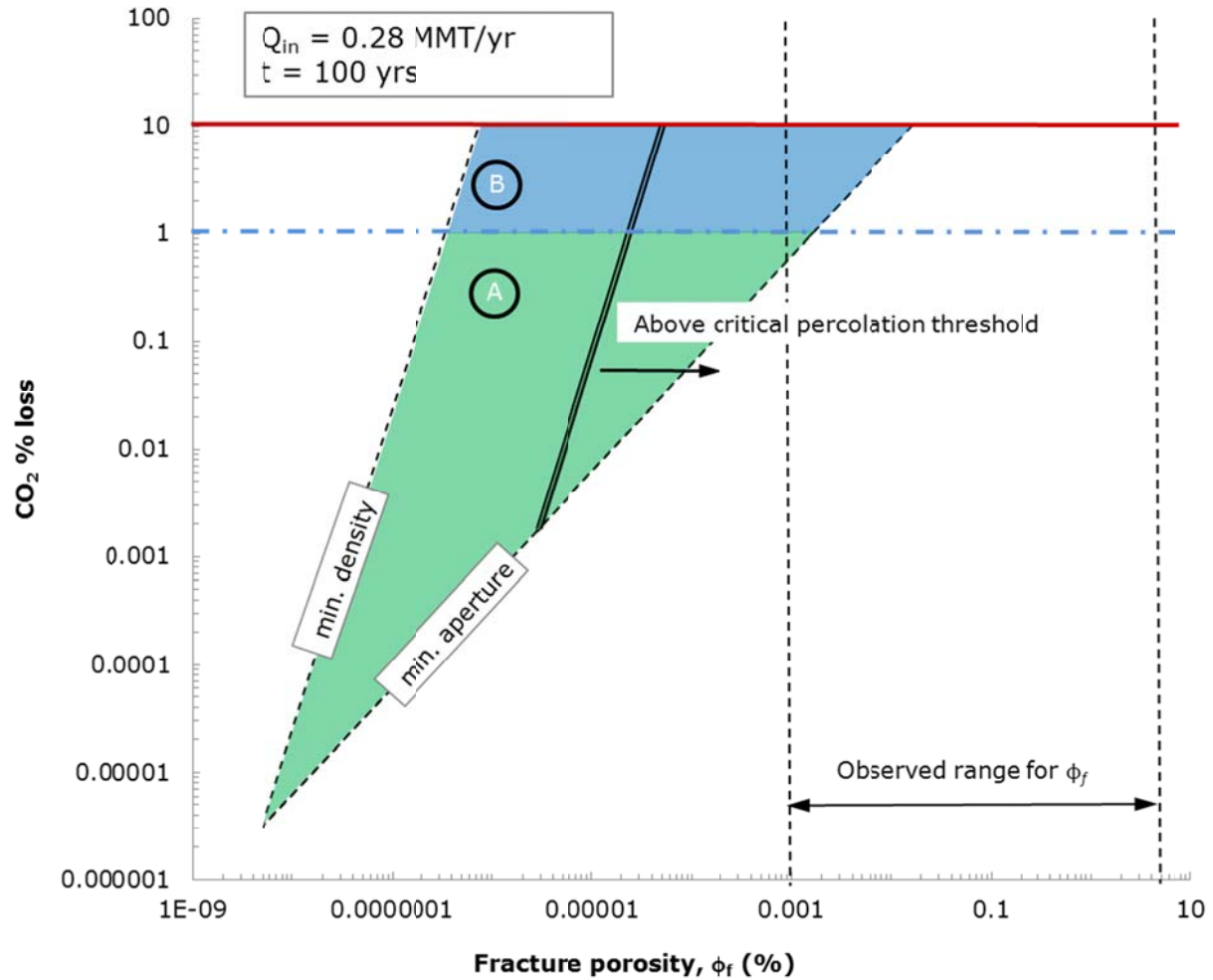
FIGURE 3.4: CO_2 loss vs. fracture porosity trend of the CO_2 loss model showing the range of values that meet the 1% (green shaded area "A") and 10% loss criteria (blue shaded area "B") given the fracture properties of Table 3.2 and 3.3. The vertical double line and arrow represent the cut-off and direction for values above the percolation threshold, p_{pc} = 5.6. Vertical dashed lines and double pointed arrows represent the overlap of modeled values with observed ranges for fracture porosities listed in Table 3.2.
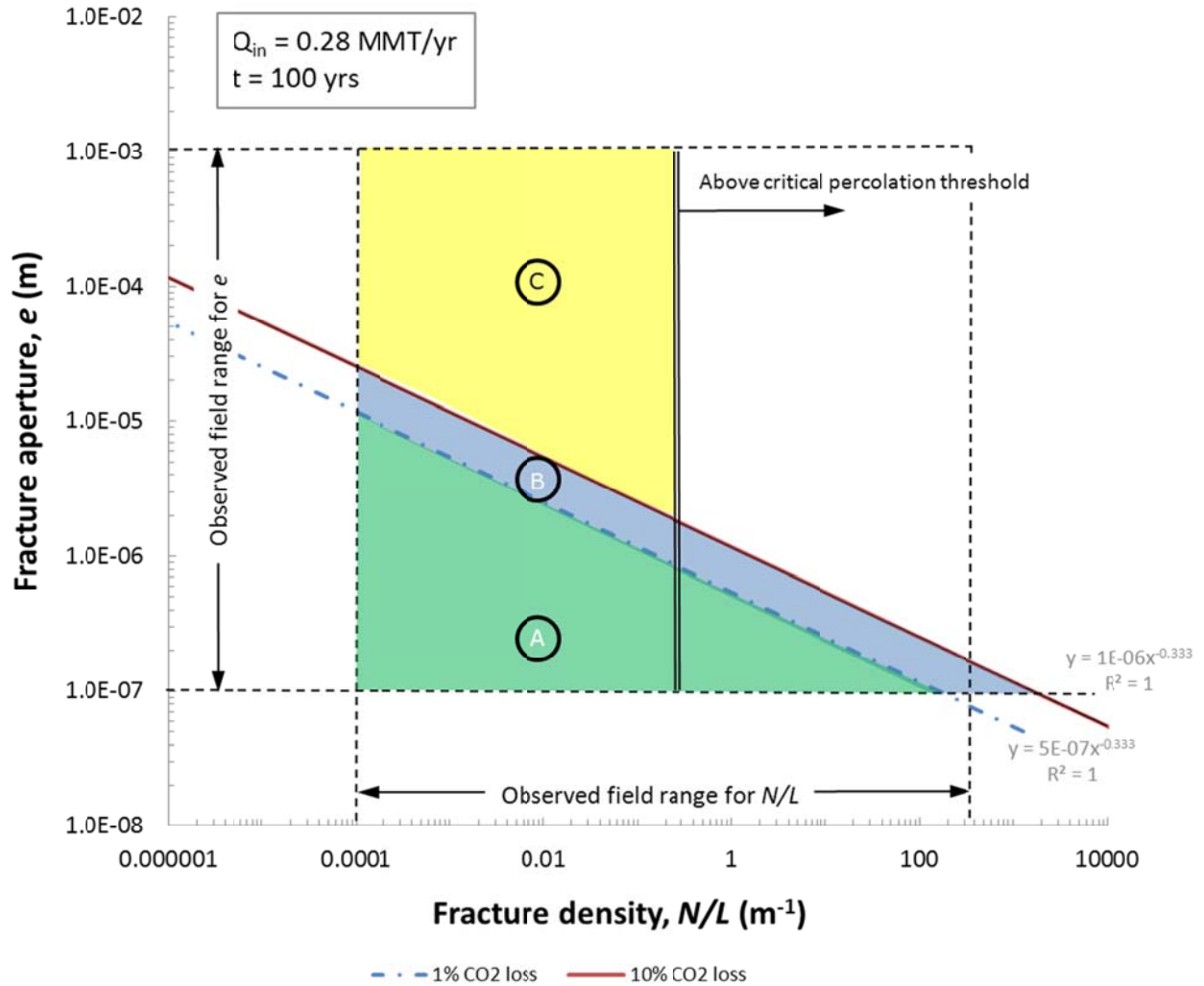
FIGURE 3.5: Fracture aperture vs. fracture density graph showing the model limits to 1% (green shaded area "A) and 10% CO_2 loss (blue shaded area "B"), given the fracture properties of Table 3.2 and 3.3. The yellow shaded area "C" respresent the range of e and N/L observed in field studies, predicted to have CO_2 loss above 10% but are limited for flow by percolation constraints. The vertical double line and arrow represent the cut-off and direction for values above the percolation threshold, p_{pc} = 5.6. Vertical dashed lines and double pointed arrows represent the overlap of modeled values with observed ranges for fracture density listed in Table 3.3.

CHAPTER 4

IMPACT OF UNCERTAINTY IN FRACTURE APERTURE AND DENSITY ON PREDICTING CO_2 LOSS AND CAPROCK HYDRAULIC FRACTURE PROPERTIES ASSOCIATED WITH LONG-TERM CO_2 STORAGE[3]

ABSTRACT

Proposed performance goals for large-scale geological storage of CO_2 include achieving 99% storage permanence within storage reservoirs. In a recent review within regions of interest for pilot and large-scale CCS projects, caprock formations showed a common occurrence of fractures. These fractures were typically not fully characterized and had unknown regional extent and connectivity. The goal of this study was to investigate how uncertainty in reservoir and caprock fracture properties affected the ability of a conceptual caprock-reservoir system to meet CO_2 storage performance goals, and to determine the sensitivity of each parameter associated with meeting these goals. This work was aimed at answering three important questions: 1) is there sufficient support from observed data to assume that < 10% CO_2 loss from a caprock is very likely (i.e. >95%) when fractures are present within the caprock? 2) Which transport properties within a fractured caprock-reservoir system are strongly associated with meeting maximum CO_2 loss targets? 3) Do these associations change significantly under increasing CO_2 loss constraints or uncertainty in system parameters? A probabilistic framework using a Generalized Sensitivity Analysis was applied to the integrated analytical CO_2 loss model of Chapter 3 to examine the influence of uncertainty in a caprock fracture properties on the ability of the caprock to contain 90% to 99% of injected supercritical CO_2 (scCO_2) over 100 years.

---

[3] Coauthored by Gregory V. Lowry, David A. Dzombak, and Mitchell J. Small. In preparation for publication in peer reviewed journal.

Results suggest (1) parameters meeting the 1 – 10% CO_2 loss criteria were rare events and more data is needed to better characterize fractures in caprocks considered for long-term CO_2 storage. (2) Suitable fracture properties are dependent on reservoir uncertainty. (3) Fracture porosity was a good diagnostic parameter for caprock suitability to meet CCS goals. Fracture porosity remained practically immeasurable (e.g. < 0.001%) with a low probability (<10%) of measured values exceeding 0.01%, and was independent of system size. (4) Fracture permeability had the strongest association with CO_2 loss, with a high probability (>90%) that caprocks which met CCS goals had values were < 10^{-17} m^2. (5) Uncertainty in the reservoir hydraulic properties exerted and increased influence on suitable caprock fracture properties as tighter constraints for CO_2 loss were placed on the system. This study suggests a low tolerance for well-connected caprock fractures within a pre-existing fracture network. Caprocks within the area of influence of stored CO_2 plume should be examined further for their aperture size distribution and connectivity.

4.1 INTRODUCTION

Proposed performance goals for large-scale carbon capture and storage (CCS) projects have either a goal of achieving 99% storage permanence in reservoirs, or a maximum CO_2 surface leakage rate of 0.01 – 0.1% of CO_2 mass inventory per year (Hepple and Benson, 2005; NETL, 2011). A critical component in meeting the performance criteria is the ability of the overlying caprock to contain the injected CO_2 permanently. In a recent review within regions of interest for pilot and large-scale CCS projects, caprock formations showed a common occurrence of fractures. These fractures were typically not fully characterized and had unknown regional extent and connectivity (Griffith et al., 2011; Chapter 2).

The goal of this study was to investigate how uncertainty in reservoir and caprock fracture properties affected the ability of a conceptual caprock-reservoir system to meet CO_2

storage performance goals, and to determine the sensitivity of each parameter associated with meeting these goals. The work was aimed at answering three questions: 1) is there sufficient support from observed data to assume that CO_2 loss from a caprock of < 10% is very likely (i.e. >95%) if fractures are present within the caprock (IPCC 2005)? 2) Which transport properties within a fractured caprock-reservoir system are strongly associated with keeping targeted CO_2 loss? 3) Do these associations change significantly under increasing CO_2 loss constraints or system uncertainty?

To address these questions, a probabilistic framework was applied to the integrated analytical CO_2 loss model of Chapter 3. The probabilistic methods employed examined the influence of uncertainty in fracture aperture and density on predicting caprock hydraulic properties associated with meeting CO_2 loss criteria for CCS.

4.2 BACKGROUND

4.2.1 RISK ASSESSMENT APPROACHES FOR CCS

Analyzing the risk associated with each CCS project is a process that primarily involves three aspects: risk identification, risk characterization, and risk management (IEAGHG 2009; NETL 2011). For CO_2 storage, risk analysis is aimed at addressing the Features, Events, and Processes (FEPs) that could contribute to, or prevent, unplanned CO_2 migration from the overlying caprock – or confining zone (NETL 2011; IEAGHG 2009). Each of the aspects of the risk analysis is impacted by uncertainty. Uncertainty can be qualitative or quantitative. For CCS, qualitative assessments seek to characterize the general state of knowledge about the risks and overall weight of evidence concerning the nature and source of the hazard (McDaniels and Small 2004). This can include the examination of possible implications, severity, and likelihood of these FEPs (McDaniels and Small 2004; NETL 2011). Once specific measures for a risk outcome are identified and methods and models are developed to predict these quantities, then quantitative uncertainty analysis can provide

insight into the probability of occurrence of different values of these measures (McDaniels and Small 2004).

Pre-existing fractures are a common occurrence within formations considered as sealing units for CO_2 storage and can be an important feature to characterize for uncertainty in their hydraulic properties, since they are considered fast paths for fluid flow and CO_2 loss (Berkowitz, 2002; Griffith et al., 2011; Shukla et al., 2010; Tsang et al., 2008). It is generally assumed that fracture patterns exhibited in outcrop rock strata are also present in subsurface with smaller aperture sizes (Nelson 2003).

4.2.2 FRACTURE CHARACTERIZATION FOR CO_2 TRANSPORT

Natural occurring fractures form a network quantitatively evaluated with the determination of fracture aperture and density, and fracture connectivity (Aguilera, 1980; Berkowitz, 2002; Lemonnier and Bourbiaux, 2010a; Lemonnier and Bourbiaux, 2010b; Nelson, 2001; Van Golf-Racht, 1982). The principal properties of a fracture network that control permeability in a fractured crystalline rock are aperture and density (Snow, 1969; Warren and Root, 1963). Data that describe the properties of a fracture network are often sparse, requiring an import of observed fracture geometries from surface outcrops (e.g. scan line, satellite image analysis) in addition to seismic, core, well logging and imaging analysis (Bonnet et al., 2001; Nelson, 2001). Uncertainty within the data collected for the fracture network parameters can affect the characterization of risk for leakage of CO_2 from the storage reservoir.

Modeling fluid transport in fractured media is generally done using either continuum or discrete models. The continuum model type is the classical engineering approach where a multi-porosity approach is adopted to represent flow in two porous systems: a rock matrix with high porosity and low permeability and a fracture network with low porosity but high permeability (Barenblatt et al., 1960; Kazemi, 1969; Warren and Root, 1963). Properties

103

used for effective fluid transport (i.e. fracture permeability) are treated as averages corresponding to a representative elementary volume (REV) of the system. Discrete network models differ from continuum models primarily in the method used for generating fracture networks. Discrete models have the ability to capture correlations between naturally hierarchical, scale-dependent effective fracture transport properties (e.g. fractal models), as well as the interconnectivity effects of the fracture network (percolation models). However, because of their complexity and substantial computational expense for simulating large systems, hybrid models have been developed (Berkowitz, 2002; Hahn et al., 2010; Jing, 2003; Sahimi, 1995)

Common to both continuum and discrete modeling approaches is the need to characterize the distribution of fracture permeability, degree of fracture connectivity, and fracture porosity within the formation (Aguilera, 1980; Berkowitz, 2002). The stochastic continuum approach taken in this study is a hybrid which honors the scaling behavior and correlation of fracture properties with system size while being relatively less computationally expensive in order to capture large-scale CO_2 transport behavior.

4.2.3 PREVIOUS STUDIES AND CURRENT APPROACH

Relatively few studies have examined the role of fracture properties on CO_2 transport across a fractured caprock, and fewer still have considered how the uncertainty in the caprock hydraulic fracture properties might influence CCS risk assessment or caprock performance (Chapter 3; Oldenburg et al., 2009; Smith et al., 2011; Zhang et al., 2010). Most studies focus on assessing the potential for geomechanical failure of a seal due to pressure buildup in a reservoir upon injection of a fluid, or wellbore leakage (Rohmer and Bouc, 2010; Rutqvist et al., 2007; Rutqvist et al., 2008; Smith et al., 2011; Celia et al., 2011; Kopp et al., 2010; Nordbotten et al., 2005; Nordbotten et al., 2009). If numerous wells exist in a potential field for CO_2 storage, poorly completed wells offer direct pathways

that can compromise the capacity of a storage unit (NETL 2009, Nordbotten et al., 2009). Caprocks are generally low permeability formations, where in an enclosed geologic structure, the potential exists for reservoir overpressure and geomechanical failure of caprock (Chapter 2; Economides 2009; Rutqvist et al., 2007; Rutqvist et al., 2008).

In this study, a generalized (or global) sensitivity Analysis (GSA) approach was used to examine the behavior of the analytical CO_2 loss model of Chapter 3 over a multidimensional region of parameter space defined by *a priori* distributions of each model input (Mishra et al. 2009; Spear and Hornberger 1980). The GSA technique provided a means for incorporating prior knowledge gained from literature or observed field data - relevant to CCS activities, to examine the uncertainty and sensitivity of reservoir and caprock fracture parameters under a set of classified CO_2 loss responses.

The GSA technique employs a Monte Carlo (MC) methodology where three simulation experiments, i.e. cases, were conducted using two different sampling schemes in order to characterize parameter associations and uncertainty within the system. One of the advantages of the GSA is that the model building process can capture non-additive behavior as well as synergy effects between input parameters (Mishra et al. 2009).

The first case (Case 1) used a simple random sampling scheme where uncertainties in the fracture aperture and density, along with several reservoir properties, propagated through the analytical CO_2 loss model to produce outputs classified under three levels of CO_2 loss: 100%, 10%, and 1%. All simulated input variables were assumed to be independent and identically distributed (iid). The simulation results of the first case were used to statistically test the probability of having < 1% loss in a fractured caprock – reservoir system, given a range of observed data and assumed probability distribution for each input variable.

The second case (Case 2) used an importance sampling (IS) scheme to increase the model outputs within the 1% and 10% classified CO_2 loss response under the system conditions of Case 1. As will be shown later, the first case revealed that CO_2 loss – and its associated hydraulic parameters, for the 1% and 10% categories were rare events (see section 4.4). Importance sampling is the principal method used to attack rare event simulation within large and/or nonlinear stochastic systems in order to obtain estimates for key performance parameters (Bucklew 2004; Helton et al 2006; Hesterberg 1995; 1988). Importance sampling (IS) is a variance-reduction technique applied to Monte Carlo simulations in order to estimate a 'target' distribution of a particular low-probability performance function (e.g. CO_2 loss), using observations from a different 'design' probability distribution. The aim is to increase the efficiency of the of the MC simulation by selecting a 'design' probability distribution that makes the occurrence of the rare event more frequent – *without* increasing the number of realizations in the MC method, and then correcting the output results with weights that compensate for the biased sampling method (Hesterberg 1998). Model outputs applying the IS scheme were then used to draw rank order correlation coefficients and descriptive statistics to address which transport properties within the system are associated with each categorical CO_2 loss

The third case (Case 3) examined the model response under a reduced level of system uncertainty using the IS Monte Carlo method. In this case, only caprock fracture properties are uncertain within the system, where reservoir conditions are held constant at benchmark conditions (Class et al. 2009). Model outputs were then used to with Kolmogorov–Smirnov tests to addresses the implications of system level uncertainty on predicting CO_2 loss.

4.3 METHODOLOGY

A global sensitivity analysis (GSA) technique was applied to the analytical CO_2 loss model of Chapter 3, using a Monte Carlo (MC) method to model parameter uncertainty and sensitivity under two different sampling schemes: Direct random sampling and importance sampling. The basic idea in the MC method is that an array (i x j) of random output results $Y_i^j(x)$ are functions of uncertain inputs X_i^j which had randomly generated values x_i described probability distribution functions (PDFs) $f_X(x_i)$ (Helton et al 2006). Generation of random sample inputs x_i is dependent not only on each associated PDF but also on the sampling scheme chosen for the MC experiment.

Direct (or simple) random sampling is a sampling design where units are collected from the entire population independently of each other, all being equally weighted and likely to be sampled (e.g. independent and identically distributed – iid) (Baron 2007). For importance sampling, samples are not equally likely, but are generated according to carefully selected PDFs designed to provide greater coverage of low probability/high consequence subset values for X_i (Helton et al. 2006).

4.3.1 DIRECT AND IMPORTANCE SAMPLING

Classical importance sampling is designed for the estimation of MC integration, or equivalently the expected value of a random variable (Hesterberg 1995; Hammersley and Handscomb 1964). The primary output function of interest is the fraction of CO_2 loss from the storage reservoir ξ_{CO2}. In the direct MC simulation of Case 1 the expected value for the fractional CO_2 loss is expressed as:

$$\mu_{\xi_{CO_2}} = \mathrm{E}\left[\xi_{CO_2}(X)\right] = \int \xi_{CO_2}(x)f(x)dx \qquad (4.1)$$

where $\xi_{CO2}(X)$ is an output function based on a set of random input variables X^j with known PDFs $f(\cdot)$. The expected value of ξ_{CO2} is estimated with:

$$\widehat{\mu}_{\xi_{CO_2}} = \frac{1}{n} \sum_{i=1}^{n} \xi_{CO_2}(X_{i=1}^j, X_2^j, \ldots, X_n^k) \tag{4.2}$$

where a sequence of $n = 10{,}000$ i.i.d random numbers $(X_1, X_2, \ldots, X_n)$ are generated from the marginal densities of k independent variables $(X^1, X^2, \ldots, X^k)$.

Under importance sampling, the expected value for the fractional CO_2 loss for Case 2 and 3 is now estimated with:

$$\widehat{\mu}_{\xi_{CO_2}} = \frac{1}{n} \sum_{i=1}^{n} \xi_{CO_2}\left({}^*X_i^j\right) \cdot \frac{\prod_{j=1}^{k} f\left({}^*X_i^j\right)}{\prod_{j=1}^{k} g\left({}^*X_i^j\right)} \tag{4.3}$$

where ${}^*X_i^j$ represent the sequence i of iid random numbers generated by a new set of densities $g(\cdot)$ for the input variables j. The densities $g(\cdot)$ are known as the importance sampling (or design) distributions and equation 4.3 is unbiased if $g(x) > 0$ when $\xi_{CO2}(x) \cdot f(x) \neq 0$ (Bucklew 2003). The product ratio:

$$W\left({}^*X_i\right) = \frac{\prod_{j=1}^{k} f\left({}^*X_i^j\right)}{\prod_{j=1}^{k} g\left({}^*X_i^j\right)} \tag{4.4}$$

is a weight function that is applied to each realization of the output function (e.g. ξ_{CO2}) to unbias results. The weight function is based on the likelihood ratio between the estimated 'target' and 'design' joint distributions (Bucklew 2003; Hesterberg 1995;1988). It is a probability ratio computed for each realization by using the known cumulative distribution functions (CDFs) of the target and design distributions, their associated parameters, and

generated random values. In summary, a simple algorithm was applied to the Microsoft®

spreadsheet for Cases 2 and 3:

1. Sample model inputs X_i from $g(^*X^j)$ instead of $f(X^j)$

2. Compute desired model outputs $Y_i^j(^*X_i)$ (e.g. ξ_{CO2}, k_f, r_{max},...) from a* and b* inputs on Table 4.1 and 4.2

3. Weight each output by $W(^*X_i)$

4. Repeat 1-3 for every row i

4.3.2 STRATIFIED DEFENSIVE MIXTURE DISTRIBUTION

In Cases 2 and 3, a stratified defensive mixture distribution was chosen to represent

the importance sampling distributions $g(\cdot)$ (Hesterberg 1995, 1988). The distribution had

the form:

$$g(^*X) = \lambda_{IS} f(X) + (1 - \lambda_{IS}) g_0(^*X) \tag{4.5}$$

where $0 < \lambda_{IS} < 1$, $f(X)$ the original input variable PDF and associated parameters, and g_0 the

original input variable PDF with parameters shifted (*) to the region known to yield ξ_{CO2} <

10%. In a stratified mixture only $n\lambda_{IS}$ realizations are taken from f and $n(1-\lambda_{IS})$ from g_0, and

for this study each set of realizations were generated independently.

Figure 4.1 illustrates the IS sampling scheme in this study where equation 4.6 is practically

in the form:

$$g(^*X) \rightarrow \lambda_{IS} U(a,b) + (1 - \lambda_{IS}) U(a^*, b^*) \tag{4.6}$$

since all the random inputs are uniform (see Table 4.1 and 4.2)and the shifted parameters

were taken from Case 1 model results for input ranges occurring within the classified ξ_{CO2} <

10%. The λ_{IS} parameter is set to 0.1, as recommended for systems demanding accurate estimation of small probabilistic that use the integration estimate (equation 4.4) for IS (Hesterberg 1995). Appendix C elaborates more on the direct and IS Monte Carlo method used in this study.

4.3.3 PARAMETER UNCERTAINTY DESCRIPTION

The three MC simulation experiments were conducted in Microsoft™ Excel® using 10,000 sample realizations of the caprock – reservoir physical scenario depicted in figure 4.2. Summaries of the three cases are given in Table 4.1 and 4.2, which also list the parameter ranges and probability distribution types assumed for each model input. Selection of input parameters subjected to MC experiments was based on two factors: 1) sensitivity to CO_2 loss and 2) model complexity. Model complexity is significantly increased if accounting for fluid phase changes at various depths. A preliminary parametric sensitivity analysis, conducted on all major variables of the analytical model, showed that the range of fluid properties were not as significant to overall CO2 loss as other parameters (Appendix C.1). Therefore, 'full' uncertainty modeling in the MC cases considers depth and fluid properties to be constant.

In all cases, each independent random variable was modeled with a uniform distribution U(a,b) based on parameter ranges (a,b) relevant to CCS activities. The exceptions were the fracture aperture and density. These two random variables had uncertain *hyper-parameters* that defined their power law (pareto) distribution. The *hyper-parameters* of the fracture aperture and density were uniformly distributed within reported limits. Fracture density was were treated as a model output that was a function of the critical number of fractures N_c necessary for percolation, fracture length PDF exponent parameter (*a*), and CO_2 plume extent (r_{max}) described below in section 4.3.4 and Appendix B.3.

4.3.4 KEY MODEL OUTPUT DESCRIPTION

The analytical CO_2 loss model of Chapter 3 considers one-dimensional vertical flow of $scCO_2$ through the fracture apertures of the caprock in contact with the $scCO_2$ plume, expanding within the reservoir (see figure 4.2):

$$\xi_{CO_2} = \frac{Mt}{2b_{res}\phi_m(1-s_{wr})} \cdot \frac{1}{\mu_c} \cdot \frac{e^3}{12} \cdot \frac{N_c}{L} \cdot \left[\frac{\overline{p_1} - p_2}{b_{cap}} - \rho_c g \right] \qquad (4.7)$$

where changes in the volumetric percent $scCO_2$ loss over time ξ_{CO2} is a function of the mobility ratio M (dimensionless)of the brine to CO_2 fluid, $scCO_2$ injection time t (sec), reservoir thickness b_{res} (m), residual brine saturation s_{wr} (dimensionless), fracture aperture e (m), critical fracture density N_c/L (m^{-1}) – i.e. number of fractures per unit length within exposed caprock above percolation threshold, $scCO_2$ viscosity μ_c (kg m^{-1} s^{-1}), dependent average reservoir pressure $\overline{p_1}$ (Pa), hydrostatic pressure above caprock p_2 (Pa), caprock thickness b_{cap} (m), $scCO_2$ density ρ_c (kg m^{-3}) density, and g (m s^{-2}) the gravitational acceleration constant.

Another key model output of focus in this study is the intrinsic fracture permeability of equation 4.1

$$k_f = \phi_f \cdot \frac{e^2}{12} = \left(\frac{N_c}{L} e \right) \cdot \frac{e^2}{12} \qquad (4.8)$$

where fracture porosity is represented by ϕ_f (dimensionless) and hydraulic fracture aperture, e (m). The critical number of fractures in the system N_c were dependent on the CO_2 plume 2D length L (aka system size), caprock thickness b_{cap}, and the coefficient of

proportionality α_c which reflected the fracture density at critical percolation threshold p_{pc} ~ 5.6 necessary for percolation.

$$N_c = \alpha_c(L) \cdot b_{cap}^{-a} \tag{4.9}$$

where $L = 2r_{max}$ for our 2D system size (see figure 4.1) and a is the power law fracture length exponent. Solutions for critical fracture density that account for the different regimes of fracture connectivity are found in Appendix B.3 and were adopted from Zhang et al. (2010) and Bour and Davy (1997).

The volumetric average reservoir pressure $\overline{p_1}$ of equation 4.7 was an approximation for pseudo-steady state pressure pressure distribution based on the derivations of (Dake, 1978; Lee and Wattenbarger, 1996) with justification for CCS applications in (Nordbotten et al., 2004).

$$\overline{p_1}(r,t) = p_i + \frac{Q_{in}}{2\pi\lambda_t b_{res}} \ln\left[\frac{r_{max}(t)}{r_w} - \frac{3}{4}\right] \tag{4.10}$$

with p_i the initial reservoir pressure, taken to be hydrostatic; Q_{in} (m^{3}s^{-1}) the volumetric flow rate of injected CO$_2$, λ_t the *total* fluid mobility of the scCO$_2$ and brine phases in the reservoir; and r_w (m) is the injection well radius - assumed to be a 7 inch diameter well (e.g. 8.89 cm). The maximum radial extent of an ideal scCO$_2$ plume over time r_{max}, migrating through a reservoir in contact with the caprock, is a model developed by Nordbotten et al. (2005):

$$r_{max} = \sqrt{\frac{MQ_{in}t}{\pi b_{res}\phi_m(1-s_{wr})}} \tag{4.11}$$

Further explanation of the parameters in equations 4.7 – 4.11 and the assumptions and constraints of the model are found in Chapter 3.2 and Appendix B. Of note were the pressure constraints, where average pressure in reservoir had to exceed capillary entry pressure for $scCO_2$ but be equal to or below 90% of the estimated fracture pressure.

4.3.5 HYPOTHESIS TESTING AND STATISTICAL ANALYSIS

Three questions were posed in this study. The first question asks how probable it is that 90 – 99% CO_2 storage will be realized (e.g. ≥ 95% probability) for large-scale projects, if fractures are present in the caprock (IPCC 2005), given the range of data examined in Chapter 2 and 3, and assumed to represent caprock fractures *in-situ*?

The data used for modeling fracture aperture and length were taken from a broad range of sources that covered core (cm) to field scale (km) fracture networks. Primarily, the data were centered around studies on fractured reservoirs or fault zones of commercial or tectonic interest. Data on the statistical fracture properties of caprocks used in CCS operations were limited. However, data on caprock thickness – used a proxy for fracture length in this study, were taken from studies covering active and potential CCS sites.

The first question was addressed by testing the hypothesis that the probability of the GSA fraction of CO_2 loss ξ_{CO2} given a categorical loss of <10% is equal to the assumed probability p_0 of 95%:

$$H_0: \qquad \widehat{p}_{\xi_{CO_2}} \Big| \xi_{CO_2} < 10\% = p_0 = 0.95 \tag{4.15}$$

$$H_A: \qquad \widehat{p}_{\xi_{CO_2}} \Big| \xi_{CO_2} < 10\% < p_0 \tag{4.16}$$

The null hypothesis H_0 was tested against a one-sided left tail alternative H_A where we are only interested if the probability of having less 10% CO_2 loss in the system falls below 95%. A one-sample Z test on proportions was performed to test the significance (P-value) of Case 1 results for fractional CO_2 loss ξ_{CO2} .

$$Z = \frac{\widehat{p}_{\xi_{CO_2}} - p_0}{\sqrt{\dfrac{\widehat{p}_{\xi_{CO_2}}(1 - \widehat{p}_{\xi_{CO_2}})}{n}}} \qquad (4.17)$$

where n is the count of total realizations that met the <100% CO_2 loss category and

$$\widehat{p}_{\xi_{CO_2}} = \frac{n_{\xi_{CO_2}}}{n} \qquad (4.18)$$

where $n_{\xi_{CO_2}}$ is the number of simulation realizations when function $\xi_{CO2} < 1\%$ or 10%.

The second question asks which transport properties within the fractured caprock-reservoir system are strongly associated with keeping targeted CO_2 loss. Scatter plots and Spearman's rank coefficients of correlation r_s were drawn from Case 1 and 2 results to address this question. The GSA technique allowed for the examination of direct and induced correlations from the classified model outputs and their associated inputs. The rank correlation coefficients provide a nonparametric measure of the degree of association (0-1) between the relative magnitudes of the parameter pairs, without the assumption of linearity (Gibbons 1976).

The third question asks if the identified transport properties associated with CO_2 loss change significantly when different loss constraints or levels of uncertainty are placed on the system. In other words, the first half of the question asks if are there any trends noticed in the association behavior among the parameters examined. The second half of the question asks if uncertainty in the reservoir can significantly affect the prediction of CO_2 loss through a fractured caprock. These were addressed by observing trends in r_s and with a two-sided Kolmogorov-Smirnov (K-S) two-sample test on the CDFs of ξ_{CO2} model output for Case 2 and Case 3. This was to test if there was a significant statistical difference in estimated CO_2 loss probabilities when modeling with fixed reservoir properties.

$$H_0: \qquad F_2(x) = F_3(x) \tag{4.19}$$

$$H_A: \qquad F_2(x) \neq F_3(x) \tag{4.20}$$

$$\text{K-S:} \qquad D = \text{maximum} \left| F_2(x) - F_3(x) \right| \tag{4.21}$$

where $F_2(x)$ and $F_3(x)$ represent the empirical CDFs of CO_2 loss in Case 2 and 3 respectively. D statistic tests if the sampling situations produce mutually independent sets of random CO_2 loss observations of from their respective case sizes, n_2 and n_3.

In addition, class membership probabilities (or 'class conditional' distributions) were derived for hydraulic fracture permeability and porosity. The class membership probabilities are Bayesian classifiers that used the observed data to describe the probability for which a measured fracture property would belong to caprocks meeting either 1% or 10% CO_2 loss criteria.

$$P(C \mid Y = y) = \frac{\hat{f}(y \mid C)P(C)}{\hat{f}(y \mid C)P(C) + \hat{f}(y \mid \overline{C})P(\overline{C})} \tag{4.22}$$

where Y is the output result for either k_f or ϕ_f data sets; y observed values of the data sets; $\hat{f}(\cdot)$ the empirical PDF of k_f or ϕ_f outputs classified under mutually exclusive sets of categorical CO_2 loss $(C, \overline{C})$; $C = \xi_{CO2} < 1\%$ or 10%; $\overline{C} = \xi_{CO2} > 1\%$ or 10%; $P(C)$ probability (prior) of any caprock having less than 1% or 10% CO_2 loss regardless of any data or information; $P(C \mid Y = y)$ probability (posterior) that a measured caprock fracture permeability or porosity value belong to caprocks meeting classified CO_2 losses of 1% or 10%. We assume an information less prior $P(C) = P(\overline{C}) = 0.5$ so that:

$$P(C \mid Y = y) = \frac{\hat{f}(y \mid C)}{\hat{f}(y \mid C) + \hat{f}(y \mid \overline{C})} \tag{4.23}$$

Each empirical PDF was estimated using a Gaussian kernel density estimator. Kernel density estimation (KDE) is similar in fashion to a histogram, where a non-parametric approach is taken for estimating a probability density from simulated data. However, a Gaussian KDE allows for a 'smoothing' curve of the density distribution using a series of standard normal curves for its kernel K (Kroese et al. 2011; Silverman 1986):

$$\widehat{f}(y) = \frac{1}{nh} \sum_{i=1}^{n} K\left(\frac{y - Y_i}{h}\right) \tag{4.24}$$

with y representing a graphical plot x-axis value for k_f or ϕ_f , Y_i the realization value of random output variable Y, n total realizations (i.e. 10,000), h bin width. Appendix D elaborates on the KDE algorithm applied to the simulated data in this study.

Descriptive statistics were also obtained for major variables of the MC simulation experiments. Statistics included minimum, maximum, median, mean, standard deviation, coefficient of variation, and 90th and 10th percentiles. Resulting statistics emphasize the central tendencies of the variables over point estimates (e.g. mean, standard deviation) since site specific data was not used. However, the mean and standard deviations were necessary for Gaussian KDE. Tabulated results of the descriptive statistics for each case are found in Appendix E.

4.4 RESULTS AND DISCUSSION

The three MC experiments addressed questions on the sufficiency of fracture aperture and length data to support CCS performance goals, as well as, the effect of uncertainty and system CO_2 loss constraints on transport properties associated with target goals. Case 1 described the geological situation where there was 'full' uncertainty among the transport properties of a reservoir and fractured caprock in a conceptual caprock-reservoir system. Case 2 examined this same system of full uncertainty under an

importance sampling MC method that was geared to examine the parameter space of rare events, which the results of Case 1 proved the conceptual system to be for the range of data applied. Case 3 examined the situation of 'partial' uncertainty, where only the caprock fracture properties were uncertain. Case 3 employed the same IS MC method except that reservoir properties are fixed based on Class et al. (2009) benchmark problem for CO_2 storage. The bulk of discussion focuses on the results from Case 2 and 3 where more statistical inferences could be drawn.

4.4.1 CO_2 LOSS PROBABILITY GIVEN RESERVOIR AND CAPROCK FRACTURE UNCERTAINTY

Figure 4.3 shows the resulting cumulative distribution functions of Case 1, 2, and 3 for the fractional loss of CO_2 from the system, under direct and importance Sampling MC methods. Analysis of the empirical CDFs addressed the first and third questions posed in this study. Three observations were taken from Figure 4.3: 1) the probability for having < 1% CO_2 loss was low (<28%) for the range of hydraulic properties sampled. 2) For a significance level of 0.01, the Z-test gave a P-value = 0. This meant that the null hypothesis of being very likely to store >90% of CO_2 was not supported by the data examined when well-connected fractures are present in an overlying caprock, assuming the analytical model of Chapter 3 and that the range of hydraulic properties used was representative of the fractured caprocks. 3) K-S test on the CDF of Case 2 and 3 showed that reservoir uncertainty significantly affected the prediction of CO_2 loss. This addressed, in part, the question of whether the range of hydraulic fracture properties within the caprocks that met < 10% CO_2 loss were statistically dependent on reservoir uncertainty.

4.4.2 FRACTURE HYDRAULIC BEHAVIOR GIVEN UNCERTAIN FRACTURE APERTURE AND DENSITY CHARACTERISTICS

Figure 4.4 and Figure 4.5 show the cumulative distribution functions of the fracture permeability and porosity under the 1% and 10% CO_2 loss constraint for Case 2. Fracture permeability and porosity were key model outputs where analysis of their empirical CDFs,

along with their probability association to a set of classified CO_2 loss, gives insight into idealized diagnostic limits for hydraulic fracture properties in a highly uncertain geological system.

Figure 4.4 shows a wide range for fracture permeability, $10^{-23} – 10^{-14}$ m^2, can exist for 1 – 10% CO_2 loss under full uncertainty within the system. The K-S statistic showed that the two trends were statistically independent within this narrow constraint window. The 90th and 10th percentiles show the central tendency of k_f, where for the categorical loss of 10% CO_2, 90% of its values lied between $10^{-20}– 10^{-16}$ m^2. The percentile range did not change significantly with an increased constraint of 1% ($10^{-20} – 10^{-17}$ m^2). This suggests that though the specific underlying distribution governing k_f was not known, it was very likely that fracture permeability was in the micro-Darcy µD (e.g. 10^{-18} m^2) range. This is in keeping with observations in Chapter 3 and is expounded in discussion of class membership probability.

Two striking features were noteworthy with fracture porosity behavior. 1) Fracture porosity, unlike permeability, did not significantly change over the level of uncertainty in the system (e.g. Case 2 vs. Case 3) or constraint of CO_2 loss (e.g. 1% vs. 10%). The 90th percentile values in figure 4.5 show the same order of magnitude, 10^{-4} %, under 10 or 1% CO_2 loss, and between full and partial (not shown) uncertainty in system. 2) Suitable ϕ_f ranges were most likely to be practically immeasurable, compared to the assumed range of observed values in Chapter 3. The results suggest that fracture porosity may be a good diagnostic parameter for suitable caprock integrity at the 1 - 10% CO_2 loss criterion level. An observation examined further in the following sections.

Uncertainty within fracture permeability and porosity stemmed from a narrow range of fracture apertures and a relatively broad range of critical fracture densities. In every case and under every system constraint, fracture aperture size had a 90th percentile values

between $10^{-8} - 10^{-6}$ m. In Case 2, critical fracture densities ranged from $10^{-3} - 2$ m^{-1} within the 90th and 10th percentiles.

4.4.3 CLASS MEMBERSHIP PROBABILITIES FOR FRACTURE PERMEABILITY AND POROSITY

Figure 4.6 and Figure 4.7 shows the trend in probability that a measured value for fracture permeability or porosity belongs to a class of caprocks meeting 1% or 10% CO_2 loss. These figures showed the trends in the posterior probability of classified CO_2 loss conditioned on MC Case 2 results and provide summary diagnostic behavior for k_f and ϕ_f given the constrained data set and analytical model examined. For example, though there was a broad range of k_f values that met the 1% or 10% CO_2 loss criteria (figure 4.5), there was only a 10% chance of having a measured value above 10^{-15} m^2 belong to a caprock exhibiting 10% CO_2 loss. Similarly, there was a 90% chance of k_f values below 10^{-17} m^2 belonging to the class of caprocks meeting less than 10% loss. The sharp transition in k_f on Figure 4.6 supports the notion that fracture permeability was a strong indicator for CO_2 loss.

Figure 4.7 showed non-unique class probability for fracture porosity, where ϕ_f plateaued in the $10^{-4} - 0.001\%$ range. However, there was a low probability ($\leq 30\%$) of having either measurable porosities (i.e. $\phi_f > 0.001\%$) or non-unique behavior occurring in the class of caprocks meeting 1% or 10% CO_2 loss.

Figure 4.8 provided a correlation between the fracture permeability and porosity for the different classes of CO_2 loss in Case 2. Figure 4.8 showed the regions within the parameter space of correlation where most of the realizations for classified losses occurred. For example, the region where most of the realizations met the 1% loss criteria, occurred when both k_f and ϕ_f were low. Caprocks with micro Darcy fracture permeability (10^{-18} m^2) also needed to have associated fracture porosity below 10^{-4} % in order to meet the 1% loss criteria. This highlights the need to characterize more than one fracture property (e.g. k_f) in

a caprock since permeability by itself does not account for the particular geometry within the fracture network, which may make the caprock unable to meet CCS goals.

4.4.4 CORRELATION OF CO_2 LOSS TO CAPROCK FRACTURE AND RESERVOIR PROPERTIES

This section examines the scaling behavior and correlations among major transport variables. Figure 4.9 depicts the range and correlation of fracture properties with system size for Case 2. Observations from Figure 4.8 include: 1) an induced negative correlation between fracture aperture and permeability with system size, and a positive correlation of fracture density. Scaling for k_f and e with L assumed a power law relationship, yielding $y = 1 \times 10^{-14} x^{-1.60}$ for fracture permeability and $y = 4 \times 10^{-5} x^{-0.83}$ for fracture aperture in the categorical loss of 1% CO_2 from system. 2) The range of k_f values meeting < 10% CO_2 loss decrease with an increase of CO_2 plume footprint. For example, k_f decreases in its maximum value for <10% CO_2 loss from 10^{-14} to 10^{-18} m^2 as the CO_2 plume grows in extent of ~ 5 km. 3) Fracture porosity did not scale with system size. This behavior re-enforces the idea that fracture porosity may be a good diagnostic indicator on its absolute scale, since there was a low probability of sample values exceeding 0.01%. Figure 4.9 reveals that k_f predicts CO_2 transport well when the size of system/CO_2 plume extent is known. However, when the extent of the CO_2 plume is uncertain, ϕ_f may play a more important role since its independent of the CO_2 plume extent.

Table 4.3 shows the Spearman rank correlation coefficient r_s matrix of Case 2 between caprock and reservoir properties only. Extended tables for all cases are available in Appendix F. Correlations in Table 4.3 were segregated into four highlighted ranges: significantly positive - bold green text with $0.45 < r_s < 1$, weakly positive - italic blue with $0 < r_s < 0.45$, weakly negative – italic red text with $-0.45 < r_s < 0$, and significantly negative – bold red text with $-1 < r_s < -0.45$. Capillary entry pressure and vertical pressure gradient

are aggregated parameters categorized under reservoir properties though they consist of individual parameters dependent on caprock properties.

Table 4.3 complements the observations in Figure 4.3 and Figure 4.9 where it shows the reservoir uncertainty affecting CO_2 loss prediction. Examining the 1% CO_2 loss category of the r_s matrix, we observe: 1) capillary entry pressure of caprock-reservoir interface was the most significant reservoir variable directly affecting CO_2 loss and caprock fracture properties. 2) Caprock fracture aperture, and the minimum size that describes its Pareto PDF, exerted more indirect influence on reservoir properties than fracture density – and the parameters describes its Pareto PDF. 3) Fracture permeability has the strongest association to CO_2 loss and it influenced the most by the minimum size of the Pareto PDF for aperture distribution.

The different classified outputs from the GSA represent snapshots of the parameters for different states of the conceptual geologic system (akin to time). Trends in parameter r_s over the classified CO_2 losses allowed insight into the relative significance of any transport or PDF parameter under increasing system constraints on CO_2 loss. Analysis of data in Table 4.3 indicated a general decrease in strength of association of caprock fracture properties to CO_2 loss (e.g. 100% -> 1%), whereas, reservoir properties showed an increased strength of association to caprock fracture properties and overall CO_2 loss. This is particularly true of capillary entry pressure, CO_2 plume/reservoir extent r_{max}, and CO_2 injection time. Therefore, another observation is: 4) reservoir uncertainty exerts and increased influence on caprock fracture properties as tighter constraints for CO_2 loss are placed on the system. A trend that is not clearly seen with Case 1 results (Table 4.4).

4.5 SUMMARY AND CONCLUSIONS

The goal of this study was to examine the uncertainty and sensitivity of fracture properties within a caprock that are associated with acceptable CO_2 storage performance. In particular, a probabilistic framework using a Generalized Sensitivity Analysis was applied to the integrated analytical CO_2 loss model of Chapter 3 to examined the influence of uncertainty in a caprock fracture aperture and density - and related fracture permeability and porosity parameters, on the ability of the caprock to contain 90% to 99% of injected supercritical CO_2 ($scCO_2$) over 100 years.

Three questions were examined with MC case simulations: 1) was there sufficient support from observed data to assume that CO_2 loss from a caprock of < 10% is very likely (i.e. >95%) if fractures were present within the caprock (IPCC 2005)? 2) Which transport properties within a fractured caprock-reservoir system were strongly associated with keeping targeted CO_2 loss? 3) Do these associations change significantly under increasing CO_2 loss constraints or system uncertainty?

Five major observations from the MC case experiments addressed the questions posed in this study. (1) Case 1 results addressed the first question, where it was suggested that the observed data did not support the assumption that CO_2 leakage through a fractured caprock would likely be insignificant. This suggested the need to collect more data that better characterized formations considered for long-term CO_2 storage. The results of Case 1 also showed that parameters meeting the 1 – 10% CO_2 loss criteria were rare events. Case 2 and 3 were designed to explore the parameter space of these rare events, from which the subsequent observations were drawn. (2) Fracture properties that met the < 10% loss criteria were dependent on reservoir uncertainty. This observation was supported with the behavior in CO_2 loss CDF under full (caprock and reservoir) and partial (caprock) system uncertainty. (3) Fracture porosity was identified as a good diagnostic parameter for caprock screening, with a high probability (>95%) that caprocks with fracture porosities < 0.01%

will meet performance goals. (4) Fracture permeability had the strongest association with CO_2 loss, with a high probability (>90%) that suitable permeabilities were $< 10^{-17}$ m^2. In addition, fracture permeability average behavior was determined by aperture distribution but its variance stemmed from critical fracture density uncertainty. (5) Correlations between reservoir parameters and caprock fracture properties became stronger as the CO_2 loss from the system became more constrained.

In an uncertain geological environment where geochemical reactions can be neglected and pressure build-up within the reservoir is managed, this study suggests a low tolerance for well-connected caprock fractures within a pre-existing network. The study suggests that caprocks within the area of influence of a stored CO_2 plume should be examined further for their aperture size distribution and connectivity. In addition, when characterizing the fracture properties of potential caprocks, fracture porosity may be a good screening/diagnostic parameter for defining suitable caprock integrity. Wherein, if a fracture porosity was detected above a threshold limit (e.g. >0.01%), it could indicate potentially unacceptable transport conditions within the caprock for long term CO_2 storage and may warrant further examination for CCS suitability.

Acknowledgments

4.6 REFERENCES

Aarnes, J. et al., 2010. CO2QUALSTORE - Guideline for Selection and Qualification of Sites and Projects for Geological Storage of CO_2. 2009-1425, Det Norske Veritas (DNV), Hovik, Norway.

Aguilera, R., 1980. Naturally fractured reservoirs. The Petroleum Publishing Company, Tulsa, Oklahoma, 703 pp.

Barenblatt, G., Zheltov, I. and Kochina, I., 1960. Basic Concepts in the Theory of Seepage of Homogeneous Liquids in Fissured Rocks. Prikl. Mat. Mekh., 24: 852-864.

Baron, M., 2007. Probability and Statistics for Computer Scientists. Taylor & Francis Group, LLC, Boca Raton.

Berkowitz, B., 2002. Characterizing flow and transport in fractured geological media: A review. Advances in Water Resources, 25(8-12): 861-884.

Bonnet, E. et al., 2001. Scaling of fracture systems in geological media. Reviews of Geophysics, 39(3): 347-383.

Bour, O. and Davy, P., 1997. Connectivity of random fault networks following a power law fault length distribution. Water Resources Research, 33(7): 1567-1583.

Brooks, R.H. and Corey, A.T., 1964. Hydrological properties of porous media, Colorado State University, Fort Collins.

Bucklew, J.A., 2004. Introduction to rare event simulation. Springer-Verlag New York, Inc., New York.

Celia, M.A., Nordbotten, J.M., Court, B., Dobossy, M. and Bachu, S., 2011. Field-scale application of a semi-analytical model for estimation cif CO_2 and brine leakage along old wells. International Journal of Greenhouse Gas Control, 5(2): 257-269.

Chalbaud, C. et al., 2009. Interfacial tension measurements and wettability evaluation for geological CO2 storage. Advances in Water Resources, 32: 98-109.

Chiquet, P., Daridon, J.-L., Broseta, D. and Thibeau, S., 2007. CO_2/water interfacial tensions under pressure and termperature conditions of CO_2 geological storage. Energy Conversion and Management, 48: 736-744.

Class, H. et al., 2009. A benchmark study on problems related to CO_2 storage in geologic formations. Computational Geosciences, 13(4): 409-434.

Condor, J., Unatrakarn, D., Wilson, M. and Asghari, K., 2011. A comparative analysis of risk assessment methodologies for the geologic storage of carbon dioxide. Energy Procedia, 4(0): 4036-4043.

Dake, L.P., 1978. Fundamentals of reservoir engineering. Developments in petroleum science. Elsevier Scientific Publishing Company, Amsterdam, The Netherlands.

DeGroot, M.H. and Schervish, M.J., 2011. Probability and Statistics Addison Wesley 912 pp.

Dressel, B. et al., 2011. CCS Activities Being Performed by the US DOE. INTERNATIONAL JOURNAL OF ENVIRONMENTAL RESEARCH AND PUBLIC HEALTH, 8(2): 300-320.

EIA, 2008. Emissions of Greenhouse Gases in the United States 2007. In: O.o.I.A.a.F. U.S. Department of Energy (Editor). Energy Information Administration.

EPA, 2008. Vulnerability evaluation framework for geological sequestration of carbon dioxide, U.S. Environmental Protection Agency.

EPA, 2011. Draft Underground Injection Control (UIC) Program Class VI Well Site Characterization Guidance for Owners and Operators. 4606M, Office of Water, Environmental Protection Agency.

Freeze, R.A. and Cherry, J.A., 1979. Groundwater. Prentice-Hall, Inc.

Griffith, C.A., Dzombak, D.A. and Lowry, G.V., 2011. Physical and chemical characteristics of potential seal strata in regions considered for demonstrating geological saline CO_2 sequestration. Environmental Earth Sciences, 64(4): 925-948.

Hahn, M., Wallmersperger, T. and Kroplin, B.H., 2010. Discrete element representation of continua: Proof of concept and determination of the material parameters. Computational Materials Science, 50(2): 391-402.

Hammersley, J.M., and Handscomb, D.C., 1964. Monte Carlo Methods. Methuen & Co., London, and John Wiley & Sons, New York.

Hepple, R.P. and Benson, S.M., 2005. Geologic storage of carbon dioxide as a climate change mitigation strategy: performance requirements and the implications of surface seepage. Environmental Geology, 47(4): 576-585.

Helton, J.C., Johnson, J.D., Sallaberry, C.J. , Storlie, C.B., 2006. Survey of sampling-based methods for uncertainty and sensitivity analysis. Reliability Engineering and System Safety, 91: 1175–1209.

Hesterberg T.C., 1988. Advances in Importance Sampling. PhD, Department of Statistics, Stanford University, Stanford California.

Hesterberg T.C., 1995. Average Importance Sampling and Defensive Mixture Distributions. Technometrics, 37(2):185-194.

IPCC, 2005. Intergovernmental Panel on Climate Change: Special Report - Carbon Dioxide Capture and Storage. Bert Metz, Ogunlade Davidson, Heleen de Coninck, Manuela Loos and Leo Meyer (Eds.), Cambridge University Press, UK, pp 431.

Jarrell, P.M., Fox, C.E., Stein, M.H. and Webb, S.L., 2002. Practical aspects of CO2 flooding. SPE Monograph Series, 22. Society of Petroleum Engineers, Richardson, TX.

Jing, L., 2003. A review of techniques, advances and outstanding issues in numerical modelling for rock mechanics and rock engineering. International Journal of Rock Mechanics and Mining Sciences, 40(3): 283-353.

Kazemi, H., 1969. Pressure Transient Analysis of Naturally Fractured Reservoirs with Uniform Fracture Distribution. Society of Petroleum Engineers Journal: 451-462.

Kopp, A., Binning, P.J., Johannsen, K., Helmig, R. and Class, H., 2010. A contribution to risk analysis for leakage through abandoned wells in geological CO_2 storage. Advances in Water Resources, 33: 867-879.

LaGoy, P.K., 1994. Risk assessment: principles and applications for hazardous waste and related sites. Noyes Publications, Park Ridge, N.J., U.S.A.

Lee, J. and Wattenbarger, R.A., 1996. Gas reservoir engineering. SPE Textbook Series. Society of Petroleum Engineers, Richardson, TX.

Lemonnier, P. and Bourbiaux, B., 2010a. Simulation of Naturally Fractured Reservoirs. State of the Art Part 1 Physical Mechanisms and Simulator Formulation. Oil & Gas Science and Technology-Revue De L Institut Francais Du Petrole, 65(2): 239-262.

Lemonnier, P. and Bourbiaux, B., 2010b. Simulation of Naturally Fractured Reservoirs. State of the Art Part 2 Matrix-Fracture Transfers and Typical Features of Numerical Studies. Oil & Gas Science and Technology-Revue De L Institut Francais Du Petrole, 65(2): 263-286.

Metz, B. and Intergovernmental Panel on Climate Change. Working, G., III, 2005. IPCC special report on carbon dioxide capture and storage. Cambridge University Press for the Intergovernmental Panel on Climate Change, Cambridge.

Nelson, R.A., 2001. Geological Analysis of Naturally Fractured Reservoirs. Gulf Professional Publishing, Woburn, Massachusetts.

NETL, 2009. Best Practices for: Monitoring, Verification, and Accounting of CO_2 Stored in Deep Geologic Formations, National Energy Technology Laboratory

NETL, 2011. Carbon Sequestration Program: Technology Program Plan - Enhancing the Success of Carbon Capture and Storage Technologies, Applied Research and Development from Lab- to Large-Field Scale, National Energy Technology Laboratory

Nordbotten, J.M., Celia, M.A. and Bachu, S., 2004. Analytical solutions for leakage rates through abandoned wells. Water Resources Research, 40: W04204.

Nordbotten, J.M., Celia, M.A., Bachu, S. and Dahle, H.K., 2005. Semianalytical solution for CO_2 leakage through an abandoned well. Environmental science & technology, 39(2): 602-611.

Nordbotten, J.M., Kavetski, D., Celia, M.A. and Bachu, S., 2009. Model for CO_2 leakage including multiple geological layers and multiple leaky wells. Environmental science & technology, 43(3): 743-749.

Oldenburg, C.M., Bryant, S.L. and Nicot, J.P., 2009. Certification framework based on effective trapping for geologic carbon sequestration. International Journal of Greenhouse Gas Control, 3(4): 444-457.

Pacala, S. and Socolow, R., 2004. Stabilization wedges: solving the climate problem for the next 50 years with current technologies. Science (New York, N.Y.), 305(5686): 968-972.

Rodosta, T. et al., 2011. US Department of Energy's Regional Carbon Sequestration Partnership Initiative: Update on Validation and Development Phases. Energy Procedia, 4(0): 3457-3464.

Rohmer, J. and Bouc, O., 2010. A response surface methodology to address uncertainties in cap rock failure assessment for CO_2 geological storage in deep aquifers. International Journal of Greenhouse Gas Control, 4(2): 198-208.

Rutqvist, J., Birkholzer, J., Cappa, F. and Tsang, C.F., 2007. Estimating maximum sustainable injection pressure during geological sequestration of CO_2 using coupled fluid flow and geomechanical fault-slip analysis. Energy Conversion and Management, 48(6): 1798-1807.

Rutqvist, J., Birkholzer, J. and Tsang, C.F., 2008. Coupled reservoir-geomechanical analysis of the potential for tensile and shear failure associated with CO_2 injection in multilayered reservoir-caprock systems. International Journal of Rock Mechanics and Mining Sciences, 45: 132-143.

Sahimi, M., 1995. Flow and transport in porous media and fractured rock - from classical methods to modern approaches. VCH Verlagsgesellschaft mbH, Weinheim Germany.

Savage, D., Maul, P.R., Benbow, S. and Walke, R.C., 2004. A generic FEP database for the assessment of long-term performance and safety of the geological storage of CO_2, Quintessa

Seto, C.J. and McRae, G.J., 2011. Reducing risk in basin scale CO_2 sequestration: a framework for integrated monitoring design. Environmental science & technology, 45(3): 845-859.

Shukla, R., Ranjith, P., Haque, A. and Choi, X., 2010. A review of studies on CO_2 sequestration and caprock integrity. FUEL, 89(10): 2651-2664.

Smith, J., Durucan, S., Korre, A. and Shi, J.Q., 2011. Carbon dioxide storage risk assessment: Analysis of caprock fracture network connectivity. International Journal of Greenhouse Gas Control, 5(2): 226-240.

Snow, D.T., 1969. Anisotropic Permeability of Fractured Media. Water Resources Research, 5(6): 1273-&.

Stenhouse, M.J., Gale, J. and Zhou, W., 2009. Current status of risk assessment and regulatory frameworks for geological CO_2 storage. Energy Procedia, 1(1): 2455-2462.

Tsang, C.F., Birkholzer, J. and Rutqvist, J., 2008. A comparative review of hydrologic issues involved in geologic storage of CO_2 and injection disposal of liquid waste. ENVIRONMENTAL GEOLOGY, 54(8): 1723-1737.

Van Golf-Racht, T.D., 1982. Fundamentals of fractured reservoir engineeering. Developments in Petroleum Science. Elsevier Scientific Publishing Company, Amsterdam, The Netherlands, 710 pp.

Warren, J.E. and Root, P.J., 1963. The Behavior of Naturally Fractured Reservoirs. Society of Petroleum Engineers Journal: 245-255.

Zhang, Y.Q., Oldenburg, C.M. and Finsterle, S., 2010. Percolation-theory and fuzzy rule-based probability estimation of fault leakage at geologic carbon sequestration sites. Environmental Earth Sciences, 59(7): 1447-1459.

TABLE 4.1: Monte Carlo (MC) simulation case summary with parameter ranges and PDFs for caprock fracture variables.

Case	Description	Fracture aperture e (m)			Fracture length, l (m)			Caprock thickness b_{cap} (m)			[**]n	$\widehat{p}_{\xi_{CO_2}}$	
		a	b	PDF	a	b	PDF	a	b	PDF		1%	10%
1	Direct MC simulation with 'well-connected' fractures in caprock with uncertain fracture properties. Includes uncertain reservoir properties	$1.5\text{-}2.5^{\dagger}$	$10^{-7}\text{-}10^{-3\dagger}$	Pareto (a,b)	$0.5\text{-}4^{\dagger}$	$l\sim b_{cap}$	Pareto (a,b)	$6^{\ddagger}$	$352^{\ddagger}$	U(a,b)	42	0.24	0.45
2	Importance Sampling MC simulation with 'well-connected' fractures in caprock with uncertain fracture properties. Includes uncertain reservoir properties	1.5-2.5	1×10^{-7}- 4.2×10^{-5}	Pareto (a[*],b[*])	0.5-2.9	$l\sim b_{cap}$	Pareto (a[*],b[*])	30	349	U (a[*],b[*])	3,273	0.28	0.56
3	Importance Sampling MC simulation of Case 2 with fixed reservoir properties.	1.5-2.5	1×10^{-7}- 4.2×10^{-5}	Pareto (a[*],b[*])	$0.5\text{-}4^{\dagger}$	$l\sim b_{cap}$	Pareto (a[*],b[*])	$100^{\diamond}$	-		293	0.15	0.41

†Source: Bonnet et al. (2001); Nelson (2001)
‡Source: Chapter 2
◇Source: Class et al. (2009)
*Values used for Importance sampling distribution – based on Case 1 results
**Total number of simulations realizations classified under 100% CO_2 loss

TABLE 4.2: Reservoir parameter range and PDFs used for Monte Carlo simulation cases.

Input Variables	Unit	Case 3 Parameter			Case 1,2 Parameter					Ref
		a	b	PDF	a	a*	b	b*	PDF	
Reservoir										
Thickness, b_{res}	m	30		-	5	90	533	530	U(a,b)	1
Porosity, φ_m	-	0.15		-	6%	6%	40%	39%	U(a,b)	2
Water saturation, s_w	-	1		-	0.3	0.31	1	0.99	U(a,b)	3
CO_2 gas saturation, s_a	-	$1 - s_w$		-	-		$1 - s_w$		U(a,b)	-
Residual water saturation, s_{wr}	-	0.2		-	0.1	0.1	0.29	0.29	U(a,b)	4
Permeability, k	m^2	2×10^{-14}		-	10^{-16}	4.5×10^{-14}	2.4×10^{-12}	2.3×10^{-12}	U(a,b)	5
CO_2 relative permeability, k_{ra}	-	0.15		-	0.022	0.023	0.15	0.15	U(a,b)	6
Brine relative permeability, k_{rw}	-	1		-	0.07	0.07	1	0.97	U(a,b)	7
Fracture pressure gradient, G_f	Pa m^{-1}	-		-	1.36×10^4	1.37×10^4	2.52×10^4	1.80×10^4	U(a,b)	8
Hydrostatic pressure gradient, G_h	Pa m^{-1}	1.05×10^4		-	1.05×10^4				-	9
Initial pressure, p_i	Pa	$p_i \approx G_h(z_{Top}+b_{cap})$		-	$p_i \approx G_h(z_{Top}+b_{cap})$				-	10
Rock compressibility, c_f	Pa^{-1}	1×10^{-9}		-	1×10^{-9}				-	11
CO_2/Brine surface tension, γ	mPa	45		-	25	45	45	45	U(a,b)	12
Fluid										
CO_2 injection rate, Q_{in}*	MMT yr^{-1}	0.28		-	0.1	0.1	1.7	1.67	U(a,b)	13
CO_2 injection time, t_{ini}	yr	100		-	0.1	0.41	100	97	U(a,b)	14
CO_2 viscosity, μ_a	Pa-s	3.95×10^{-5}		-	3.95×10^{-5}				-	15
CO_2 density, ρ_a	kg m^{-3}	479		-	479				-	16
CO_2 compressibility, c_a**	Pa^{-1}	$c_g \approx 1/\bar{p}_l$		-	$c_g \approx 1/\bar{p}_l$				-	17
Brine viscosity, μ_w	Pa-s	2.54×10^{-4}		-	2.54×10^{-4}				-	18
Brine density, ρ_w	kg m^{-3}	1045		-	1045				-	19
Brine compressibility, c_w	Pa^{-1}	4.4×10^{-10}		-	4.4×10^{-10}				-	20

Table 4.2:   Cont'd

*Upper limit based on CO_2 emissions from the Electric Power Sectors' energy consumption of coal for existing coal power plants in 2008 [i.e. (CO_2 emission = 1,979.7 MMT/yr)/(No. coal power plant = 1,445)]

**Approx. for depth and range of hydrostatic pressures considered in study

1.)   Chapter 2
2.)   NETL (2009); Rodosta et al. (2011)
3.)   Brooks and Corey (1964)
4.)   Brooks and Corey (1964)
5.)   NETL (2009); Rodosta et al. (2011)
6.)   Jarrell et al. (2002)
7.)   Brooks and Corey (1964); Jarell et al. (2002)
8.)   EPA (2011)
9.)   Class et al. (2009)
10.)   Dake (1978)
11.)   Lee and Wattenbarger (1996)
12.)   Chalbaud et al. (2009); Chiquet et al. (2007)
13.)   EIA (2008); NETL (2009)
14.)   Chapter 1; Metz et al. 2005
15.)   Class et al. 2009
16.)   Class et al. 2009
17.)   Dake (1978); Lee and Wattenbarger (1996)
18.)   Class et al. (2009)
19.)   Class et al. (2009)
20.)   Freeze and Cherry (1979)

TABLE 4.3: Rank order correlation coefficient rs matrix for Case 2 caprock-reservoir associations.

Model parameter	Fracture aperture			Fracture density			Fracture porosity			Fracture permeability		
System CO_2 loss constraint:	100%	10%	1%	100%	10%	1%	100%	10%	1%	100%	10%	1%
CAPROCK FRACTURE PROPERTIES AND CO_2% LOSS CORRELATIONS												
Fracture aperture	1.00	1.00	1.00									
Fracture density	-0.18	-0.41	-0.46	1.00	1.00	1.00						
Fracture porosity	0.11	0.09	0.09	0.83	0.79	0.77	1.00	1.00	1.00			
Fracture permeability	0.47	0.77	0.79	0.13	-0.06	-0.16	0.62	0.51	0.46	1.00	1.00	1.00
Aperture Pareto PDF: exponent	-0.07	-0.10	-0.07	-0.04	-0.03	-0.07	-0.03	-0.03	-0.04	-0.02	0.00	0.03
Aperture Pareto PDF: min. length	0.50	0.82	0.83	-0.45	-0.55	-0.60	0.04	-0.01	-0.03	0.72	0.79	0.81
Fracture length Pareto PDF: exponent	-0.22	-0.37	-0.37	0.72	0.71	0.69	0.66	0.66	0.65	0.20	0.10	0.07
Caprock thickness/ Fracture length Pareto PDF: min. length	0.02	0.10	0.16	-0.39	-0.38	-0.42	-0.33	-0.31	-0.33	-0.10	-0.01	0.05
CO_2% Loss	0.36	0.55	0.55	0.23	0.12	0.04	0.62	0.55	0.52	0.82	0.79	0.77
RESERVOIR PROPERTIES AND CO_2 INJECTION CORRELATIONS												
CO_2 injection rate	-0.06	-0.09	-0.11	0.12	0.14	0.13	0.11	0.12	0.10	0.03	0.02	0.00
Injection time	-0.16	-0.36	-0.45	0.06	0.13	0.20	-0.06	-0.08	-0.08	-0.23	-0.35	-0.41
CO_2 gas saturation	0.01	0.03	0.01	0.01	0.01	0.01	0.00	0.02	0.02	-0.01	0.01	0.01
Relative CO_2 permeability	-0.07	-0.16	-0.13	0.05	0.10	0.11	-0.01	0.03	0.04	-0.10	-0.10	-0.10
Reservoir water saturation	-0.01	-0.03	-0.01	-0.01	-0.01	-0.01	0.00	-0.02	-0.02	0.01	-0.01	-0.01
Reservoir residual water saturation	-0.03	-0.03	-0.01	0.00	0.02	0.03	-0.02	0.00	0.01	-0.03	-0.03	-0.02
Relative brine permeability	0.08	0.14	0.14	-0.06	-0.08	-0.07	0.02	0.01	0.04	0.14	0.13	0.17
Reservoir thickness	-0.07	-0.04	-0.06	-0.15	-0.14	-0.15	-0.09	-0.08	-0.09	0.06	0.09	0.08
Reservoir porosity	0.06	0.15	0.15	-0.05	-0.07	-0.10	0.02	0.03	0.01	0.11	0.16	0.16
Reservoir permabilty	-0.04	-0.03	-0.03	-0.01	-0.01	0.00	0.02	-0.01	0.00	-0.01	0.00	0.00
Fracture pressure gradient	-0.04	-0.05	-0.03	-0.07	-0.08	-0.12	-0.05	-0.06	-0.10	0.00	0.02	0.02
Capillary entry pressure	-0.53	-0.86	-0.88	0.49	0.57	0.62	-0.03	0.02	0.03	-0.76	-0.82	-0.84
Pressure gradient, Δp/L-pg	0.22	0.27	0.23	0.28	0.27	0.29	0.22	0.21	0.23	0.02	-0.02	-0.05
Bouyancy Factor	-0.06	0.01	0.00	-0.18	-0.20	-0.20	-0.14	-0.13	-0.13	0.01	0.07	0.08
Reseroir extent	-0.20	-0.46	-0.51	0.20	0.28	0.33	0.02	0.01	-0.01	-0.28	-0.42	-0.49

TABLE 4.3: Cont'd

Model parameter	Aperture Pareto PDF: exponent			Aperture Pareto PDF: min. length			Fracture length Pareto PDF: exponent			Caprock thickness/ Fracture length Pareto PDF: min. length			CO$_2$% Loss		
System CO$_2$ loss constraint:	100%	10%	1%	100%	10%	1%	100%	10%	1%	100%	10%	1%	100%	10%	1%
CAPROCK FRACTURE PROPERTIES AND CO$_2$% LOSS CORRELATIONS															
Fracture aperture															
Fracture density															
Fracture porosity															
Fracture permeability															
Aperture Pareto PDF: exponent	**1.00**	**1.00**	**1.00**												
Aperture Pareto PDF: min. length	0.04	0.03	0.07	**1.00**	**1.00**	**1.00**									
Fracture length Pareto PDF: exponent	0.03	0.06	0.03	-0.25	-0.28	-0.29	**1.00**	**1.00**	**1.00**						
Caprock thickness/ Fracture length Pareto PDF: min. length	-0.01	0.00	0.03	0.14	0.18	0.24	0.00	0.01	-0.02	**1.00**	**1.00**	**1.00**			
CO$_2$% Loss	0.01	0.01	0.04	**0.53**	**0.55**	**0.56**	0.12	0.08	0.07	-0.08	-0.01	0.02	**1.00**	**1.00**	**1.00**
RESERVOIR PROPERTIES AND CO$_2$ INJECTION CORRELATIONS															
CO$_2$ injection rate	-0.03	0.00	-0.01	-0.04	-0.06	-0.05	0.11	0.03	0.03	0.01	0.01	0.00	0.04	0.01	0.00
Injection time	0.01	-0.01	0.00	-0.21	-0.33	-0.38	-0.06	-0.09	-0.03	0.03	0.01	-0.04	0.12	0.05	0.02
CO$_2$ gas saturation	0.02	0.01	0.02	0.00	0.01	0.00	-0.01	0.01	0.04	0.00	0.02	0.04	-0.02	0.01	0.03
Relative CO$_2$ permeability	0.04	0.03	0.01	-0.10	-0.12	-0.12	-0.04	0.02	0.03	-0.01	-0.02	-0.04	0.06	0.08	0.09
Reservoir water saturation	-0.02	-0.01	-0.02	0.00	-0.01	0.00	0.00	-0.01	-0.04	0.00	-0.02	-0.04	0.02	-0.01	-0.03
Reservoir residual water saturation	-0.02	-0.02	0.02	-0.04	-0.03	-0.04	-0.02	0.00	-0.01	0.03	0.00	-0.01	-0.02	0.00	0.00
Relative brine permeability	-0.02	0.01	0.02	0.14	0.13	0.16	0.02	0.02	0.04	-0.03	0.00	0.01	-0.05	-0.04	0.01
Reservoir thickness	0.01	0.02	0.04	0.14	0.15	0.14	0.02	0.02	0.03	-0.03	-0.04	-0.03	-0.08	-0.04	-0.05
Reservoir porosity	-0.03	-0.05	-0.01	0.11	0.14	0.14	0.03	0.02	0.00	-0.04	-0.02	-0.03	-0.05	0.01	-0.01
Reservoir permabilty	-0.03	-0.05	-0.07	-0.01	-0.01	0.00	0.02	0.00	0.00	0.01	0.01	0.02	-0.03	-0.02	0.01
Fracture pressure gradient	0.00	0.00	-0.01	0.03	0.05	0.07	-0.05	-0.01	-0.04	0.00	-0.02	-0.01	-0.01	0.00	-0.03
Capillary entry pressure	-0.01	-0.03	-0.06	**-0.94**	**-0.96**	**-0.96**	0.27	0.30	0.31	-0.15	-0.19	-0.24	**-0.55**	**-0.56**	**-0.58**
Pressure gradient, Δp/L-ρg	-0.25	-0.29	-0.31	-0.14	-0.15	-0.20	-0.17	-0.18	-0.16	-0.27	-0.25	-0.24	0.06	0.01	-0.02
Bouyancy Factor	0.00	-0.01	0.00	0.10	0.15	0.15	0.03	-0.01	0.00	-0.03	-0.04	-0.01	-0.10	-0.04	-0.02
Reseroir extent	0.02	0.00	0.00	-0.33	**-0.45**	**-0.49**	-0.13	-0.06	-0.03	0.06	0.03	-0.01	0.20	0.09	0.04

TABLE 4.4: Rank order correlation coefficient rs matrix for Case 1 caprock-reservoir associations

	Model parameter	Fracture aperture			Fracture density			Fracture porosity			Fracture permeability		
	System CO_2 loss constraint:	100%	10%	1%	100%	10%	1%	100%	10%	1%	100%	10%	1%
CAPROCK FRACTURE PROPERTIES AND CO_2% LOSS CORRELATIONS	Fracture aperture, e	1.00	1.00	1.00									
	Fracture density, N/L	-0.41	-0.78	-0.98	1.00	1.00	1.00						
	Fracture porosity, φ_f	0.02	-0.36	-0.81	0.72	0.82	0.88	1.00	1.00	1.00			
	Fracture permeability, k_f	0.56	0.80	0.79	-0.27	-0.30	-0.67	0.42	0.22	-0.43	1.00	1.00	1.00
	Aperture Pareto PDF: (exponent)	0.28	0.19	0.24	-0.10	-0.30	-0.28	0.00	-0.31	-0.47	0.13	-0.03	-0.04
	Aperture Pareto PDF: (min. size)	0.65	0.96	0.92	-0.66	-0.76	-0.86	-0.01	-0.40	-0.69	0.88	0.76	0.86
	Fracture length Pareto PDF: (exponent)	-0.25	-0.51	-0.77	0.82	0.82	0.84	0.78	0.74	0.89	0.05	-0.01	-0.35
	Caprock thickness/Fracture length Pareto PDF: (min. length)	-0.24	0.12	0.28	-0.29	-0.20	-0.21	-0.34	-0.30	-0.09	-0.08	0.11	0.56
	CO_2% Loss	0.50	0.42	0.37	-0.06	0.06	-0.26	0.48	0.51	0.12	0.77	0.75	0.54
RESERVOIR PROPERTIES AND CO_2 INJECTION CORRELATIONS	CO_2 injection rate	-0.23	-0.42	-0.37	0.35	0.41	0.42	0.39	0.38	0.65	0.03	-0.11	-0.21
	Injection time	-0.44	-0.58	-0.59	0.39	0.41	0.66	-0.06	0.20	0.56	-0.60	-0.48	-0.41
	CO_2 gas saturation	-0.08	0.05	-0.32	-0.09	-0.07	0.28	-0.21	-0.10	-0.08	-0.24	-0.09	-0.26
	Relative CO2 permeability	-0.12	0.29	0.30	-0.08	-0.18	-0.31	-0.12	-0.01	-0.39	-0.09	0.30	0.20
	Reservoir water saturation	0.08	-0.05	0.32	0.09	0.07	-0.28	0.21	0.10	0.08	0.24	0.09	0.26
	Reservoir residual water saturation	0.11	0.09	0.02	-0.12	-0.15	-0.07	0.02	-0.26	-0.13	0.13	-0.03	0.07
	Relative brine permeability	0.08	0.27	0.55	-0.08	-0.07	-0.53	0.06	0.02	-0.50	0.19	0.25	0.54
	Reservoir thickness	0.07	0.29	-0.12	0.09	-0.03	0.04	0.31	0.18	-0.28	0.36	0.36	-0.39
	Reservoir porosity	-0.09	0.04	-0.49	-0.17	0.00	0.54	0.00	0.06	0.56	0.29	0.10	-0.16
	Reservoir permabilty	-0.22	-0.24	-0.70	0.01	0.12	0.64	0.06	0.19	0.65	0.08	-0.16	-0.81
	Fracture pressure gradient	0.07	0.39	0.09	-0.07	-0.26	-0.07	0.05	-0.07	-0.39	0.04	0.25	0.10
	Capillary entry pressure	-0.63	-1.00	-1.00	0.68	0.80	0.98	0.02	0.39	0.81	-0.87	-0.78	-0.79
	Pressure gradient, $\Delta p/L-\rho g$	0.11	-0.26	-0.02	0.32	0.21	0.08	0.22	0.07	0.25	-0.16	-0.22	0.12
	Bouyancy Factor, Γ	-0.05	0.25	-0.22	-0.11	-0.17	0.14	0.01	0.01	-0.12	0.20	0.19	-0.42
	Reseroir extent	-0.42	-0.73	-0.56	0.45	0.48	0.59	-0.01	0.24	0.66	-0.65	-0.56	-0.58

	Model parameter	Fracure aperture power law parameter #1 (exponent)			Fracure aperture power law parameter #2 (miniumum length)			Frac length power law parameter #1 (exponent)			Caprock thickness			CO₂% Loss		
	System CO₂ loss constraint:	100%	10%	1%	100%	10%	1%	100%	10%	1%	100%	10%	1%	100%	10%	1%
CAPROCK FRACTURE PROPERTIES AND CO₂% LOSS CORRELATIONS	Fracture aperture, e															
	Fracture density, N/L															
	Fracture porosity, φf															
	Fracture permeability, kf															
	Aperture Pareto PDF: (exponent)	**1.00**	**1.00**	**1.00**												
	Aperture Pareto PDF: (min. size)	0.16	0.29	0.36	**1.00**	**1.00**	**1.00**									
	Fracture length Pareto PDF: (exponent)	-0.12	-0.39	-0.50	-0.31	-0.51	-0.67	**1.00**	**1.00**	**1.00**						
	Caprock thickness/Fracture length Pareto PDF: (min. length)	-0.19	-0.18	-0.53	0.08	0.15	0.22	-0.08	0.18	0.07	**1.00**	**1.00**	**1.00**			
	CO₂% Loss	0.04	-0.23	-0.52	0.61	0.38	0.37	0.06	0.06	0.01	-0.03	-0.30	0.25	**1.00**	**1.00**	**1.00**
RESERVOIR PROPERTIES AND CO₂ INJECTION CORRELATIONS	CO₂ injection rate	-0.01	-0.04	-0.08	-0.14	-0.38	-0.19	0.39	0.43	0.38	0.13	0.25	-0.13	0.06	-0.05	0.27
	Injection time	-0.08	-0.02	0.16	-0.63	-0.47	-0.33	-0.06	0.03	0.37	0.11	-0.23	-0.39	-0.15	-0.11	-0.04
	CO₂ gas saturation	0.23	0.13	0.42	-0.11	0.07	-0.20	-0.15	-0.12	-0.05	0.01	-0.21	-0.07	-0.25	-0.19	-0.82
	Relative CO2 permeability	-0.17	-0.16	-0.31	-0.09	0.19	0.15	-0.05	0.04	-0.04	0.04	0.25	0.39	-0.21	0.08	0.08
	Reservoir water saturation	-0.23	-0.13	-0.42	0.11	-0.07	0.20	0.21	0.12	0.05	-0.01	0.21	0.07	0.25	0.19	0.82
	Reservoir residual water saturation	0.13	-0.11	-0.21	0.16	0.12	-0.01	0.02	-0.12	-0.33	0.13	0.29	0.30	0.01	-0.09	-0.04
	Relative brine permeability	0.04	-0.05	0.32	0.21	0.25	0.63	0.06	-0.02	-0.54	-0.14	0.02	0.25	-0.06	-0.06	-0.19
	Reservoir thickness	0.31	0.34	0.60	0.17	0.21	-0.18	0.18	0.04	-0.12	-0.01	0.00	-0.26	0.21	0.27	-0.65
	Reservoir porosity	-0.02	0.02	-0.14	0.31	0.08	-0.29	0.01	0.24	0.45	0.21	0.41	0.32	0.10	-0.17	-0.10
	Reservoir permabilty	-0.23	-0.23	-0.15	0.01	-0.38	-0.77	0.12	0.30	0.53	-0.07	0.05	-0.56	-0.01	-0.15	-0.05
	Fracture pressure gradient	-0.09	0.02	0.42	0.04	0.31	0.14	0.05	-0.24	-0.31	-0.04	-0.10	0.01	0.10	0.16	-0.33
	Capillary entry pressure	-0.13	-0.20	-0.24	-0.98	-0.96	-0.92	0.34	0.54	0.77	-0.09	-0.13	-0.28	-0.61	-0.40	-0.37
	Pressure gradient, Δp/L-ρg	0.05	0.04	-0.07	-0.21	-0.11	0.18	0.11	-0.11	-0.07	-0.23	-0.41	-0.37	0.07	0.12	0.54
	Bouyancy Factor, Γ	0.05	0.13	0.30	0.14	0.10	-0.37	0.00	0.02	0.15	-0.11	0.03	-0.12	0.00	0.02	-0.60
	Reseroir extent	-0.17	-0.24	-0.28	-0.72	-0.70	-0.53	0.12	0.21	0.43	0.13	-0.10	-0.33	-0.15	-0.11	0.25

FIGURE 4.1: Illustration of the shift in parameter ranges from the original uniform PDFs used to represent the importance sampling distributions U(a*,b*) of Case 2 and 3. Parameters a* and b* were chosen based on Case 1 simulation results for input parameters with classified CO_2 loss of < 10%.

FIGURE 4.2: Conceptual model CO_2 plume transport through reservoir and fractured caprock given uncertain physical and transport parameters. Plan view map illustrates geometric coverage of fractures in caprock in contact with CO_2 plume in reservoir.
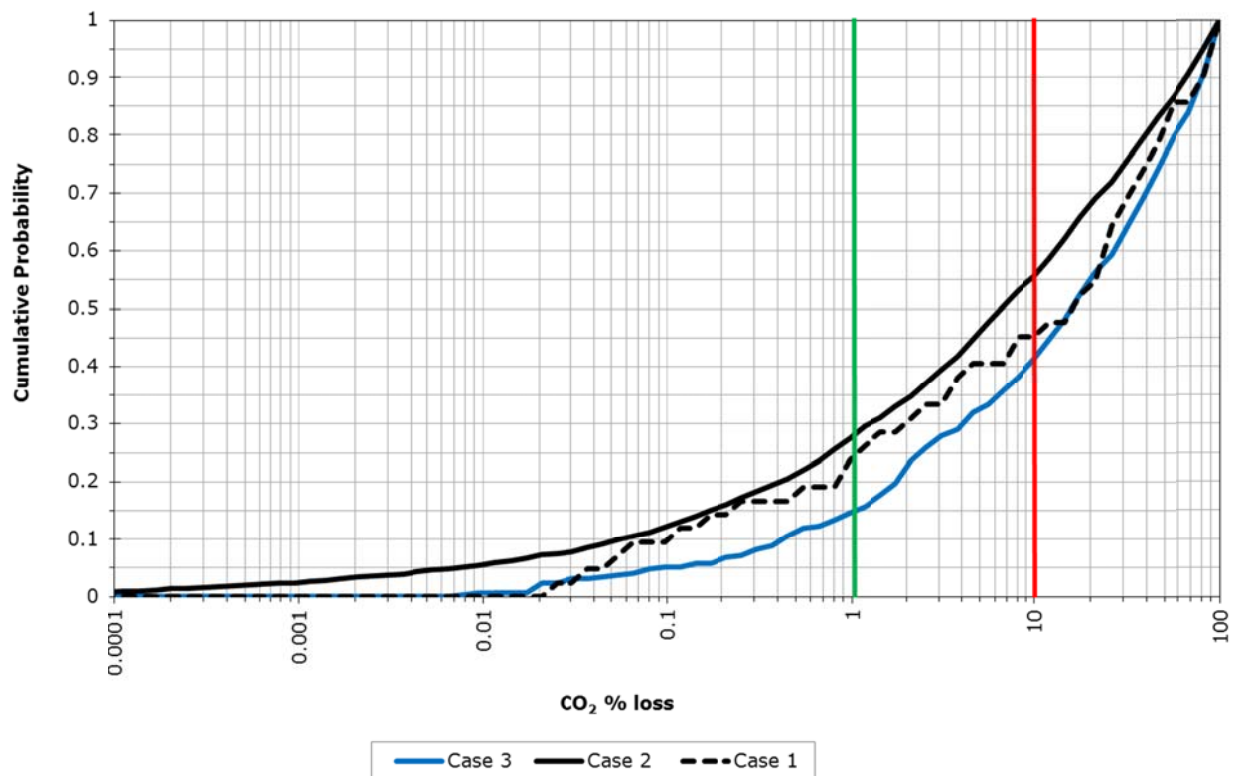
FIGURE 4.3: Cummulative distribution function of the resulting $CO_2\%$ loss for the three MC cases examined. Black dashed line represents Case 1 where full system uncertainty (caprock and reservoir) was considered using a direct sampling MC approach. Solid black and blue lines represent Case 2 and 3, respectivity, where importance sampling MC approach was applied. Case 2 considers full system uncertainty while Case 3 considered partial uncertainty (caprock only). Vertical green and red lines represent the CCS performance criteria for 1-10% CO_2 loss over 100 years, respectively.
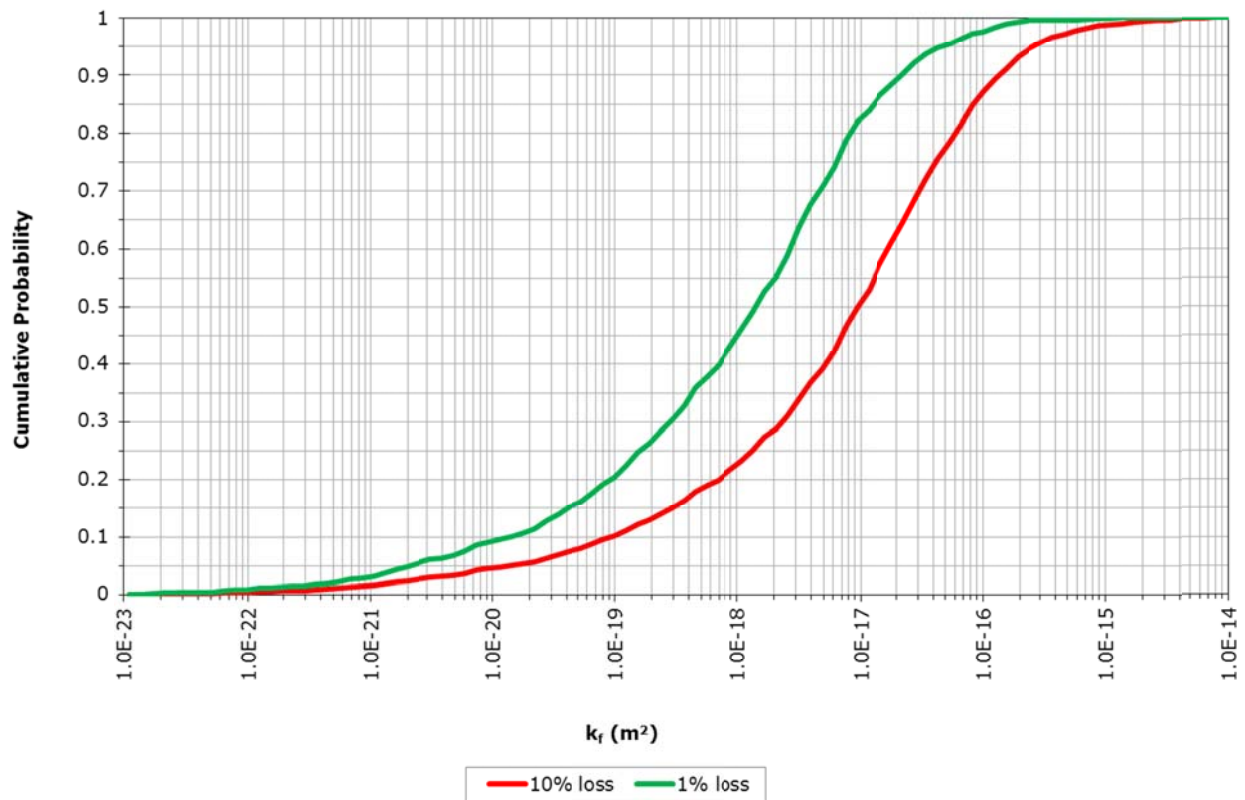
FIGURE 4.4: Cummulative probabilities of resulting fracture permeabilities for Case 2. Green and red lines represent the CDF of fracture permeability under the classified loss of 1% and 10% CO_2 loss in system, respectively.
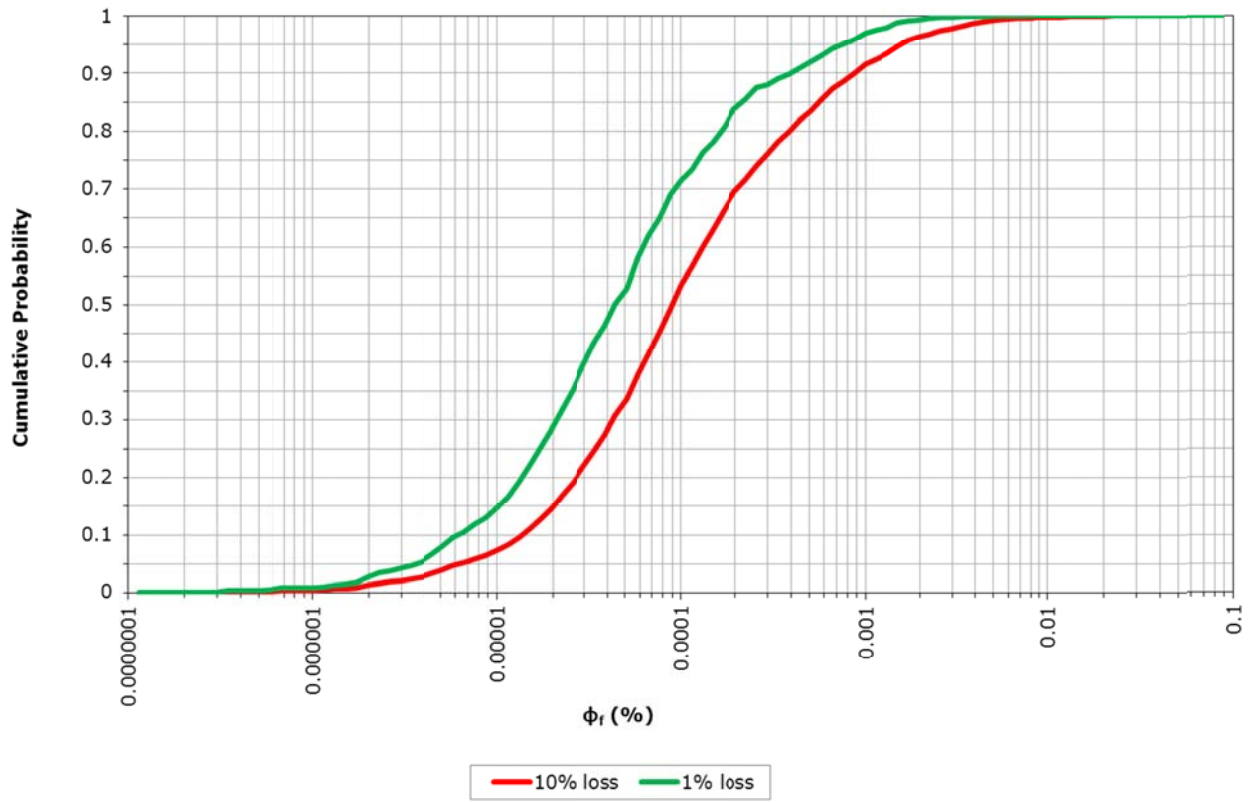
FIGURE 4.5: Cummulative probabilities of resulting fracture porosity for Case 2. Green and red lines represent the CDF of fracture porosity under the classified loss of 1% and 10% CO_2 loss in system, respectively.
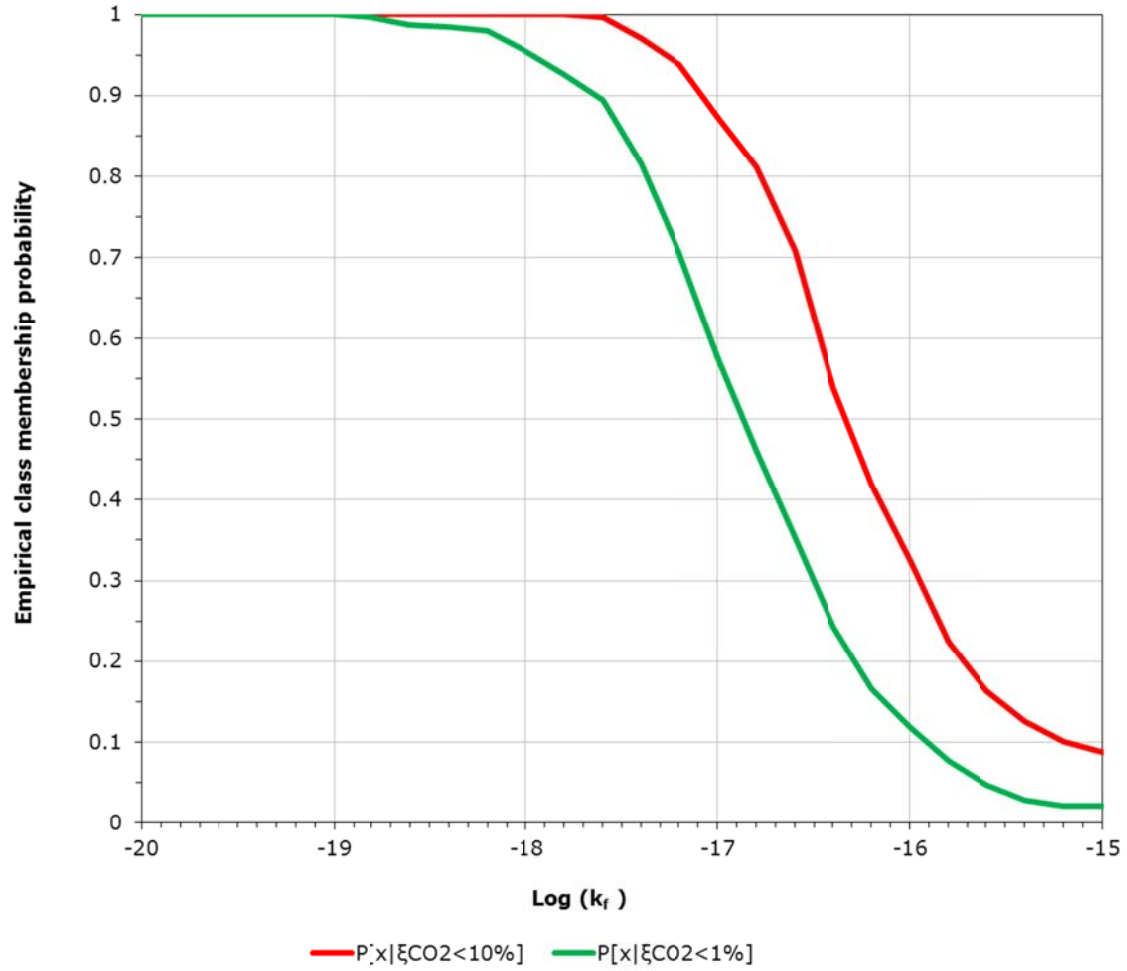
FIGURE 4.6: Empirical class membership probability for caprock fracture permeablity in Case 2. Depicts the probability of a given caprock fracture permeability meeting either a 1% (dash) or 10% (solid) classified CO_2% loss criteria.
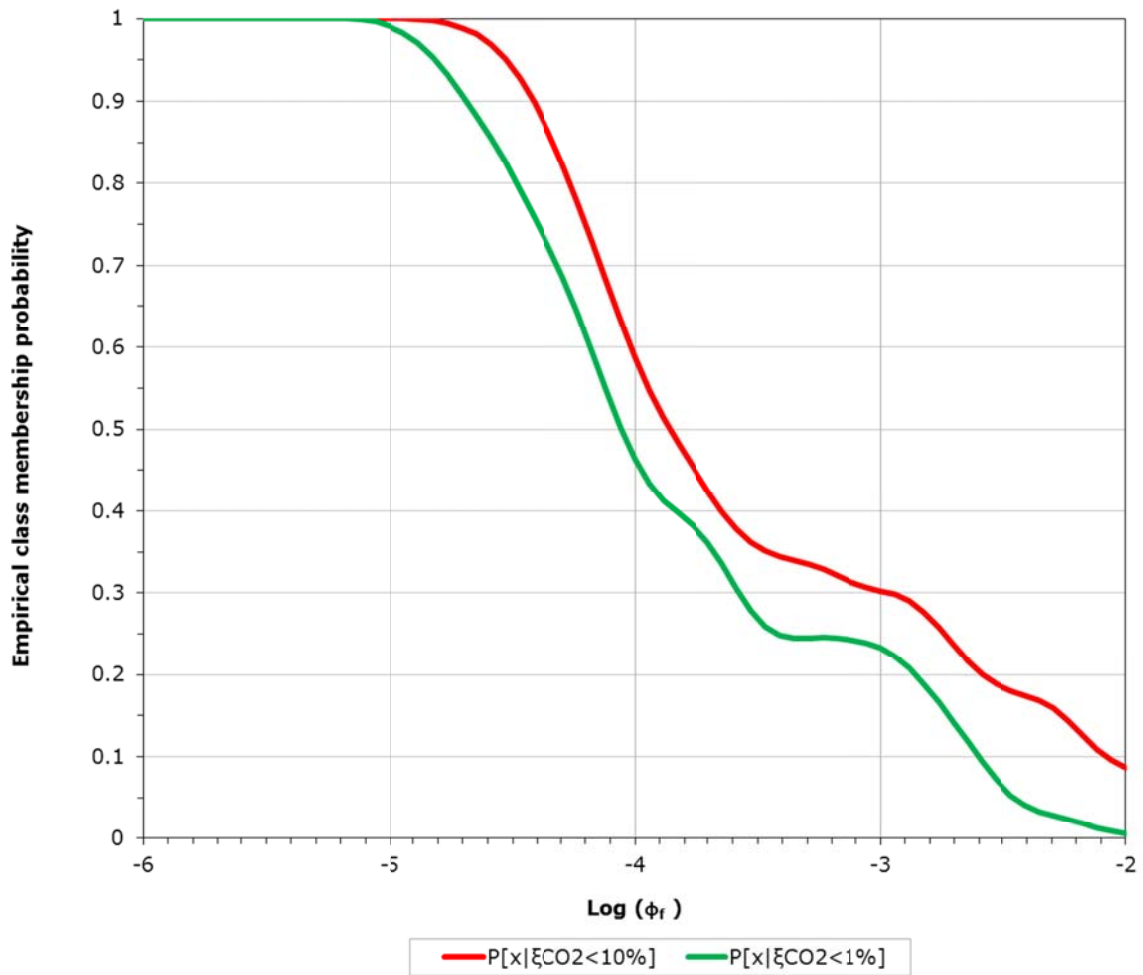
FIGURE 4.7: Empirical class membership probability for caprock fracture porosity in Case 2. Depicts the probability of a given caprock fracture porosity meeting either a 1% (dash) or 10% (solid) classified CO_2% loss criteria in system.
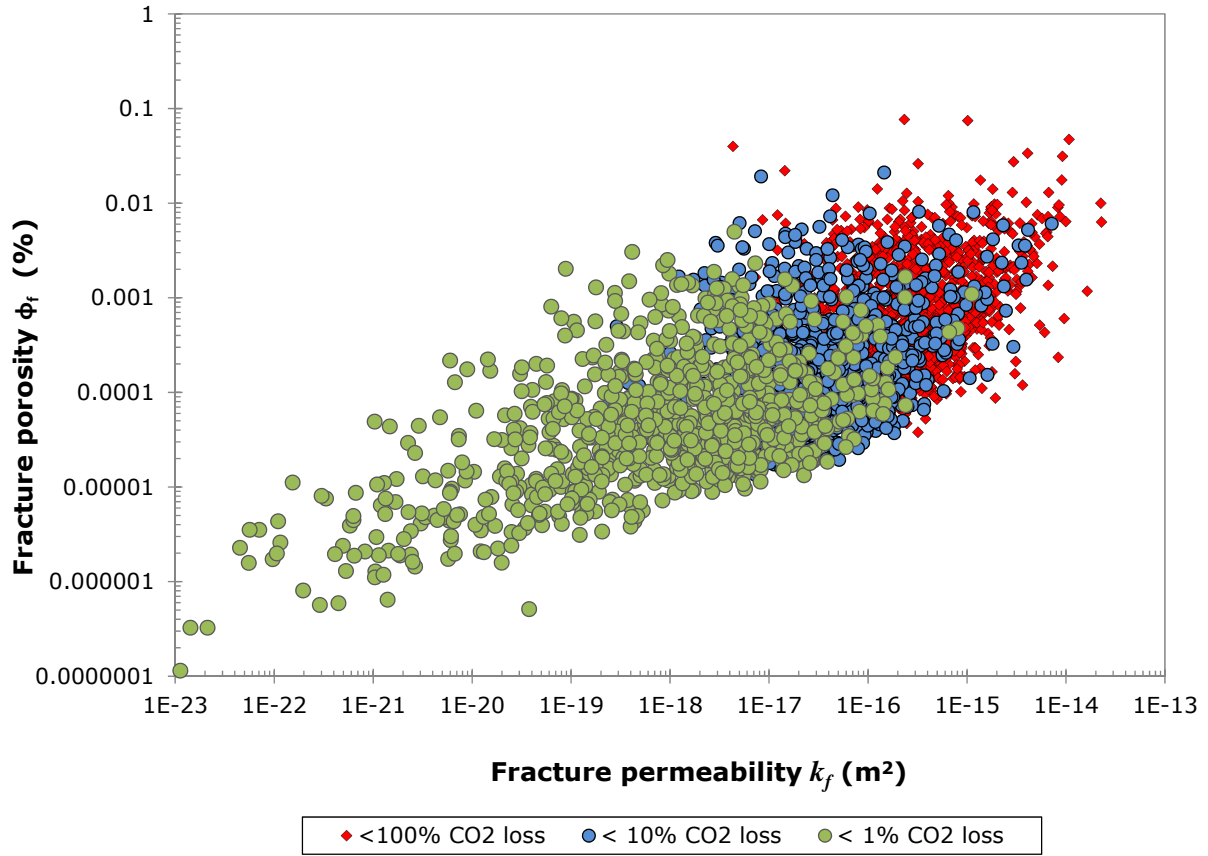
FIGURE 4.8:   Scatter plot of fracture permeability vs. fracture porosity for the different classes of CO_2 loss in Case 2. (Red) dots are realizations with <100% CO_2 loss, (Blue) <10%, and (Green) < 1% CO_2 loss.
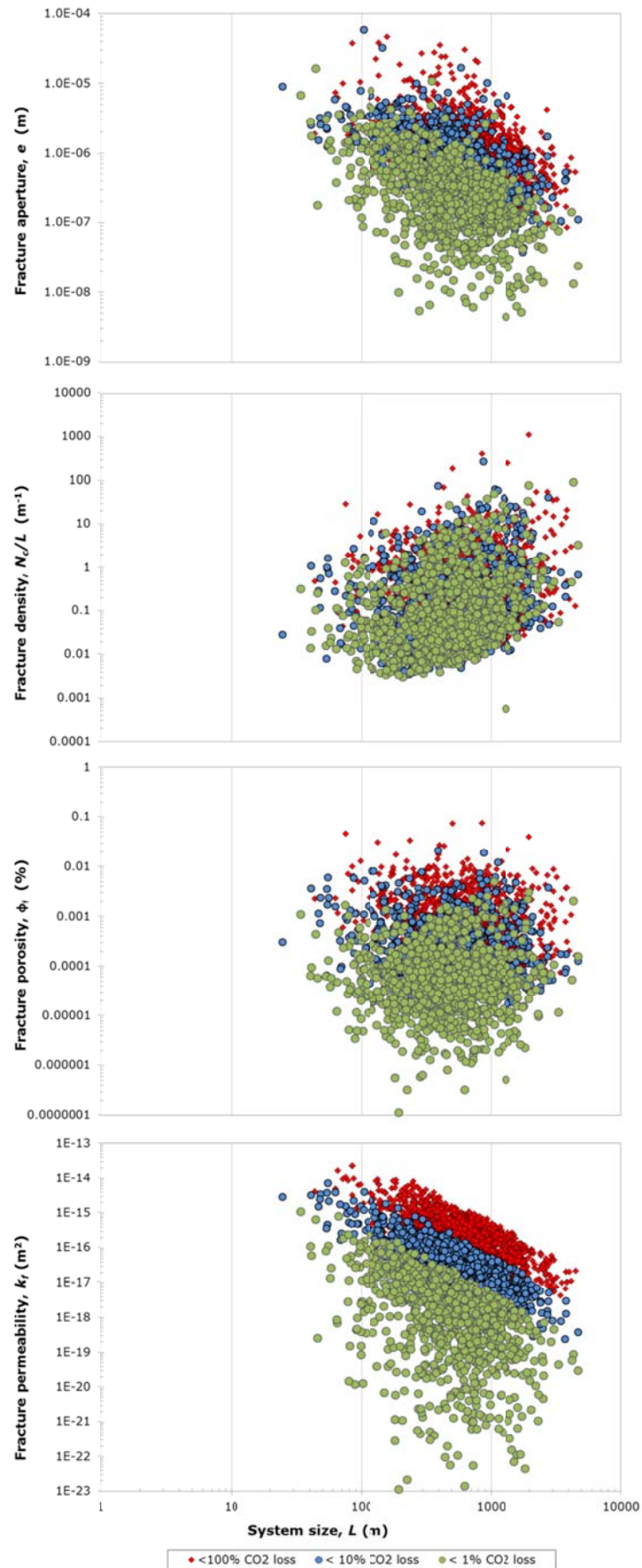
FIGURE 4.9: Scatter plots for Case 2 fracture hydraulic properties as a function of system size L. (Red) dots are realizations with <100% CO_2 loss, (Blue) <10%, and (Green) < 1% CO_2 loss.

144

CHAPTER 5

CONCLUSIONS AND RECOMMENDATIONS FOR FUTURE WORK

The overall goals of this research were to examine the physical and lithological characteristics of caprock formations considered for saline CO_2 sequestration, and to investigate the impact of uncertainty in hydraulic properties of a fractured caprock on the ability to meet long-term CO_2 storage goals. This chapter discusses the major findings of the research, original contributions, and recommendations for future work.

5.1 SUMMARY OF MAJOR FINDINGS OF RESEARCH

5.1.1 REVIEW OF PHYSICAL AND LITHOLOGIC CHARACTERISTICS OF CAPROCKS CONSIDERED FOR CO_2 STORAGE WITHIN SELECTED U.S. GEOLOGIC BASINS

The purpose of this effort was to review available information on the physical and lithological features of caprock strata within some candidate basins considered for CO_2 storage in saline reservoirs in the U.S., and to identify characteristics that could be relevant in assessing the permanence of CO_2 storage. Several caprock strata were examined for their lithology and dominant mineral phases. Based on available data, a subset of these caprocks were also examined for their structural features and physical properties.

The main conclusions were: 1) caprock (primary seal) formations are regionally extensive, and are generally thick with low permeability. 2) There is substantial spatial variability in the lithologic composition, thickness, and fluid transport properties of the seal formations within the basins. 3) Fractures and faults penetrate seal strata throughout the basins examined, highlighting the importance of site–specific evaluations in the selection of a storage reservoir. 4) Some of the seal rock strata are oil and gas sources; and 5) each

145

basin has unique regional features that could be relevant to CO_2 storage, such as the presence of salt piercements, previous seismic activity, and proximity of water resource aquifers. The significance of these features with regards to site–specific seal integrity is currently the focus of investigations conducted by the U.S. DOE regional partnerships.

Caprocks examined were generally thick and exhibited low permeability. However, they were not continuous or uniform in lithology throughout the regions examined. Caprocks exhibited lateral facies changes, fractures, and spatial variability in thickness, permeability, porosity, and other physical properties that could affect CO_2 storage. Fractures reported in caprock formations were not fully characterized and had unknown regional extent and interconnectivity. Faults and fault zones were also common within each of the regions examined. The influence of fault proximity, extent of deformation, and fluid conductivity on seal strata performance at a potential site merits investigation.

This review of physical and chemical characteristics of the caprock formations overlying candidate saline reservoirs highlighted features that merit focused attention when investigating candidate sites for long-term CO_2 storage within these selected basins. The common characteristics identified in this study regarding heterogeneity in caprock composition, physical attributes, and regional structural features can help guide the development of laboratory and field studies for site–specific assessments. The range of hydraulic properties examined can be used as a basis for comparison to values determined by CO_2 transport models to meet storage permanence goals.

5.1.2 DEVELOP AN INTEGRATED ANALYTICAL MODEL FOR ESTIMATING FRACTURE HYDRAULIC PROPERTIES OF CAPROCKS RELIED UPON FOR LONG-TERM CO_2 STORAGE

The purpose of this effort was to develop an integrated analytical model to estimate the limits of hydraulic fracture properties within a caprock that are consistent with storage performance criteria, and with observed ranges for aperture size and density within field studies on fracture networks. An idealized reservoir and caprock system was used as the

basis for analysis. The integrated model was used to evaluate how fracture aperture, density, and connectivity affect transport of supercritical CO_2 ($scCO_2$) through caprock.

Major findings in this study were: (1) microfractures (e.g. 10^{-7} to 10^{-6} m range) can yield CO_2 loss rates of concern under certain conditions. (2) Fracture permeability was the key parameter governing CO_2 loss and apart from fracture density, its constitutive parameters could only vary within a limited range. (3) Fracture permeability that gave less than 10% CO_2 loss lied in the nano- to micro-Darcy (μD) range (i.e. 10^{-21} – 10^{-18} m^2), which may be indistinguishable from caprock matrix permeabilities. (4) Fracture porosities were low ($\leq$0.02 %). (5) Apart from fracture permeability, no other single fracture parameter (e.g. fracture porosity, aperture, and density) uniquely predicted CO_2 transport in caprock. (6) Compared to reported measurements of fracture systems, interpretation of hydraulic flow within a 1 – 10% CO_2 loss window may be difficult depending on degree of fracture connectivity.

5.1.3 INVESTIGATING THE IMPACT OF UNCERTAINTY IN FRACTURE APERTURE AND DENSITY ON PREDICTING CO_2 LOSS AND CAPROCK HYDRAULIC FRACTURE PROPERTIES ASSOCIATED WITH MEETING LONG-TERM CO_2 STORAGE GOALS

The purpose of this effort was to use the analytical model of Chapter 3 to examine the impact of uncertainty in caprock fracture aperture and density on predicting CO_2 loss and hydraulic fracture properties associated with meeting CO_2 storage criteria. Unlike Chapter 3, which focused on parameter bounds that met CCS criteria, this study focused on the probability of a measured fracture property meeting CCS criteria, and the associations (direct and induced) they have under increasing CO_2 loss constraints of the system. In particular, a stochastic framework was applied to the integrated analytical model for a generalized sensitivity analysis (GSA), using three Monte Carlo case experiments to evaluate the influence of uncertain caprock fracture and reservoir properties on $scCO_2$ leakage through an idealized caprock-reservoir system.

Major findings of this study suggest: (1) combinations of parameters meeting the 1 – 10% CO_2 loss criteria were rare events and more data is needed to better characterize fractures in caprocks considered for long-term CO_2 storage. (2) Fracture porosity was identified as a good diagnostic parameter for caprock screening, with a high probability (>95%) that caprocks with fracture porosities < 0.01% will meet performance goals. (3) Fracture permeability had the strongest association with CO_2 loss, with a high probability (>90%) that caprocks which met CCS goals had values < 10^{-17} m^2. (4) Correlations between reservoir parameters and caprock fracture properties became stronger as the CO_2 loss from the system became more constrained.

5.2   RELEVANCE OF STUDY TO SITE CHARACTERIZATION

In an uncertain geological environment where geochemical reactions can be neglected and pressure build-up within the reservoir is managed, this study suggests a low tolerance for well-connected caprock fractures within a pre-existing network. The study suggests that caprocks within the area of influence of a stored CO_2 plume should be examined with respect to their structural enclosures (in any, e.g. anticlines and domes), sharp changes in lithologic composition, influence on water resources, tectonic activity, or historical use like oil and gas exploration and production.

For a pre-existing fracture network within a potential caprock, further characterization of fracture connectivity, aperture size, fracture porosity, and fracture permeability distribution are needed since these are important factors influencing a caprock's ability to meet CCS goals. Hydraulic properties that met CO_2 storage goals, as determined from the analytical model, were based on the assumption that fracture connectivity was established. Therefore, an important first step in the analysis is to determine if a critical density of fractures is present in the caprock such that connectivity is established. For connected fracture networks, determination of the porosity and the permeability will help to assess the potential to meet CO_2 storage goals. Caprock fracture

properties that meet CCS goal are tied to the uncertainty of estimating the CO_2 plume extent. However, fracture porosity, which is independent of system size, may be a good screening/diagnostic parameter for defining caprock integrity. Wherein, if fracture porosity was detected above a threshold limit (e.g. >0.01%), it could indicate potentially unacceptable CO_2 leakage rates. In addition, the interdependence of these caprock fracture properties with reservoir properties that govern CO^2 plume migration plays a significant role in predicting CO_2 loss. This study suggests that the reservoir and caprock fracture properties need to be modeled together in order to assess the potential of caprock meeting CO_2 storage criteria.

5.3   ORIGINAL CONTRIBUTIONS

Original contributions of this dissertation to the development of CCS include: 1) A detailed synthesis of the physical and lithologic characteristics of sixteen regional caprock formations considered for CCS in the US, including structural, hydrological and lithological data relevant of CO_2 storage. The basin-wide information could provide reference to Features, Events, and Processes (FEPs) characterizations used for current risk assessments for CCS projects. 2) An integrated analytical model for $scCO_2$ transport that can be used to estimate suitable fracture properties of a fractured caprock, given the performance criteria for CCS projects. 3) Estimated bounds and probability associations of fracture properties suitable for meeting CCS performance criteria under various levels of system uncertainty and CO_2 loss constraints. 4) Identification of fracture porosity as a parameter that could serve as a diagnostic for determining the ability of a fractured caprock to contain $scCO_2$ and meet CCS goals.

5.4   RECOMMENDATIONS FOR FUTURE WORK

This research has determined how caprock fracture properties affect the ability of a caprock formation to meet CCS performance objectives, and how uncertainty in

measurements of those properties affect our ability to predict the probability of a specific caprock meeting CCS performance objectives. Uncertainty in characterizing the effect of fracture network properties on CO_2 transport can influence the risk assessment of a potential CCS project. There are several immediate areas for follow-up research:

- Reduce the number of assumptions in the analytical model. CO_2 loss predicted in the model assumes constant fluid properties for the $scCO_2$ and brine. Changes in fluid properties under non-isothermal conditions, which can occur as the CO_2 is transported vertically through fractures, can affect the reservoir pressure distribution and CO_2 flow rate through fractures.

- This study proved that uncertainty in fracture properties like aperture size, density, porosity and permeability impact the ability to predict CO_2 loss. However, detailed fracture analysis can be difficult to perform on the scale needed, and are costly. Therefore, it may be useful to perform a value–of–information study to assign benefits or penalties to project site characterization and/or costs, where measures taken to decrease the probability of CO_2 loss due to fracture property uncertainty are weighed against the cost of doing that activity.

- Compare the analytical loss model developed in this study to other models used to address risk of leakage through a caprock, particularly via wellbore leakage or mechanical failure due to reservoir overpressure. A comparative analysis of this type could help to identify the sources of greatest risk in a particular CCS operation.

- Address the question of whether measurement limitations of current tools used for fracture characterization can significantly affect CO_2 loss prediction and the

150

determination of the caprocks' ability to meet performance goals for long-term storage.

- Develop improved understanding of the geochemical factors affecting fracture aperture and connectivity. For example, conduct experiments on caprock dissolution or mineral precipitation as $scCO_2$ flow occurs under CCS conditions.

APPENDIX A

ADDITIONAL LITHOLOGY AND PETROLOGY OF SELECTED CAPROCKS AND RESERVOIRS CONSIDERED FOR CO_2 STORAGE IN U.S

APPENDIX A.1:

ISMAY-DESERT CREEK RESERVOIRS AND GOTHIC AND CHIMNEY ROCK SHALES SEALS: GEOLOGY, LITHOLOGY, MINERALOGY AND CO_2 STORAGE IMPLICATIONS

A.1.1   INTRODUCTION

In 2003 the U.S Department of Energy (U.S. DOE) initiated regional partnership programs to address the concern for rising atmospheric CO_2. These partnerships were formed to explore regional and economical means for geologically sequestering CO_2 across the United States and to set the stage for future commercial applications. Several options exist for geological sequestration and among these sequestering CO_2 into deep saline aquifers is one of the most promising. This is due, in part, to the possibility of stabilized permanent storage through mineral precipitation from chemical interactions of the injected carbon dioxide with the brine and reservoir rock. To mitigate CO_2 emissions successfully, the rock seal(s) considered for geological CO_2 sequestration need to be assessed for risk and be proven effective for containment of the injected CO_2 gas.

In the Southwest Regional Partnership (SWP) there is one test sites in Utah chosen to demonstrate Enhanced Oil Recovery (EOR) and CO_2 injection into a saline reservoir, the Ismay-Desert Creek formation. The test site lies within the Aneth Unit of the Greater Aneth Oil Field near Bluff, Utah in San Juan County (Figure 1). The data on the geological seals used for these sites were collected from literature sources in peer reviewed journals, open reports, and thesis dissertations containing geological data near the location of the demonstration site.

153

There are many mechanisms governing CO_2 escape from a potential storage reservoir, mainly through primary and secondary porosity. In order to properly assess the effectiveness of a geological seal by these mechanisms, it is important to consider the seal in the broader context of the prevailing structural features, lithostratigraphy, mineral, and physical characteristics that compose and influence the seal(s) at each field demonstration site. Of primary interest is the presence of soluble minerals in the seal rock that could be vulnerable to dissolution upon contact with supercritical CO_2 and CO_2-brine solutions.

A.1.2   GENERAL GEOLOGIC FRAMEWORK

The demonstration site lies in the southeastern part of the Paradox Basin, which is in the west-central part of the larger, Colorado Plateau (Figure 1)(Grout and Verbeek 1998). It is located on the shallow shelf area in the southeast where the Paradox basin trends northwest-southeast asymmetrically, thickening in a wedge-shaped sequence to the northwest with its deepest point adjacent to the Uncompahgre Plateau (Figures 2, 3) (Raup and Hite 1996; Hite and Lohman 1973). The present sedimentary basin covers an area of approximately 11,000 mi^2 with its boundaries are defined by the limit of the halite deposits in the Paradox Formation (Raup and Hite 1992).

The Paradox Basin is a large elongate, northwest-southeast trending structural depression that was predominantly developed during the Pennsylvanian (Desmoinesian) period with exposed sediments, Pennsylvanian through Cretaceous, over vast areas of the Basin(Grout and Verbeek 1998; McClure et al. 2003). Through continental collisions of North America with South America, and South Africa and rapid subsidence during the Pennsylvanian (and continuing into Permian) the Paradox Basin was created(Kluth and Coney 1981; McClure et al. 2003). The Paradox Basin is bounded by uplifts and basins of late Cretaceous – early Tertiary age but was infilled with arkosic material, intertongued with evaporitic and marine sediments during Pennsylvanian and Permian time period (Figure 2)(Hintze 1993; McClure et al. 2003). Quaternary erosion has left the infilled, wedge-

shaped basin with sediments up to 18,000 feet thick in the northeast by the Uncompahgre Plateau and approximately 6,000 feet in the southwest regions near the Monument Upwarp(Hite and Lohman 1973) (Figure 3).

Folds

The most outstanding structural features of the Paradox Basin are the evaporite-cored anticlines collectively known as the Paradox fold and fault belt to the northern and the Blanding sub basin to the south-southwest (Figure 3)(McClure et al. 2003; Grout and Verbeek 1998). The Paradox fold and fault belt trend about parallel to the Uncompahgre Uplift to the northeast of Basin and are unique to the continental Americas(Grout and Verbeek 1998). The fold and fault belt contain Middle Pennsylvanian through Upper Cretaceous rocks that are cut by nine regional sets of extension joints while the Blanding sub-basin remains relatively undeformed (Figure 3)(McClure et al. 2003; Grout and Verbeek 1998).

In the Paradox fold and fault belt, there exist an array of anticlines that overlie thick deposits of salts and occupy a rectangular shaped area about 50 miles wide and 120 miles long along the northeast margin of the basin (Hite and Lohman 1973) (p.24) (Figure 3). These salt deposits are of Middle Pennsylvanian age and can be divided geographically and structurally into five major systems(Hite and Lohman 1973). The major salt anticline systems are (1) Lisbon Valley – Dolores Valley, (2) Moab Valley – Spanish Valley – Pine Ridge, (3) Gypsum Valley, (4) Castle Valley – Paradox Valley and (5) Salt Valley – Cache Valley – Fisher Valley – Sinbad Valley (Figure 3). Smaller anticlines not associated with these major salt systems include the: Cane Creek and Lockhart anticline, and the Shafer, Rustler, and Gibson domes.

Some of the anticlines can be diapiric, where areas along the axis of the anticlines which were not covered by young sediments, allowed for large-scale migration of Paradox

155

strata toward and up the holes in the sediment cover(Hite and Lohman 1973). Non-diapiric anticlines, like the Shafer and Gibson domes have simple disharmonic folding. Other nondiapiric anticlines, such as the Lisbon Valley anticline are considerably more complex but retain the statigraphic identity of its evaporite core(Hite and Lohman 1973).

Faults

Most of the faults that occur within the Paradox Basin are associated with Paradox fold and fault belt in the northern region of the basin bordering the Uncompahgre Plateau. In this region, the salt deposits of the Paradox formation are faulted down against the Precambrian core of the uplift and covered by a thick wedge of Permian clastics(Hite and Lohman 1973) (Figures 4, 5).

Faults within the major salt anticline systems are commonly low-angle reverse faults or high-angle normal faults, where dip angles of nondiapiric structures seldom exceed 10° and angles of diapiric anticlines may exceed 30°(Hite and Lohman 1973). Within the Paradox formation strata, the salt anticlines have their base units deformed by block and strike-slip faulting(Hite and Lohman 1973). Below the Paradox formation, sediments are cut by normal faults with reliefs reaching a maximum of 5,615 feet(Hite and Lohman 1973).

In relation the demonstration site in the Blanding sub-basin, the Ismay and Desert Creek storage reservoir(s) along with the Gothic and Chimney Rock shale seals of the Paradox formation are uniform with respect to folds and unconformities. However, there exists many faults and fractures within the shales and storage reservoir, reported within the vicinity of the test site(Hite and Lohman 1973). Some of these faults exist north and northeast (< 50 miles), within San Juan County. Examples include the Lisbon and Paradox Valley anticlines (see Figures 3, 4, 5). Fractures in the Gothic and Chimney Rock shales in the Blanding sub-basin have veins are coated and filled with halite and other salts(Hite and Lohman 1973).

Other structural features

Other noteworthy structural features within the Paradox Basin include the presence of natural CO_2 reservoirs at the McElmo Dome in Montezuma County, Colorado and in the Lisbon field in San Juan County, Utah(Cappa and Rice 1995); and, CO_2 geysers along the Little Grand Wash fault and Salt Wash faults in Utah(Allis et al. 2005; Shipton et al. 2004).

The McElmo Dome is a natural carbon dioxide deposit within the Mississippian age Leadville formation, and was likely formed during the Late Cretaceous to early Tertiary Laramide orogeny(Cappa and Rice 1995; Stevens, Fox, and Melzer 2001). It is located at near the southern end of the Paradox Basin in Montezuma, Colorado where the domal structure that forms its closure measures approximately 22 miles north-south by 20 miles east-west, giving 440 mi^2 of closure(Stevens, Fox, and Melzer 2001)(Figure 6). There are significant internal faulting within the McElmo Dome, but reservoir simulations demonstrated that the flow of CO_2 is not affected by these faults (Stevens, Fox, and Melzer 2001).

The Lisbon field in San Juan County, Utah is similar to the McElmo dome in Colorado in that they both have natural CO_2 deposits within the Leadville formation but they differ in lithology and purity of produced CO_2(Cappa and Rice 1995).

The Little Grand Wash and Salt Wash faults in Grand and Emery County, Utah are structural elements whose geological timing are poorly understood but are estimated to be of Early Tertiary to Middle Cretaceous in age. The faults are part of a west-northwest trending group of normal faults, dipping at 70 - 80°that offset Pennsylvanian, Jurassic, and Cretaceous stratas(Shipton et al. 2004). The depth extension of the Little Grand Wash and Salt Wash faults are not fully known but speculated to sole into the salt sequences of the Paradox formation(Shipton et al. 2004).

There are localized CO_2 – charged springs situated along the Little Grand Wash and Salt Wash faults with the most widely known are the Crystal Geyser and Tenmile Geyser, respectively(Shipton et al. 2004). The Crystal Geyser has spring erupting up to a height of 82 feet every 4 – 12 hours while the Tenmile erupts infrequently only up to 5 feet high (Shipton et al. 2004).

A.1.3 DEMONSTRATION SITE GEOLOGY OF STORAGE RESERVOIR(S) AND GEOLOGICAL SEAL(S)

The Southwest Regional Partnership has undertaken multiple large and pilot - scale demonstration projects for CO_2 sequestration, primarily based on EOR and Enhance Coalbed Methane (ECBM) with one site potentially injecting also into a saline reservoir(Litynski et al. 2008; McPherson 2007). Discussion is limited to the site with potential injection into saline reservoirs, the Ismay and Desert Creek formations, within the Paradox Basin.

The demonstration site for EOR and saline CO_2 sequestration in the Paradox Basin lies in Utah within the Blanding sub-basin and the Greater Aneth Oil Field (Figure 3). The oil field has been extensively drilled since its discovery in 1956 and has produced 149 million barrels of an estimated 421 million barrels of oil in place(McPherson 2006). Also since 1998, multi-lateral horizontal wells have been used for a CO_2 water-alternating-gas pilot project to improve oil production(Hall 1998). The history of this site with its economic benefit along with technology in place for CO_2 injections made the site a prime choice for field testing within the SWP.

The primary purpose of the demonstration in the Greater Aneth Oil field is to demonstrate the capability of using Enhance Oil Recovery (EOR) to store significant amounts of CO_2 in a depleted oil reservoir while injecting into a saline reservoir. The results of which would improve CO_2 monitoring technologies and our understanding of CO_2 migration and storage capacity within potential reservoirs of the Paradox Basin(McPherson 2006).

CO₂ storage reservoirs

The target storage reservoirs are the informally named Ismay and Desert Creek zones of the Paradox formation. The Paradox formation is part of the Middle Pennsylvanian (Desmoinesian) Hermosa Group and contains 29 to 33 "cycles" or beds of halite separated by a sequence of clastic and penesaline interbeds (Figures 7, 8). These evaporite beds are unique in that they provide a record of sedimentation that is unequaled by other known evaporite sequences, both in number and completeness, where the saline facies below the Akah member of the Paradox formation can thicken up to 15,000 feet in northeast region of the basin (Figures 4,7) (Rueger 1996; Hite 1960).

The Ismay and Desert Creek zones occur 5,600 to 5,800 feet below the surface with planned CO_2 injections of up to 450,000 tons CO_2 into the reservoir(s) and 20,000 tons CO_2 into a saline formation below(McPherson 2006; Litynski et al. 2008) (Figure 7). The cumulative thickness of the reservoirs and seals is approximately 360 feet in the Monument upwarp area with reports of Ismay and Desert Creek thickness ranging from 15 – 30 feet(Chidsey, Eby, and Wray 2003; Nuccio and Condon 1996).

Geological seal(s)

The geological seals for the targeted storage reservoirs are the Gothic and Chimney Rock shales of the Paradox formation. The shales were developed during periods of glacioeustatic sealevel rise and fall with mud and terrigenous plant remains being transported into the basin from the Silverton delta which was situated in the southwest of Colorado(Schamel 2006; Fetzner 1960).

The Gothic and Chimney Rock shales are cycles 3 and 5 respectively within the 29 to 33 cycles of the Paradox formation (Figure 8). The shales also occur 5,600 to 5,800 feet below the surface with thicknesses up to 360 feet near the Monument Upwarp region (Nuccio and Condon 1996)(Figure 7).

A.1.4   MINERAL AND PHYSICAL CHARACTERISTICS OF STORAGE RESERVOIR, SEAL(S), AND OTHER RELEVANT GEOLOGICAL FEATURES

To estimate the impact of CO_2 injection into the Ismay and Desert Creek zones of the Paradox formation, it is important to know the mineral composition and physical traits of the potential reservoir(s), seal(s), and other relevant structural features that could impact the storage of the CO_2. Changes in the mineral composition of the Ismay, Desert Creek, Gothic or Chimney rock formations, due to lithological facies variation or CO_2 injection, could reduce or enhance injectivity and storage capacity at the site. Likewise, changes in the physical traits of these formations due to CO_2 injection could result in increased risk for leakage and migration of the gas, where interaction with other prominent structural features could impact the permanency of the CO_2 storage.

Figure 7 and Table 1 describe the lithology, mineralogy, and physical traits of the targeted storage reservoir(s) and seal(s), along with other geological features surrounding the site. Mineral characteristics are discussed in terms of the lithology and dominant minerals present in the reservoir(s), seal(s) rocks, and other relevant structural features. Physical traits of these formations are described in terms of permeability, porosity, fractures and fluid transport behavior. Emphasis is given to the description of the geological seal(s) due to their immediate relevance to CO_2 containment.

A.1.4.1   MINERAL CHARACTERISTICS

Storage reservoir(s)

The informally named Ismay and Desert Creek zones of the Paradox formation are contained within what is traditionally called the 'Ismay-Desert Creek interval', which comprise the first five cycles of the 29 – 33 found in the formation across the Paradox Basin(see Figure 8). The cycles are sequences of alternating layers of halite, anhydrite, dolostone, limestone, and black shale, with penesaline and siliciclastic rock interbeds at the base and a halite bed at the top(Schamel 2006; Raup and Hite 1992).

160

In the Blanding sub-basin, the Ismay zone is dominantly limestone comprising equant buildups of phylloid-algal material with small, locally variable subfacies of calcarenites and bryozoan mounds, and capped by anhydrite (Eby, Chidsey, McClure et al. 2003)(Figure 7). The Desert Creek zone is dominantly dolomite with regional, nearshore, shoreline trends with highly aligned, linear facies tracts(Eby, Chidsey, McClure et al. 2003). Both the Ismay and Desert Creek zonese have complex reservoir heterogeneity due to extensive diagenesis and various facies changes(Eby, Chidsey, McClure et al. 2003)

The dominant minerals of the Ismay and Desert Creek zones as seen by SEM and Thin Sections are dolomite, anhydrite, and pyrobitumen, with trace amounts of calcite, quartz, and smectite(Chidsey., Eby, and Taylor 2003; Thomas C. Chidsey and Eby 2003)(Table 1).

Geolgocial Seals

The geological seals considered for the demonstration site in the Greater Aneth Oil field are the informally named Gothic and Chimney Rock shales. The lithology of the Gothic and Chimney Rock shales are described in Figure 7 with the mineral and physical characteristics listed in Table 1. The term of 'shales' to describe the Gothic and Chimney Rock zones can be somewhat misleading in that they significant amounts of carbonates in their composition, as will be discussed later(Nuccio and Condon 1996). The shales occur in the "Ismay-Desert Creek interval' of the Paradox formation represented by cycles 3 and 5, respectively, and are located near the centers of the cycles designated(Schamel 2006)(Figure 8).

In the Blanding sub-basin, core descriptions of cycles 3 and 5, which contain the Gothic and Chimney Rock shales, were taken from the following wells: U.S. Department of Energy Elk Ridge No.1, Carbonit Exploration State No.1, and Southland Royalty West Water Creek No.1, E.L. and B.R. Cox Aztec Federal No.1, McCullah Oil and gas Corp – Pickett

Federal No.1-33, and Santa Fe Energy Lake Canyon Prospect Federal No.1-27 in San Juan County, Utah(Tuttle et al. 1996; Tromp 1995).

The well cores show the Gothic shale within cycle 3 to an organic-rich, dark-grey to black shale containing fine-sand to silt size quartz, feldspar, carbonate, and well ordered muscovite grains. Authigenic minerals include sparse patches of microcrystalline calcite cement, silt-size dolomite rhombs, abundant pyrite, and possibly marcasite. Micritic carbonates disseminated anhedral pyrite and minor pyrite cement. The rest of cycle 3 is shown to have fossiliferous, shaly limestone with calcareous siltstone and laminated dolostone(Tuttle et al. 1996)

The cores also show that the Chimney Rock shale (cycle 5) is a zone is composed of interbeds of light-to-dark limestone, medium-to-dark gray siltstone, dark-grey siltstone and dolostone, anhydrite, and gray-black shale. The black Chimney rock shale is laminated and platy, containing mostly dolomite with abundant reddish organic matter, silt-size quartz, calcite and dolomite with muscovite and large grains of pyrite. The limestone present in cycle 5 is fossilerous with the detrital grains of quartz and large rhombs of calcite. Marcasite may also be present in cycle 5(Tuttle et al. 1996).

In terms of abundance, whole rock petrographic analysis show that the Gothic and Chimney Rock shale consist of approximately 1/3 silt and clay-sized quartz, 1/3 carbonates, and 1/3 clay minerals and organic material(Tromp 1995; Hite, Anders, and Ging 1984). The 1/3 amount of quartz also includes Potassium and Plagioclase feldspars where, in the Blanding sub-basin near the Monument upwarp region, Plagioclase feldspar is found in minor amounts. The carbonates are 15 - 37 percent by weight, divided equally between dolomite and calcite, being more calcareous in the vicinity of test site, near the Monument Upwarp region, and act as cementing agents in the shales(Figure 3) (Tuttle et al. 1996; Tromp 1995). The clay minerals present, by XRD, show that illite/smectite is the

predominant clay minerals in cycle 5 (Chimney Rock), and a uniform distribution of chlorite/smectite and illite/smectite are present in cycle 3 (Gothic)(Tromp 1995) (Table 1).

Calcite and dolomite act as cementing agents between the clay minerals with anhydrite and halite present as vein filling mineral in fractures and micofractures(Tromp 1995). Both the Gothic and Chimney Rock shales contain significant amounts of pyrite with rare halides (sylvite, sinjarite, and tachyhydrite) also filling veins in fractures(Tromp 1995).

The Total Organic Carbon (TOC) present in the Gothic and Chimney rock shales in the vicinity of the test site, range from 0.1 – 5.85%(Tromp 1995). Throughout the Paradox Basin in the Ismay-Desert Creek interval, TOC ranges 0.3 – 10.98%(Nuccio and Condon 1996).

Other geological features

In addition to the mineralogy of the seals and reservoir, there exists within the Paradox Basin other structural features that could be relevant to geological sequestration. These include the salt anticlines of the Paradox fold and fault belt and the natural CO_2 deposit in the McElmo Dome and Lisbon Field (Figures 3, 6).

The McElmo Dome and the Lisbon field both have their natural CO_2 deposits in the Mississippian Leadville Limestone formation. The formation is composed of densely crystalline dolomite and limestone; and based on facies changes, is informally divided into upper and lower members in the subsurface (Cappa and Rice 1995; Baars 1966; Fouret 1982) (Figure 7).

The upper member of the Leadville Limestone is predominatly limestone marked by a zone of intraclastic carbonate with intraformational conglomerates, crinoidal biomicrite, and grain supported oolitic pelsparite lithofacies(Cappa and Rice 1995). The zone marker within the upper member of the Leadville Limestone formation, which signifies the boundary of the facies change from crinoidal to terrigenous material, is composed of dolomite, quartz,

kaolinite, calcite cemented siltstones and fine-grained sandstones, chert, and shale. Also, the lithoclasts (siltstone, sandstone, chert) range up to cobble in size and have abundant strauolite, in the heavy mineral fractions, with disseminated pyrite and nodular anhydrite(Fouret 1982) (Figure 7, Table1).

The lower member of the Leadville Limestone is composed of finely crystalline dolomite with leached crinoidal fragments and brecciation, and is overlain with coarse grained dolomite(Cappa and Rice 1995). The lower member of the Leadville Limestone also has a zone marker similar in composition to the upper member which separates it from the underlying formations. The marker is composed of dolomite, chert, sparry calcite cement, anhydrite, terrigenous clastics and organics. Also present in lesser amounts are feldspar, mica, and heavy minerals including opaques, pyrite, garnet, zircon, and epidote, with insoluble quartz, clay and organics(Fouret 1982).

The Paradox formation, which contains the storage reservoir(s) and seal(s) in the southern region of the Paradox Basin, transition facies to the north in the salt anticlines of the Paradox fold and fault belt region (Figure 3). Each salt anticline has up to 33 evaporite cycles with each cycle being composed of 70 – 80% halite (with or without potash), with the remainder being composed of anhydrite, silty dolomite, and black shale(Hite and Lohman 1973). The halite rock within each cycle is predominantly halite with an average grain size of 5 mm containing less than 2 – 3% of anhydrite, dolomite, quartz, clay, and talc. More than 50% of the halite rocks contain potash minerals sylvite (KCl) and carnallite ($KMgCl_3·6H_2O$)(Hite and Lohman 1973). The anhydrite rock is the least abundant constituent and has anhydrite nodules with fine-grained dolomitic mud laminae or matrix. The dolomite rock contains fine-grained dolomite with up to 50 percent by weight of well-sorted quartz silt. The black shales contain 20 – 30 weight percent carbonate with a nearly equal amount of dolomite and calcite. The black shales also contain clay-sized detritus

consisting of quartz, feldspar, and clay minerals, with up to 15% organic matter found locally(Hite and Lohman 1973) (Table 1).

The evaporites cycles of the salt anticlines show lateral changes in facies in addition to the vertical changes described previously. The lateral changes trend similarly to the vertical bed cycles with transitions from halite to dolomite from the northeast to southwest, respectively, in the basin(Hite and Lohman 1973).

A.1.4.2   *PHYSICAL CHARACTERISTICS*

Storage Reservoirs

Physical characteristics of the Ismay-Desert Creek zones of the Paradox formation were drawn from case studies performed on the Cherokee and Bug fields in the Blanding sub-basin near Greater Aneth Oil field. The Ismay zone was characterized at the Cherokee oil field and the Desert Creek zone was characterized at the Bug oil field (Thomas C. Chidsey, Eby, and Wray 2003).

The Cherokee field produces from a porous algal limestone and dolomite interval in the upper Ismay zone, which is separated from the Ismay-Desert Creek interval in that its facies contain more anhydrite-rich, intra-shelf basins(Eby, Thomas C. Chidsey et al. 2003). The Ismay reservoir has a thickness of 27 feet, extending over 0.5 square miles with a porosity average of 12% with permeability of 8 millidarcies (mD). The permeability is primarily due to vuggy and intercrystalline channels(Thomas C. Chidsey, Eby, and Wray 2003). The Ismay also has a water saturation of 38.1%(Thomas C. Chidsey, Eby, and Wray 2003).

The Bug field produces from a porous dolomitized bafflestone to a packstone or wackestone of the lower Desert Creek zone, which is segregated from the Ismay-Desert Creek interval with a facies change of abundant intra-shelf evaporite basins(Eby, Thomas C. Chidsey et al. 2003). The Desert Creek reservoir has a thickness of 15 feet with an areal

extent of 4 square miles with an average porosity of 11% and a permeability ranging from 1 – 500 mD (average: 25 – 30 mD) with water saturation of 32%(Thomas C. Chidsey, Eby, and Wray 2003). The porosity is due is moldic, vuggy, and intercrystalline networks with intervals containing open and closed fractures(Thomas C. Chidsey, Eby, and Wray 2003; Gournay 1999).

Geological Seals

The general chemical and physical characteristics of the Gothic and Chimney Rock shales are listed in Table 1.The black Gothic and Chimney Rock shales are represented by cycles 3 and 5 respectively and are relatively uniform (i.e. no folds or unconformities) in the vicinity of the test site (Figure 3). There is limited data on the porosity and permeability of the Gothic and Chimney Rock shales. The porosity and permeability listed in Table 1 are modeled values.

The shales are physically characterized by high porosity and low permeability except where fractured and as a general rule, the fractures range from hairline in size to 3 inches in width in the northern region of the Paradox basin (Hite 1960; Hite and Lohman 1973; Spangler, Naftz, and Peterman 1996).

Other geological features

The natural CO_2 deposits at the McElmo Dome and Lisbon field in the Paradox basin are found within the Mississippian Leadville Limestone. The McElmo Dome has a regional extent of 309 – 315 mi^2 occurring at 5,906 – 8,530 feet deep (averaging 6,890 feet)(Allis et al. 2001; Stevens, Fox, and Melzer 2001). The McElmo Dome has thickness ranging from 295 – 328 feet, porosity ranging from 3 – 25% (averaging 11%) , and permeability ranging from 0.1 to over 500 millidarcies (averaging 23 mD)(Stevens, Fox, and Melzer 2001; Allis et al. 2001; Cappa and Rice 1995) (see Table 1). The McElmo produces gases with 98 – 99% CO_2(Stevens, Fox, and Melzer 2001).

The Leadville Limestone formation at the Lisbon field has regional extent of approximately 12 – 20 mi^2 occurring at depths ranging 7,520 – 9,150 feet(Fouret 1982)(See Table 1). At the Lisbon field, the Leadville Limestone has a thickness of 400 – 500 feet but throughout the Paradox Basin it ranges from 100 – 800 feet(excluding one anomalous reading)(Fouret 1982; Cappa and Rice 1995). The Leadville formation has a porosity range of 5 – 25% (averaging 5%) and permeability range of 0.01 – 1000 millidarcies (averaging 22 mD) due to facies changes and detrital clay between the upper and lower members of the formation(Cappa and Rice 1995; Fouret 1982). The most important type of porosity at the Lisbon field is moldic and intercrytalline, with porosity being affected by dolomitization, leaching, and fracturing of the reservoir(Miller 1985; Fouret 1982). The produced gas from the Lisbon field is 17 – 35% CO_2(Cappa and Rice 1995).

The salt anticlines in the northern Paradox fold and fault belt region of the Paradox Basin have units that are correlated to the Paradox formation in the Blanding sub-basin. These salt anticlines have evaporite cycles 2,500 – 14,000 feet thick, where thickness may vary from zero to greater than 10,000 feet within 3 geographic miles(Hite and Lohman 1973). The evaporite cycles of the salt anticlines have dense anhydrite and dolomite rocks but have areas intensely fractured. Observed flow of brine and/or oil and gas has been seen in cores from these anticlines(Hite and Lohman 1973). The black shales within these cycles are characterized by high porosity and low permeability except where fractured. Within these black shales, fracturing is widespread where they are commonly filled with halite and other potash minerals(Hite and Lohman 1973).

The salt anticlines have caprocks that are porous and can be saturated with brine, such as in the Paradox valley. The caprocks of the salt anticlines have an average thickness of 1,000 feet and consist mainly of gypsum and anhydrite, with minor amounts of clay. These salt anticlines have been resistant to dissolution as seen through their geologic

persistence, with an estimated halite removal rate range of 3 – 900 feet per million years(Hite and Lohman 1973).

In addition to the natural CO_2 deposits and salt anticlines present in the San Juan County, Utah where the demonstration site is located, there exists salinization of drinking waters in the Navajo aquifer, which includes the Entrada, Navajo, and Wingate sandstones from the brine of the Cutler formation(Spangler, Naftz, and Peterman 1996) (Figure 9). The salinization of drinking water occurs at the Greater Aneth Oil field and could be derived from natural pathways or from an in situ source which pre-dates the development of the oil field(Spangler, Naftz, and Peterman 1996). This documented phenomenon occurs in the Permian Cutler formation through to the Triassic – Jurassic Navajo sandstone and is stratigraphically situated above the Hermosa group, which contains the target reservoir(s) and seal(s) for CO_2 sequestration at the Greater Aneth Oil field.

A.1.5   IMPLICATIONS FOR CO_2 SEQUESTRATION RESERVOIR LEAKAGE

Carbon capture and storage into geological media has as part of its goal, the need to estimate the risk associated with CO_2 injection. Some have proposed a framework to assess risk through the use of quality factors assigned to various reservoir and seal characteristics like thickness, lithology, and proximity to faults and fracture networks(Oldenburg 2005). This study helps to address some of these factors at the EOR/saline demonstration site at Greater Aneth Oil field, San Juan County, Utah, by focusing on mineral phases that are susceptible to CO_2 attack that are present in the surrounding structural features and influenced by the hydrogeological behavior of the sediments.

Based on the information reviewed in the previous sections, implications for the permanence of CO_2 storage at this demonstration site can be categorized into the following topics centered on lithology, structural geology, and reservoir fluid behavior along with oil

and gas production history. These topics will be discussed further with an emphasis on soluble minerals present in each of these categories.

In terms of lithology, there are significant amounts of carbonate (15 – 37%) in the composition of the primary seal(s) that could be susceptible to CO_2 attack depending on exposure to brine fluids. Calcite and dolomite appear also as cementing agents between the illite/smectite and chlorite/smectite clay minerals(Tuttle et al. 1996; Tromp 1995). The composition of the Gothic and Chimney Rock seals at the Greater Aneth Oil field change laterally as the Paradox Basin trends north. The carbonate-rich Gothic and Chimney Rock shales trend into evaporite cycles of the Paradox 'fold and fault belt' in the northwest – northeast region of the Paradox Basin where they are interbedded among thick beds of halite, with anhydrite and silty dolomite(Hite and Lohman 1973).

Comparing the clay mineralogy and the high organic content of the Gothic and Chimney Rock shales to other organic rich shales across the U.S. we find that shales with the expandable clays, similar to the composition of illite/smectite and chlorite/smectite found in Gothic and Chimney rock shales in the southeast region of the Paradox Basin, have been reported to sequester CO_2 (Nuttall 2003, 2007; U.S. Department of Energy 2006).

The Gothic and Chimney Rock shales, along with increasing amounts of evaporite, have by inference demonstrated to be a naturally effective seal to the CO_2 deposits at the McElmo Dome and Lisbon field of the Paradox Basin. The CO_2 deposits are found in the Leadville Limestone formation underlying the mid-Pennsylvanian units of the Paradox formation, where the CO_2 gas exists with purity up to 99% in this saline reservoir(Stevens, Fox, and Melzer 2001) (Figure 7).

No leakage of the CO_2 gas produced from the McElmo Dome has affected the surrounding community in 15 years of operation(Stevens, Fox, and Melzer 2001). However, in the subsurface, the effectiveness of the evaporites and black shales of the Paradox

formation to contain the CO_2 deposits of the Leadville formation is offset by regional faults, fractures, and lateral changes in lithology, which is evidenced in the vertical migration of CO_2 gas into multiple sediments(Allis et al. 2001).

The Lisbon field, along with other regions within the Paradox basin containing natural occurrences of CO_2, has faults and fractures within the Paradox formation and younger sediments (see Figure 5). The faults not only can cause vertical migration of CO_2 gas in the subsurface but can also have high CO_2 fluxes near the surface, as seen with Crystal Geyser and Tenmile Geyser(Shipton et al. 2004; Allis et al. 2005). Fractures present in the Gothic and Chimney Rock shale are filled with carbonates (i.e. calcite, dolomite) and halides (i.e. halite, sylvite) along with gypsum and pyrite which could potentially be soluble and reactive with CO_2(Tromp 1995; Tuttle et al. 1996).

In terms of relevant hydrogeological behavior surrounding the Aneth site, there is documented salinization of the drinking waters of the Navajo aquifer from the Cutler formation below(Spangler, Naftz, and Peterman 1996). Some of the ideas postulated for the salinization of the drinking waters include: a network of natural fractures, an in situ brine source, and flow through old well casings.

The reported salinization of the Navajo aquifer system is important to note for sequestration efforts at the Greater Aneth site because it demonstrates the ability of brine waters of the Cutler formation to flow through the 1,200 feet thick Chinle-Moenkopi formation to the Navajo aquifer system. The Chinle-Moenkopi is considered a hydraulic seal and in other areas, within the Colorado plateau, is primarily composed of quartz, calcite, dolomite, hematite, feldspar, illite, chlorite, and Montmorillonite(Cadigan and Stewart 1971; Schultz 1963). The cements of the Chinle-Moenkopi are similar to what is found in the Gothic and Chimney Rock shales. Also, the Cutler formation overlies the Hermosa group that contains the target reservoir and seals. If CO_2 were to escape from the Ismay-Desert

Creek interval it could travel through similar natural fracture paths, bringing along with it any exsolved minerals or substances.

There has been extensive horizontal well drilling in this area due to oil and gas exploration. It is likely that fractures were hydraulically induced into the Gothic and Chimney Rock shales, in addition to the fractures that occurred naturally over tectonic history. In addition, the Gothic and Chimney Rock shales also serve as source rocks for hydrocarbon production, where leakage of hydrocarbons through geologic seals of this type are a common phenomenon (Watts 1987; McPherson 2006).

A.1.6   SUMMARY

In examining the literature available for the mineral, physical, and surrounding structural characteristics of the Gothic and Chimney Rock seals used at the Greater Aneth Oil field, the study showed that their exists the potential for slow leakage. This is based on several factors: 1.) the extensive horizontal drilling techniques used during oil and gas exploration which could have hydraulically created fractures in the seals (or accentuated pre-existent ones), 2.) the presence of soluble minerals in the matrix, cement, and veins of the shale cycles and their reported fractures, 3.) documented salinization of drinking waters from formations above the targeted reservoir(s) and seal(s), indicating a possible fracture network liable for CO_2 transport, and 4.) the behavior of natural CO_2 deposits of similar mineralogy to leak CO_2 into multiple horizons above their storage reservoir.

The study of the Gothic and Chimney Rock shales of the Paradox Basin at the Greater Aneth site revealed that dolomite, calcite and halite are abundant soluble minerals present in the shales that could be susceptible to CO_2 attack. This information can then be used to guide experiments and modeling efforts aimed as understanding the dominant chemistries that could impact leakage and risk assessment.

A.1.7 REFERENCES

Allis, R., S. P. White, T. C. Chidsey Jr, W. Gwynn, C. Morgan, and M. Adams. 2001. Natural CO2 reservoirs on the colorado plateau and southern rocky mountains: Candidates for CO2 sequestration. Paper read at Proceedings fo the First National Conference on Carbon Sequestration, May 14-17, 2001, at Washington, D.C.

Allis, Rick, Deborah Bergfeld, Joe Moore, Kevin McClure, Craig Morgan, Thomas Chidsey, Jason Heath, and Brian McPherson. 2005. Implications of results from CO2 flux surveys over known CO2 systems for long-term monitoring. In *Fourth Annual Conference on Carbon Capture and Sequestration*. Alexandria, VA.

Baars, D.L. 1966. Pre-Pennsylvanian paleotectonics - Key to basin evolution and petroleum occurences in the Paradox Basin, Utah and Colorado. *American Association of Petroleum Geologists Bulletin* 50 (10):2082-2111.

Cadigan, Robert A., and J.H. Stewart. 1971. Petrology of the Triassic Moenkopi Formation and Related Strata in the Colorado Plateau Region. United States Government Printing Office, Washington, D.C.: U.S. Geological Survey

Cappa, James A., and Dudley D. Rice. 1995. Carbon Dioxide in Mississippian Rocks of the Paradox Basin and Adjacent Areas, Colorado, Utah, New Mexico, and Arizona. In *Evolution of Sedimentary Basins - Paradox Basin*: U.S. Geological Survey

Carter, F.W. 1970. Geology of the salt anticline region in southwestern Colorado: U.S. Geological Survey Professional Paper.

Chidsey, Thomas C., David E. Eby, and Laura L. Wray. 2003. Deliverable 2.1.1, Porosity/permeability cross-plots: Cherokee and Bug Fields, San Juan County, Utah, and Little Ute and Sleeping Ute Fields, Montezuma County, Colorado. In *Heterogeneous shallow-shelf carbonate buildups in the Paradox Basin, Utah and Colorado: Targets for increased oil production and reserves using horizontal drilling techniques*: Utah Geological Survey.

Chidsey., Thomas C., David E. Eby, and Louis H. Taylor. 2003. Deliverable 1.2.3, Scanning Electron Microscopy and pore casting: Cherokee and Bug Fields, San Juan County, Utah. In *Heterogeneous shallow-shelf carbonate buildups in the Paradox Basin, Utah and Colorado: Targets for increased oil production and reserves using horizontal drilling techniques*: Utah Geological Survey.

Eby, David E., Thomas C. Chidsey, Kevin McClure, and Craig D. Morgan. 2003. Semi-Annual Technical Progress Report: October 6, 2002 - April 5, 2003 In *Heterogeneous shallow-shelf carbonate buildups in the Paradox Basin, Utah and Colorado: Targets for increased oil production and reserves using horizontal drilling techniques*: Utah Geological Survey.

Eby, David E., Thomas C. Chidsey, Craig D. Morgan, Kevin McClure, and Thomas C. Chidsey, Jr. 2003. Regional facies trends in the upper Ismay Zone of the Blanding Sub-basin of the Paradox Basin, Utah; aids for identifying possible targets for horizontal drilling. In *Annual Meeting Expanded Abstracts - American Association of Petroleum Geologists, vol.12*.

Eby, David E., Jr. Thomas C. Chidsey, Kevin McClure, and Craig D. Morgan. 2003. Semi-Annual Technical Progress Report: October 6, 2002 - April 5, 2003 In *Heterogeneous shallow-shelf carbonate buildups in the Paradox Basin, Utah and Colorado: Targets for increased oil production and reserves using horizontal drilling techniques*: Utah Geological Survey.

Fetzner, R.W. 1960. Pennsylvanian paleotectonics of Colorado Plateau. *AAPG Bulletin* 44:1371-1413.

Fouret, Kent Leslie. 1982. Depositional and diageneitc environments of the Leadville formation at Lisbon Field, Utah. Master of Science, Texas A&M University.

Gournay, Jonas Paul. 1999. Phylloid Algal Biotherms and Ooid Grainstones: Characterization of Reservoir Facesi Utilizing Subsurface Data from the Aneth Platform and Outcrop Data Along the San Juan River, Paradox Basin, Southeastern Utah, University of Texas at Austin.

Grout, Marilyn A., and Earl R. Verbeek. 1998. Tectonic and Paleostress Significance of the Regional Joint Network of the Central Paradox Basin, Utah and Colorado. In *Laccolith Complexes of Southeastern Utah: Tectonic Control and Time of Emplacement -- Workshop Proceedings*, edited by J. D. Friedman and A. C. Huffman, Jr.: U.S. Geological Survey Bulletin.

Hall, Scott D. 1998. Multilaterals convert 5 spot to line drive waterflood in SE Utah. Paper read at Proceedings of the International Oil & Gas Conference and Exhibition in China, IOGCEC, at Beijing, China.

Hintze, L.F. 1993. Geologic history of Utah. *Brigham Young University Studies Special Publication* 7:202.

Hite, R. J. 1960. Stratigraphy of the saline facies of the Paradox Member of the Hermosa Formation of southeastern Utah and southwestern Colorado. In *Four Corners Geological Society Guidebook 3rd Field Conference*.

Hite, R. J., D.E. Anders, and T.G. Ging. 1984. Organic-rich source rocks of Pennsylvanian age in the Paradox basin of Utah and Colorado. In *Hydrocarbon Source Rocks of the Greater Rocky Mountain Region*, edited by J. Woodward, F. F. Meissner and J. L. Clayton. Denver, CO: Rocky Mountain Association of Geologists Guidebook.

Hite, R. J., and D. H. Buckner. 1981. Stratigraphic correlations, facies concepts and cyclicity in Pennsylvanian rocks of the Paradox Basin. *Field Conference - Rocky Mountain Association of Geologists* 1981:147-159.

Hite, R. J., and S.W. Lohman. 1973. Geological Appraisal of Paradox Basin Salt Deposits for Waste Emplacement. In *United States Department of the Interior Geological Survey*: United States Department of the Interior Geological Survey.

Hite, Robert J., and S. W. Lohman. 1973. Geologic Appraisal of Paradox Basin Salt Deposits for Waste Emplacement: U.S. Geological Survey.

Hite, Robert J., and Stanley William Lohman. 1973. Geological Appraisal of Paradox Basin Salt Deposits for Waste Emplacement. Denver, Colorado: U.S. Geological Survey.

Kelly, V.C. 1958a. Tectonics of the region of the Paradox Basin. In *Guidebook to the Geology of the Paradox Basin*, edited by A. F. Sanborn: Intermountain Association of Petroleum Geologists.

———. 1958b. Tectonics of the Black Mesa region of Arizona. In *Guidebook of the Black Mesa Basin, Northeastern Arizona*, edited by R. Y. Anderson and J. W. Harshbarger: New Mexico Geological Society.

Kluth, C.F., and P.J. Coney. 1981. Plate tectonics of the Ancestral Rocky Mountains. *Geology* 9:10-15.

Litynski, John T., Sean Plasynski, Howard G. McIIvried, Christopher Mahoney, and Rameshwar R. Srivastava. 2008. The United States Department of Energy's Regional Carbon Sequestration Partnerships Program Validation Phase. *Environ Int.* 34:127-138.

McClure, Kevin, Craig D. Morgan, Thomas C. Chidsey, and David E. Eby. 2003. Deliverable 1.1.1 Regional Paradox Formation Structure and Isochore Maps, Blanding Sub-Basin, Utah. In *Heterogeneous shallow-shelf carbonate buildups in the Paradox Basin, Utah and Colorado: Targets for increased oil production and reserves using horizontal drilling techniques*. Salt Lake City, Utah: Utah Geological Survey.

McPherson, Brian. 2006. CO2 Sequestration in Saline Formations - II: Southwest Regional Partnerships on Carbon Sequestration (SWP). Paper read at Regional Carbon Sequestration Partnerships Initiative Review Meeting, October 3-4 at Pittsburgh, PA.

———. 2007. Large Scale Projects: Southwest Regional Partnerships on Carbon Sequestration (SWP). Paper read at Regional Carbon Sequestration Partnerships Annual Review Meeting, December 12-13, at Pittsburgh, PA.

Miller, J.A., ed. 1985. *The depositional and reservoir facies of the Mississippian Leadville Formation, Northwest Lisbon field, Utah*. Edited by P. Roehl and P. Choquette, *Carbonate petroleum reservoirs (Casebooks in Earth Sciences)*. New York: Springer-Verlag.

Nuccio, Vito F., and Steven M. Condon. 1996. Burial and thermal history of the Paradox Basin, Utah and Colorado, and petroleum potential of the Middle Pennsylvanian Paradox Basin. In *Evolution of Sedimentary Basins - Paradox Basin*, edited by A. C. Huffman. United States Government Printing Office, Washington, D.C.: U.S. Geological Survey.

Nuttall, Brandon. 2003. ANALYSIS OF DEVONIAN BLACK SHALES IN KENTUCKY FOR POTENTIAL CARBON DIOXIDE SEQUESTRATION AND ENHANCED NATURAL GAS PRODUCTION. Lexington, Kentucky: Kentucky Geological Survey.

———. 2007. Analysis of Devonian Shale in Eastern Kentucky for Carbon Sequestration Possibilites. *Energeia, University of Kentuck Center for Applied Energy Research*, 1-3.

Oldenburg, Curtis M. 2005. Health, Safety, and Environmental Screening and Ranking Framework for Geologic CO2 Storage Site Selection.: Lawrence Berkeley National Laboratory Paper.

Raup, Omer B., and Robert J. Hite. 1992. Lithology of evaporite cycles and cycle boundaries in the upper part of the Paradox Formation of the Hermosa Group of Pennsylvanian age in the Paradox Basin, Utah and Colorado.

———. 1992. Lithology of evaporite cycles and cycle boundaries in the upper part of the Paradox Formation of the Hermosa Group of Pennsylvanian age in the Paradox Basin, Utah and Colorado. In *Evolution of sedimentary basins - Paradox Basin*, edited by A. C. Huffman. United States Government Printing Office, Washington, DC: U.S. Geological Survey bulletin.

———. 1996. Bromine geochemistry of chloride rocks of the Middle Pennsylvanian Paradox Formation of the Hermosa Group, Paradox Basin, Utah and Colorado.

———. 1996. Bromine geochemistry of chloride rocks of the Middle Pennsylvanian Paradox Formation of the Hermosa Group, Paradox Basin, Utah and Colorado. In *Evolution of Sedimentary Basins - Paradox Basin*, edited by A. C. Huffman, Jr. United States Government Printing Office, Washington, D.C.: U.S. Geological Survey.

Rueger, Bruce F. 1996. Palynology and its relationship to climatically induced depositional cycles in the Middle Pennsylvanian (Desmoinesian) Paradox Formation of southeastern Utah.

Schamel, Steven. 2006. Shale Gas Resources of Utah: Assessment of Previously Undeveloped Gas Discoveries. Salt Lake City, Utah: GeoX Consulting, Inc. and the Utah Department of Natural Resources, Utah Geological Survey.

Schultz, Leonard G. 1963. Clay Minerals in Triassic Rocks of the Colorado Plateau. In *Contributions to the Geology of Uranium*. United States Government Printing Office, Washington, D.C: U.S. Geological Survey.

Shipton, Z.K., J.P. Evans, D. Kirschner, P.T. Kolesar, A.P. Williams, and J. Heath. 2004. Analysis of CO2 leakage through 'low-permeability' faults from natural reservoirs in the Colorado Plateau, east-central Utah. In *Geological Storage of Carbon Dioxide*, edited by S. J. Baines and R. H. Worden. London: The Geological Society of London 2004.

Spangler, L. E., D. L. Naftz, and Z. E. Peterman. 1996. Hydrology, Chemical Quality, and Characterization of Salinity in the Navajo Aquifer in and near The Greater Aneth Oil Field, San Juan County, Utah. Salt Lake City, Utah: U.S. Geological Survey.

Spangler, L.E., D.L. Naftz, and Z.E. Peterman. 1996. Hydrology, Chemical Quality, and Characterization of Salinity in the Navajo Aquifer in and near The Greater Aneth Oil

Field, San Juan County, Utah. In *Water-Resources Investigations Report* U.S. Geological Survey.

Stevens, Scott H., Charles E. Fox, and L. Stephen Melzer. 2001. McElmo Dome and St. Johns Natural CO2 deposits: Analogs for Geologic Sequestration. In *Greenhouse Gas Control Technologies: Proceedings of the 5th International Conference on Greenhouse Gas Control Technologies*, edited by R. A. Durie, D. J. Williams, A. Y. Smith, P. McMullan and C. A. J. Paulson. Cairns, Australia: CSIRO Publishing.

Thomas C. Chidsey, Jr., and David E. Eby. 2003. Deliverable 1.2.1A, Thin section descriptions: Cherokee and Bug Fields, San Juan County, Utah. In *Heterogeneous shallow-shelf carbonate buildups in the Paradox Basin, Utah and Colorado: Targets for increased oil production and reserves using horizontal drilling techniques*: Utah Geological Survey.

Thomas C. Chidsey, Jr., David E. Eby, and Laura L. Wray. 2003. Deliverable 2.1.1, Porosity/permeability cross-plots: Cherokee and Bug Fields, San Juan County, Utah, and Little Ute and Sleeping Ute Fields, Montezuma County, Colorado. In *Heterogeneous shallow-shelf carbonate buildups in the Paradox Basin, Utah and Colorado: Targets for increased oil production and reserves using horizontal drilling techniques*: Utah Geological Survey.

Tromp, Dirck E. 1995. Clays as indicators of depositional and diagenetic conditions in Pennsylvanian black shales, Paradox Basin, Utah and Colorado. Master's, Department of Geology, Colorado School of Mines, Golden.

Tuttle, Michele L., Timothy R. Klett, Mark Richardson, and George N. Breit. 1996. Geochemistry of two interbeds in the Pennsylvanian Paradox Formation, Utah and Colorado: a record of deposition and diagenesis of repetitive cycles in a marine basin. In *Evolution of sedimentary basins - Paradox Basin*, edited by A. C. Huffman. United States Government Printing Office, Washington, D.C.: U.S. Geological Survey bulletin.

U.S. Department of Energy, National Energy Technology Laboratory. 2006. 2006 Carbon Sequestration Atlas of the United States and Canada. Morgantown, WV: U.S. Department of Energy, Office of Fossil Energy, National Energy Technology Laboratory.

Watts, N.L. 1987. Theoretical aspects of cap-rock and fault seals for single- and two-phase hydrocarbon columns. *Marine and Petroleum Geology* 4 (11):274-307.

Wengerd, S.A., and M.L. Matheny. 1958. Pennsylvanian system of the Four Corners region. *American Association of Petroleum Geologists Bulletin* 42 (9):2048–2106.

White, S.P., R.G. Allis, J. Moore, T.Chidsey, C.Morgan, W. Gwynn, and M. Adams. 2002. Natural CO2 Reservoirs on the Colorado Plateau and Southern Rocky Mountains, USA, A Numerical Model. In *Proc. Greenhouse Gas Control Technologies 6th Conference*. Kyoto, Japan

———. 2003. Injection of CO2 into an Unconfined Aquifer Located beneath the Colorado, Central Utah, USA. In *Second Annual Conference on Carbon Sequestration, NETL Proceedings*. Alexandria, Virginia.

Table A.1.1: Stratigraphic and lithologic description of the Gothic and Chimney Rock Shale with surrounding units in the Monument Upwarp region of the Paradox Basin. N = north, NE = northeast, NW = northwest, SW = southwest.

System	Series	Group	Formation/member			Thickness (ft)	Description
Pennsylvanian	Middle and Upper Pennsylvanian (Desmoinesian)	Hermosa Group	Honaker Trail Formation			900[1]	Composed of cyclically deposited of limestone, sandstone, and shale with varying amounts of sandstone and shale. Grades to dolomite, arkose, and mica siltsone in NE [1,2].
			Paradox Formation	Upper Pennsylvanian Ismay-Desert Creek Interval	Ismay	15 – 30[3] 40 – 50[4]	Dominantly limestone composed of small, phylloid-algal buildups; locally variable, inner-shelf, skeletal calcarenites; and rare open-marine, bryozan mounds. Capped by anhydrite[5,6].
					Gothic Shale	? – 200[7]	Also named 'cycle 3' in deposition by Hite and others (1970). Contains beds of halite with successive interbeds of silt, dolomite, black shale, silty dolomite, and anhydrite. Shale is dolomitic with numerous vertical fractures filled with halite (chalcedony and pyrite to a lesser extent) becoming more pronounced in N. and NW regions of the basin. These interbeds are vertically symmetrical with respect to lithology. The base of this interval is anhydrite[7,8].
					Desert Creek	15 – 30[3] 40 – 50[4]	Dominantly dolomite in SE Utah area of interest Halite (majority), trace Anhydrite laminations[5,8].
					Chimney Rock Shale	30 – 40[7]	Also named 'Cycle 5' in deposition [9]. Contains beds of halite with successive interbeds of silt, dolomite, black shale, silty dolomite, sylvinite (Potash salts) and anhydrite Shale is calcerous and dolomitic and with fractures in and outside of site area, extending to the N and NE regions with veins filled with halite, anhydrite and to a lesser extent pyrite [7,8].
	Atokan			Middle Penn.	Akah	700[1]	Dark-grey siltstone, arkosic granulite overlain by gypsum. Includes dolomite and black shales to N and cherty limestone and porous dolomite and gray shales in SW [2].
					Barker Creek		
					Cane creek cycle		Predominantly rock Halite and Anyhdrite laminae with small amounts of sylvite. Considered Cycles 13-26 [10].
			Pinkerton Trail Formation			84 – 195[2]	Consist of fossiliferous, marine limestone interbedded and overlain with dark shale[1,2].
	Morrowan		Molas Formation			150[2] 325[1]	Consists of marine limestone with redbed sequence of siltstone, waxy red shale, calcareous sandstone and limestone lentils.of marine limestone [1,2]

360[1] (Paradox Formation total thickness)
700[1] (Atokan interval thickness)

Mississippian	Osagean - Kinderhookian	Leadville Limestone	450[1]	Predominantly limestone with dolomite[1,11]. Upper member predominantly limestone with a zone of intraclastic carbonate with intraformational facies[12]. Lower member is composed of finely crystalline dolomite with leached fossil fragments and brecciation, and overlain with coarse grained dolomite[11]

Table A.1.1: Cont'd

- ☐ - Shaded unit represents seal rock

- ⌇ - Represents stratigraphic unconformity

1.) Nuccio and Condon (1996)
2.) Wengerd and Matheny (1958)
3.) Chidsey, Eby, and Wray (2003)
4.) Spangler, Naftz, and Peterman (1996)
5.) Eby, Chidsey, Morgan et al. (2003)
6.) McClure et al. (2003)
7.) Tuttle et al. (1996)
8.) Raup and Hite (1992)
9.) Hite and Lohman (1973)
10.) Rueger (1996)
11.) Cappa and Rice (1995)
12.) Fouret (1982)

TABLE A.1.2: Physical and chemical properties of the Gothic and Chimney Rock shales, Leadville Limestone, and the Salt Anticlines in the Paradox Basin.

Characteristic	Gothic & Chimney Rock Shale	Leadville Limestone (McElmo Dome & Lisbon field)	Salt Anticlines	Comments
Physical properties				
Depth (ft)	5,000 - 6,000[1]	McElmo: 5,906 – 8,530[2] (av: 6,890)[3] Lisbon: 7,520 – 9,150[4,5]	-	Lisbon depth estimated from Figures 5,9,22, and 24 of source[5]
Thickness (ft)	360[6]	McElmo: 295 – 328[2-4] Lisbon: 400 – 515[4,5]	2,500 – 14,000 (cycles) 1,000 (caprock)[7]	Table 3 of source[6]; Lisbon thickness estimated from Figure 5,9,22, and 24 of source[5]; Caprock within cycles of salt anticline[7]
Porosity (%)	10[8,9]	McElmo: 3 – 25% (av: 11%)[2,3] Lisbon: 0 – 25% (av: 5%)[4,5]	-	Modeled CO_2 injection[9]; Lisbon values taken from Figures 20, 21 of source[5]
Permeability (md)	0.1[9]	McElmo: 0.1 – 500 (av: 23)[2,3] Lisbon: 0.001 – 1,000 (av: 22)[4,5]	-	Modeled CO_2 injection[9]; Lisbon values taken from Figures 20, 21 of source[5]
Areal extent (mi^2)	11,000[10]	McElmo: 309 - 315[2,3] Lisbon: 12 – 20[5]	-	Lisbon extent estimated from Figure 5 of source[5]
Major Mineral Components (> 20 wt%)				
Quartz	20 – 40 wt%[6,11]	>20 wt%[5]	-	
Halite	-	-	70 – 80 wt%[7]	Halite rocks including potash[7]
Sylvite	-	-	>20 wt%[7]	Potash mineral in halite rocks[7]
Carnallite	-	-	>20 wt%[7]	Potash mineral in halite rocks[7]
Carbonates	20 – 30 wt%; 15 – 37 wt%[6,12,7]	>20 wt%[4,5]	-	Carbonates present in Gothic and Chimney Rock are of the two types listed[6,12,7]; Upper member is mostly calcite, lower member mostly dolomite[5]
- Calcite	-	-	-	
- Dolomite	-	-	-	
Clays	~ 33 wt%[12]	-	-	Clays in Gothic and Chimney rock shale are of the two types listed[12]
- Illite/smectite	-	-	-	
- Chlorite/smectite	-	-	-	
Minor minerals Component (< 20 wt%)				
Quartz	-	-	<20 wt%[7]	Present in black shales, halite, and dolomite rocks[7]
Dolomite	-	-	<20 wt%[7]	Present in halite, dolomite, and anhydrite rocks, and 20 – 30% of black shales[7]
Calcite	-	<20 wt%[5]	<20 wt%[7]	Cement of upper member siltstones and in zone 'marker' lithoclasts[5]; Present in 20 – 30% of black shales[7]
Halite	< 20 wt%[13]	-	-	Value not calibrated against standards; Fracture vein filling[13]
Anhydrite	< 20 wt%[13]	<20 wt%[5]	<20 wt%[7]	Value not calibrated against standards; Fracture vein filling[13]; In zone 'marker' lithoclasts[5]; Present in black

178

				shales, halite, dolomite, and anhydrite rocks[7]
Gypsum	< 20 wt%[13]	-	-	Value not calibrated against standards[13]
Potassium Feldspar	< 20 wt%[13]	-	-	Value not calibrated against standards[13]
Sodium Feldspar	< 20 wt%[13]	-	-	Value not calibrated against standards[13]
Feldspar	-	<20 wt%[5]	-	In zone 'marker' lithoclasts and in lesser amount than other 'marker' minerals[5]; Present in black shales[7]
Apatite (fluorapatite)	< 20 wt%[13]	-	-	Value not calibrated against standards[13]
Pyrite	< 20 wt%[13]	< 20 wt%[5]	-	Fracture vein filling[13]; In zone 'marker' lithoclasts and in lesser amount than other 'marker' minerals[5]
Garnet	-	<20 wt%[5]	-	In zone 'marker' lithoclasts and in lesser amount than other 'marker' minerals[5]
Zircon	-	<20 wt%[5]	-	In zone 'marker' lithoclasts and in lesser amount than other 'marker' minerals[5]
Epidote	-	<20 wt%[5]	-	In zone 'marker' lithoclasts and in lesser amount than other 'marker' minerals[5]
Strauolite	-	<20 wt%[5]	-	Heavy mineral fraction in member zone 'marker' lithoclasts[5]
Clays	-	-	<20 wt%[7]	Present in black shales and halite rocks[7]
- Kaolinite	-	<20 wt%[5]	-	In zone 'marker' lithoclasts[5]
Mica	-	<20 wt%[5]	-	In zone 'marker' lithoclasts and in lesser amount than other 'marker' minerals[5]
Talc	-	-	<20 wt%[7]	Present in halite rocks[7]
Organic content				
Relative TOC	0.5 - 11%[6]	-	-	
Insoluble organic matter	-	<20 wt%[5]	<20 wt%[7]	In zone 'marker' lithoclasts and in lesser amount than other 'marker' minerals[5]; Composes 15% of black shales in the formation[7]

1.) Spangler, Naftz, and Peterman (1996)
2.) Stevens, Fox, and Melzer (2001)
3.) Allis et al. (2001)
4.) Cappa and Rice (1995)
5.) Fouret (1982)
6.) Nuccio and Condon (1996)
7.) Hite and Lohman (1973)
8.) White et al. (2003)
9.) White et al. (2002)
10.) Raup and Hite (1996)
11.) Raup and Hite (1992)
12.) Tromp (1995)
13.) Tuttle et al. (1996)
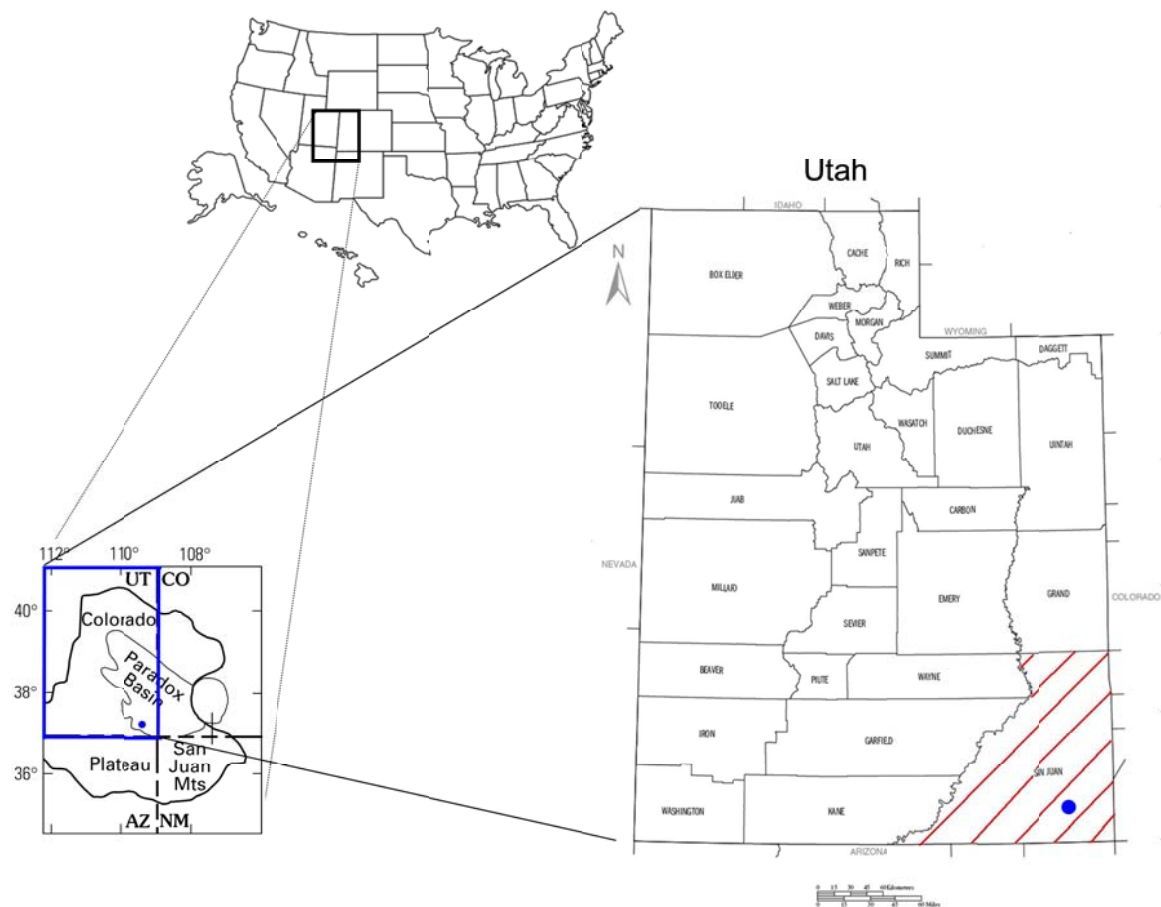
FIGURE A.1.1: Map showing location of proposed demonstration site for CO_2 saline sequestration in San Juan County, Utah. County is striped and field location is approximated by the blue dot. Modified from (Grout and Verbeek 1998) and U.S. Census 2000 map.
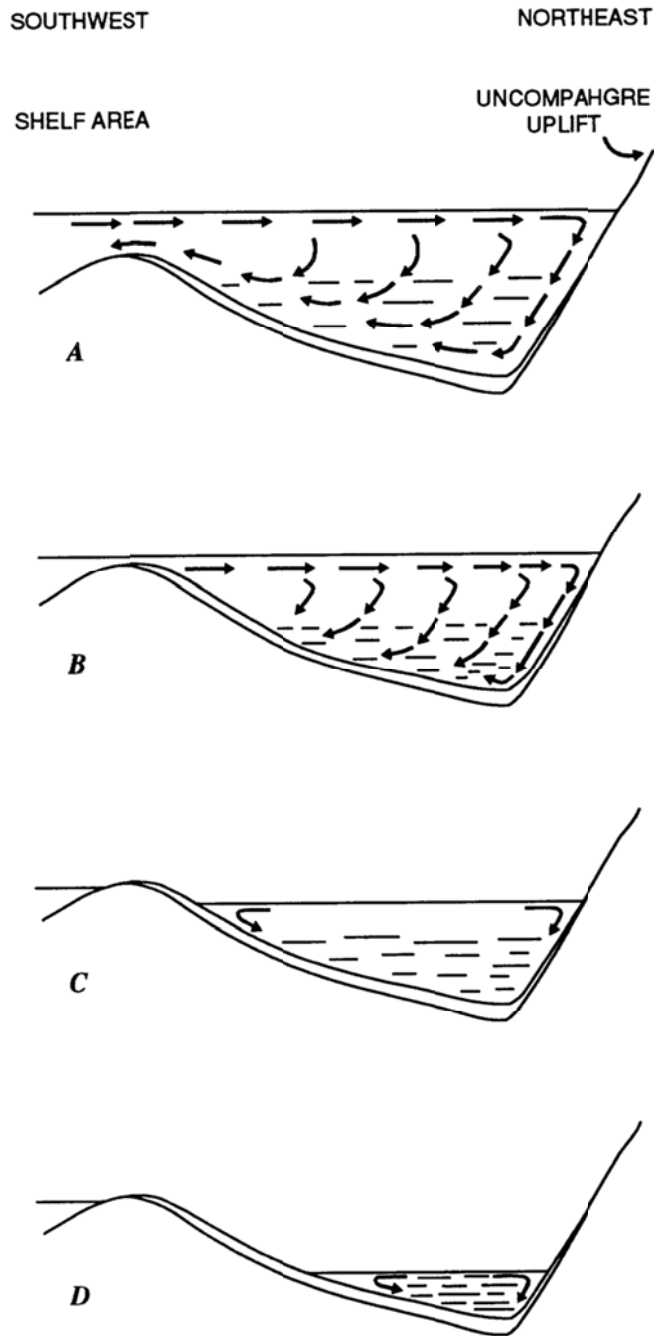
FIGURE A.1.2: Schematic southwest to northeast cross-section of the Paradox Basin showing the stages of evaporite drawdown that formed the many cycles observed in the Basin (Raup and Hite 1996).
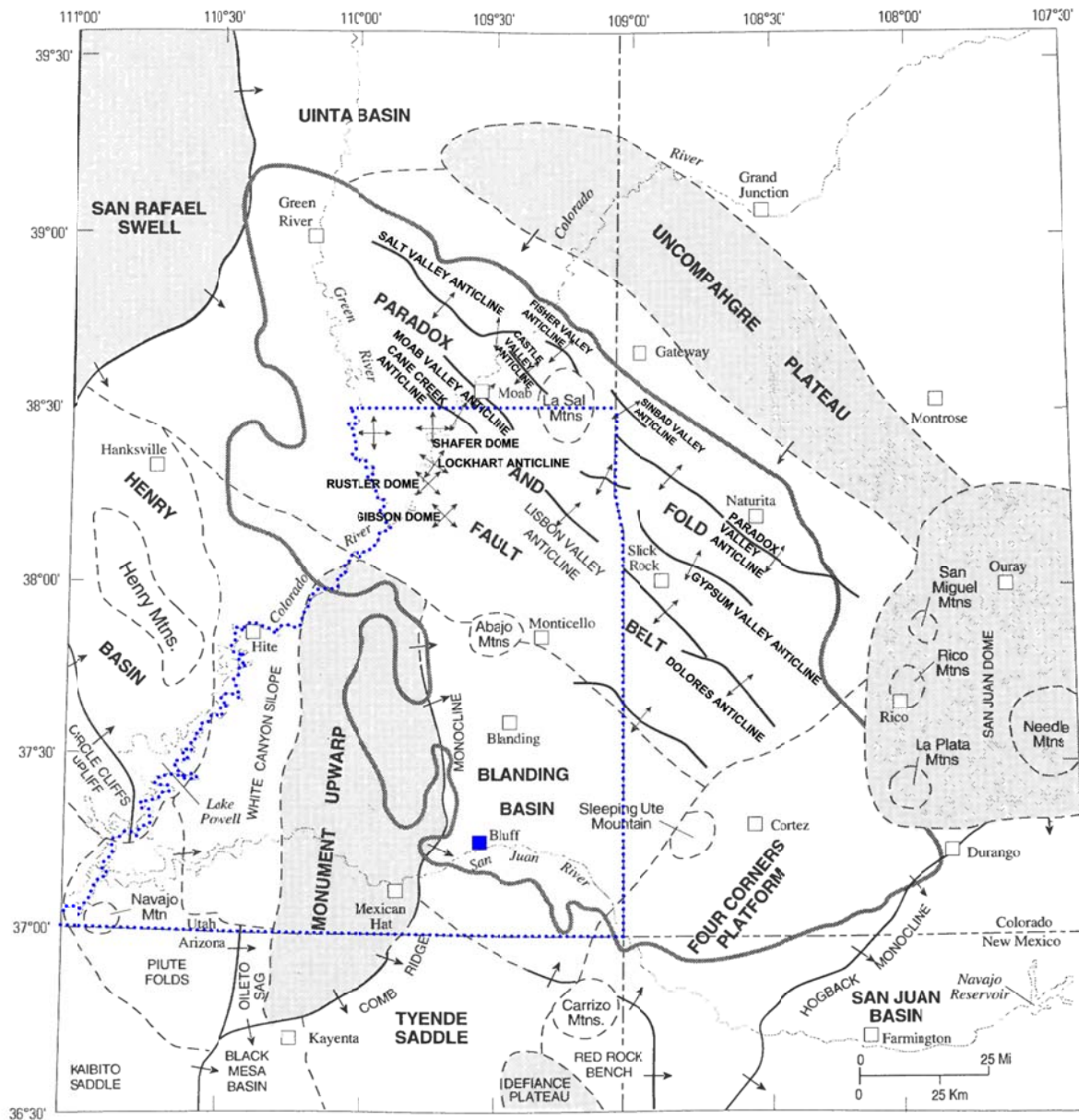
FIGURE A.1.3: Map showing the major salt anticline and other structural elements in and around the Paradox Basin. San Juan County, Utah is outlined with dotted (blue) line. Bluff is shaded box (blue). Dashed lines indicate transitional or indefinite boundaries between elements. Modified from (Kelly 1958a, 1958b).
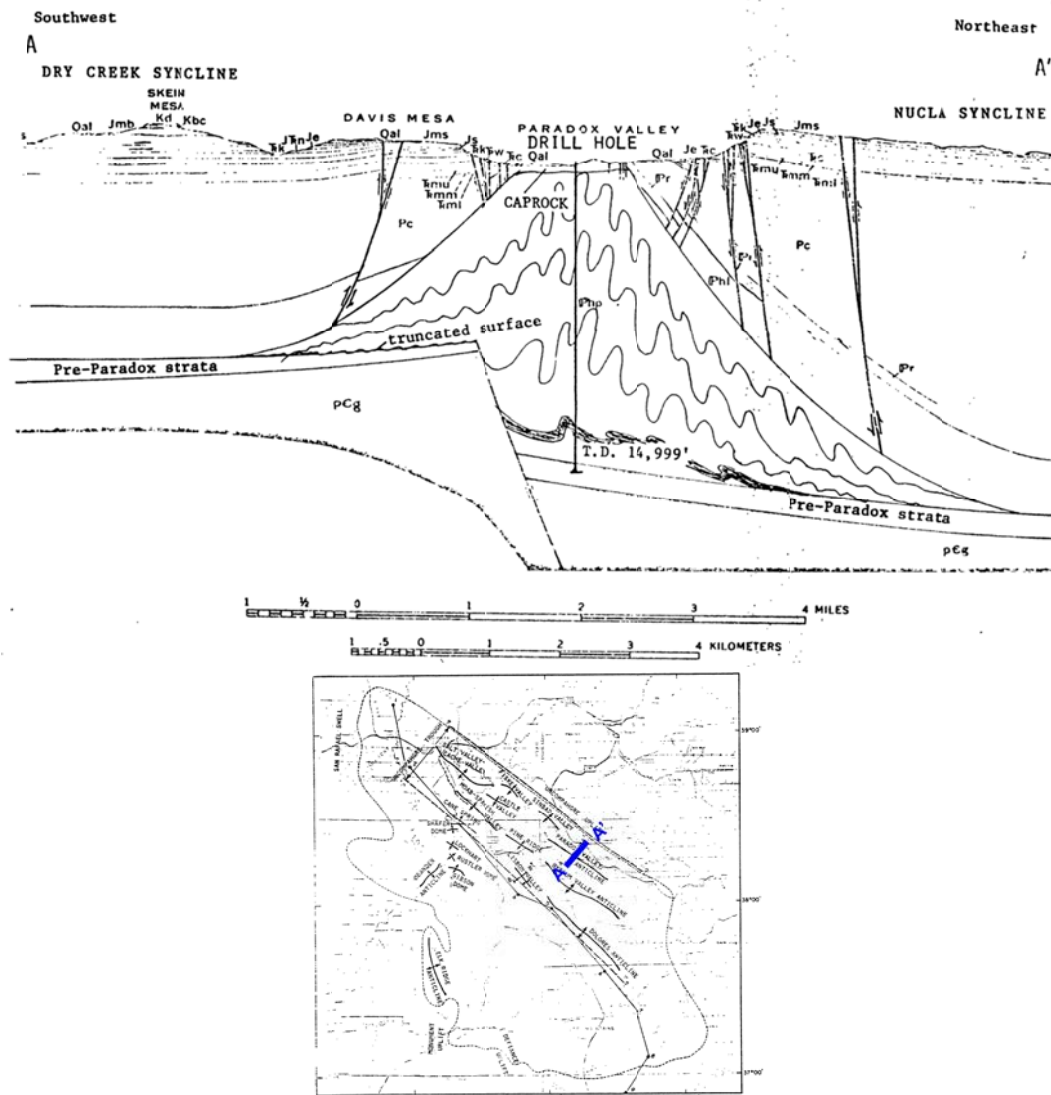
FIGURE A.1.4: Cross section through Paradox Valley Anticline. Adapted from (Carter 1970; Hite and Lohman 1973).
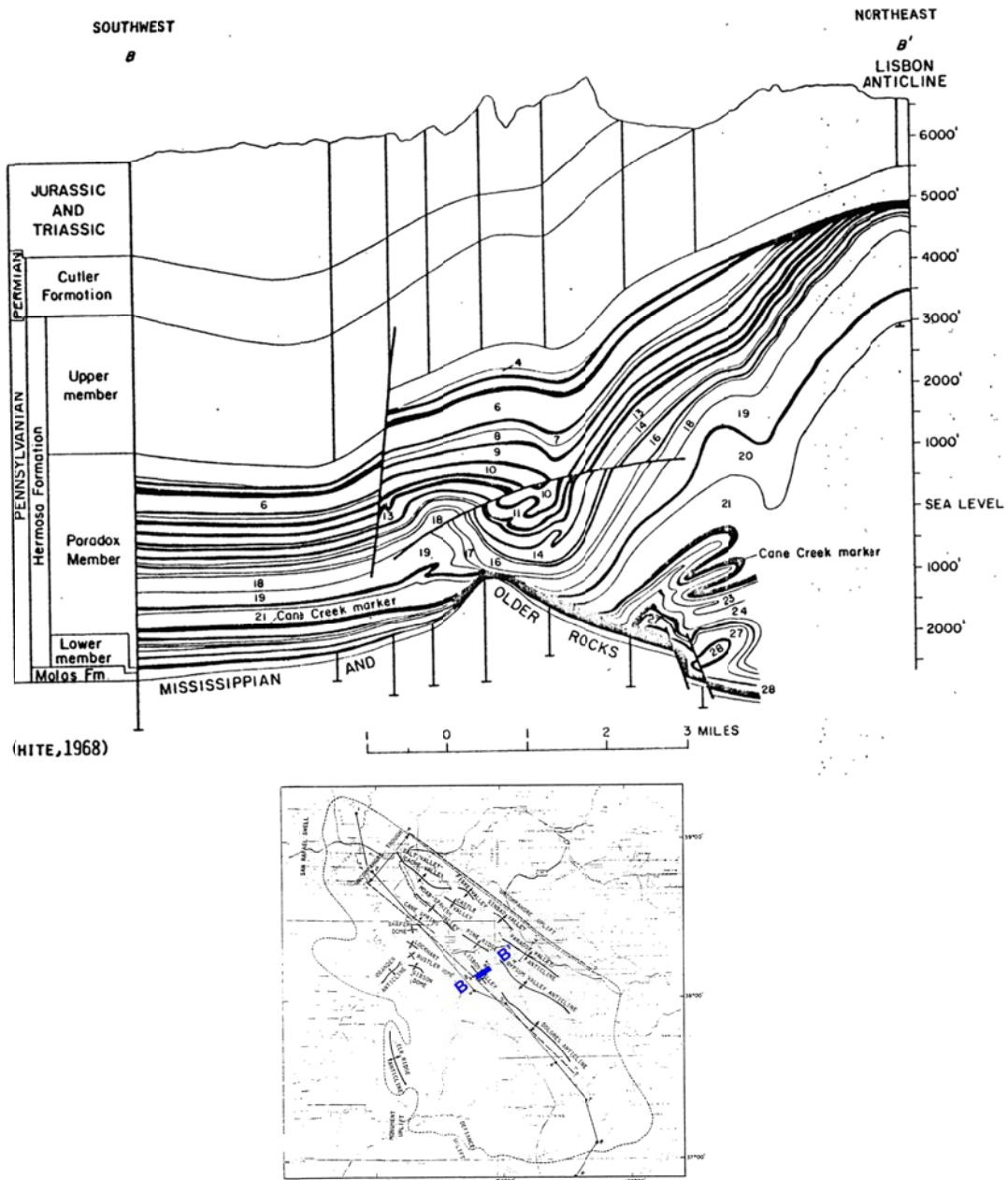
FIGURE A.1.5: Cross section of Lisbon Valley Anticline, Utah. Halite beds are numbered with interbedded dark layers of clastic-penesaline marker beds(Hite and Lohman 1973).

184
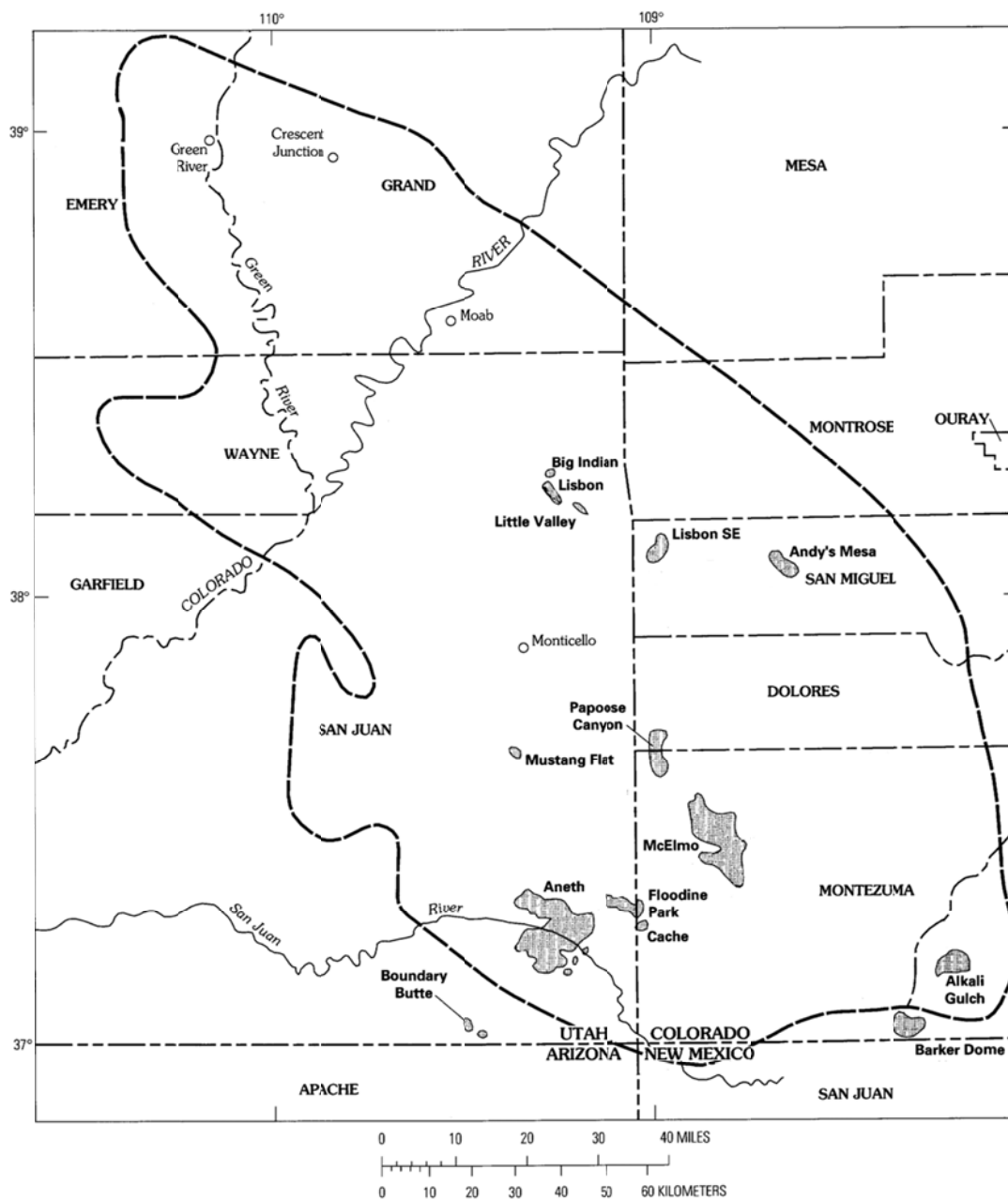
FIGURE A.1.6: Map showing location of the Paradox Basin and the gas reservoirs within the basin. Modified from (Cappa and Rice 1995).
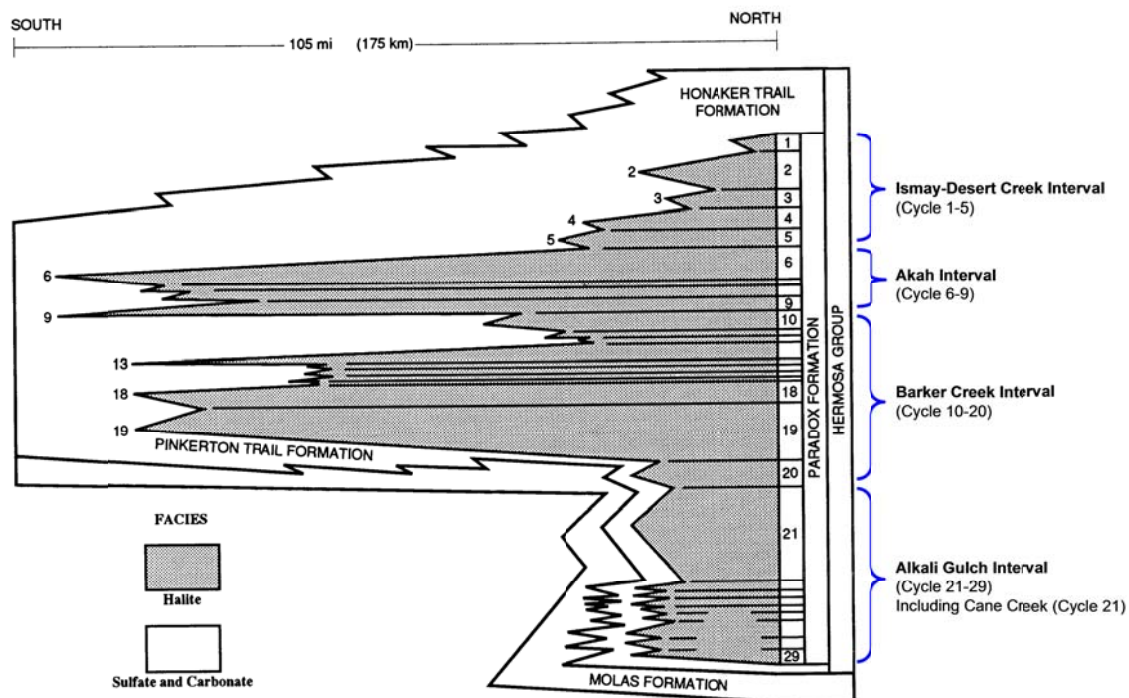
FIGURE A.1.7: Diagrammatic south-north strategraphic cross-section of the Paradox Formation across the Utah- Colorado state line. 29 cycles are shown with cylces 3 and 5 representing the Gothic and Chimney Rock shale respectively. The carbonate facies of the Gothic and Chimney Rock shale are more abundant in the southern region of the formation. Modified from (Hite and Buckner 1981)

South

North

Westwater Canyon Sandstone Member
Recapture Shale Member
Salt Wash Sandstone Member

Cretaceous
Dakota Sandstone

Upper Mesozoic
aquifers and
confining layers

M aquifer
Morrison aquifer

D aquifer
Dakota aquifer

San Juan River

Brushy Basin Shale Member
(Morrison Formation)

Middle Mesozoic
aquifers

N aquifer
Entrada–Navajo aquifer
Navajo aquifer

(Bluff Sandstone Member)

Jurassic   Morrison Formation

Wanakah Formation

Lower Mesozoic
confining layers

Triassic-
Jurassic   Entrada—Navajo—Wingate Sandstones

P aquifer
C aquifer
DeChelly aquifer

Triassic   Chinle—Moenkopi Formations

**Upper Paleozoic
aquifer**

P aquifer

White Rim Sandstone Member
DeChelly Sandstone Member
Organ Rock Shale Member
Cedar Mesa Sandstone Member

Upper Paleozoic
aquifers and
confining layers

Permian   CUTLER FORMATION

Halgaito Member

Pennsylvanian   HERMOSA GROUP

Honaker Trail Formation

Redwall aquifer

Paradox Formation

Pinkerton Trail Formation

Middle
Paleozoic
aquifers

Mississippian   Redwall—Leadville Limestone

Aquifer terminology written in regular
typeface is from Avery (1986); in italic
typeface is from Thomas (1989) and
Howells (1990); and in bold typeface is
as used in this report

Aquifer terminology written in
regular typeface is from Taylor and
others (1986); and in bold
typeface is as used in this report

EXPLANATION

⟵ **Arrow indicates direction of potential ground-water movement resulting from hydraulic-head
differences**—Direction of ground-water movement summarized from Thomas (1989); Freethey and Cordy (1991);
and Weiss (1991)

AVERAGE DEPTH BELOW LAND SURFACE TO TOP OF HYDROGEOLOGIC UNITS

Morrison Formation—Bluff Sandstone = 265 feet	Cutler Formation = 2,640 feet
Entrada Sandstone = 550 feet	Hermosa Group = 4,585 feet
Navajo Sandstone = 775 feet	Leadville Limestone = 6,910 feet
Chinle Formation = 1,475 feet	

FIGURE A.1.8:   Schematic cross section of hydrogeologic units in the vicinity of the
Greater Aneth Oil Field (Spangler, Naftz, and Peterman 1996).

APPENDIX A.2:

LOWER TUSCALOOSA MASSIVE SAND RESERVOIR WITH TUSCALOOSA MARINE SHALE AND SELMA CHALK AS GEOLOGICAL SEALS: GEOLOGY, LITHOLOGY, MINERALOGY AND CO_2 STORAGE IMPLICATIONS

A.2.1 INTRODUCTION

In 2003 the U.S Department of Energy (U.S. DOE) initiated regional partnership programs to address the concern for rising atmospheric CO_2. These partnerships were formed to explore regional and economical means for geologically sequestering CO_2 across the United States and to set the stage for future commercial applications. Several options exist for geological sequestration and among these sequestering CO_2 into deep saline aquifers is one of the most promising. This is due, in part, to the possibility of stabilized permanent storage through mineral precipitation from chemical interactions of the injected carbon dioxide with the brine and reservoir rock. To mitigate CO_2 emissions successfully, the rock seal(s) considered for geological CO_2 sequestration need to be assessed for risk and be proven effective for containment of the injected CO_2 gas.

In the Southeast Regional Carbon Sequestration Partnership (SECARB) there are two sites in Mississippi chosen to demonstrate CO_2 injection into a saline reservoir, the Lower Tuscaloosa Massive Sand. The sites are at Plant Daniel in Jackson County and Denbury's Cranfield unit in Adams County (Figure 1). The data on the geological seals used for these sites were collected from literature sources in peer reviewed journals, open reports, and thesis dissertations containing geological data near the location of the demonstration site. There are many mechanisms governing CO_2 escape from a potential storage reservoir, mainly through primary and secondary porosity. In order to properly assess the

effectiveness of a geological seal by these mechanisms, it is important to consider the seal in the broader context of the prevailing structural features, lithostratigraphy, mineral, and physical characteristics that compose and influence the seal(s) at each field demonstration site. Of primary interest is the presence of soluble minerals in the seal rock that could be vulnerable to dissolution upon contact with supercritical CO_2 and CO_2-brine solutions.

A.2.2 GENERAL GEOLOGIC FRAMEWORK

The U.S. DOE demonstration sites for CO_2 saline sequestration in Mississippi are located in Jackson and Adams County and lie within the northern region of what is called the Gulf Coast Province of North America (Figure 1). The target reservoir unit is the Lower Tuscaloosa Massive Sand, and the overlying seal units are the Tuscaloosa Marine Shale and the Selma Chalk. Both geological units considered for storage and containment fall within the Gulfian and Paleocene series of the Upper Cretaceous System during the Mesozoic Era. Broadly speaking, the Mesozoic (and Cenozoic) strata of the coastal province form a syncline. A large trough was linearly filled with vast amounts of sediment accompanied by folding, and faulting of the deposits with intrusion of crystalline igneous rock and regional uplifts along the axis of the trough . The overall dip of the beds within the syncline are seaward where the degree and seaward slope of the units have in the past been modified by Paleozoic, Cenozoic, and late Cretaceous orogenies and are still are being modified by large vertical positive and negative warping by extended fault and fracture systems of varying magnitude, and by igneous and salt emplacements (Murray 1961).

The major structural features that surround the demonstration sites, along with their extent and relationship to other structural features within the Gulf Coast Province can be seen in Figure 2. The northern region of the Gulf Coast Province, where the demonstration sites lie, are characterized by fault systems, uplifts, and salt piercement. These features are further described with an emphasis on elements in Mississippi pertinent to the locality of the demonstration sites.

Folds

The Hatchetigbee anticline, located principally in southwest Alabama in Choctaw, Washington, and Clarke Counties, is gently plunging and complexly faulted with its northwestern limb traced at the surface and subsurface into Clarke and Wayne Counties of Mississippi. It has associated faulting and contains early Tertiary age marine deposits(Murray 1961).

The Wiggins uplift is an irregular, bifurcating feature in southwestern Alabama, southeastern Mississippi, and eastern Florida parishes of Louisiana(Murray 1961). The uplift splits in Stone County, Mississippi with one lobe extending to the northwest and the other, called the Hancock ridge, plunging southwest and disappearing under St. Bernard Parish, Louisiana (Figures 1, 3). It is associated with Quaternary and later Tertiary (Miocene-Pliocene) sediments with the subsurface having zones of pronounced downfaulting creating strike faults in portions of the modern Mississippi coast and southern Louisiana(Murray 1961). The Wiggins uplift is the most prominent structural feature closest to the demonstration site Jackson County, Mississippi but is not of the same age as the storage or seal rock units of the older Upper Cretaceous sediments below. Its influence on the storage and seal rocks are not clear.

Monroe Uplift is a Mesozoic-Cenozoic structural feature in northeastern Louisiana, southeastern Arkansas, and west-central Mississippi (see Figure 2).The overall form and shape of the uplift is variable in both position and structure with small to nonexistent structural closure in the north and northwest portions. Variations in structure are due to emplacement of relatively large igneous masses with pronounced angular unconformities between certain sequences of the Mesozoic sequences. The Gulfian strata are arenacous-arigillaceous in the lower part and calcareous in upper part with an appreciable amount of volcanic material interbedded in lower and upper sequences.

Faults

Along the Gulf Coast Province there exist numerous faults and fault zones, particularly in Louisiana and Texas and it is important to understand how these affect the sediment layers (Figure 2). The flexures describe zones of rapid, inconsistent thickening of sedimentary beds. Historically they were called flexures or flexure zones but now they are called fault zones(Murray 1961). Figure 3 shows these types of fault zones that extend through Mississippi. The flexure zones in Mississippi do not extend to Gulfian and Paleocene series where the storage reservoir or related geological seals occur. The fault zones occur, with significant magnitude, in the Jurassic age and in the Coahulian – Comanchean strata affecting early Cretaceous beds.

The most predominant type of fault in the Gulf Coast province is the normal fault, but high-angle reverse faults are known to exist in southwestern Alabama region(Murray 1961). The faults dip from 35° to 70° with higher angles near the coast where the demonstration site in Jackson County, Mississippi is located (Figures 1, 4). The majority appear to be steepest near the surface and decease in dip at greater depths. In Mississippi, the major fault system is the Pickens-Gilbertown graben which is part of a relatively uninterrupted system that extends into Alabama, Louisiana, Arkansas, and Texas (see Figure 2). The graben fault system is a concave system stretching 1,000 miles, and affecting surface and subsurface rocks. The faults are 5 – 8 miles wide and run parallel or subparallel to regional strike of Jurassic and early Cretaceous, and salt structures. The Picken-Gilbertown graben faults are known to increase in sediment displacement at greater depths, with up to 5,000 feet displacement recorded in central Mississippi. The graben faults penetrate both the Lower Massive Sand storage reservoir and all the geological seals considered for the two demonstration sites (Figure 5). This includes the primary seal, Tuscaloosa Marine Shale (TMS), the secondary seal which is the Selma Chalk group, and the tertiary seal which is the Midway Shale formation. Other faults exist in Jasper, Wayne, Jones, and Perry County, Mississippi that are documented to penetrate the secondary Selma Chalk seal rock(Murray 1961) (Figure 6).

Other structural elements

Salt structures in Mississippi

Salt structures are present throughout Mississippi and occur as spikes, stocks or large elongated masses where they can exist in many varied relationships to their host sediments(Murray 1961). The salt domes were formed through the folding and flowage of salt due to differential specific and sedimentary loading. The domes have moved relatively upward in various stages of growth which are related to thicker than normal Gulfian and early Tertiary age sediments(Murray 1961). In areas where appreciable amounts of salt piercenents are grown, the enclosing strata experiences upwarping and thinning of beds adjacent to the salt rock(Murray 1961) (Figure 7).

Salt structures are typically associated with normal faulting with simple offsets, however, some salt piercements are associated with multiple offset faults and compound fractures(Murray 1961). A dome was reported in Adams County, Mississippi, one of the two locations for CO_2 saline sequestration demonstration (Figure 8). Piercements with compound fractures and multiple offset faults are reported to penetrate the Eutaw formation and Tuscaloosa group in Jasper and Lincoln Counties, Mississippi (Figure 9).

The Jackson dome is a very prominent Mesozoic and Cenozoic uplift in Hinds and Rankin Counties in west-central Mississippi. It has a high relief asymmetric feature 25 miles in diameter with a quadrate shape. The form and shape of the uplift near the surface are similar to those of the deeper structure where Jurassic to early Gulfian strata were tilted, truncated and overlain with angular unconformity(Murray 1961).

Mississippi Embayment

An important structural feature within Mississippi is the Mississippi Embayment. It is a system that dominates the northern sections of the Gulf Coast Province with sedimentary rocks exceeding 25,000 feet deep. The thickness of the embayment decreases northward from the Gulf at a fairly even rate to a feather edge in southernmost Illinois (see Figures 2,

4). From southern Illinois it extends southward and underlies portions of Louisiana, Kentucky, Tennessee, Arkansas, Mississippi, and Alabama.

The embayment contains Cretaceous and early Tertiary system age sediment in which the CO_2 storage reservoir and seal rocks for the demonstration sites are located. The sediments plunge Gulfward in the embayment and change rock facies, particularly in the Gulfian sediment series, as they grade southward in Mississippi, merging with the coastal syncline (Figure 10).

A.2.3   DEMONSTRATION SITE GEOLOGY OF STORAGE RESERVOIR(S) AND GEOLOGICAL SEAL(S)

The Southeast Regional Carbon Sequestration Partnership (SECARB) has two field demonstration sites for CO_2 saline sequestration in Mississippi. One of its field demonstration sites is operating at Plant Daniel, located in Jackson County and the other at the Denbury Cranfield unit in Adams County. Both sites share the same reservoir and seal units for CO_2 storage, however, in this study, only the seal units beneath Plant Daniel will be discussed in detail.

A.2.3.1   *CO$_2$ STORAGE RESERVOIR(S)*

The stratigraphic horizon into which CO_2 will be injected is the Lower Tuscaloosa formation. In southern Mississippi it is divided into an upper "Stringer" member and a bottom "Massive Sand", it is into the "Massive Sand" at Cranfield, in Adams Co. that up to 1,500,000 Tons/yr of CO_2 will be injected as well as 3,000 Tons (short) at Plant Daniel(Nemeth 2007). The Lower Tuscaloosa Massive Sand beneath Plant Daniel is at a depth of 8,600 feet with a thickness of approximately 190 feet(Rhudy 2006). Within the southeast region of Mississippi the Lower Massive Sand can be greater that 400 feet thick(Braunstein 1950).

The Lower Tuscaloosa formation has a history of oil and gas production dating back to the 1940s with the discovery of the Brookhaven and Mallalieu fields in Lincoln County and

Cranfield field in Adams County(Gruebel and Ewing). However, exploration has mostly focused on the "Stringer" member of Lower Tuscaloosa in southwest Mississippi where, in a few wells, more than 5 million billion barrels (bbl) of oil and 12 billion cubic feet (bcf) of gas had been recovered between 1981 and 1986(Moody and Dowty 1991; Wiygul et al.). The incentive for pursuing this oil and gas 'play' in the southwest of Mississippi was the fact that oil could be found at relatively shallow depths with reasonable drilling and engineering costs (Gruebel and Ewing). This trend is not extensive in the southeast counties of Mississippi where significant quantities of oil are absent from the Lower Tuscaloosa(Braunstein 1950).

A.2.3.2   GEOLOGICAL SEAL(S)

Beneath Plant Daniel, the primary, secondary, and tertiary geological seal units of the Tuscaloosa Marine Shale, Selma group, and Midway Shale formation respectively. In this study, the Midway Shale tertiary seal is excluded from further discussion due to its distance of 1,800 – 3,800 feet above the proposed Lower Tuscaloosa Massive Sand CO_2 injection horizon. The Selma Group (Selma Chalk) occurs at a depth range of 5,500 – 7,800 feet with a thickness of approximately 1,000 feet(Rhudy 2006) (Figure 11). The Tuscaloosa Marine Shale is at a depth range of 7,675 – 8,150 feet with a thickness of 450 – 475 feet(Rhudy 2006).

The Tuscaloosa Marine Shale has little oil and gas production history with a few reports in southeast counties of Mississippi and central Louisiana containing wells producing 2,500 – 20,000 barrels of oil from this formation at 11,073 – 11,644 feet(John et al. 1997). In 1997, it was estimated that recoverable reserves from the Tuscaloosa Marine Shale is approximately 7 bbl of oil(John et al. 1997).

The structural features that could affect the performance of the Lower Massive Sand, Tuscaloosa Marine Shale, and the Selma 'Chalk' Group formations below Plant Daniel include flexures and fault zones, such as the Pickens-Gilbertown graben fault system, as well as the

Hatchetigbee anticline, Wiggins uplift, Monroe Uplift, Jackson Dome, and piercement salt domes (Figure 3).

A.2.4 MINERAL AND PHYSICAL CHARACTERISTICS OF STORAGE RESERVOIR, SEAL(S), AND OTHER RELEVANT GEOLOGICAL FEATURES

To estimate the impact of CO_2 injection into the Lower Tuscaloosa Massive Sand formation, it is important to know the mineral composition and physical traits of the potential reservoir(s), its seal(s), and other relevant structural features that could impact the storage of the CO_2. Changes in the mineral composition of the Lower Tuscaloosa Massive Sand formation or its seals, the Tuscaloosa Marine Shale and Selma Chalk, due to lithological facies variation or chemical reactions with CO_2 injection, could reduce or enhance injectivity and storage capacity at the site. Likewise, changes in the physical traits of these formations due to CO_2 injection could result in increased risk for leakage and migration of the gas, where interaction with other prominent structural features could impact the permanency of the CO_2 storage.

Figure 11 and Table 1 describe the lithology, mineralogy, and physical traits of the targeted storage reservoir(s) and seal(s), along with other geological features surrounding the site. Typically, the descriptions of the storage reservoir and geologic seals near the surface are generally not used in subsurface descriptions further Gulfward, where the sediments are much deeper. Also, names for equivalent units differ across states in the northern region of the Gulf Coast Province. This difference is illustrated in Figure 12.

Mineral characteristics are discussed in terms of the lithology and dominant minerals present in the reservoir(s), seal(s) rocks, and other relevant structural features. Physical traits of these formations are described in terms of permeability, porosity, fractures and fluid transport behavior. Emphasis is given to the description of the geological seal(s) due to their immediate relevance to CO_2 containment.

A.2.4.1 MINERAL CHARACTERISTICS

Storage reservoir(s)

The CO_2 storage reservoir used at Plant Daniel is the Lower Tuscaloosa Massive Sand. In the subsurface of Mississippi, the Massive Sand is the bottom member of Lower Tuscaloosa formation. This distinction is lost as the formation extends across the Gulf Coast states of Alabama, Louisiana, and Texas; and, is described by equivalent formations near the surface within the Mississippi Embayment (see Figures 10, 12). Within Mississippi, the equivalent names for the Lower Tuscaloosa Massive Sand describe facies changes the formation undergoes as it progresses from the subsurface near the Gulf Coast to the outcrops in southern Arkansas and Tennessee, and northern Mississippi and Alabama (Murray 1961; Cushing, Boswell, and Hosman 1964; Braunstein 1950).

In the subsurface of southeast Mississippi, the Massive Sand is described as a white, finely micaceous, fine to medium grained, sandstone(Braunstein 1950). The Massive Sand has a fine clay matrix and is interbedded with thin red, gray, and green waxy mudstone with siderite nodules(Braunstein 1950). The sand section of the Massive Sand may be over 90% sand in southeast Mississippi (Braunstein 1950).

Petrographic analysis of the Lower Tuscaloosa is typically performed on the upper "Stringer" member of the Lower Tuscaloosa in southwest Mississippi, where oil is reported to be produced (Wiygul et al. 1987; Klicman, Cameron, and Meylan 1988). The Stringer member, which represents a transgressive sequence within the Lower Tuscaloosa, is a coarse to fine-grained sandstone that is quartz rich with a high percentage of rock fragments that may be of volcanic origin (Wiygul et al. 1987). The sandstones are shale arenites and are cemented by quartz overgrowths, iron-rich carbonates, and chlorite (Wiygul et al. 1987).

The sandstone from the Stringer member is composed of 65% quartzarenites and 35% sublitharenites. Stringer samples analyzed from the North Hustler and Thompson Fields of Amite County, Mississippi, had and average composition of 67.3% framework grains, 14.8% matrix, 9.2% cement, and 8.7% pore space. Minerals within the sandstone

are: quartz (88.7%), polycrystalline quartz (6.6%), potassium feldspar (0.3%), plagioclase (0.1%), chert (1.9%), volcanic rock fragments (0.5%), metamorphic rock fragments (0.2%), and sedimentary rock fragments (0.2%)(Klicman, Cameron, and Meylan). The matrix is mainly composed of pore-filling clays, secondary pyrite, and organic matter. The clay minerals are authigenic and include chlorite, kaolinite, mixed-layer ilite/smectite, and illite(Hamlin and Cameron 1987). Cements are mostly quartz, ankerite, siderite (nodules), and calcite(Klicman, Cameron, and Meylan).

Geologica Seal(s)

Tuscaloosa Marine Shale

The Tuscaloosa Marine Shale (TMS) in the subsurface of southeast Louisiana is described as a light-dark grey or brown, splintery, brittle, micaceous, calcareous silty shale with occasional stringers of white to light-gray sand(John et al. 1997). In southern Mississippi it is described as a fissile, fine-grained, dark-gray micaceous shale with minor interbeds of calcareous, glauconitic sandstone with some argillaceous limestone lentils, laminated claystone, and mudstones, and calcareous siltstone(Braunstein 1950; Miranda 1988) (see Figure11).

Mineral composition data are not available for the primary seal, the Tuscaloosa Marine Shale (TMS). The composition of the TMS was inferred from the equivalent Eoline member of the Coker formation near the surface (see Figures 10, 11) which outcrops in Alabama. As indicated in Table 1, the TMS is predominantly composed of quartz, kaolinite, and illite minerals with minor amounts of montmorillonite, muscovite, glauconite, chlorite and feldspar. The TMS also contains significant amounts of total organic carbon (> 0.5%) that is thermally mature and thus the unit is capable of producing oil and gas(Miranda and Walters 1992).

Selma Chalk group

The secondary geologic seal, the Selma group, contains chalks, chalky marl, and limestone members (see Figure 11). The predominant minerals within the Selma group are

manganese, ferrous, and magnesium carbonates with marls containing kaolinite, montmorillonite, illite, and glauconite. There may also be significant beds of gypsum within the Selma. Some horizons within the Selma group in Mississippi, Alabama, and particularly Texas have been the source of natural gas reservoirs(Scholle 1977).

Other geologic features

The composition of the salt structures within Mississippi and the northern region of Gulf Coast Province are discussed in this study because of their abundance and ability to influence the geological seals. The salt structures are composed mainly of halite, with the upper regions of the structure characterized as a caprock consisting mainly of sulfur, carbonates, gypsum, and anhydrite, respectively increasing in abundance (see Table 1).

A.2.4.2   *PHYSICAL CHARACTERISTICS*

Storage reservoir(s)

The porosity of the Lower Tuscaloosa Massive Sand reservoir is mostly of the secondary type, ranging from 3-27% with an average of 19% in Amite Co., caused by partial dissolution of framework rock fragments and carbonate cements(Hamlin and Cameron 1987; Klicman, Cameron, and Meylan). The primary porosity of the Lower Tuscaloosa Massive Sand can average 17 – 31% in across southern Mississippi and parts of Louisiana(Nelson and Kibler 2003; *The Lower Tuscaloosa Formation* 2006). The horizontal permeability of the Massive Sand ranges from 0.01 – 193 millidarcies (mD) in Louisiana and from 0 – 2 darcies in Mississippi owing to certain areas having abnormally high porosities and 'overpressures' (*The Lower Tuscaloosa Formation* 2006; Bloch, Lander, and Bonnell 2002; Weedman et al. 1996).

In certain regions within the Gulf Coast, the Lower Tuscaloosa formation can be described as having fluid overpressure, where the fluid within the reservoir is greater than the hydrostatic gradient for the fluid from the top of the water column(Bloch, Lander, and Bonnell 2002; Dickinson 1953). This phenomenon can be caused by differences in the rate

of reservoir fluid release versus pore volume reduction during the basin development and can preserve high porosities and permeabilities found throughout the Lower Tuscaloosa(Bloch, Lander, and Bonnell 2002). The presence of chlorite coating on the quartz is thought to play a role in the sandstone developing higher porosities (Weedman et al. 1996).

Geological Seal(s)

Available descriptions of the physical characteristics (permeability, porosity) of the TMS and Selma group in Mississippi are limited to a few reports stating which horizons have had oil and gas produced(John et al. 1997; Scholle 1977). Hydrogeologic reports from throughout the Mississippi Embayment have been used to gain information about the TMS and Selma group units based on their outcrop characteristics elsewhere in the Mississippi Embayment (Table 1). These data also give insight into the level of hydraulic communication between the units in the subsurface.

In general, the Selma group is more permeable and porous in the subsurface than the TMS but is thicker and has the same water transmission properties as the TMS, based on aquifer test estimates (see Table 1). There exists extensive fracturing within the TMS in the southwest region of Mississippi and the fractures are suspected to be interconnected(John et al. 1997). This implies that there exist zones with higher permeability and/or porosity in the TMS which could create higher risks for leakage in southwest Mississippi. This may be particularly true of the demonstration site in Adams County which lies in that region of the state.

Other geological features

The salt structures in Mississippi have no reported permeability, porosity, or hydraulic conductivity values to compare. What is known about these structures are that they penetrate through many layers of sediment in the subsurface and are usually associated with faults near their caprocks, which can be of significant extent in the salt structure (see Table 1). The fractures and faults near the caprocks of the salt

piercements/domes may extend into sediments considered for geologic storage and containment of CO_2 (see Figures 8, 9).

A.2.5   IMPLICATIONS FOR CO_2 SEQUESTRATION STORAGE AND LEAKAGE

Carbon capture and storage into geological media has as part of its goal, the need to estimate the risk associated with CO_2 injection. Some have proposed a framework to assess risk through the use of quality factors assigned to various reservoir and seal characteristics like thickness, lithology, and proximity to faults and fracture networks(Oldenburg 2005). This study helps to address some of these factors at the proposed saline demonstration sites in Jackson and Adams County, Mississippi by focusing on mineral phases susceptible to CO_2 attack that are present in the surrounding structural features and influenced by the hydrogeological behavior of the sediments.

Based on the information reviewed in the previous sections, implications for the permanence of CO_2 storage at this demonstration site can be categorized into the following topics centered on lithology, structural geology, and reservoir fluid behavior along with oil and gas production history. These topics will be discussed further with an emphasis on soluble minerals present in each of these categories.

In terms of lithology, the composition of the Tuscaloosa Marine Shale and Selma Group formations are very different. The TMS has more clay and silca content than the Selma group, but both units contain significant amounts of calcite in their structure which could potentially be susceptible to CO_2 attack.

The TMS and Selma Group undergoes significant facies changes across the state, and may result in permeable zones or channels through which the CO_2 may seep and react. This would be particularly true with the Selma Group whose members change composition and porosity significantly from south to north Mississippi. Figure 11 and Figure 12 depict the change in facies from subsurface (south) to surface (north) and from east to west. Reactions of the CO_2 with the predominant soluble minerals present in these seal rock units,

especially manganese carbonates and glauconite (an iron rich illite), could result in increased seal rock permeability.

In terms of the structural geology in southern Mississippi, both seals are laterally continuous and relatively thick in the proposed area of injection. Also, Plant Daniel is situated near a regional anticline (Wiggins anticline) less than 50 miles away which could act as a structural barrier for CO_2 migration. Further north of Plant Daniel and Cranfield are faults and salt piercements that penetrate the storage and seal units. Faults like the Pickens-Gilbertown grabens to the north and those associated with nearby (< 100 miles) salt piercements pose an increased risk for leakage. Faults of the Pickens-Gilbertown graben system cut through Cretaceous sediments and are connected to the surface(Murray 1961).

A benefit to sequestration at this site is that the seal rocks are thick and continuous and the flexures that downfault thousands of feet of sediments adjacent to the Gulfian rocks, near the coast, provide structural barriers in the subsurface as opposed to the Pickens-Gilbertown fault system further north which exposes thousands of feed of sediment (Murray 1961).

Considering the physical attributes of the seals, the Selma is more susceptible to CO_2 migration than the TMS due to its higher reported values of porosity and permeability along with numerous vertical microfractures observed in core samples. The TMS is also observed to have vertical microfractures but they are cemented with carbonates and other minerals.

There exists a history of oil and gas production from both the TMS and Selma group. The TMS has reported oil production, with possible interconnected fractures, in the southeast region of the state and the Selma has reports of natural gas production, with porosities ranging as high as the storage reservoir in the Tuscaloosa group, in the central regions of Mississippi(John et al. 1997; Scholle 1977). Their production history indicates that there exist transmissive zones within the sediments that may pose an increased risk for leakage.

Depending on the methods used for oil and gas recovery from the TMS and Selma Group, additional leakage risk may be introduced. Apart from the faults that may have naturally occurred in the TMS and Selma Chalk seal through tectonic history, there may be potential leakage pathways created through fractures induced during oil and gas production. Fractures are induced in the formations (especially shales) through hydraulic stimulation, where horizontal wells can be drilled with long, multiple laterals that are tightly spaced (500 – 1,500 feet apart) that are capable of simultaneously setting off hydraulic fractures sequentially. Techniques like the one described could be extremely effective in increasing oil and gas production rates in the TMS and Selma group, but would run contrary to the principles of storage. The induced fractures by these techniques can be widespread and not all can easily captured by current seismic monitoring methods. It is therefore necessary to account for the types of techniques used in the past (or currently) for oil and gas production from the TMS and Selma Chalk. Extensive oil and gas exploration/production in potential seals may increase the risk of leakage at a geological sequestration site.

In regards to potential gas migration, the CO_2 injected into the Lower Tuscaloosa Massive Sand will most likely travel laterally inland to regions of higher elevation. As it does, there are numerous structural deformities that could act as structural barriers or as a fast path for escape. The nearest structural features that would affect CO_2 migration in Gulfian age sediments are the salt dome piercements. Each dome rises through the sedimentary bed layers and is associated with compound offset faulting (see Figure 3). Vertical migration of the CO2 gas could be hindered by the structural trap created by the Wiggins-Hancok Ridge anticlines of younger Quaternary – Tertiary sediment.

A.2.6   SUMMARY

In examining the literature available for the mineral, physical, and surrounding structural characteristics of the Tuscaloosa Marine Shale and Selma Group seals used in Mississippi, the study showed that their exists a potential for leakage and transport. The

extent for leakage and transport is limited by several factors: 1.) the thickness of the seal units which can be greater than 1,000 feet and the thousands of feet of flexure above the units, 2.) no open reports of hydraulic communication of the subsurface saline reservoirs in the south with potable aquifers in the northern regions of the state, 3.) salt piercements that possibly extend through the TMS and Selma formations nearby the demonstration sites in Adams and Jackson County, 4.) faults that transect the Selma and TMS and other Cretaceous sediments less than 100 miles north from sites 5.) structural traps to vertical migration created by the Wiggins-Hancock anticlines near by Plant Daniel. These factors indicate that commerciality of geological CO_2 sequestration in the Tuscaloosa Massive Sand is limited in Mississippi, without incurring great risks for leakage.

The study of the TMS and Selma, along with other relevant geologic features, across proposed demonstration sites in Mississippi reveal that carbonates (primarily calcite), quartz, halite, anhydrite, gypsum, sulfur, glauconite, kaolinite, illite, montmorillonite, and muscovite, are abundant minerals present in the seals and piercements that could be susceptible to CO_2 –brine attack. This information can then be used to guide experiments and modeling efforts aimed at understanding the dominant chemistries that could impact leakage and risk assessment.

A.2.7 REFERENCES

Beebe, B. Warren, and Bruce F. Curtis, eds. 1968. *Natural Gas in Post-Paleozoic Rocks in Mississippi*. 2 vols. Vol. 1, *Natural Gases of North America*. Tulsa, Oklahoma: American Association of Petroleum Geologist.

Bergenback, Richard E. 1964. Petrology of pre-Selma strata from core holes in western Alabama. In *Studies of Pre-Selma Cretaceous Core Samples from the Outcrop area in Western Alabama*. United States Government Printing Office, Washington, D.C.: U. S. Geological Survey.

Bingham, Patrick S., and Charles E. Savrda. 2006. Paleoenvironmental context of the Ingersoll Shale, an Upper Cretaceous Konservat-Lagerstaette, Eutaw Formation, eastern Alabama. In *Geological Society of America, Southeastern Section, 55th annual meeting*. Knoxville, Tennesse: Geological Society of America (GSA)

Bloch, Salman, Robert H. Lander, and Linda Bonnell. 2002. Anomalously high porosity and permeablity in deeply buried sandstone reservoirs: Origin and predictability. *AAPG Bulletin* 86 (2):301-328.

Boswell, Ernest H. 1963. Cretaceous aquifers of northeastern Mississippi: Mississippi Board of Water Commissioners Bulletin.

Brahana, J.V., and T.O. Mesko. 1988. Hydrogeology and preliminary assessment of regional flow in the Upper Cretaceous and adjacent aquifers int he northern Mississippi embayment In *Water Resources Investigations Report*: U.S. Geological Survey.

Braunstein, Jules. 1950. *Subsurface stratigraphy of the Upper Cretaceous in Mississippi*, *Guidebook, field trip*: Mississippi Geological Society.

Condon, S. M., and T. S. Dyman. 2006. 2003 geologic assessment of undiscovered conventional oil and gas resources in the Upper Cretaceous Navarro and Taylor Groups, Western Gulf Province, Texas. In *Petroleum Systems and Geologic Assessment of Undiscovered Oil and Gas, Navarro and Taylor Groups, Western Gulf Province, Texas*, edited by U. S. G. S. W. G. P. A. Team. Reston, Virginia: U.S. Geological Survey

Cushing, E.M., E.H. Boswell, and R.L. Hosman. 1964. General Geology of the Mississippi Embayment. In *Water Resources of the Mississippi Embayment*. United States Government Printing Office, Washington, D.C.: U.S. Geological Survey

Czerniakowski, Lana Ann, Kyger C. Lohmann, and James Lee Wilson. 1984. Closed-system marine burial diagenesis: isotopic data from the Austin Chalk and its components. *Sedimentology* 31:863-877.

Dickinson, G. 1953. Geological aspects of abnormal reservoir pressures in the Gulf Coast, Louisiana. *AAPG Bulletin* 37:410-432.

Dyman, T.S., and S.M. Condon. 2006. Assessment of Undiscovered Conventional Oil and Gas Resources - Upper Jurassic - Lower Cretaceous Cotton Valley Group, Jurassic

Smackover Interior Salt Basins Total Petroleum System, in the East Texas Basin and Louisiana-Mississippi Salt Basin Provinces: U.S. Geological Survey Digital Data Series.

Freed, R. L. 1980. X-ray study of the bulk mineralogy and clay content of six samples from the Austin Formation, Bexar and Medina counties, Texas. *Bulletin of the South Texas Geological Society* 20 (5):7-9.

Gruebel, Ralph D., and Thomas E. Ewing, eds. *Exploring the Lower Tuscaloosa in Southwest Mississippi*: Gulf Coast Association of Geological Societies, New Orleans, LA.

Hamlin, Kenneth H., and Christopher P. Cameron. 1987. Sandstone Petrology and Diagenesis of Lower Tuscaloosa Formation Reservoirs in McComb and Little Creek Field Areas, Southwest Mississippi. *AAPG Bulletin* 71 (9):1117.

Holston, Ira, David T. King, Jr., and Enid Bittner. 1989. Porosity and cementation in Upper Cretaceous Mooreville and Demopolis chalks, central Alabama. *AAPG Bulletin* 73 (9):1184.

John, Chacko J., Bobby L. Jones, James E. Moncrief, Reed Bourgeois, and Brian J. Harder. 1997. An Unproven Unconventional Seven Billion Barrel Oil Resource - the Tuscaloosa Marine Shale. In *The Basin Research Institute Bulletin*: Louisiana State University.

Klicman, Douglas P., Christopher P. Cameron, and Maurice A. Meylan. Petrology and depositional environments of lower Tuscaloosa Formation (Upper Cretaceous) sandstones in North Hustler and Thompson Field areas, southwestern Mississippi. *Gulf Coast Association of Geological Societies and Gulf Coast Section SEPM meeting; abstracts AAPG Bulletin* 72 (9):1115.

The Lower Tuscaloosa Formation 2008. Vision Exploration, LLC 2006 [cited August 8 2008]. Available from http://www.visionexploration.com/lower%20tusc.htm.

Mancini, Ernest A. 1989. Upper Cretaceous and Paleogene Biostratigraphy and Lithostratigraphy of Eastern Gulf Coastal Plain. Paper read at 28th International Geological Congress, at Washington, D.C.

———. 2005. Resource Assessment of the In-Place and Potential Recoverable Deep Natural Gas Resource of the Onshore Interior Salt Basins, North Central and Northeastern Gulf of Mexico. Tuscaloosa, AL: University of Alabama.

Mancini, Ernest A., Puckett T. Markham, B. H. Tew, and Charles C. Smith. 1995. Upper Cretaceous sequence stratigraphy of the Mississippi-Alabama area. *AAPG Gulf Coast Section meeting; abstracts AAPG Bulletin* 79 (10):1563.

McGlothlin, Tom. 1944. General geology of Mississippi. *American Association of Petroleum Geologists Bulletin* 28 (1):29-62.

Miranda, R. M., and C. C. Walters. 1992. Geochemical variations in sedimentary organic matter within a "homogeneous" shale core (Tuscaloosa Formation, Upper Cretaceous, Mississippi, USA). *Organic Geochemistry* 18 (6):899-911.

Miranda, Roger M. 1988. Geochemical variations in sedimentary organic matter within a one hundred meter shale core of uniform lithology and thermal history (middle Tuscaloosa, Upper Cretaceous). M.S., The University of Texas at Dallas, United States -- Texas.

Moody, Jack S., and Sandra G. Dowty. 1991. Lower Tuscaloosa and Frio of Southwestern Mississippi. *AAPG Bulletin* 75 (9):1533-1534.

Murray, Grover E. 1961. *Geology of the Atlantic and Gulf Coastal Province of North America*. Edited by C. Croneis, *Harper's Geoscience Series*. New York: Harper & Brothers.

Nelson, Philip H., and Joyce E. Kibler. 2003. A Catalog of Porosity and Permeability from Core Plugs in Siliciclastic Rocks: U.S. Geological Survey.

Nemeth, Kenneth J. 2007. Factsheet for Partnership Field Validation Test - Large Scale Storage Projects: Southeast Regional Carbon Sequestration Partnership (SECARB). Paper read at Regional Carbon Sequestration Partnerships Initiative Review Meeting, December 12-13, at Pittsburgh, PA.

Oldenburg, Curtis M. 2005. Health, Safety, and Environmental Screening and Ranking Framework for Geologic CO2 Storage Site Selection.: Lawrence Berkeley National Laboratory Paper.

Planert, M., and S.L. Sparkes. 1985. Estimation of vertical hydraulic conductivity of the clay layer between the Eutaw and Gordo aquifers in teh vicinity of Faunsdale, Marengo County, Alabama. In *Water Resources Investigations Report*: U.S. Geological Survey.

Pryor, W.A., and H.D. Glass. 1961. Cretaceous-Tertiary Clay Mineralogy of the Upper Mississippi Embayment. *Journal of Sedimentary Petrology* 31 (1):38-51.

Report on selected oil and gas fields, Arkansas, Louisiana, Texas, and Misssissippi. 1987. *Shreveport Geological Society Reference Volume VII*: Shreveport Geological Society

Rhudy, Richard. 2006. Pilot Tests Fact Sheets: CO2 Sequestration in Saline Formations - I, Mississippi Salt Basin, SECARB. Paper read at Regional Carbon Sequestration Partnerships Initiative Review Meeting, 3-4 October, at Pittsburgh, PA.

Scholle, Peter Allen. 1977. Current oil and gas production from North American Upper Cretaceous chalks. Arlington, Virginia: U.S. Geological Survey

Slack, Larry, and Daphne Darden. 1991. Summary of Aquifer Tests in Mississippi, June 1942 through May 1988. In *Water-Resources Investigations Report*: U.S. Geological Survey.

Spooner, H.V. 1964. Basal Tuscaloosa Sediments, East Central Louisiana. *American Association of Petroleum Geologists Bulletin* 48:1-21.

Strom, Eric W., and Micheal J. Mallory. 1995. Hydrogeology and Simulation of Ground-Water Flow in the Eutaw-McShan Aquifer System in Northeastern Mississippi: U.S. Geological Survey.

Stromm, Erick W., and Micheal J. Mallory. 1995. Hydrogeology and simulation of ground-water flow in the Eutaw-McShan aquifer and in the Tuscaloosa aquifer system in the

northeastern Mississippi. In *Water-Resources Investigations Report*: U.S. Geological Survey.

Tarbutton, R. J. 1979. Petrography of some selected Upper Cretaceous Selma Group sediments in parts of Humphreys, Sharkey, and Yazoo counties, Mississippi. Master's, University of Southern Mississippi, Hattiesburg.

Tew, Berry H. Depositional setting of the Arcola Limestone Member (Campanian) of the Mooreville Chalk, eastern Gulf Coastal Plain; assessment of the pelagic and benthonic depositional models. *Enriched: AAPG Gulf Coast Section (GCAGS) meeting; abstracts AAPG Bulletin* 84 (10):1692.

Watkins, H. Henderson. 1985. The petrology and diagenesis of the lower Tuscaloosa, Fayette Field, Jefferson County, Mississippi. Master's, Graduate School, University of Southern Mississippi, Hattiesburg.

Weedman, Suzanne D., Susan L. Brantley, Ryoji Shiraki, and Simon R. Poulson. 1996. Diagenesis, Compaction, and Fluid Chemistry Modeling of a Sandstone Near a Pressure Seal: Lower Tuscaloosa Formation, Gulf Coast. *AAPG Bulletin* 80 (7):1045-1064.

Wiygul, Gary J., Leonard M. Young, William P. Wilbert, and Leslie P. Jones, eds. *A subsurface study of the lower Tuscaloosa Formation at Olive Field, Pike and Amite counties, Mississippi*: Gulf Coast Association of Geological Societies, New Orleans, LA.

TABLE A.2.1: Stratigraphic and lithologic description of the system, series, group, formations and members surrounding the Tuscaloosa Massive Sand unit in Jackson County, Mississippi. Inset boxes represent dominant but not continuous members in the formations.

System	Series	Group	Formation/Member North	Formation/Member South	Thickness (ft)	Description
Upper Cretaceous	Gulfian	Selma (Navarro)	Owl Creek	Prairie Bluff Chalk	30 – 70[2]	Prairie Bluff Chalk in the extreme northernmost region of the Mississippi Embayment is present as the Owl Creek Formation[2]. The Prairie Bluff Chalk is a gray-white sandy massive chalk with calcareous shale that grades to a dark-grey, fine micaceous silty sand, and clay in the TN, represented as the Owl Creek[2]. The Ripley formation contains clay, sandy clay, calcareous shale, chalk, and thin beds of sandstone; with, Coon Creek Tongue member containing glauconitic micaceous, fossiliferous fine sand with interbedded clay[2,3]. The Monroe Gas Rock is white, sandy, micritic limestone in the Monroe Uplift region in the western region of MS[3]. Demopolis chalk is a relatively pure chalk with a chalky marl member within the top 50ft [2] and a basal member that contains chert, quartz pebbles, and beds of calcareous, glauconitic, fine sand[3]. Mooreville chalk consists of an impure chalk or chalky marl containing scattered thin beds of very fine glauconitic sands as well as hard bored limestone[2]. The Arcola Limestone member consists of hard bored limestone rhythmically interbedded with chalky marl[2,4] The Mooreville chalk grades into the Coffee Sand in N. MS. Coffee Sand contains a series of stratified and crossbedded micaceous, pyritic, and glauconitic sands and carbonaceous clays[2].
		Selma (Navarro)	Ripley	Coon Creek Tongue Member	1 - 400 [2]	(see above)
		Selma (Taylor)	Demopolis Chalk	Bluffport Marl Member	1 - 500[2]	(see above)
		Selma (Austin)	Coffee Sand	Arcola Limestone Member / Mooreville Chalk	1 – 250[2]	(see above)
		(Eagle Ford)	Eutaw	Tombigbee Sand Member	0 – 400[2] / 0 – 900[3]	Eutaw composed of gray clay interbedded with fine glauconitic, somewhat calcareous sands that are crossbedded or stratified[2,3]. The Tombigbee Sand Member is a persistent, massive, highly glauconitic, calcareous, and fossiliferous sand in upper part of Eutaw[2]. In the area of the Monroe Uplift it contains various volcanic detritus with brown waxy mudstone and fine to coarse fragments of igneous rock[3]. It overlies the McShan in AL and MS, recognized by their outcrop, but at subsurface the McShan and Eutaw are mapped together[2].
		(Eagle Ford)	McShan (Eagle Ford Shale)		150[5] / 1 – 200[2]	Eagle Ford shale consists of dark colored shale, sandy shale, and subordinate beds of sand[2]. The McShan consists of laminated micaceous glauconitic gray clay, fine sand, glauconitic sand[2].
		Tuscaloosa Group	Gordo (Upper Tuscaloosa)		100 – 150 [5] / 100 – 400[2]	Gordo formation is composed of thick beds of sand and chert gravel in lower part and multicolored clay and shale interbedded with sand in upper part[2,6].

Note: Column spanning "(Jackson Gas Rock?)" appears in the South Formation/Member area spanning the upper Selma rows. Overall Selma thickness range: 1 - 1,000[1]. Eutaw/McShan overall thickness: 150[5].

Lower Cretaceous	Comanche	Washita - Fredricksburg Undifferentiated Group	Coker (Tuscaloosa Marine Shale)		450 – 475[5]	1 – 400[2]	The marine shale is mostly gray to black, fine grained fissile, silty, micaceous, fossiliferous, calcareous, laminated claystone interbedded with dark gray silty, micaceous, fossiliferous, glauconitic, calcareous siltstone and very fine-grained sandstone, and also contains mudstones[1,7,8]. The equivalent Eoline member of the Coker formation is predominantly sand and consists of thin-bedded clay, sandy clay, shale, and sand of marine origin[2,9].
			Massive Sand (Lower Tuscaloosa)	(Stringer Member)		1- 500[2] 1-400[9]	The Massive sand has medium to coarse grained sands with interbedded shale and clay occurring in thick beds of course sand, chert, and quartz gravel [2,10]. The Stringer unit has course grained, lenticular sands with interbedded shale, sandstone, silty shale, and silty sandstone[11]. The Massive sand predominately contains nonmarine medium to course quartz, chert and gravel[6].
				(Massive Sand Member)	190[1]		
			Dantzler		0 – 1000[12]	1,1160 [13]	Washita-Fredricksburg group composed of black calcareous shales interbedded with thin, gray fossiliferous limestone and some fine grained sandstones [11,14]. Washita-Fredricksburg group is also described as comprising shale, clay sand, gravel, and calcareous strata[6,15]. The lower Andrew formation is an undifferentiated, unit predominantly composed of limestone[16,17] .
			Andrew (Undifferentiated "Limestone Unit")			800 – 1,500[13]	

▨ Shaded units represent seal rocks

( ) Subsurface equivalent to given surface unit
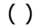
⌇ Represents a transition from one rock facies to another

1.) Rhudy (2006)
2.) Cushing, Boswell, and Hosman (1964)
3.) Tarbutton (1979)
4.) Tew (2000)
5.) Richard Esposito, personal communication with author, 2008
6.) Strom and Mallory (1995)
7.) John et al. (1997)
8.) Miranda and Walters (1992)
9.) Braunstein (1950)
10.) McGlothlin (1944)
11.) Watkins (1985)
12.) Murray (1961)
13.) Beebe and Curtis (1968)
14.) Spooner and Basal (1964)
15.) Boswell (1963)
16.) Mancini et al. (1995)
17.) Mancini (2005)

TABLE A.2.2: Correlation of geological formations across the northern and western regions of the Gulf Coast Province. Correlations based on hydrological (Cushing, Boswell, and Hosman 1964; Mancini 1989) and oil and surveys(Condon and Dyman 2006; Braunstein 1950; Dyman and Condon 2006). Inset boxes represent dominant but not continuous members in the formations.

Symbols (Table A.2.2 below):

▢   - Shaded units represent seal rocks

⦚   - Represents a transition from one rock facies to another in the subsurface

( )   - Subsurface equivalent to surface unit

SYSTEM	EAST TEXAS	LOUISIANA AND/OR ARKANSAS		MISSISSIPPI WEST-CENTRAL	MISSISSIPPI NORTH	MISSISSIPPI EAST	ALABAMA WEST	ALABAMA CENTRAL
UPPER CRETACEOUS	NAVARRO GROUP — ARKADELPHIA MARL	MONROE GAS ROCK ?	SELMA GROUP	JACKSON GAS ROCK? — PRAIRIE BLUFF CHALK	OWL CREEK	PRAIRIE BLUFF CHALK		PROVIDENCE SAND
	NAVARRO GROUP — NACATOCH SAND			JACKSON GAS ROCK? — RIPLEY FORMATION	McNAIRY SAND	RIPLEY FORMATION		
	NAVARRO GROUP — SARATOGA CHALK				COON CREEK TONGUE MEMBER			
	TAYLOR GROUP — MARLBROOK MARL			BLUFFPORT MARL MEMBER	COFFEE SAND	DEMOPOLIS CHALK	BLUFFPORT MARL MEMBER	
	TAYLOR GROUP — ANNONA CHALK			DEMOPOLIS CHALK			DEMOPOLIS CHALK	
	TAYLOR GROUP — OZAN FORMATION			ARCOLA LIMESTONE MEMBER		MOOREVILLE CHALK	ARCOLA LIMESTONE MEMBER	
	AUSTIN GROUP — BROWNSTOWN MARL			MOOREVILLE CHALK			MOOREVILLE CHALK	
	AUSTIN GROUP — TOKIO FORMATION				TOMBIGBEE SAND MEMBER			
	AUSTIN GROUP — AUSTIN				EUTAW FORMATION			
	EAGLE FORD GROUP — EAGLE FORD SHALE			McSHAN FORMATION				
	WOODBINE GROUP — TUSCALOOSA		TUSCALOOSA GROUP	GORDO (UPPER TUSCALOOSA) FORMATION	UNDIFFERENTIATED	GORDO (UPPER TUSCALOOSA) FORMATION		
				COKER (MIDDLE TUSCALOOSA) FORMATION — MARINE SHALE		COKER (MIDDLE TUSCALOOSA) FORMATION — MARINE SHALE	COKER	UNAMED UPPER MEMBER
								EOLINE MEMBER
				MASSIVE SAND (LOWER TUSCALOOSA)		LOWER TUSCALOOSA (MASSIVE SAND)		
LOWER CRETACEOUS	WASHITA – FREDRICKSBURG UNDIFFERENTIATED	WASHITA-FREDRICKSBURG GROUP		DANTZLER FORMATION				
				ANDREW FORMATION (UNDIFFERNTIATED LIMESTONE)				

TABLE A.2.3: Physical and mineral characteristics of the Tuscaloosa Marine Shale, Selma Group, and Midway Group.

Characteristic	Reported Values			Comments
	Marine Tuscaloosa Shale	Selma Group	Salt piercements	
Physical Properties				
Depth (ft)	7,675 - 8,150[1]	5,550 – 7,800[1]	0 – 25,000[2]	Reported depths of sediment analyzed for mineral components
Thickness	450 – 475[1]	1,000[1]	> 1,000[2]	Thickness of salt dome caprock[2]. Values reported near site of injection[1]
Porosity (%)	2.3 – 8.0[3]	1 – 45[4] 31 – 35[5]	-	Unpublished records from A.C. Moore in southwestern region of MS. Shale fractured and fractures interconnected [6]. Selma Group's Demopolis - Mooreville Chalk[5]. Selma permeability include reports from TX[4]
Permeability (md)	0.01 – 0.06[3]	<0.5 - 10[4] 0.9 – 0.13[5]	-	
Horizontal Hydraulic Conductivity (ft/day)	10 - 75[7] 48 - 200[8] 14 - 81[9]	10 - 75[7] 1 - 37[9]	-	Estimated from aquifer tests in northern Mississippi embayment[7-9]
Vertical Hydraulic Conductivity (ft/day)	1×10^{-5} – $1 \times 10^{-6(10)}$	1×10^{-5} – $1 \times 10^{-6(10)}$	-	Estimation based reported values of the Eutaw and Gordo aquifer clays in Alabama[10]
Hydraulic Transmissivity (ft[2]/day)	270 – 4,300[7]	270 – 4,300[7] 76 – 1,400[9]	-	Estimated from aquifer tests in northern Mississippi embayment[7]
Hydraulic Storage Coefficient	0.0001 – 0.0008[7]	0.0001 – 0.0008[7]	-	Estimated from aquifer tests in northern Mississippi embayment[7]
Area extent (mi[2])	48,434	48,434	48,434	Limited to the state of Mississippi
Major Mineral Components (> 20 wt%)				
Carbonates:			> 20%[2]	Third most abundant mineral in caprock of salt dome, primarily calcite[2]
Crystalline carbonate cement	39 – 45%[11]	8 – 58%[11]	-	Mooreville chalk of Selma group (Table 1,11)[11]. Marine Shale equivalent to Eoline member composition of Coker formation[11]
Low-Magnesium Calcite	-	> 20%[12]	-	Taken from equivalent Austin Chalk in TX[12]
Manganese Calcite	-	> 20%[13]	-	Taken from equivalent Austin Chalk in TX[13]
Ferrous Calcite	-	> 20%[13]	-	Taken from equivalent Austin Chalk in TX[13]
Argillaceous calcilluite	-	14 – 87%[11]	-	Mineral constituent of Mooreville chalk in Selma group(Table 1,11)[11]
Chalky Marl	-	50 – 60%[5]	-	Selma Group's Demopolis - Mooreville Chalk[5]
Marl	-	30 – 50%[5]	-	Selma Group's Demopolis - Mooreville Chalk[5]
Glauconite	-	8 – 28%[11]	-	Mineral constituent of Marl in Mooreville chalk of Selma group (Table 47)[11]
Halite	-	-	97 – 99%[2]	Main composition of salt dome structure[2]
Anhydrite	-	-	> 20%[2]	Most abundant mineral in caprock of salt dome[2]
Gypsum	-	> 20%[12]	> 20%[2]	Taken from Austin Chalk in TX[12]. Second most abundant mineral in caprock of salt dome[2]
Insoluble Residues	-	20 – 50%[4]	-	Insoluble residues are not reactive to

				dilute HCL[4]
Sulfur	-	-	> 20%[2]	Mineral in caprock of salt dome[2]
Quartz	2 – 33%[11]	-	-	Eoline member of Coker equivalent (Table 7,9,10)[11]
Clay paste	1 – 68%[11]	-	-	Clay sized particles and minerals (Table 9,10)[11]
Clay minerals:				
Kaolinite	19 – 100% (av.: 57%)[14]	7 – 94% (av.: 12 - 73%)[14]	-	Upper Mississippi embayment clays reported in parts of 10[14]. Marine Shale clay composition base from Tuscaloosa group values[14]. Average range over subunits of Selma group and Tuscaloosa[14]
Illite	0 – 81% (av.: 34%)[14]	1 – 85% (av.: 15 – 30%)[14]	-	Upper Mississippi embayment clays reported in parts of 10[14]. Marine Shale clay composition base from Tuscaloosa group values[14]. Average range over subunits of Selma group and Tuscaloosa [14]
Montmorillonite	0 – 28% (av.: 9%)[14]	0 – 92% (av.: 6 – 73%)[14]	-	Upper Mississippi embayment clays reported in parts of 10[14]. Marine Shale clay composition base from Tuscaloosa group values[14]. Average range over subunits of Selma group and Tuscaloosa [14]
Muscovite	1 – 22%[11]	-	-	Eoline member of Coker equivalent (Table 7,9,10)[11]
Minor Mineral Components (< 20 wt%)				
Quartz	-	1 – 9%[11]	-	Mooreville chalk of Selma group (Table1,11)[11]
Kaolinite		< 20%[12]	-	Taken from Austin Chalk in TX[12]
Feldspar	1 – 8%[11]	< 20%[12]	-	Taken from Austin Chalk in TX[12]. Eoline member of Coker equivalent (Table 7,9,10)[11]
Glauconite	1 – 15%[11]	-	-	Eoline member of Coker equivalent (Table 7,9,10)[11]
Mixed lattice clay		< 20%[14]	-	Upper Mississippi embayment clays[14]
Chlorite	1 – 10%	< 20%[14]	-	Upper Mississippi embayment clays[14] Eoline member of Coker equivalent (Table 7,9,10)[11]
Organic Content				
Oil	0.7 – 4.3 (%vol)[3]	-	-	
Total Organic Carbon (TOC)	0.21 – 1.13%[15]	1.2 – 1.8%[16]	-	Marine Shale values from Pike Co., Mississippi[15]. Ingersoll shale within the Eutaw formation[16]
Total Inorganic Carbon (TIC)	0.07 – 3.15%[15]	-	-	Marine Shale values from Pike Co., Mississippi[15].

av. – average of source data set

1.) Rhudy (2006)
2.) Murray (1961)
3.) John et al. (1997)
4.) Scholle (1977)
5.) Holston, King, and Bittner (1989)
6.) John et al. (1997)
7.) Brahana and Mesko (1988)
8.) Stromm and Mallory (1995)
9.) Slack and Darden (1991)
10.) Planert and Sparkes (1985)
11.) Bergenback (1964)
12.) Freed (1980)
13.) Czerniakowski, Lohmann, and Wilson (1984)
14.) Pryor and Glass (1961)
15.) Miranda & Walters (1992)
16.) Bingham and Savrda (2006)
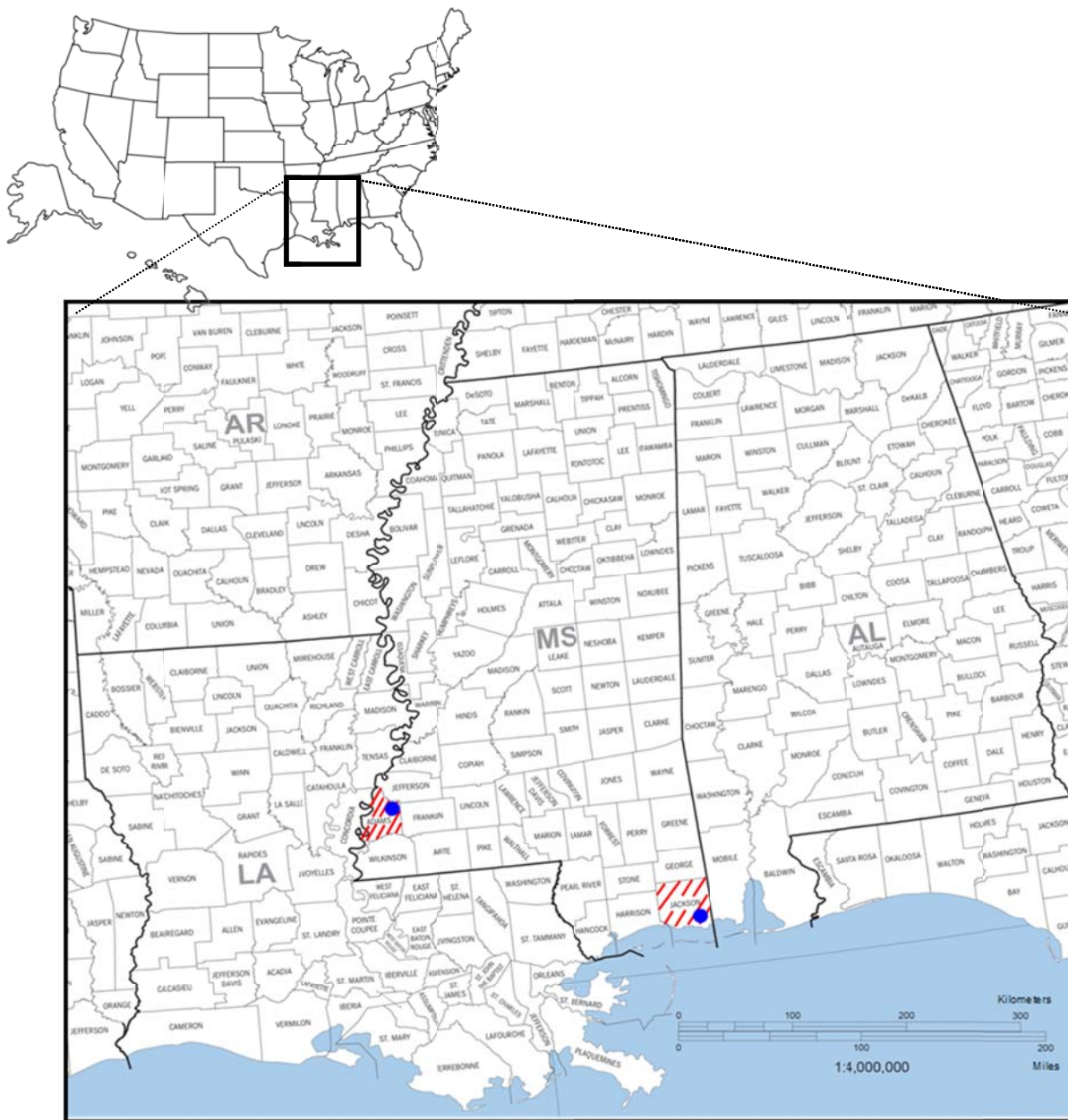
FIGURE A.2.1:   Map showing location of proposed demonstration sites for CO_2 Saline sequestration in Mississippi at Plant Daniel, Jackson County and Cranfield, Adams County in the northern region of the Gulf Coast Province of North America. Counties are striped and field locations are approximated with dots. Modified from U.S. Census 2003 map.
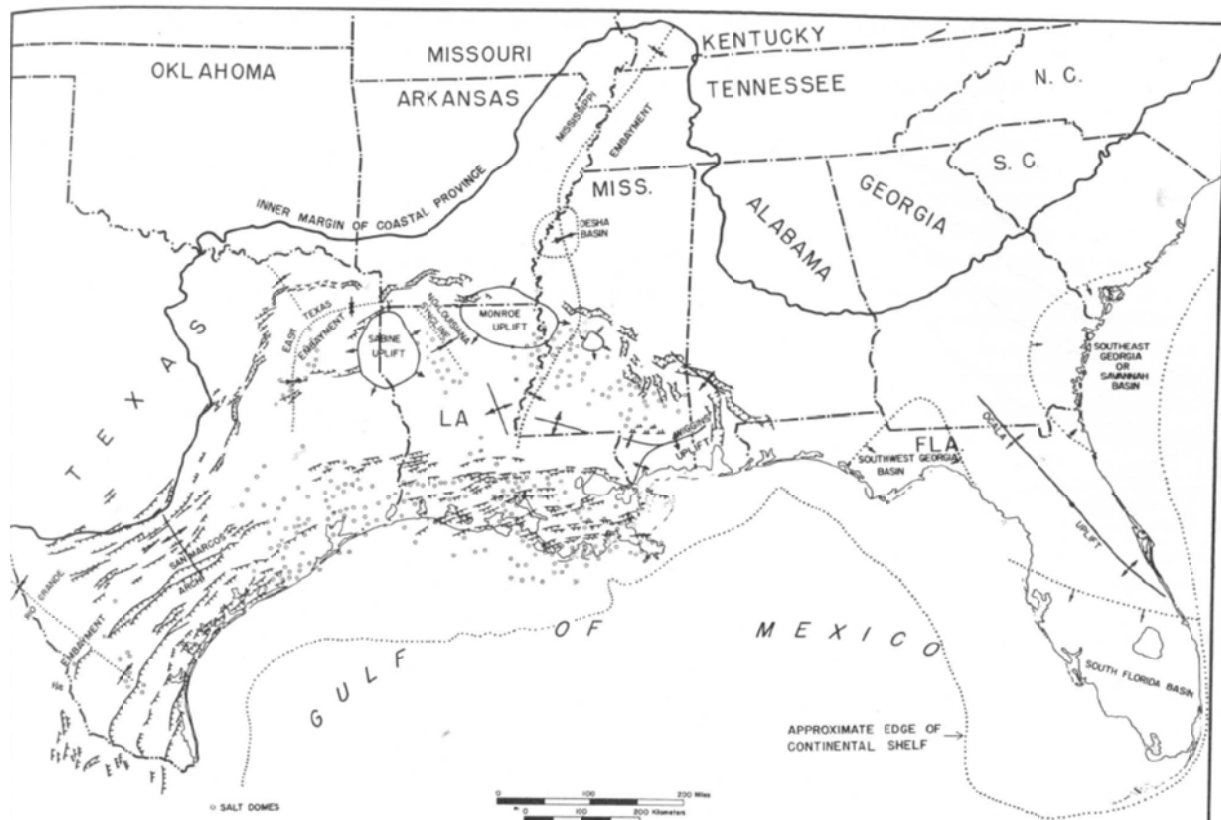
FIGURE A.2.2: Diagrammatic map of major structural features of the Northern and Western regions of the Gulf Coast Province (Murray 1961).
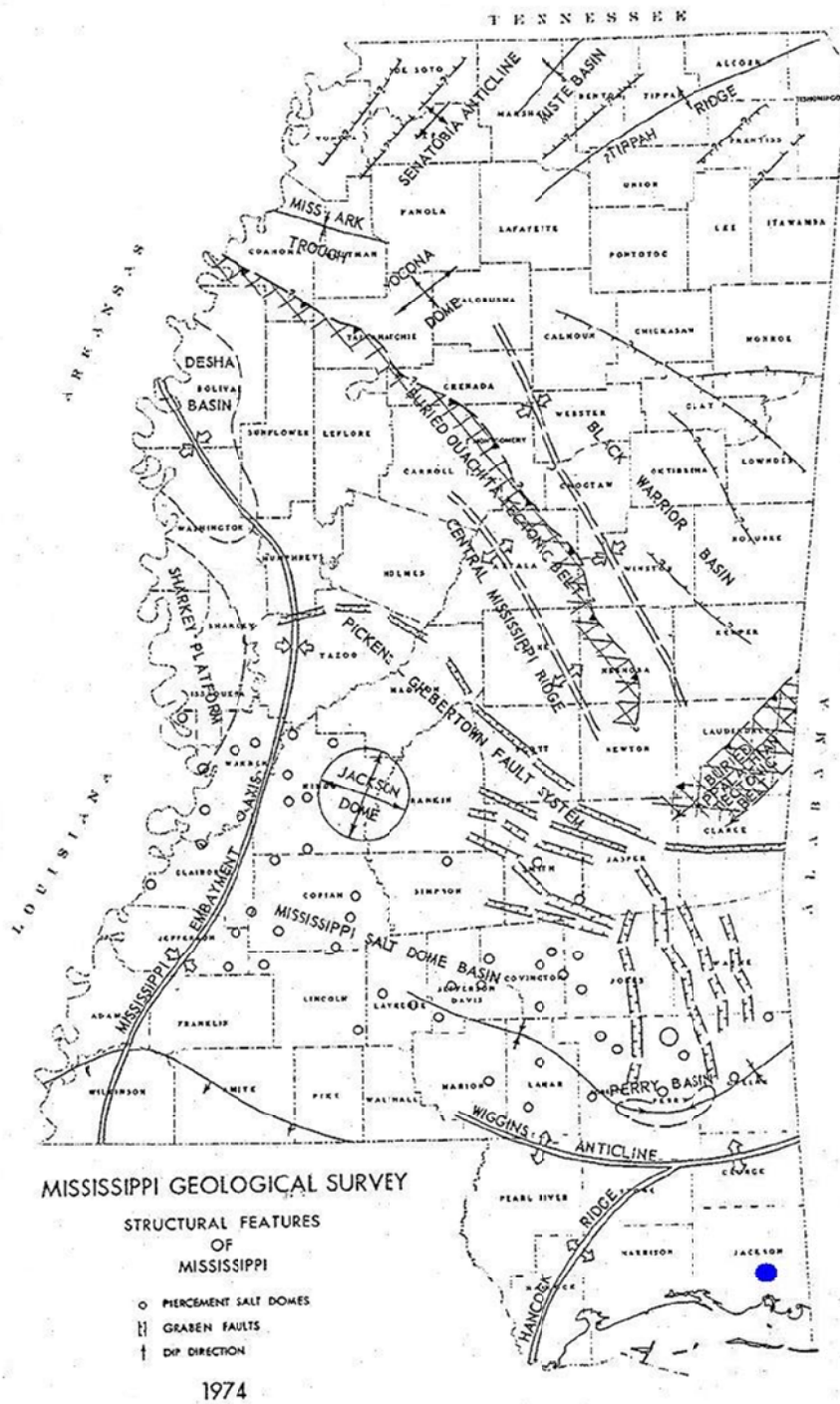
FIGURE A.2.3: Structural features of Mississippi in relation to Plant Daniel (blue dot) demonstration site (Tarbutton 1979).
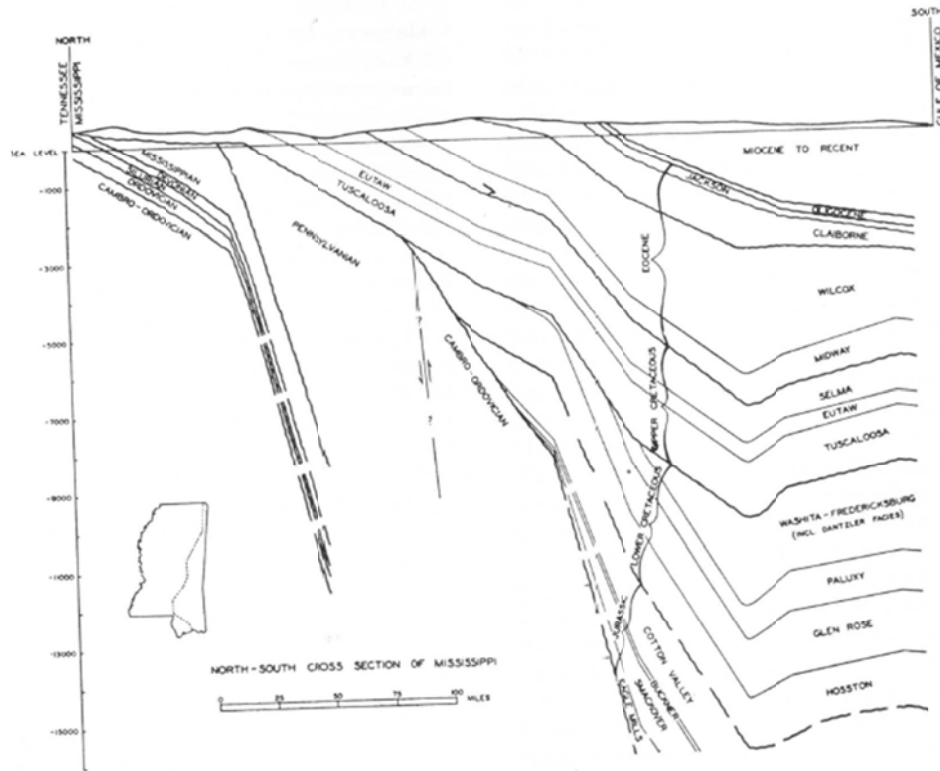
FIGURE A.2.4: Cross Section showing stratigraphy of Mississippi coastal sequence - Gulfward, of the central portion of the northern Gulf coastal province (Murray 1961).
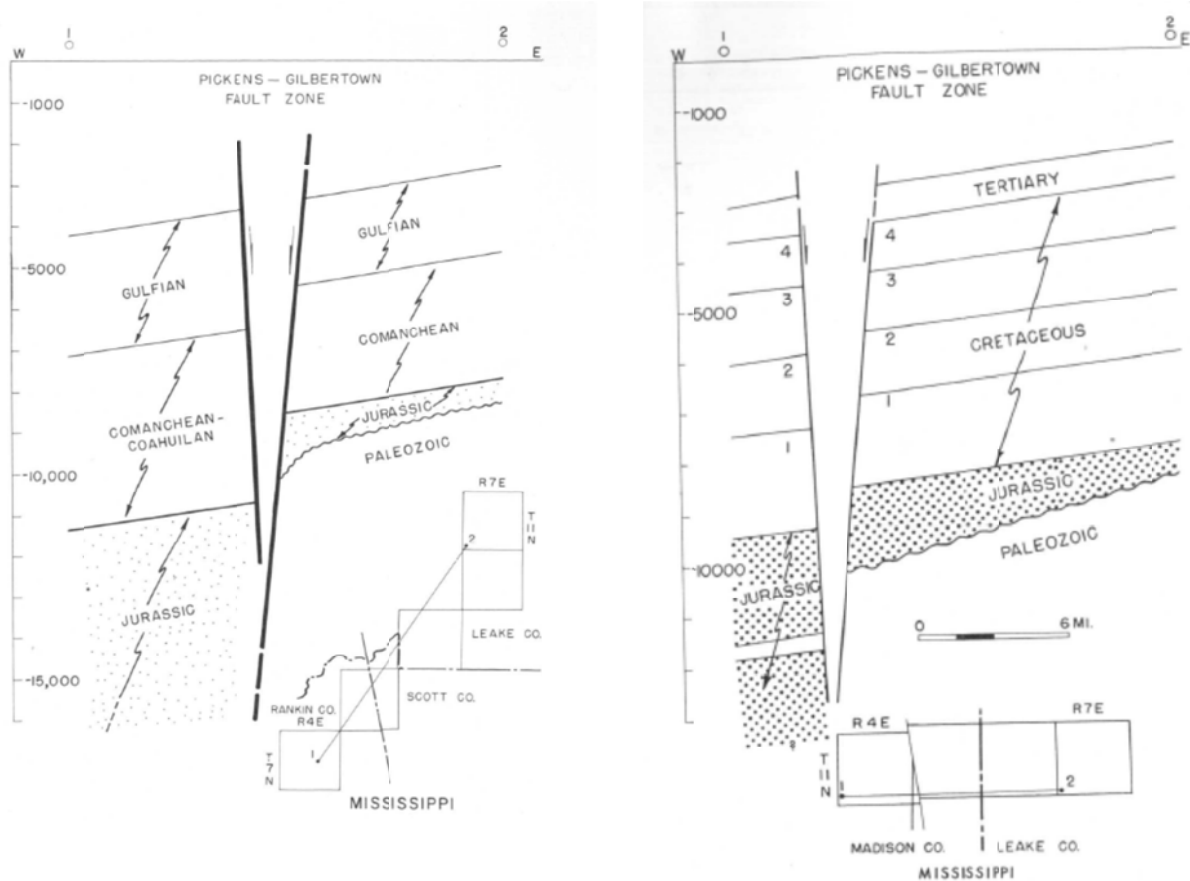
FIGURE A.2.5: Cross sections of the Pickens - Gilbertown Fault in Mississippi. Leake and Rankin Counties (left), Madison and Leake Counties (right). Circles represent control wells (Murray 1961).
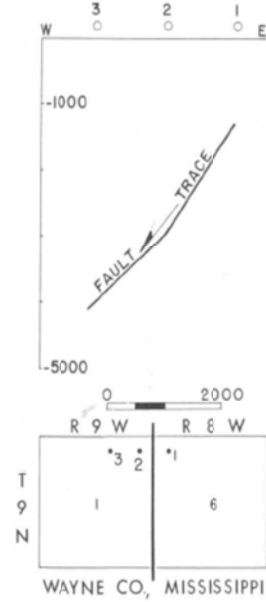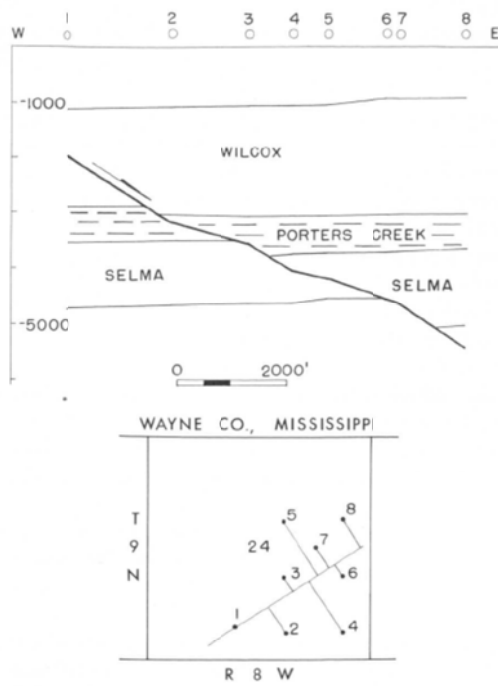
FIGURE A.2.6: Recorded fault transecting Selma Group in the Eucutta field - Wayne County, Mississippi. Circles represent well locations (Murray 1961).
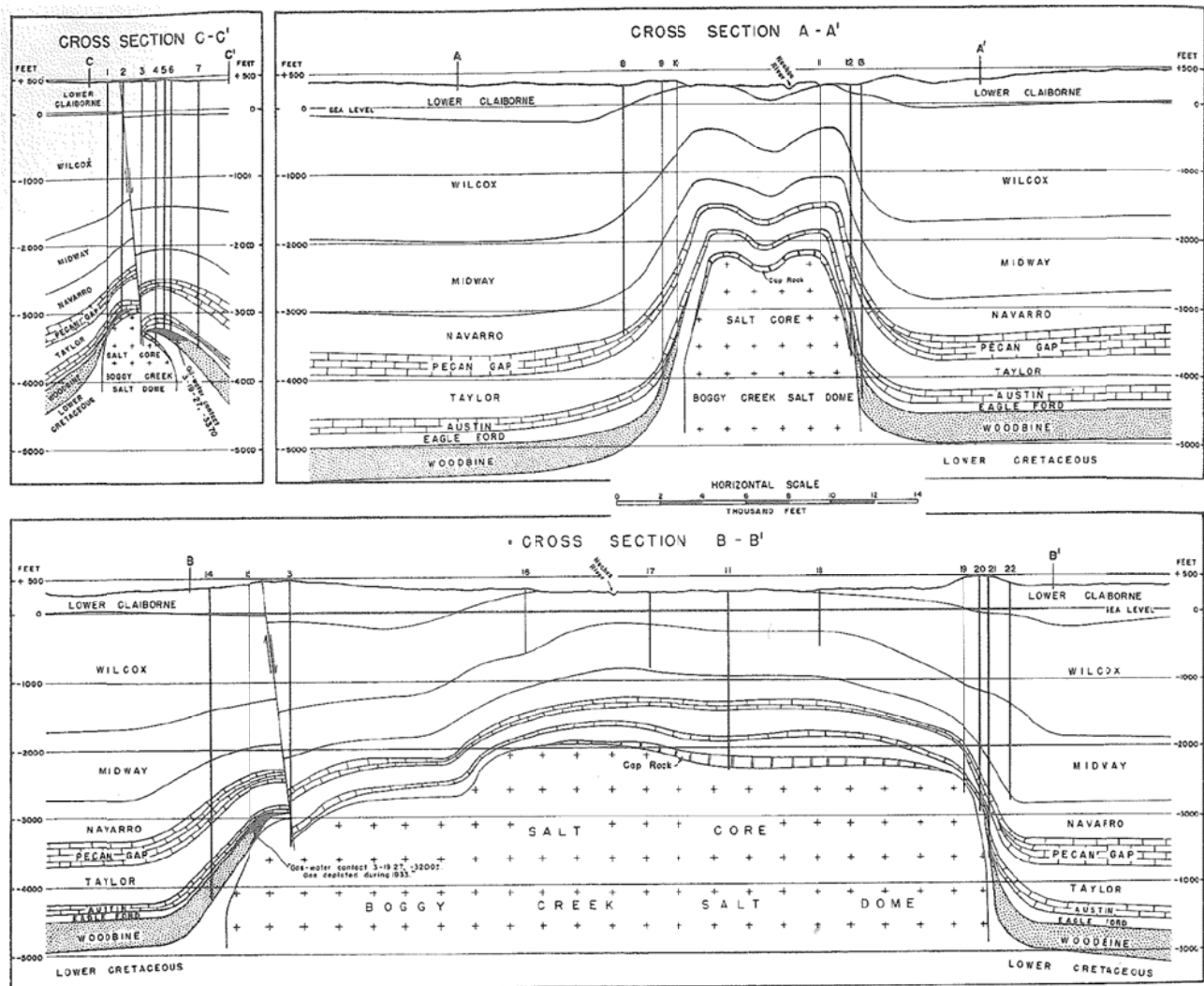
FIGURE A.2.7: Cross-section example of salt domes and piercements throughout the Gulf Coast Province of North America that extend through the reservoir and seal sediments for CO_2 sequestration in SECARB. Salt dome depicted is the Boggy Creek in Anderson and Cherokee Counties of Texas.
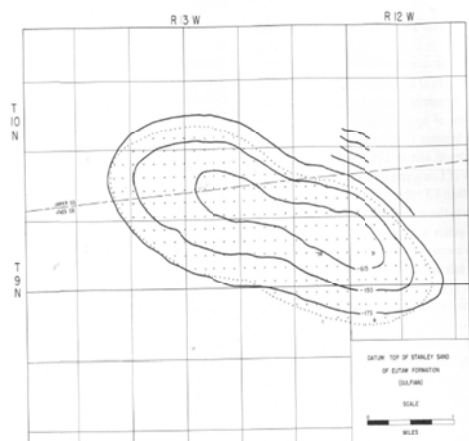
FIGURE A.2.8: Salt domes that pierce through the Tuscaloosa group and Eutaw formation in Adams, Lincoln, and Jasper County Mississippi (Murray 1961).
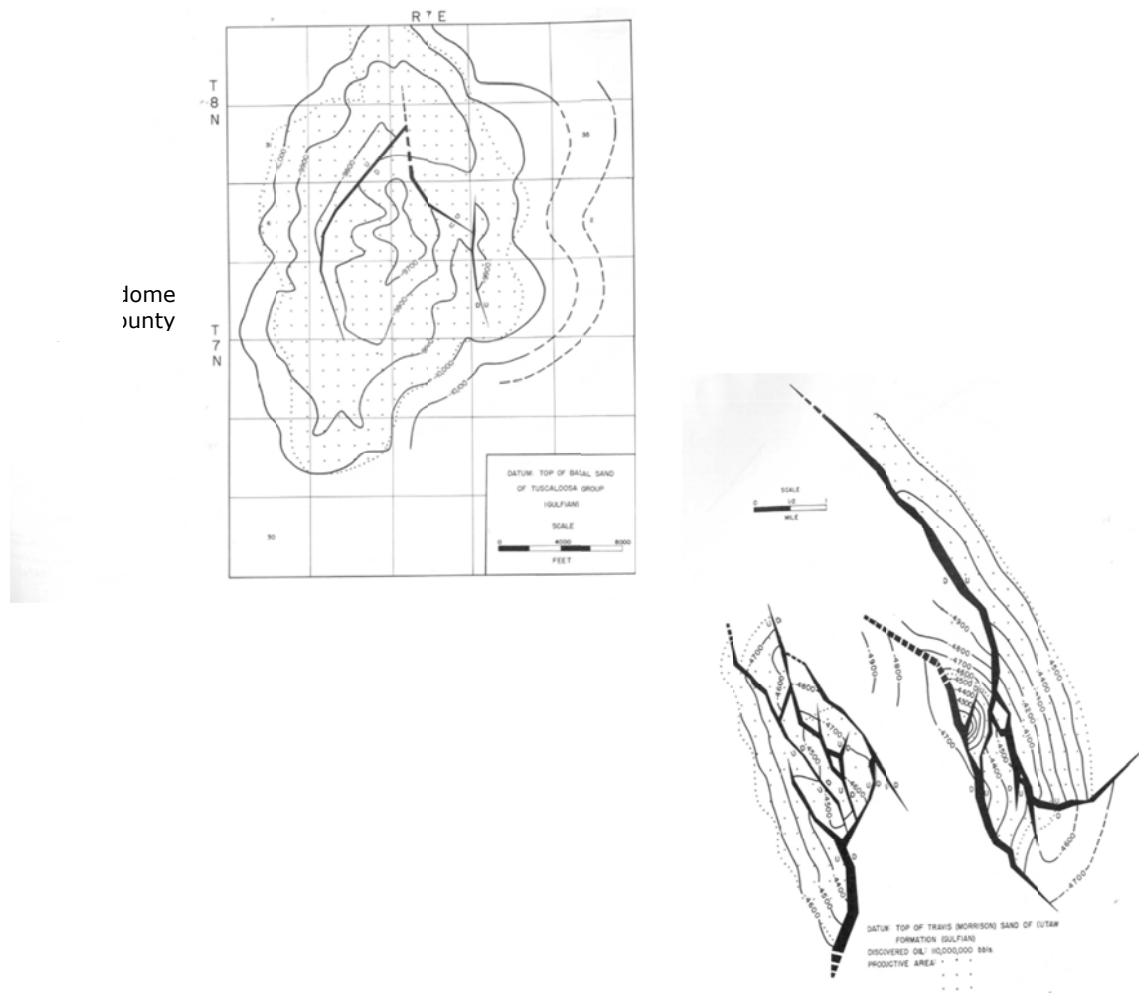
FIGURE A.2.9: Salt dome piercements through the Eutaw and Lower Tuscaloosa formations in Jasper and Lincoln County, Mississippi. Salt piercements show compound fractures (Murray 1961).
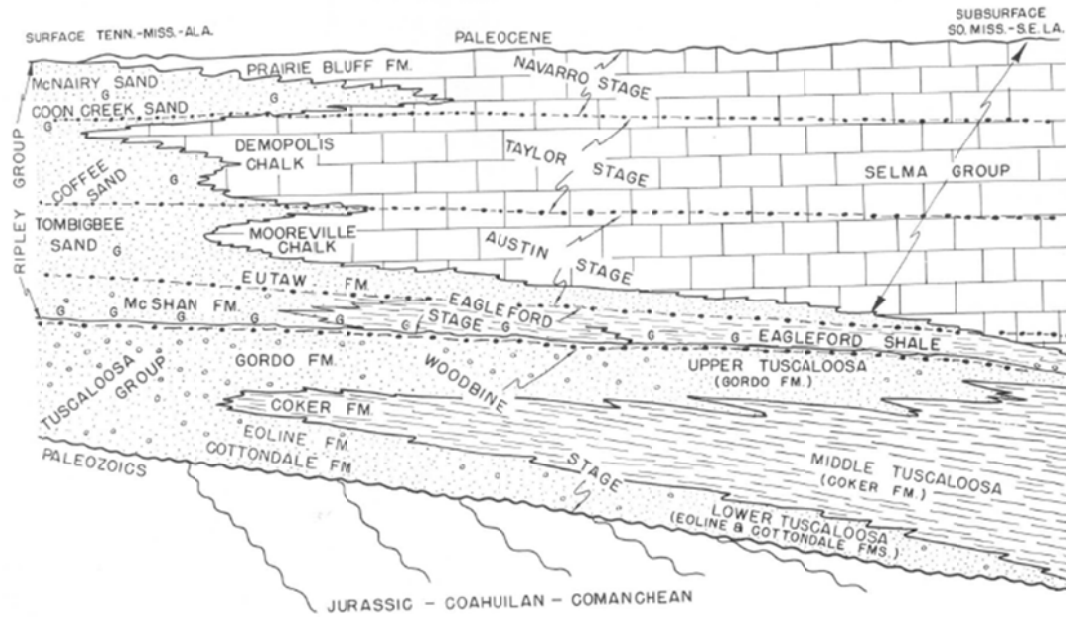
FIGURE A.2.10: Diagrammatic correlation of reservoir and seal formation lithology between the surface and subsurface units in North to Southern Mississippi. G = glauconite, dots = sandstone, small open circles = gravel, brick symbol = limestone or chalk, dotted and dashed line = approximate boundary of each group (or stage) within the Upper Cretaceous system (Murray 1961). Modified for Chapter 2, Figure 2.6. (See Table A.2.2 for regional correlation of Upper Creteaceous system).

Appendix A.3:

Mount Simon reservoir with Eau Claire formation as geological seals: Geology, Lithology, Mineralogy and CO_2 Storage Implications

A.3.1   Introduction

In 2003 the U.S Department of Energy (U.S. DOE) initiated regional partnership programs to address the concern for rising atmospheric CO_2. These partnerships were formed to explore regional and economical means for geologically sequestering CO_2 across the United States and to set the stage for future commercial applications. Several options exist for geological sequestration and among these sequestering CO_2 into deep saline aquifers is one of the most promising. This is due, in part, to the possibility of stabilized permanent storage through mineral precipitation from chemical interactions of the injected carbon dioxide with the brine and reservoir rock. To mitigate CO_2 emissions successfully, the rock seal(s) considered for geological CO_2 sequestration need to be assessed for risk and be proven effective for containment of the injected CO_2 gas.

In Illinois there are four sites proposed to demonstrate CO_2 injection into a saline reservoir, the Mount Simon. Three by the Midwest Geological Sequestration Consortium (MGSC) in the Louden and Mattoon oil fields of Fayette and Coles County, respectively; and, one by the FutureGen Alliance, near the town of Mattoon in Coles County (Figure 1)(Finley and Leetaru 2006; Pacheco 2007). The data on the geological seal used for these sites were collected from literature sources in peer reviewed journals, open reports, and thesis dissertations containing geological data near the location of the demonstration sites.
Given the types of mechanisms governing CO_2 escape from a potential storage reservoir, it is important to consider the effectiveness of the geologic seal in the broader context of the

prevailing structural features, lithostratigraphy, mineral, and physical characteristics that compose and influence the seal(s) at each field demonstration site. Of primary interest is the presence of soluble minerals in the seal rock that would be vulnerable to dissolution upon contact with supercritical CO_2 and CO_2-brine solutions.

A.3.2 GENERAL GEOLOGIC FRAMEWORK

The proposed locations for CO_2 saline sequestration in Illinois, and the sediments used for storage and seals, lie within the Illinois Basin (Figure 1). The Illinois Basin is spoon shaped, asymmetrical shallow intracratonic structural depression that trends northwest-southeast and covers an area of 135,000 mi^2, reaching into parts of Indiana, Kentucky, and Tennessee with the deepest part of the basin (15,000 feet) near the intersection of Illinois, Indiana, and Kentucky (Figure 1)(Willman et al. 1975; McBride and Nelson 1999).

The basin extends to the top of bordering epeirogenic arches and domes to the north, east and west, where the direction of the regional slopes is reversed, and is overlapped in the south by the Mississippi Embayment(McBride and Nelson 1999). The arches and domes include: Wisconsin Arch to the north, the Kankakee Arch to the northeast, the Cincinnati Arch to the east, the Nashville Dome to the southeast, Pascola Arch to the south, the Ozark Dome to the southwest and the Mississippi River Arch to the west and northwest (Figures 1, 2)(Finley 2005; McBride and Nelson 1999). The southern part of the basin approaches the New Madrid Rift System and the Rough Creek Graben (including the Moorman Syncline), a region that contains the thickest sedimentary beds within the basin and is complexly faulted and also having a history of reactivation(McBride and Nelson 1999) (see Figure 2).

In Illinois, the rocks above the Precambrian basement, which contain the CO_2 storage reservoir and seal(s), are dominantly marine sediments deposited in the Paleozoic Era. The Paleozoic rocks (Cambrian through Pennsylvanian) have a maximum thickness of about 14,000 feet in the deepest part of the basin(Willman et al. 1975). The layers of

sedimentary strata can dip up to 20 degrees from the epeirogenic arches and domes around the Illinois Basin and expose 2,000 – 3,000 feet of sediment in east-central part of Illinois(Willman et al. 1975).

The major structural features that surround the demonstration sites in the Illinois Basin can be seen in Figure 2. The Illinois Basin is characterized by sub-basins, and systems of folds and faults. These features will be further described with an emphasis on elements in Illinois pertinent to the locality of the demonstration sites.

Folds

In the southern part of the state of Illinois, near the Louden and Mattoon oil fields, the Illinois Basin is sub-divided into two main regions: the Fairfield Basin and the Sparta Shelf. The Fairfield Basin a relatively unfaulted area region that extends from the southern end of the La Salle Anticlinoium to the similar but shorter east-facing Du Quoin Monocline (Figure 2) (Willman et al. 1975; McBride and Nelson 1999). The Fairfield Basin is a ovoid structure containing 13,780 feet of Paleozoic sediments with the Sparta Shelf being flat and broad and containing 8,202 feet of strata (McBride and Nelson 1999). Both the Fairfield Basin and the Sparta Shelf are dominated by north-trending monoclines, and asymmetrical anticlines (see Figure 2) and are spanned below by the Cottage grove fault system, which is a series of transgressional reverse faults forming a strike-slip zone that affects the entire Paleozoic strata and Precambrian basement(McBride and Nelson 1999; McBride 1998). In describing the folds and faults in southern Illinois, only relevant structural elements within the Fairfield sub-basin will be discussed.

The dominant folds that occur between the Fairfield sub-basin are north-trending, asymmetrical anticlines and monoclines(McBride and Nelson 1999). They were developed during the late Mississippian through early-middle Pennsylvanian age and are elongate, branched, and with sinuous axes(McBride and Nelson 1999). Oval-shaped domes are arranged along the crests of anticlines, like beads on a string, separated by synclines that are flat troughs with poorly defined axes.

226

Major anticlines, monoclines, and synclines that are present or in close proximity (< 30 miles) from the counties in which CO_2 saline sequestration is being demonstrated include: the Louden anticline, the Du Quoin monocline, the La Salle Anticlinorium and Clay City anticline.

The Louden anticline hosts the second-largest oil field in the Illinois Basin and was progressively folded asymmetrically from the Chesterian through Pennsylvanian time with steep flexure(McBride and Nelson 1999). The anticline is steep on its northwest flank and has an elongated, oval outline with some 197 feet of closure in Devonian and younger sediments(Nelson 1995; McBride and Nelson 1999). On the Louden anticline is where the MGSC has one of its demonstration sites.

The Du Quoin monocline is a north-trending fold that has two branches that separates the Fairfield basin in the east from the Sparta Shelf on the west (Figure 2). The eastern branch runs northeast and recoils before meeting the Salem and Louden anticlines while the western branch runs northward (Figure 2). The monocline was uplifted during the Morrowan through Missourian time (late Mississippian – early Pennsylvanian)(Nelson 1995). As a consequence, structural relief increases with depth through Pennsylvanian strata(McBride and Nelson 1999). This monocline is in close proximity (< 30 miles) to the MGSC demonstration site in the Louden oil field of Fayette County.

The La Salle Anticlinorium (also called 'anticlinal belt') is a zone of anticlines, domes, monoclines, and synclines that trend north-northwest for approximately 248 miles across Illinois (Figure 2). The western margin of the anticlinal belt has is mostly west-facing monoclines with a relief up to 2,460 feet(McBride and Nelson 1999). The other folds present in the belt are anticlines with axes that are sinuous and branching and domal closures that are arranged in a "string-of-beads"fashion(McBride and Nelson 1999). The anticlinorium was developed during the Chesterian to Virgilian time (early to late Pennsylvanian)(Nelson 1995; McBride and Nelson 1999). This anticlinal belt extends in close proximity (< 30 miles) to the MGSC and FutureGen project demonstration sites in Macon and Coles County.

Contributing to the complex structural geology of southern Illinois is the Clay City anticline near the southern margin of the La Salle Anticlinorium. The Clay City anticline is a long, sinuous fold between the Don Quoin Monocline and La Salle Anticlinorium with distinct asymmetric folding affecting the entire Paleozoic sediments(McBride 1998). Its structure affects both the storage and geological seal(s) used in nearby (~ 30 miles) demonstration sites in Coles County.

Faults

The folds previously mentioned are important for CO_2 storage implications due to recent high-resolution seismic studies in the southern Illinois that reveal normal, reverse, and antithetic faults that cut through the CO_2 storage reservoir and the seal(s).

A high resolution seismic study on the Louden anticline revealed high-angle (shallow to near vertical) reverse faults that were interpreted to penetrate the Precambrian through Knox Group sediments (Figures 3a, 4)(McBride and Nelson 1999). The interpreted dominant fault in the Louden anticline was estimated to have about 60° dip(McBride and Nelson 1999).

The Du Quoin monocline is interpreted to have steep west-dipping reverse faults that penetrate the Precambrian strata to the New Albany Shale with a possible antithetic (backthrust) fault extending from Precambrian to Knox group sediments (Figure 3b). The dip of the Du Quoin monocline faults average 70° – 75°. In the east flank of the Du Quoin the faults are normal and transect sediments of the Knox group through middle Chesterian (Beech Creek) (Figure 3c).

Faulting accounts for only a minor part of the relief in the La Salle Anticlinorium, although deep-seated faulting in Precambrian rocks may account for the deformation of the overlying sedimentary rocks(Willman et al. 1975). The La Salle Anticlinorium has more complex faulting in the Precambrian basement that may extend to the Mount Simon storage reservoir but may not penetrate the Eau Claire seal (Figures 4, 5). The faults throughout the southern margin of the anticlinorium have high-angle reverse, antithetic thrust faults that appear to steepen with depth(McBride and Nelson 1999).

The Clay City anticline shows evidence of reverse faulting that appears to penetrate sediments of the Precambrian basement, Mount Simon, and Knox group (including the Eau Claire) up to what might be the New Albany Shale (Figures 4, 6). This may have implications for CO_2 storagae at demonstration sites in Coles County.

Anticlines present in the Fairfield Basin provide a positive benefit to sequestration because they offer a means for structural closure/trap which is beneficial to oil and gas storage, but existing high-angle, near vertical faults that transect primary, secondary, and tertiary seals (which are thousands of feet apart) create an elevated risk for leakage in southern Illinois region. In addition, the faults within the Fairfield sub-basin, seen in Figures 3, 5, and 6, give indication of having strike-slip components that could provide a structural fabric capable of reactivation(McBride and Nelson 1999; McBride 1998).

Other structural features

A unique feature of the Illinois Basin is the occurrence of numerous seismic activities around structural deformations in the southern portion of the Basin. Earthquakes are spatially associated with the La Salle Anticlinorium (LSA) and Wasbash Valley Fault System (WVFS) in the Fairfield sub-basin, and also in the New Madrid seismic zone (NMSZ)(McBride 1998; Finley 2005).

The NMSZ is a structurally complex zone of faults with a long history of reactivation(McBride 1998; Kolata and Nelson 1991). The NMSZ is located in the central Mississippi River valley, centered within the northern Reelfoot rift (see Figure 1). Earthquakes associated with NMSZ follow a relatively discrete zone of strike-slip faulting and have been well studied (see Figure 7).

There are recent studies associating the discrete seismic patterns of the NMSZ with the diffuse seismic patterns found in southern Illinois region around the LSA and WVFS(McBride 1998). The WVFS is a system 60 miles long and 15 miles wide and is an active area of recent faulting, with sediments with up to 480 feet of displacement(Finley 2005) (see Figure 2). Although it is unclear how the LSA and WVFS are kinematically related

the NMSZ, due to low magnitude seismicity ($m_{bLg} \leq 4.0$) in NMSZ and high seismicity in LSA ($m_{bLg} \geq 5.0$), it is postulated that they are connected through an array of faults that penetrate the Precambrian and widen northward from the NMSZ to the LSA and WVFS of the southern Illinois Basin(Finley 2005; McBride 1998).

A.3.3   DEMONSTRATION SITE GEOLOGY OF STORAGE RESERVOIR(S) AND GEOLOGICAL SEAL(S)

In Illinois, there are two programs that endeavor to demonstrate the feasibility of CO_2 saline sequestration, one is the MGSC and the other is the FutureGen Alliance. The MGSC has three potential sites: the Lounden and Mattoon oil fields and the Archer Daniels Midland, Company (AMD) ethanol plant, located in three separate counties: Fayette, Coles, and Macon, respectively. The FutureGen Alliance has its proposed plant built near the town of Mattoon in Coles County. All of these sites have proposed to inject CO_2 into the Mount Simon reservoir and use the overlying Eau Claire formation of the Knox group, as its primary seal. The geological Additional geological seals include the Maquoketa formation and the New Albany Shale, 3,000 – 3,700 feet above the Eau Claire respectively. In this study, the geological units underneath the Louden and Mattoon oil fields will be described, as all sites share the same storage reservoir and seal units. Only the Mount Simon and the lower members of the Knox group, the Eau Claire and Galesville sandstone, will be discussed in detail.

Currently, and for about 50 years, the Mount Simon sandstone has been used for successful natural gas storage. It is its success in natural gas storage that elevates the Mount Simon reservoir as a most likely candidate for CO_2 saline sequestration in Illinois, in addition to the multiple overlying formations that have also proven to be adequate for natural gas storage(Finley 2005). Reports from several natural gas projects suggest that the Eau Claire should be an effective reservoir rock(Finley 2005). However, rates for gas migration were not available but only general descriptions of the reservoir performance.

Reports show that the Mount Simon is particular effective when situated on anticlines with closures on top of the Mount Simon ranging from 100 – 290 feet. However, some natural gas storage projects, like the Troy Grove Project, has the Mount Simon cut by at least four faults with evidence of gas migration into overlying formation, indicating that fractures are present in the seal (Finley 2005).

The Galesville Sandstone, above the Eau Claire, represents a possible sink which could be though of a pseudo-seal. It also represents a possible risk in that it has been proven to leak in natural gas storage fields (Herscher and Herscher NW fields(Finley 2005; Buschbach and Bond 1974)) with source of leak being unresolved.

It is important to note that likely candidates for CO_2 sequestration are on anticlines because they are known to have the necessary structural closure for storage and containment of hydrocarbons and natural gas. Natural gas ultilites are currently using many of the anticlines in northern Illinois(Finley 2005).

A.3.3.1 CO$_2$ STORAGE RESERVOIR(S)

The Mount Simon sandstone is the proposed storage reservoir for 10,000 – 1,000,000 Tons of CO_2 in Illinois(Finley and Leetaru 2006; Finley 2007). At the Loudon oil field site, the Mount Simon occurs at depth of 7,000 – 8,300 feet(Finley and Leetaru 2006) with a thickness of 1,300 feet(Finley and Leetaru 2006). At the Mattoon oil field the Mount Simon is estimated to start at depth of 6,500 – 6,950 feet(Tetra-Tech 2007) at the with an approximate thickness of 1,300 – 1,400 feet(Tetra-Tech 2007).

The Galesville sandstone is described with the overlying Ironton sandstone due to the difficultly in differentiating them in the subsurface. The Ironton-Galesville sandstones have an approximate depth of 5,650 feet with a combined thickness of 0 – 150 feet near the sites. (Figure 4)(Willman et al. 1975; Finley 2005).

A.3.3.2 CO$_2$ STORAGE RESERVOIR SEAL(S)

The target formation for CO_2 injection is the Mount Simon formation with the Eau Claire formation acting as its primary seal(Finley 2005; Finley and Leetaru 2006). Stratigraphically, the Mount Simon and the Eau Claire formation are Cambrian in geological age and of the Dresbachian series; with, the Eau Claire formation being associated with the Knox group (see Figure 4). The Eau Claire formation, which acts as the primary seal at both sites, starts approximately at a depth of 5,800 – 6,450 feet(Tetra-Tech 2007) at the Mattoon oil field, interpreted from reported thickness of 500 – 700 feet(Tetra-Tech 2007). The Eau Claire formation is expected to also have a thickness of 500 – 700 feet in the Loudon oil field area (see Figures 4, 8) (Tetra-Tech 2007).

A.3.4 MINERAL AND PHYSICAL CHARACTERISTICS OF STORAGE RESERVOIR, SEAL(S), AND OTHER RELEVANT GEOLOGICAL FEATURES

To estimate the impact of CO_2 injection into the Mount Simon formation, it is important to know the mineral composition and physical traits of the potential reservoir(s), its seal(s), and other relevant structural features that could impact the storage of the CO_2. Changes in the mineral composition of the Mount Simon or the Eau Claire formation, due to lithological facies variation or CO_2 injection, could reduce or enhance injectivity and storage capacity at the site. Likewise, changes in the physical traits of these formations due to CO_2 injection could result in increased risk for leakage and migration of the gas, where interaction with other prominent structural features could impact the permanency of the CO_2 storage.

Figure 4 and Table 1 describe the lithology, mineralogy, and physical traits of the targeted storage reservoir(s) and seal(s), along with other geological features surrounding the site. Mineral characteristics are discussed in terms of the lithology and dominant minerals present in the reservoir(s), seal(s) rocks, and other relevant structural features. Physical traits of these formations are described in terms of permeability, porosity, fractures

and fluid transport behavior. Emphasis is given to the description of the geological seal(s) due to their immediate relevance to CO_2 containment.

A.3.4.1   MINERAL CHARACTERISTICS

Storage reservoir(s)

The Mount Simon is a fine-to-course grain sandstone with some layers interbedded with dark-grey shale laminae(Finley 2005). Based on core descriptions and wireline log analysis, the general lithological description of the Mount Simon storage reservoir can be divided into three zones: upper, middle, and lower(Finley 2005; KunleDare 2005). The upper zone is a thin, very fine-to-medium grained sandstone cemented with hematite with alternating white sandstone horizons(KunleDare 2005; Finley 2005). The middle zone is thicker than the upper unit and is a coarse grained , white, well sorted sandstone with lag pebbles and interbedded mud/clay seams(KunleDare 2005; Finley 2005). The lower zone is a thicker, gray-white, fine to medium grained sandstone with shale partings, dolomite cement, hematite stains, glauconite, pyrite, and siltstone interclasts(KunleDare 2005).

The Mount Simon is quartz arenite to subarkose due to concentration of fine grained feldspars. Its detrial mineralogy is composed of 85 – 90% quartz with less than 15% feldspars(KunleDare 2005). Quartz grains have inclusions of heavy minerals, biotite, microcline and K-feldspars, and hematite and quartz cement(KunleDare 2005).

The Mount Simon is the proposed storage reservoir for 10,000 – 1,000,000 Tons of CO_2 but in the upper segments of the formation, there exists interbedded shales that could hinder CO_2 migration. The shale interbeds can approach 500 feet in thickness in the north. The upper segment is composed of sandstone, siltstone, and shale(Nicholas, Sherrill, and Young 1987; Bond 1972). The interbeds are described as red shales with Illite, quartz, and potassium feldspar being the dominant minerals(Nicholas, Sherrill, and Young 1987)(see Table 1).

Geological Seal(s)

In general Eau Claire is composed of silty, argillaceous dolomitic sandstone or sandy dolomite in northern Illinois and trends to a siltstone or shale in the central part of the Illinois Basin (Figure 9)(Willman et al. 1975; Finley 2005). In the southern part of Basin, the Eau Claire is a mixture of dolomite and limestone with some fine-grained siliciclastic rocks where near the Missouri border it is a relatively pure dolomite(Finley 2005). The regional cross-sections in the central part of Illinois show the Eau Claire to have a persistent shale interval above the Mount Simon sandstone (Figure 10). The siltstone facies contain clay seams and laminae and is commonly interbedded with very dark green to black shale(KunleDare 2005). Literature available on the mineralogy of the Eau Claire show that the formation is dominantly Illite, quartz, and dolomite; with, glauconite or chlorite also being a major component in some reports (see Table 1).

Other geological features

The Ironton sandstone is a relatively poorly sorted, fine- to –coarse grained dolomitic sandstone with the underlying Galesville sandstone being of similar composition but fine grained and well sorted, having better porosity than the Ironton(Finley 2005). The Ironton and Galesville are not present in the southern portion of the Illinois Basin and grade to a non-sandy dolomite above the Eau Claire in the north (Figure 11) (Finley 2005).The dominant minerals within the Galesville formation is quartz with minor amounts of dolomite and calcite (see Table 1). The dolomite present occurs as cement and in discrete bands(KunleDare 2005).

A.3.4.2   PHYSICAL CHARACTERISTICS

Storage reservoir(s)

The paucity of well penetrations into the Mount Simon and Eau Claire in the southern region of the Illinois Basin limits the interpretation accuracy of reports on its permeability and porosity. At Manlove Field and Media field, in Champaign and Henderson Co., the Mount Simon has a porosity average of 11.1% and 13%, respectively, with a range of 13 – 14.5%

over several other well studies(Finley 2005; KunleDare 2005). The Mount Simon, at Manlove Field, has an average geostatistical horizontal permeability range of 0.01 – 300 (average: 29.7 millidarcies (md)) and 0.001 – 150 md vertical permeability(Finley 2005). At Media field in Henderson Co., the Mount Simon has a horizontal permeability average of 110 md with a range over other wells between 91 – 178 md, the vertical permeability averages 60 md with a ranges over other wells between 30 – 104 md(KunleDare 2005). The Mount Simon also has observed quartz filled fractures, microfaulting and reactivation surfaces at the base its upper zone(KunleDare 2005).

There are shaley interbeds of the upper zone of the Mount Simon formation in northern Illinois and they have not been readily correlated across the subsurface of the oil fields and were assessed to represent baffling for the CO_2 injection but not an perform as an effective cap(Finley 2005). However, in the northeastern parts of Illinois these shalely interbeds are hydraulically effectively as a confining unit, along with the predominant shale beds of the Eau Claire in the region, to water movement of the Mount Simon saline aquifer(Mills, Nazimek, and Halford 2002; Nicholas, Sherrill, and Young 1987).

Geological Seal(s)

There are only 25 penetrations of the Eau Claire in southern Illinois so there are relatively few data on the formation to map the changes in lithology at the sequestration site (Section 2, p.32 (Tetra-Tech 2007)). The paucity of well penetrations into the Mount Simon and Eau Claire in the southern region of the Illinois Basin limits the interpretation accuracy of reports on its permeability and porosity. The porosity and permeability of the Eau Claire and Galesville are reported in Table 1. In general, the Eau Claire has low vertical permeability but significant porosity as compared to the Galesville sandstone. This may indicate that the rock may be more prone to chemical attack than physical diffusion of CO_2. The Eau Claire is considered a geological seal throughout Illinois. In the northern parts of Illinois it is further subdivided into the Proviso Siltstone, Lombard Dolomite, and Elmhurst members. The lower Elmhurst member of the Eau Claire acts as hydrological aquifer in

north Illinois (Nicholas, Sherrill, and Young 1987). This may indicate that the subsurface interface between the Mount Simon and the Eau Claire in Macon, Coles, and Fayette County may not be a distinct barrier. The Mount Simon brine may have access to the more dolomitic portions of the formation which might be more porous, based on previous reports. Movement of water around the Eau Claire has been modeled to have input from the waters of the Mount Simon below and from the Ironton-Galesville above range from < 0.25 cm/year (< 0.01 inch/year)(Gupta and Bair 1997). It is estimated that 17% of the water entering the Mount Simon leaks through the Eau Claire geological seal and the remaining 83% moves laterally through the formation(Gupta and Bair 1997).

Other geological features

The Ironton and Galesville Sandstones are reported as one unit because they occur as a single aquifer in the northern Illinois and are hard to distinguish using wireline logs in the subsurface. It is included in the discussion because it overlies the Eau Claire and is a porous, permeable saline reservoir capable of acting as a sink and transport of CO_2 gas. The Ironton – Galesville sandstones are a major source of potable drinking water in the northern regions of Illinois and is six times more conductive of an aquifer than the Mount Simon, where transport of leaked CO_2, and other dissolved species, to potable water is possible over shorter time periods(Nicholas, Sherrill, and Young 1987; Finley 2005).

In the northern regions of Illinois, groundwater flows from west to east; and in the southern region, had been reported (questionably) to flow deeper into the Illinois Basin(Bond 1972). In some areas flow seem to be random but in general the Mount Simon sandstone waters move slow (inches per year). In some areas, groundwater flows upward from the Mount Simon aquifer to the Ironton-Galesville in the Chicago area, where pumpage has lowered pressures in the Ironton-Galesville(Bond 1972).

It is documented that Volatile Organic Compounds (VOCs) and other contaminants were detected in Cambrian-Ordovician age sediments at Superfund sites in northeast Illinois where migration of toxic substances were due to fractures and (or) unused wells that

penetrated the confining units(Mills et al. 2002). Preferential local pathways were created for the VOC movement to sandstone aquifers. This was noted in Galena-Platteville aquifer, a system in the Ordovician sediments above the Ironton-Galesville and Eau Claire formation but below the secondary Maquoketa Shale Group confining unit. This documented migration of contaminants could potentially be useful in that it shows evidence that fractures that pass through geological seals in these Cambrian-Ordovician age sediment are active conduits for limited movement of injected CO_2.

Observations from the Superfund groundwater simulation showed that the greatest percentage of water flow was through the conductive (vuggy) intervals of the matrix and through discrete fractures and bedding-plane partings. This observation validates the notion that matrix composition matters in a caprock/seal where dissolution can create water flow; and nearby fracture and its mineral filling can also create locally preferential pathways for leakage. Another observation was the effects of heterogeneity of hydraulic properties were scale dependant (primarily on a local scale) even though fractures were inclined and networked.

A.3.5 IMPLICATIONS FOR CO2 SEQUESTRATION STORAGE AND LEAKAGE

Carbon capture and storage into geological media has as part of its goal, the need to estimate the risk associated with CO_2 injection. Some have proposed a framework to assess risk through the use of quality factors assigned to various reservoir and seal characteristics like thickness, lithology, and proximity to faults and fracture networks(Oldenburg 2005). This study helps to address some of these factors at the proposed saline demonstration sites in Fayette, Coles, and Macon County, Illinois by focusing on mineral phases susceptible to CO_2 attack that are present in the surrounding structural features and influenced by the hydrogeological behavior of the sediments.

Based on the information reviewed in the previous sections, implications for the permanence of CO_2 storage at this demonstration site can be categorized into the following

topics centered on lithology, structural geology, and reservoir fluid behavior along with oil and gas production history. These topics will be discussed further with an emphasis on soluble minerals present in each of these categories.

In terms of lithology and areal extent, both the Mount Simon and Eau Claire formations are regionally extensive, stretching into other states, such as Kentucky and Indiana, where other Regional Partnerships plan to use the same formations for storage and seal. The lithofacies of the Eau Claire change more significantly throughout the Illinois Basin than the Mount Simon. Even though the Eau Claire is generalized as a dolomite with dolomitic sandstone, siltstone, and shale, it grades from abundant sandstone in north Illinois to siltstone and shale in central Illinois, to dolomite and limestone in southern Illinois(Willman et al. 1975). These generalization of lithologic facies changes in southern Illinois are based on limited available information(Willman et al. 1975; Finley 2005). The shale beds of the Eau Claire and other Cambrian sediments are regionally continuous with thicker units existing in the southern regions of Illinois in the area of fields considered for CO_2 saline sequestration(Finley 2005; Willman et al. 1975). The shales within the upper portions of the Mount Simon should be considered as a potential seal and baffle for CO_2 migration due to capability to perform as an effective hydrological confining unit in northern Illinois.

In terms of the surrounding structural geology in the southern region of Illinois, there exists faults and relatively extensive seismically active zones(McBride 1998). Near the counties of Macon, Coles, and Fayette where demonstration sites are proposed to be established, there may exist high angle reverse thrust faults and fractures, evidenced by high-resolution seismic studies on the bedrock that indicate fractures present in bedrock may extend through the Eau Claire and other Cambrian age sediments; and, may be a source for leakage through secondary porosity in the geologic seal(McBride and Nelson 1999).

There may exist faults and fractures that penetrate the Eau Claire formation, creating fast paths of escape into the overlying Ironton – Galesville aquifer. This aquifer is a major source of potable water in north Illinois where it is six times more transmissive of its waters than the Mount Simon, thereby creating a higher risk for contamination transport despite the presence of the secondary and tertiary seals considered for saline sequestration in the area(Nicholas, Sherrill, and Young 1987).

Also, a history of earthquake events surrounding the structural deformation of the LSA, WVFS, and Precambrian basement, contribute to an elevated risk for fault reactivation, making the folds and faults surrounding the possible demonstration sites dynamic features capable of releasing CO_2 stored in the Mount Simon sandstone(Finley 2005).

Hydraulic properties of the sediments at Superfund sites in northeast Illinois provide inside into how fluid might move in the subsurface in southern Illinois in the Fairfield Basin. It is observed that water flows through vuggy intervals in matrix of Cambrian-Ordovician sediments, within discrete fractures and bedding partings, but being limited in transport thereby remaining localized(Mills et al. 2002). This may not be directly applicable the CO_2 behavior in Mount Simon/Eau Claire subsurface formations, but they provide a relative comparison for subsurface fluid movement.

A substantial history of successful natural gas storage into the Mount Simon has proven the Eau Claire to be an effective seal in central and north Illinois. However, data on leakage rates and performance with mixed gas blends containing CO_2 would have to be reviewed.

In addition to the faults that may have naturally occurred in the Eau Claire seal through tectonic history, there may be potential leakage pathways created in the secondary and tertiary geologic seals through fractures induced during current oil and gas production in the organic rich New Albany Shale and Maquoketa formation. Fractures are induced in the formations through hydraulic stimulation, where horizontal wells are drilled with long, multiple laterals that are tightly spaced (500 – 1,500 feet apart) that are capable of

simultaneously setting of hydraulic fractures sequentially. These techniques, which are extremely effective in increasing oil and gas production rates in the New Albany Shale, run contrary to the principles of storage. The induced fractures by these techniques can be widespread and not all can easily captured by current seismic monitoring methods. It is a point to note that extensive oil and gas exploration/production in potential seals may increase the risk of leakage at a geological sequestration site.

Natural gas storage projects in Illinois have proven that the Galesville is not a suitable for storage and that leakage was sometimes profound(Finley 2005). This is another piece of evidence that raises concern about transport of CO_2 by the Galesville if CO_2 escaped through the Eau Claire by way of faults.

A.3.6   SUMMARY

In examining the literature available for the mineral, physical, and surrounding structural characteristics of the Eau Claire seal used in Illinois, the study showed that their exists the potential for slow localized leakage but fast transport to potable water sources. This is based on several factors: 1.) the successful history of natural gas storage throughout the Illinois Basin in the Mount Simon but no available leakage rates, 2.) the evidence for high-angel reverse faults through the primary seal in Fayette and Coles County, which may or may not be transmissive of fluid, 3.) regional facies changes within the Eau Claire seal across the Illinois Basin, and 4.) possible transport of CO_2 and CO_2-enriched fluids, along with other released compounds, by the Ironton-Galesville sandstone above the primary Eau Claire seal, into potable water sources in northern Illinois, as seen by failed gas storage attempts and hydraulic transmission tests.

The study of the Eau Claire formation, along with other relevant geologic features, across proposed demonstration sites Illinois reveal that quartz, potassium feldspar, dolomite, glauconite, and chlorite are abundant minerals present in the shales that could be susceptible to CO_2 attack. This information can then be used to guide experiments and

240

modeling efforts aimed as understanding the dominant chemistries that could impact leakage and risk assessment.

A.3.7 REFERENCES

Bond, D.C. 1972. Hydrodynamics in deep aquifer of the Illinois Basin. Urbana, Illinois: Illinois State Geological Survey

Buschbach, T.C. 1964. Cambrian and Ordovician strata of northeastern Illinois. In *Report of Investigation*: Illinois Geological Survey.

Buschbach, T.C., and D.C. Bond. 1974. Underground storage of natural gas in Illinois - 1973. In *Illinois Petroleum*: Illinois State Geological Survey.

Finley, Robert. 2005. An Assessment of Geological Carbon Sequestration Options in the Illinois Basin: Illinois State Geological Survey.

———. 2007. Project Fact Sheets: Large Scale Storage Projects, Demonstrating CO2 Storage in the Mount Simon Sandstone of the Illinois Basin. Paper read at Regional Carbon Sequestration Partnerships Annual Review Meeting, 12-13 December at Pittsburgh, PA.

Finley, Robert, and Hannes Leetaru. 2006. Pilot Tests Fact Sheets: CO2 Sequestration in Saline Formations - II, Illinois Basin, MGSC. Paper read at Regional Carbon Sequestration Partnerships Initiative Review Meeting, 3-4 October at Pittsburgh, PA.

Gupta, N., and E.S. Bair. 1997. Variable-density flow in the midcontinental basins and arches region of the United States. *Water Resources Research* 33 (8):1785-1802.

Kolata, D.R. 2005. Bedrock Geology Map of Illinois In *Illinois State Geological Survey*.

Kolata, D.R., and W.J. Nelson. 1991. Tectonic history of the Illinois Basin. In *Interior Cratonic Basins*, edited by M. W. Leighton, D. R. Kolata, D. F. Oltz and J. J. Eidel: American Association of Petroleum Geologists Memoir.

KunleDare, Mojisola Abosede. 2005. Petrographic investigation into the development of secondary porosity in sandstones: A case study of the Cambrian Mount Simon and Galesville Sandstones, Illinois Basin. PhD, Department of Geological Sciences & Engineering, University of Missouri-Rolla, Rolla, Missouri.

McBride, J.H. 1998. Understanding basement tectonics of an interior cratonic basin: southern Illinois Basin, USA. *Tectonophysics* 293:1-20.

McBride, J.H, and W.J Nelson. 1999. Style and origin of Mid-Carboniferous deformation in the Illinois Basin, USA - Ancestral Rockies deformation? *Tectonophysics* 305 (1/3):249-273.

Mills, P.C., J.E. Nazimek, and K.J. Halford. 2002. Hydrogeology and Simulation of Ground-Water Flow in the Aquifers Underlying Belvidere, Illinois. In *Water-Resources Investigations Report*: U.S. Geological Survey.

Mills, P.C., J.E. Nazimek, K.J. Halford, and D.J. Yeskis. 2002. Hydrogeology and Simulation of Ground-Water Flow in the Aquifers Underlying Belvidere, Illinois. Urbana, Illinois: U.S. Geological Survey.

Nelson, W.J. 1995. Structural features in Illinois: Illinois State Geological Survey.

Nicholas, J.R., M.G. Sherrill, and H.L. Young. 1987. Hydrogeology of the Cambrian-Ordovician Aquifer System at a test well in northeastern Illinois. In *Water Resources Investigations Report*. Denver, CO: U.S. Geological Survey.

Oldenburg, Curtis M. 2005. Health, Safety, and Environmental Screening and Ranking Framework for Geologic CO2 Storage Site Selection.: Lawrence Berkeley National Laboratory Paper.

Pacheco, Lawrence. 2008. *FutureGen Alliance Selects Mattoon, Illinois as the Final Site for the First-of-a-kind, Near-Zero Emissions Coal-fueled Power Plant*. FutureGen Alliance, Inc., May, 2008 2007 [cited July 9 2008]. Available from http://www.futuregenalliance.org/news/releases/pr_12-18-07.stm.

Tetra-Tech. 2007. Final Risk Assessment Report for the FutureGen Project Environmental Impact Statement: Tetra Tech, Inc.

Willman, H.B., Elwood Atherton, T.C. Buschback, Charles Collinson, John C. Frye, M.E. Hopkins, Jerry A. Lineback, and Jack A. Simon. 1975. *Handbook of Illinois Stratigraphy*. Urbana, Illinois: Illinois State Geological Survey Bulletin 95.

TABLE A.3.1: Stratigraphic and lithologic description of the Eau Claire and Mount Simon formations with surrounding Cambrian age sediments in Illinois of the greater Illinois Basin.

System	Series	Group	Formation/member	Thickness (ft)		Description
Cambrian	St. Croixan	Knox Group	Eminence dolomite	0 – 200[1]		Dolomites[2]. Light colored[3]. Composed of light gray to brown or pink, sandy, fine-to medium grained dolomite that has thin beds of oolitic chert and sandstone[4].
			Potosi dolomite	0 – 250[1]		Relatively pure dolomites[2,4]. Fine-grained, gray to brown, drusty quartz that fills cavities[3,4]. Consists of finely crystalline, pure to slightly argillaceous, brown to pinkish gray dolomite with some glauconite in top layers and more at base of unit[4].
			Franconia formation	50 – 400[1]		Sandstone, dolomitic, Interbedded dolomite in upper part, siltstone interbedded with -shale, vuggy dolomite with a flat pebble conglomerate zone[2]. Consists of glauconitic, argillaceous sandstone and dolomite with various amounts of red and green shale becoming more abundant in southern Illinois[4].
			Ironton sandstone	0 – 150[4]	50 – 100[1]	Coarse-grained sandstone, dolomitic (very, in upper part) dark shale partings in lower part where in northern Illinois the sandstones become thinner, medium-grained, and poorly sorted with pinkish buff dolomite as cement[2,4]. To the south it grades to a sandy dolomite[4].
			Galesville sandstone		40 – 100 [1]	Clean unfossiliferous sandstone, almost complete absence of dolomite stringers, grading from lateral zones of dolomitic sandstone to nonsandy dolomite to the south[2,4]. In some localities it has silty, fine-grained, moderately well sorted, friable, nondolomitic sandstone with dolomite as cementing material[5].
			Eau Claire formation	500 – 700[6]	300 – 1,000[1,7]	Composed of alternating layers of dolomite, limestone, sandstone, shale and siltstone[7]. In north and western Illinois it is dominantly dolomitic, fine- to medium grained, gray sandstone, with shaly siltstone and silty, sandy, glauconitic, brownish gray dolomite. The Eau Claire in north Illinois it is composed of three members: Proviso siltstone, Lombard Dolomite, and Elmhurst Sandstone, from youngest to oldest respectively. Dolomite, glauconitic sandstone,, sandy dolomite with gray to red shales, characterize these members[4]. In central and eastern Illinois it is dominantly dolomitic, orange to pink gray siltstone with green, gray or red shale and glauconitic, partly oolitic limestone and dolomite[4]. In southern Illinois it is dominantly fine-grained, gray dolomite or limestone but includes beds of siltstone, shale, and sandstone where basal "sooty" zone has sand grains coated with pyritic black powder[4].

			Mount Simon sandstone	$1,300^{7,8}$	$500 – 3,000^{1}$	Consists of fine –to coarse grained, partly pebbly, friable sandstone, with sandstone varying in color from white to red.[4]. The basal zone is strongly arkosic with bed partings of red and green micaceous shale (up to 15 ft thick) in upper 200-300 ft and lower 600 ft of formation[2,4]. Also described as a composition of stacked clean sandstone units capped with thin interbeds of fine sandstone, siltstone, and shale[7]. In northeast Illinois, the upper 140ft of sandstone is part of Elmhurst-Mount Simon aquifer, below are interbedded with red shale for 500ft with the lower 1,185 ft of the Mount Simon being porous and with brine[9].
			Precambrian Middle Proterozoic			Medium to coarse grained granite and ryholite[1]

☐ -   Shaded unit represents seal rock

1.) Kolata (2005)
2.) KunleDare (2005)
3.) Mills et al. (2002)
4.) Willman et al (1975)
5.) Buschbach (1964)
6.) Tetra Tech Inc. (2007)
7.) Finley (2005)
8.) Finley and Leetaru (2006)
9.) Nicholas, Sherrill, and Young (1987)

TABLE A.3.2: Physical and mineral characteristics of the Eau Claire and Galesville formations, along with the shale interbeds of the Mt. Simon.

Characteristic	Reported Values				Comments
	Mt. Simon Shale Interbeds	Eau Claire	Galesville		
Physical Properties					
Location*	Champaign County, IL	Henderson County, IL	Putnam County, IL	Henderson County, IL	
Depth (ft)	4,128 – 4,1865.5[1]	2,235 – 2,519[2]	2,833 – 2,851[1]	2,120 – 2,235[2]	Depth from which samples were analyzed for mineral components
Porosity (%)	-	0.4 – 15.4 (av. 7.7)[2]	-	19.2 (av. 17.2)[2]	Sub surface Galesville formation average (av.) porosity taken from several well locations in Illinois, Appendix D[2]
Vertical Permeability (md)	-	0.000001 – 0.485[b] (av. 0.001144[b])[2]	-	509[a] (av. 354[a]) 0.496[b2]	Sub surface Galesville formation average (av.) permeability taken from several well locations in Illinois, Appendix D[2]
Horizontal Permeability (md)	-	-	-	667[a] (av. 448[a])[2]	Sub surface Galesville formation average (av.) permeability taken from several well locations in Illinois, Appendix D[2]
Horizontal Hydraulic Conductivity (ft/day)	1.5 – 3.8[3] 1.3 – 1.5[4]	1.5 – 3.8[3] 1.3 – 1.5[4]	1.3 – 1.5[4]	10.0 – 13.6[3]	Galesville-Ironton sandstone and Eau Claire values from a 1,143 – 1,932 ft interval of 3,475 ft deep well in northeast, Illinois (Lake County)[4]. For Eau Claire the lower Elmhurst member and the shale interbeds of Mt. Simon yielded values[4]. Estimates from discrete-interval drawdown tests in Rockford and Chicago, Illinois[3].
Hydraulic Transmissivity (ft²/day)	-	200 – 840[4] 1,900[3]	200 – 840[4] 1,900[3]	1,100[4] 1,750[3]	Galesville-Ironton sandstone and Eau Claire values from a 1,143 – 1,932 ft interval of a 3,475 ft deep well in northeast, Illinois (Lake County)[4]. For Eau Claire the lower Elmhurst member and the shale interbeds of Mt. Simon yielded values[4]. Derived from geometric mean of estimated horizontal conductivity tests in Rockford, IL and Chicago, IL[3]
Area extent (mi²)	57,918	57,918	57,918	57,918	Limit discussion to state of Illinois
Major Mineral Components (> 20 wt%)					
Quartz	17.89 – 23.99%[1]	> 20%[2]	10.30 – 33%[1]	92.03 – 98.20%	Qualitative and Quantitative (%vol)

245

				(av. 95%)[2]	values from whole rock XRD analysis[1,2]. Point count data from Galesville[2].
K-feldspar	19.23 – 20.21%[1]	-	20.27 – 37.31%[1]	-	Qualitative and Quantitative (%vol) values from whole rock XRD analysis[1,2]
Dolomite	-	> 20%[2]	3.58 – 26.33%	-	Qualitative and Quantitative (%vol) values from whole rock XRD analysis[1,2]
Illite	35.92 – 41.30% (82.23 – 82.85%)[1]	> 20%[2]	5.49 – 51.36% (57 – 90.69%)[1]	-	Qualitative based on XRD bulk clay analysis of shale layers[2]. Quantitative (%vol) values from whole rock XRD analysis with clay size vol% in (_)[1]
Glauconite	-	> 20%[2]	-	-	Qualitative based on XRD scan of bulk clay analysis of shale layers[2]
Chlorite	-	-	0.46 – 3.40% (6.43 – 38.88%)[1]	-	Quantitative (%vol) values from whole rock XRD analysis with *clay size* vol% in (_)[1]
Minor Mineral Components (< 20 wt%)					
Quartz	-	-	-	0 – 13.30%[2]	Point count data from whole rock analysis, representing chert, rock fragments, and overgrowths[2]
K-feldspar	-	< 20%[2]	-	0.70 – 5.97%[2]	Qualitative from whole rock XRD analysis for Eau Claire. Point count data for Galesville[2]
Plagioclase	1.18 – 2.51%[1]	-	0.82 – 3.28%[1]	-	Quantitative (%vol) values from whole rock XRD analysis[1]
Calcite	0.74 – 2.41%[1]	-	0.72 – 1.97%[1]	< 20%[2]	Quantitative (%vol) values from whole rock XRD analysis[1]. Qualitative from petrographic analysis, calcite embays dolomite[2]
Dolomite	1.19 – 3.37%[1]	-	-	< 20%[2]	Qualitative from petrographic analysis, dolomite is cement and void filling[2]
Hornblende	0.38 – 0.48%[1]	-	0.22 – 0.44%[1]	-	Quantitative (%vol) values from whole rock XRD analysis[1]
Pyrite	0.14 – 0.45%[1]	-	0 – 1.71%[1]	-	Quantitative (%vol) values from whole rock XRD analysis[1]
Marcasite	0.08 – 0.47%[1]	-	0.59 – 3.16%[1]	-	Quantitative (%vol) values from whole rock XRD analysis[1]
Expandable clays	0.96 – 1.43% (1.10 – 1.61%)[1]	-	0.30 – 3.18% (1.11 – 2.61%)[1]	-	Quantitative (%vol) values from whole rock XRD analysis with clay size vol% in (_)[1]
Kaolinite	4.95 – 7.39% (10.05 – 10.36%)[1]	< 20%[2]	0.25 – 1.46% (1.45 – 3.01%)[1]	-	Qualitative based on XRD bulk clay analysis of shale layers[2]. Quantitative (%vol) values from whole

					rock XRD analysis with clay size vol% in (_)[1]
Chlorite	1.98 – 4.09% (5.18 – 6.61%)[1]	< 20%[2]	-	< 20% [2]	Qualitative based on XRD bulk clay analysis of shale layers in Eau Claire and pore filing, grain rim with patches in petrographic analysis of Galesville [2]. Quantitative (%vol) values from whole rock XRD analysis with clay size vol% in (_)[1]
Zircon	-	-	-	< 20% [2]	Qualitative from petrographic analysis[2]
Glauconite	-	-	-	< 20%[2]	Qualitative from petrographic analysis near top of unit[2]
Organic Content					
Total Organic Carbon (TOC)	?	?	?	?	Information on organic content not readily retrieved
Total Inorganic Carbon (TIC)	?	?	?	?	Information on organic content not readily retrieved

[a]**Permeablity in gas**
[b]**Permeability in water**
*Characteristic values taken from location unless otherwise stated in comments

1.) Finley (2005)
2.) KunleDare (2005)
3.) Mills et al. (2002)
4.) Nicholas, Sherrill, and Young (1987)
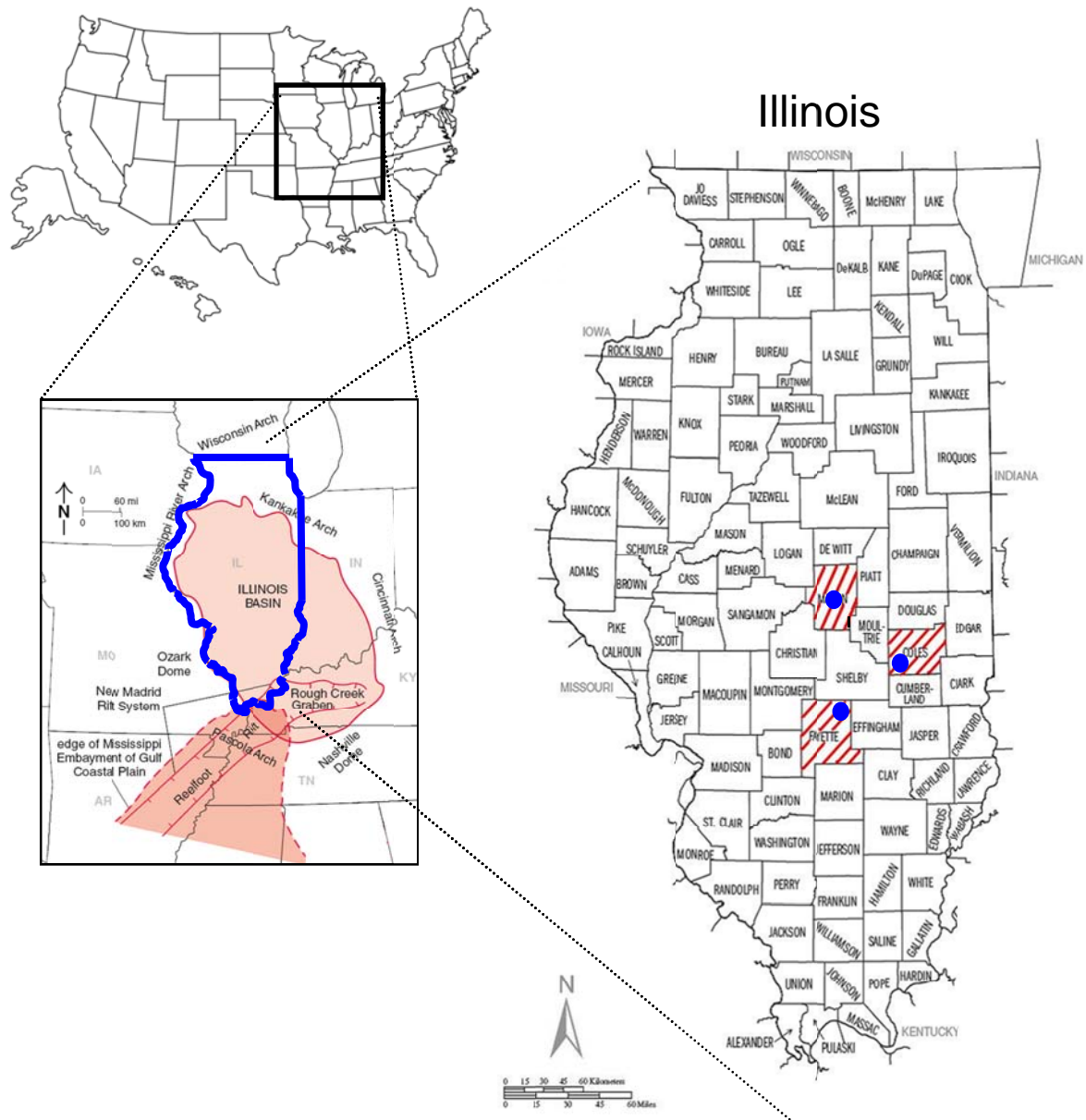
FIGURE A.3.1:   Regional map showing the major tectonic features surrounding the Illinois Basin and the locations of proposed demonstration sites for CO2 saline sequestration. Louden field (Fayette County), Matton field (Coles County), and Decatur (Macon County) have striped counties with field locations approximated with (blue) dots. Modified from U.S. Census 2000 map and on unpublished work of Kolata (Finley 2005).
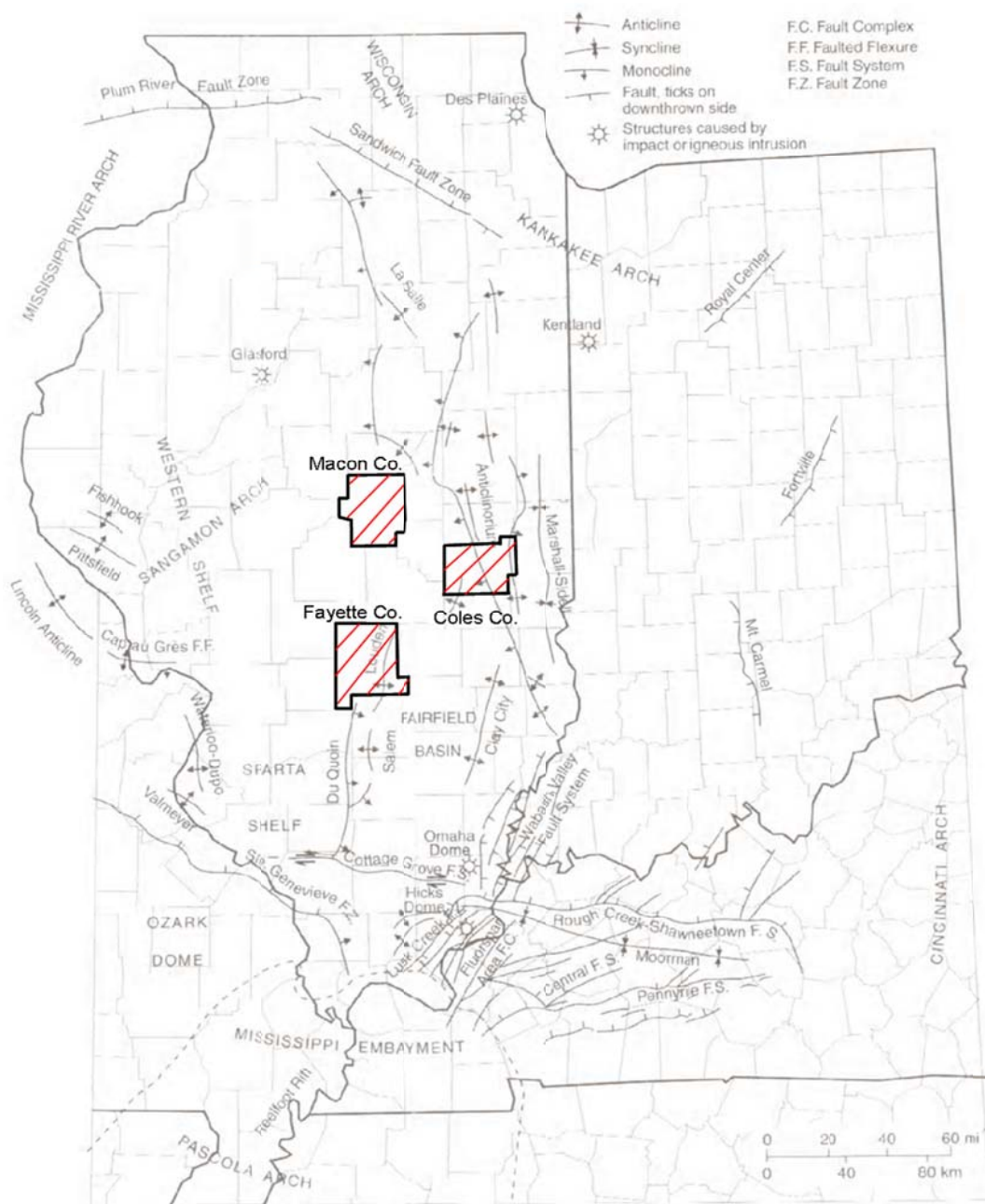
FIGURE A.3.2:   Regional map showing major structural features in the Illinois Basin. Striped boxes represent counties considered for demonstration of CO_2 saline sequestration. Modified from (Nelson 1995) in (Kolata 2005)
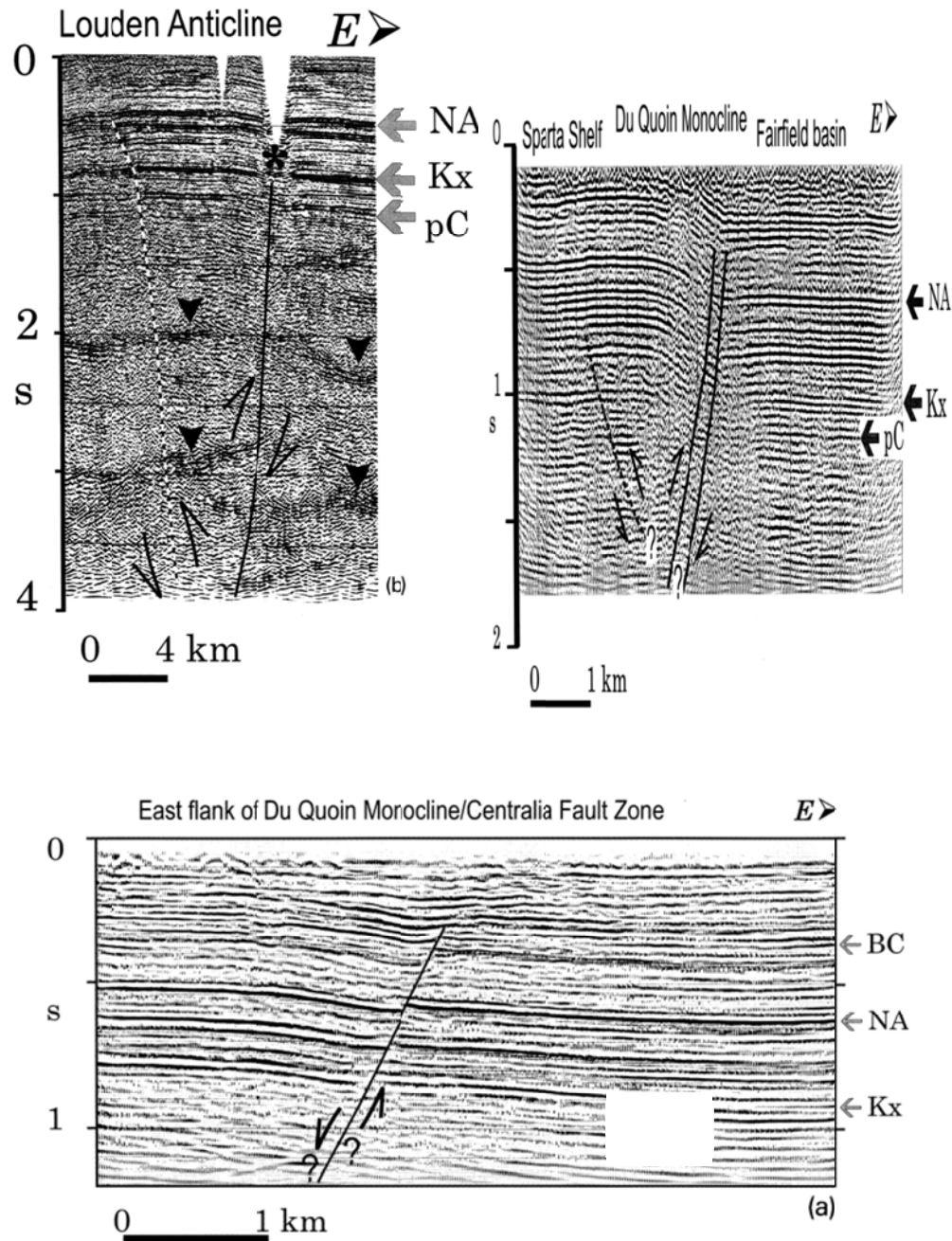
FIGURE A.3.3: Vertically exaggerate high-resolution migrated seismic profile of the southern end of (a) Louden Anticline, (b) Du Quoin Monocline, and (c) Centralia Fault Zone within the Fairfield Basin. Black lines show interpreted dominant faults associated with overall vergence direction; dashed line represents interpreted subordinate faults; asterisk represent position of forward hinge point on folded Paleozoic reflector. Kx = base of Knox Supergroup, pC = base of Precambrian, NA = base of New Albany Shale, BC = Beech Creek reflector (McBride and Nelson 1999).
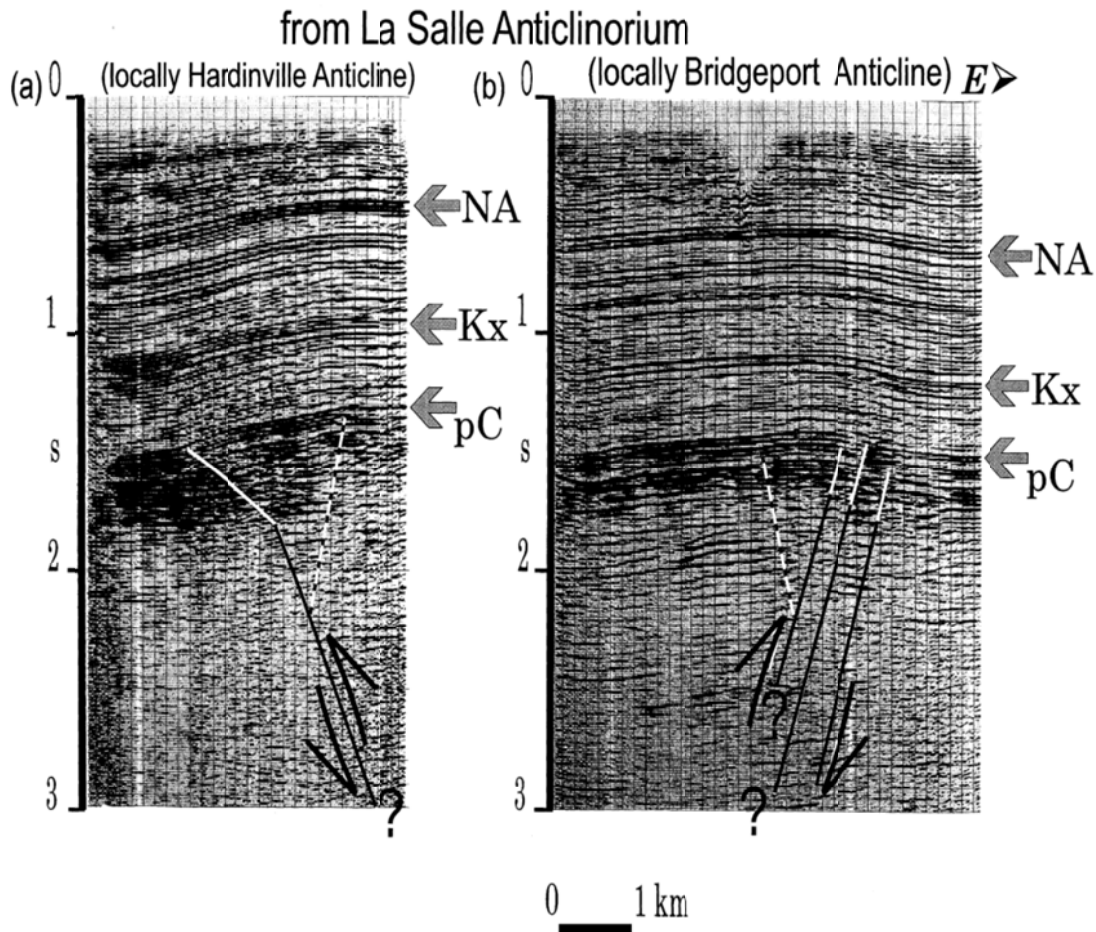
FIGURE A.3.4:   High-resolution migrated seismic profile showing interpreted faulting in the La Salle Anticlinorium that extend below and through the Cambrian strata. Dominant faults shown as solid black or dashed lines. White lines are added for clarity. NA = approx. boundary for New Albany shale, Kx = approx. boundary for Knox formation group, pC = approx. Precambrian basement boundary (McBride and Nelson 1999).
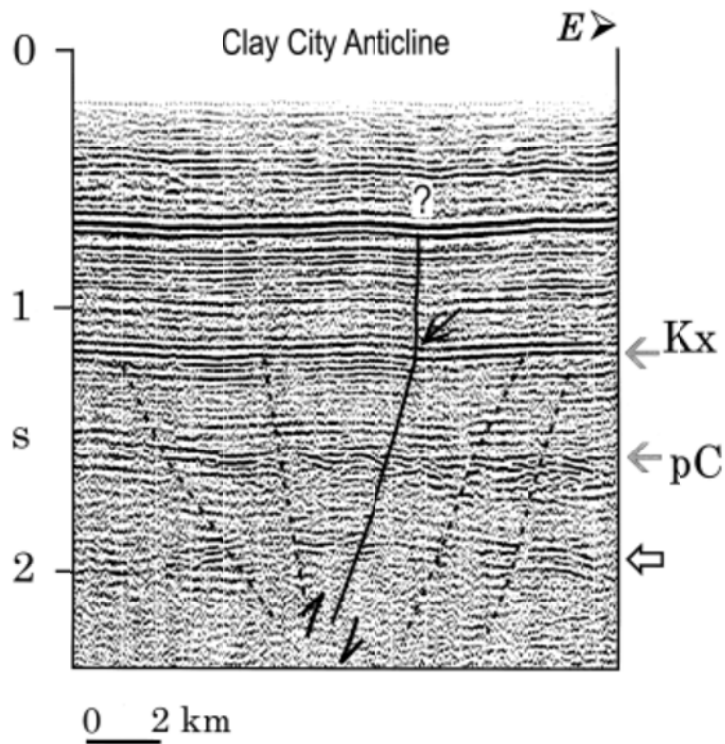
FIGURE A.3.5:   High-resolution migrated seismic profile of interpreted faulting within the Clay City Anticline. Kx = approx. boundary for Knox formation group, pC = approx. Precambrian basement boundary (McBride and Nelson 1999).
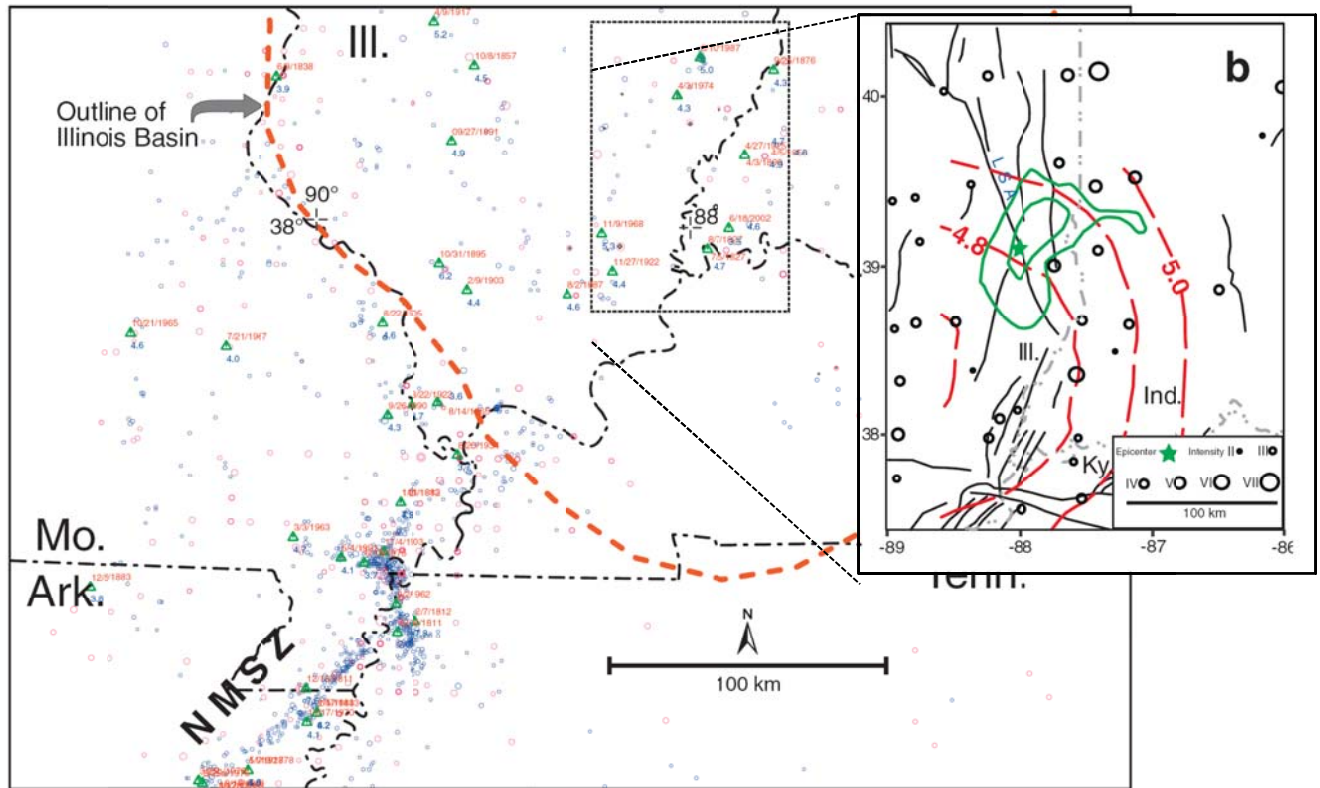
FIGURE A.3.6: Distribution of earthquakes surrounding the southern region of the Illinois Basin through 2004, with magnitudes and epicenters in the New Madrid seismic zone and southern Illinois. Sources: green triangles = Bakun and Hopper (2004), red circles = Nuttli and Brill (1981), blue circles = Center for Earthquake Research and Information, 1974-2004. Relative magnitudes of earthquakes in inset picture are given by size of circles. Image taken from (Finley 2005)
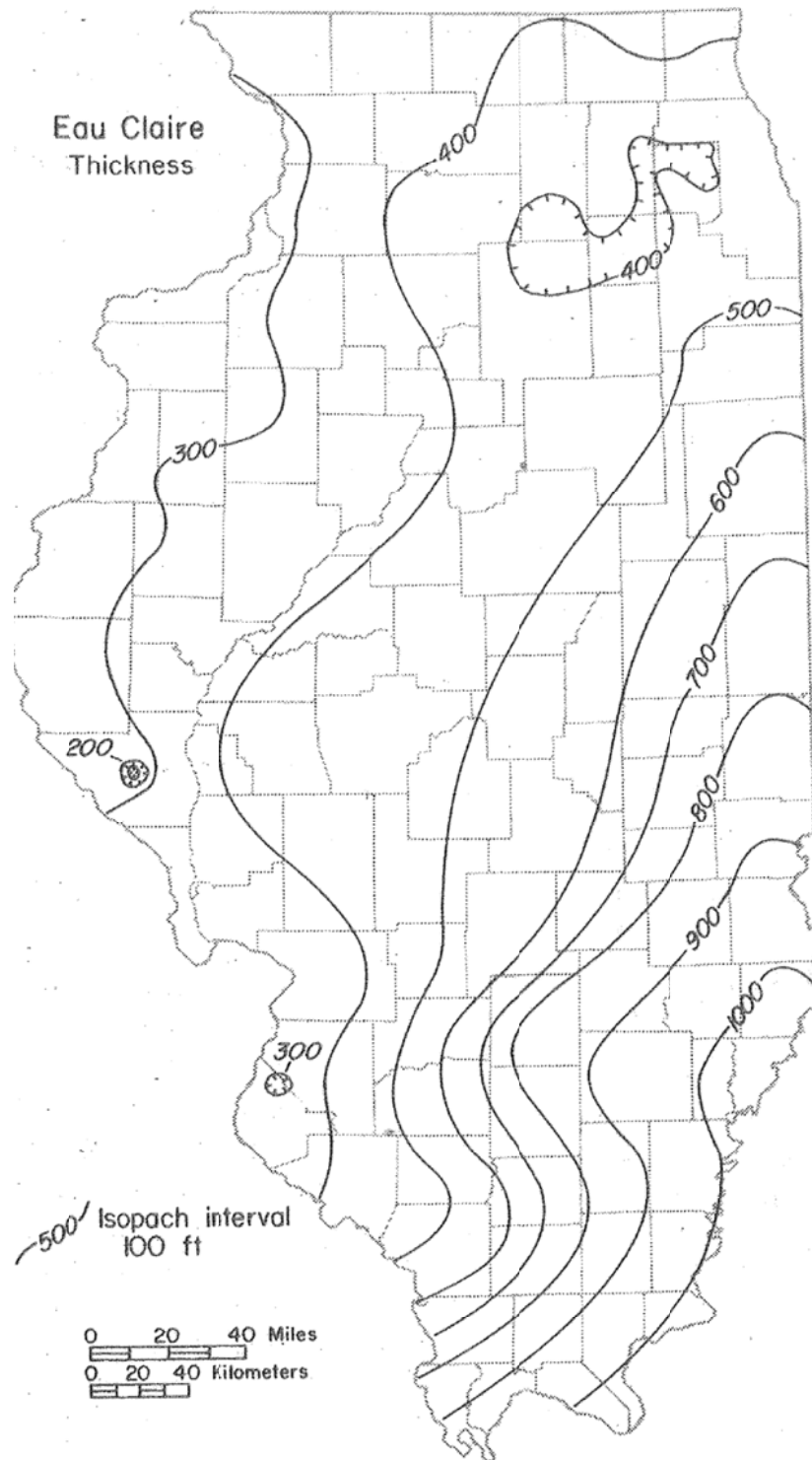
FIGURE A.3.7: Eau Claire thickness isopach throughout Illinois (Willman et al. 1975)

FIGURE A.3.8: Facies change in the Eau Claire formation throughout Illinois (Willman et al. 1975).
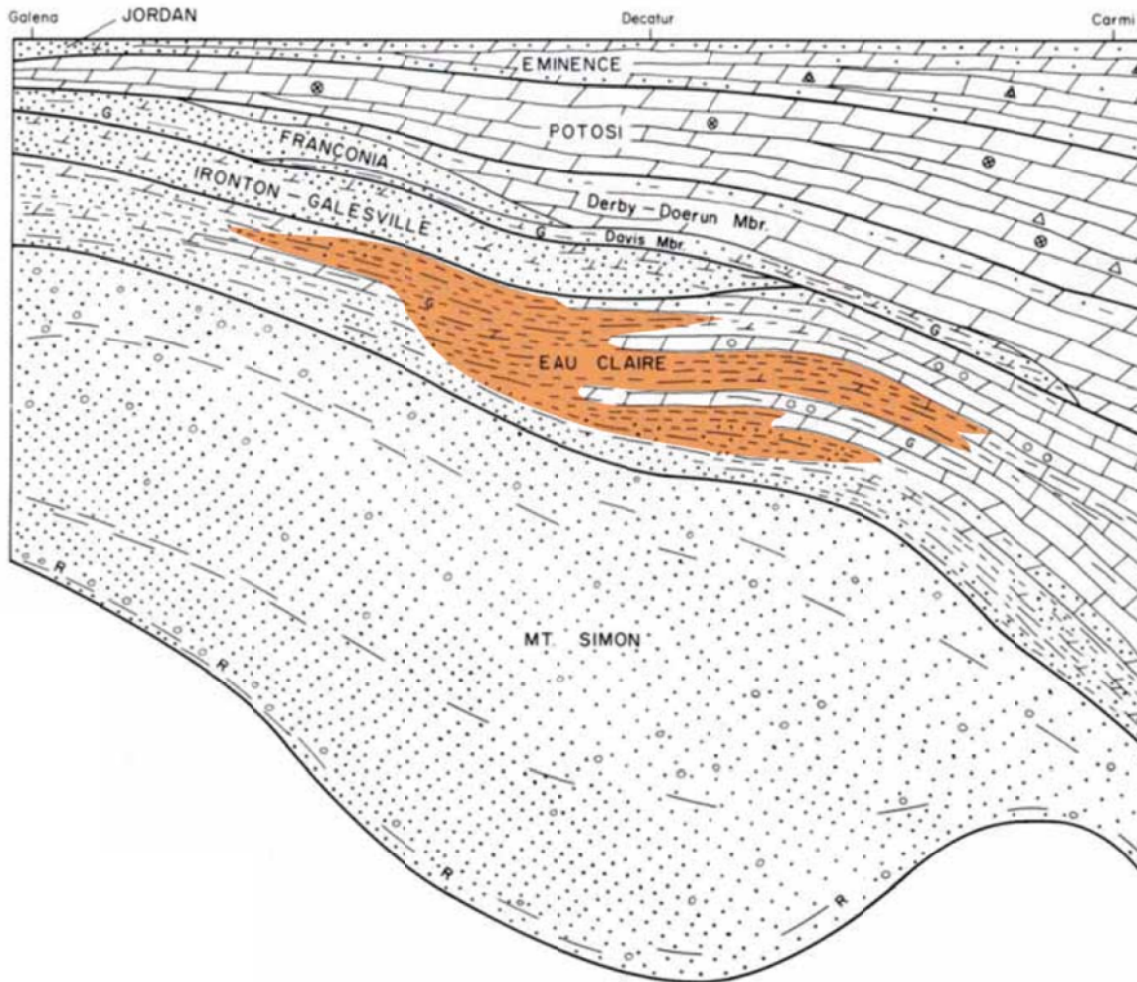
FIGURE A.3.9:   Diagrammatic cross section of the Cambrian System from northwest to southeast Illinois. Orange color depicts areas where Eau Claire if primarily shale and should be a good seal. Uncolored portions of the Eau Claire represent areas that have higher leakage risk due to fracturing. Modified after (Willman et al. 1975) in (Finley 2005).
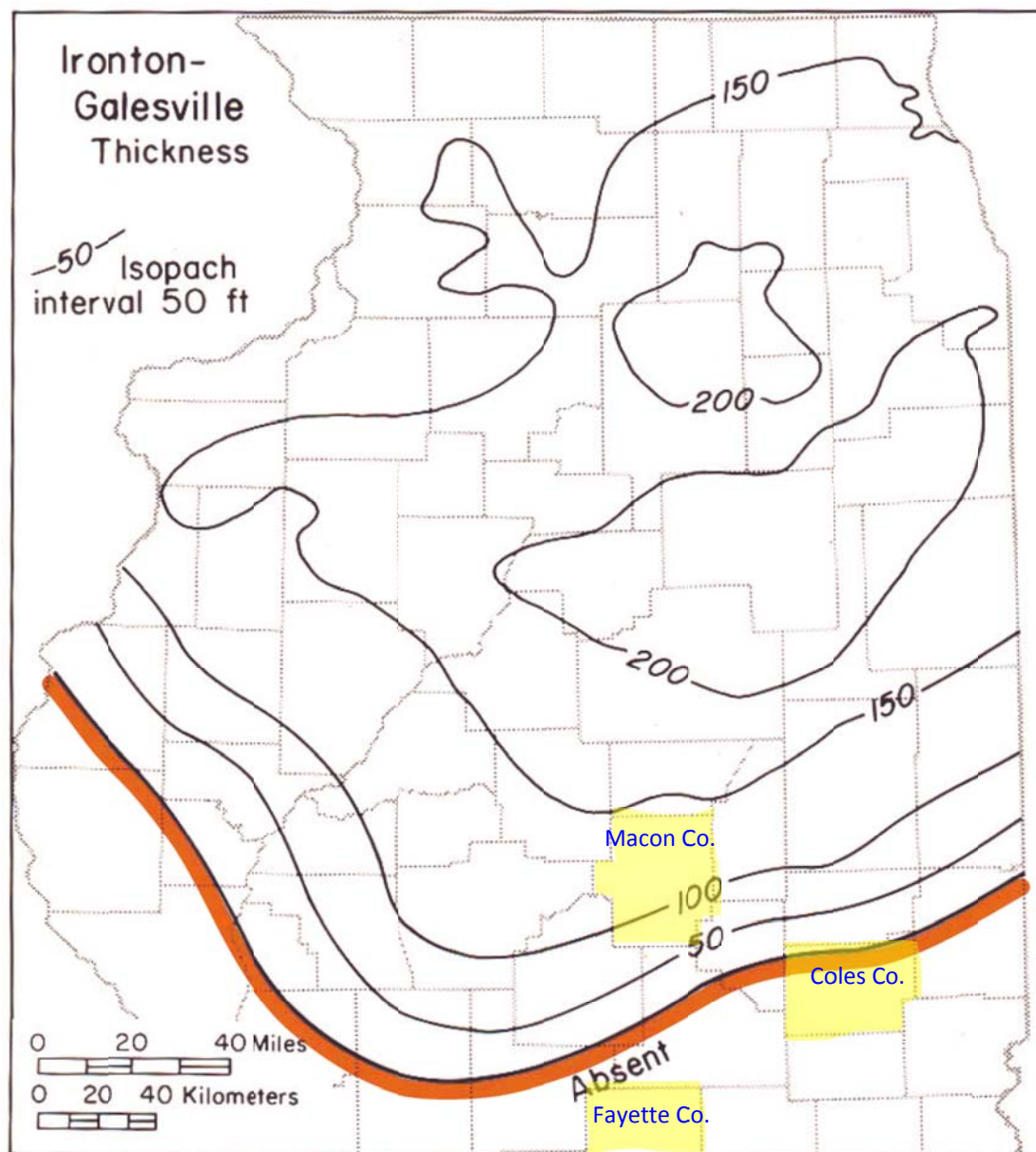
FIGURE A.3.10: Isopach of the Ironton-Galesville sandstone above the Eau Claire in northern Illinois. The orange line signifies the limit of the sandstone facies. Yellow shaded areas represent counties considered for CO_2 injection into saline formation. Modified from (Willman et al. 1975).

APPENDIX A4

SELECTED REPRODUCED DATA FOR THE EAU CLAIRE AND TUSCALOOSA MARINE SHALE HYDRAULIC PERMEABILITY

TABLE A.4.1: Selected well data reproduced from KunleDare (2005) for the Eau Claire vertical hydraulic permeability in Illinois.

No.	Direction	Formation	Location	Depth (ft)	Porosity	**Permeablity, k_v (mD)	k, m^2	Lnk
1	Vertical	Eau Claire	Henderson County	2400	8.2	0.005	4.93E-18	-39.850
2	Vertical	Eau Claire	Henderson County	2401	10.8	0.006	5.92E-18	-39.668
3	Vertical	Eau Claire	Henderson County	2402	8.8	0.003	2.96E-18	-40.361
4	Vertical	Eau Claire	Henderson County	2403	6.8	0.005	4.93E-18	-39.850
5	Vertical	Eau Claire	Henderson County	2404	7.6	0.002	1.97E-18	-40.767
6	Vertical	Eau Claire	Henderson County	2405	11.8	0.1	9.87E-17	-36.855
7	Vertical	Eau Claire	Henderson County	2406	9.8	0	-	
8	Vertical	Eau Claire	Henderson County	2407	8.9	0.007	6.91E-18	-39.514
9	Vertical	Eau Claire	Henderson County	2408	11.8	0.003	2.96E-18	-40.361
10	Vertical	Eau Claire	Henderson County	2409	13.6	0.003	2.96E-18	-40.361
11	Vertical	Eau Claire	Henderson County	2410	10.2	0.000821	8.10E-19	-41.657
12	Vertical	Eau Claire	Henderson County	2411	11	0	-	
13	Vertical	Eau Claire	Henderson County	2412	11.5	0	-	
14	Vertical	Eau Claire	Henderson County	2413	15.4	0.093	9.18E-17	-36.927
15	Vertical	Eau Claire	Henderson County	2414	6.3	0.125	1.23E-16	-36.631
16	Vertical	Eau Claire	Henderson County	2415	8.9	0.004	3.95E-18	-40.073
17	Vertical	Eau Claire	Henderson County	2416	7.8	0	-	
18	Vertical	Eau Claire	Henderson County	2417	11.3	0.005	4.93E-18	-39.850
19	Vertical	Eau Claire	Henderson County	2418	10.1	0	-	
20	Vertical	Eau Claire	Henderson County	2419	5.9	0	-	
21	Vertical	Eau Claire	Henderson County	2420	6	0.00213	2.10E-18	-40.704
22	Vertical	Eau Claire	Henderson County	2421	8.6	0.002	1.97E-18	-40.767
23	Vertical	Eau Claire	Henderson County	2422	8.4	0	-	
24	Vertical	Eau Claire	Henderson County	2423	12.9	0.002	1.97E-18	-40.767
25	Vertical	Eau Claire	Henderson County	2424	13	0.003	2.96E-18	-40.361
26	Vertical	Eau Claire	Henderson County	2425	13.4	0	-	
27	Vertical	Eau Claire	Henderson County	2426	5	0	-	
28	Vertical	Eau Claire	Henderson County	2427	10.3	0.048	4.74E-17	-37.588
29	Vertical	Eau Claire	Henderson County	2428	9.5	0.485	4.79E-16	-35.276
30	Vertical	Eau Claire	Henderson County	2429	11.3	0.015	1.48E-17	-38.752
31	Vertical	Eau Claire	Henderson County	2430	9.1	0.000643	6.35E-19	-41.901
32	Vertical	Eau Claire	Henderson County	2431	9	0.007	6.91E-18	-39.514
33	Vertical	Eau Claire	Henderson County	2432	4.9	0	-	
34	Vertical	Eau Claire	Henderson County	2433	7	0	-	
35	Vertical	Eau Claire	Henderson County	2434	6.5	0	-	
36	Vertical	Eau Claire	Henderson County	2435	10.4	0	-	
37	Vertical	Eau Claire	Henderson County	2436	4	0	-	
38	Vertical	Eau Claire	Henderson County	2437	7.9	0	-	
39	Vertical	Eau Claire	Henderson County	2438	4.8	0	-	
40	Vertical	Eau Claire	Henderson County	2439	1.5	0	-	
41	Vertical	Eau Claire	Henderson County	2440	4.3	0.000037	3.65E-20	-44.757

42	Vertical	Eau Claire	Henderson County	2441	8.7	0	-	
43	Vertical	Eau Claire	Henderson County	2442	7.6	0.001	9.87E-19	-41.460
44	Vertical	Eau Claire	Henderson County	2443	7	0.002	1.97E-18	-40.767
45	Vertical	Eau Claire	Henderson County	2444	7.4	0	-	
46	Vertical	Eau Claire	Henderson County	2445	7	0.002	1.97E-18	-40.767
47	Vertical	Eau Claire	Henderson County	2446	8.6	0.004	3.95E-18	-40.073
48	Vertical	Eau Claire	Henderson County	2447	5.2	0	-	
49	Vertical	Eau Claire	Henderson County	2448	7.1	0	-	
50	Vertical	Eau Claire	Henderson County	2449	8.6	0	-	
51	Vertical	Eau Claire	Henderson County	2450	4.2	0.00137	1.35E-18	-41.145
52	Vertical	Eau Claire	Henderson County	2451	7.5	0	-	
53	Vertical	Eau Claire	Henderson County	2452	4.5	0	-	
54	Vertical	Eau Claire	Henderson County	2453	9	0	-	
55	Vertical	Eau Claire	Henderson County	2454	6.3	0	-	
56	Vertical	Eau Claire	Henderson County	2455	7.3	0	-	
57	Vertical	Eau Claire	Henderson County	2456	7.8	0	-	
58	Vertical	Eau Claire	Henderson County	2457	6.6	0	-	
59	Vertical	Eau Claire	Henderson County	2458	7.8	0.002	1.97E-18	-40.767
60	Vertical	Eau Claire	Henderson County	2459	11.1	0	-	
61	Vertical	Eau Claire	Henderson County	2460	6.8	0.000837	8.26E-19	-41.638
62	Vertical	Eau Claire	Henderson County	2461	4.9	0	-	
63	Vertical	Eau Claire	Henderson County	2462	7.3	0	-	
64	Vertical	Eau Claire	Henderson County	2463	6.7	0	-	
65	Vertical	Eau Claire	Henderson County	2464	6.5	0	-	
66	Vertical	Eau Claire	Henderson County	2465	4.8	0.104	1.03E-16	-36.815
67	Vertical	Eau Claire	Henderson County	2466	9.5	0	-	
68	Vertical	Eau Claire	Henderson County	2467	1.4	0	-	
69	Vertical	Eau Claire	Henderson County	2468	8.1	0.008	7.90E-18	-39.380
70	Vertical	Eau Claire	Henderson County	2469	7.8	0.00402	3.97E-18	-40.068
71	Vertical	Eau Claire	Henderson County	2470	6.8	0.019	1.88E-17	-38.515
72	Vertical	Eau Claire	Henderson County	2471	5.5	0	-	
73	Vertical	Eau Claire	Henderson County	2472	8.4	0	-	
74	Vertical	Eau Claire	Henderson County	2473	3.1	0.305	3.01E-16	-35.739
75	Vertical	Eau Claire	Henderson County	2474	9.7	0	-	
76	Vertical	Eau Claire	Henderson County	2475	7.9	0	-	
77	Vertical	Eau Claire	Henderson County	2476	11.9	0	-	
78	Vertical	Eau Claire	Henderson County	2477	11.5	0	-	
79	Vertical	Eau Claire	Henderson County	2478	12.6	0	-	
80	Vertical	Eau Claire	Henderson County	2479	6.3	0.00042	4.15E-19	-42.327
81	Vertical	Eau Claire	Henderson County	2480	5.3	0	-	
82	Vertical	Eau Claire	Henderson County	2481	6.6	0	-	
83	Vertical	Eau Claire	Henderson County	2482	6.3	0	-	
84	Vertical	Eau Claire	Henderson County	2483	6.7	0	-	
85	Vertical	Eau Claire	Henderson County	2484	8.6	0	-	
86	Vertical	Eau Claire	Henderson County	2485	0.4	0	-	
87	Vertical	Eau Claire	Henderson County	2486	6.4	0	-	
88	Vertical	Eau Claire	Henderson County	2487	8	0	-	

89	Vertical	Eau Claire	Henderson County	2488	3.9	0	-	
90	Vertical	Eau Claire	Henderson County	2489	2	0	-	
91	Vertical	Eau Claire	Henderson County	2490	3.3	0	-	
92	Vertical	Eau Claire	Henderson County	2491	4.6	0	-	
93	Vertical	Eau Claire	Henderson County	2492	6.6	0	-	
94	Vertical	Eau Claire	Henderson County	2493	12.3	0	-	
95	Vertical	Eau Claire	Henderson County	2494	5.2	0	-	
96	Vertical	Eau Claire	Henderson County	2495	7.2	0	-	
97	Vertical	Eau Claire	Henderson County	2496	10.2	0	-	
98	Vertical	Eau Claire	Henderson County	2497	7.7	0	-	
99	Vertical	Eau Claire	Henderson County	2498	7.9	0	-	
100	Vertical	Eau Claire	Henderson County	2499	7.2	0	-	
101	Vertical	Eau Claire	Henderson County	2500	8.2	0	-	
102	Vertical	Eau Claire	Henderson County	2501	12.7	0	-	
103	Vertical	Eau Claire	Henderson County	2502	2.1	0	-	
104	Vertical	Eau Claire	Henderson County	2503	12.8	0	-	
105	Vertical	Eau Claire	Henderson County	2504	5.4	0	-	
106	Vertical	Eau Claire	Henderson County	2505	7	0	-	
107	Vertical	Eau Claire	Henderson County	2506	7.5	0	-	
108	Vertical	Eau Claire	Henderson County	2507	5.5	0	-	
109	Vertical	Eau Claire	Henderson County	2508	5.3	0	-	
110	Vertical	Eau Claire	Henderson County	2509	6.9	0	-	
111	Vertical	Eau Claire	Henderson County	2510	5.4	0	-	
112	Vertical	Eau Claire	Henderson County	2511	6.6	0	-	
113	Vertical	Eau Claire	Henderson County	2512	9.8	0	-	
114	Vertical	Eau Claire	Henderson County	2513	8.7	0	-	
115	Vertical	Eau Claire	Henderson County	2514	3.3	0	-	
116	Vertical	Eau Claire	Henderson County	2515	4.5	0	-	
117	Vertical	Eau Claire	Henderson County	2516	9.2	0	-	
118	Vertical	Eau Claire	Henderson County	2517	11.9	0	-	
119	Vertical	Eau Claire	Henderson County	2518	9.2	0	-	
				No. of samples :	119	119	37	37
				Max :	15.4	0.485	4.79E-16	-35.276
				Min :	0.4	0.001	3.65E-20	-44.757
				Average:	7.73	1.16E-02	3.68E-17	-39.799
				Std Dev. :	2.851	0.055	9.379E-17	1.940

**zero mD = "0.001-" reported in KunleDare (2005)

Note : 1 Darcy = 9.87 x 10^{-13} m^2

TABLE A.4.2: Selected well data reproduced from Visocky et al. (1985) for the Eau Claire horizontal hydraulic permeability in Illinois.

No.	Formation	Location	Depth (m)	*Est. Thickness (m)	*Thickness uncert., ± (m)	Transmissivity (m^2/s)**	$-\ln(k_h)m^2$	Ln(k$_h$) uncert., ± (m^2)
1	Eau Claire	Rock Island County 20N2E-18.1h	549	91	15	-	-	-
2	Eau Claire	Cook County 37N14E-27.6g	517	122	15	-	-	-
3	Eau Claire	Ford County 24N7E-19.4c	1,295	168	8	-	-	-
4	Eau Claire	LaSalle County 33N1E-8.2f	842	137	15	2.52E-03	26.929	0.012
5	Eau Claire	Knox County 11N1E-14.7e	747	91	8	8.92E-03	25.258	0.007
6	*Eau Claire*	*Henry County 15N5E-33.5h4*	741	91	8	2.99E-04	28.653	0.007
7	Eau Claire	Henry County 15N5E-33.5h4	741	91	8	2.98E-03	26.353	0.007
8	Eau Claire	Whiteside County 21N5E-18.8c1	616	91	30	2.12E-03	26.697	0.111
9	Eau Claire	Cook County 35N13E-1.1d	538	122	15	2.21E-03	26.942	0.016
10	Eau Claire	Will County 36N11E-31.8b	506	152	15	1.51E-03	27.545	0.010
11	Eau Claire	Will County 33N9E-12-1g	501	152	15	3.70E-03	26.650	0.010
12	Eau Claire	Cook County 39N13E-21.6g	498	122	15	1.49E-03	27.336	0.016
13	Eau Claire	Will County 36N10E-21.4a	491	152	15	3.81E-04	28.922	0.010
14	Eau Claire	Cook County 37N12E-2.8h2	491	122	15	1.04E-03	27.699	0.016
15	Eau Claire	Will County 35N10E-14.6h	490	152	15	2.46E-03	27.057	0.010
16	Eau Claire	Whiteside County 21N7E-28.2h	484	91	30	8.48E-04	27.610	0.111
17	Eau Claire	Grundy County 32N6E-29.4e	471	122	15	2.09E-03	26.999	0.016
18	Eau Claire	Lake County 45N11E-14-5a	462	122	8	-	-	-
19	Eau Claire	Will County 35N10E-30.1e	460	152	15	9.78E-04	27.979	0.010
20	Eau Claire	Grundy County 33N7E-9.3h	458	122	15	1.51E-03	27.322	0.016
21	Eau Claire	Lake County 46N12E-8.1d	457	122	8	-	-	-
22	Eau Claire	Grundy County 33N7E-4.4c	446	122	15	2.44E-03	26.840	0.016
23	*Eau Claire*	*Grundy County 33N7E-4.4c*	446	122	15	3.09E-03	26.605	0.016
24	Eau Claire	Kane County 38N8E-8.3e	445	122	8	-	-	-
25	*Eau Claire*	*DuPage County 40N11E-13.8e*	440	122	8	3.11E-03	26.600	0.004
26	Eau Claire	DuPage County 40N11E-13.8e	440	122	8	3.31E-03	26.537	0.004
27	Eau Claire	Knox County 43N10E-14.7d	427	91	8	2.79E-03	26.419	0.007
28	Eau Claire	Kendall County 37N7R-28.8b	425	122	4	1.15E-03	27.594	0.001
29	Eau Claire	LaSalle County 36N1E-33.3h	421	137	15	7.62E-04	28.123	0.012
30	*Eau Claire*	*LaSalle County 36N1E-33.3h*	421	137	15	1.33E-03	27.569	0.012
31	Eau Claire	Lake County 44N10E-12.8a	421	122	8	1.99E-03	27.047	0.004
32	Eau Claire	Kendall County 37N8E-20.8h	420	122	4	2.88E-03	26.677	0.001
33	Eau Claire	Lake County 43N12E-30.7e	418	122	8	4.60E-04	28.510	0.004
34	Eau Claire	Cook County 42N11E-5.1g	409	122	15	1.62E-03	27.253	0.016
35	Eau Claire	Lake County 43N10E-21.5e	406	122	8	1.89E-03	27.098	0.004
36	Eau Claire	Carroll County 24N3E-10.2e	399	91	15	-	-	-
37	Eau Claire	Lake County 45N10E-15.7e	392	122	8	8.46E-04	27.901	0.004
38	*Eau Claire*	*Jo Daviess County 27N2E-11.2d*	389	91	15	2.73E-04	28.743	0.028
39	*Eau Claire*	*Jo Daviess County 27N2E-11.2d*	389	91	15	7.33E-04	27.756	0.028
40	*Eau Claire*	*Jo Daviess County 27N2E-11.2d*	389	91	15	1.01E-03	27.439	0.028

41	Eau Claire	Jo Daviess County 27N2E-11.2d	389	91	15	1.18E-03	27.281	0.028
42	Eau Claire	Lake County 44N09E-24.5d	385	122	8	-	-	-
43	Eau Claire	DeKalb County 40N3E-23.6e	382	137	15	2.16E-03	27.079	0.012
44	Eau Claire	Kane County 42N8E-27.1e	378	122	8	2.66E-03	26.755	0.004
45	Eau Claire	Kane County 41N8E-11.3f	373	122	8	-	-	-
46	Eau Claire	Lee County 20N10E-22.2g	337	122	8	1.60E-03	27.262	0.004
47	Eau Claire	Carroll County 24N6E-5.5e	336	91	15	2.16E-03	26.677	0.028
48	Eau Claire	Jo Daviess County 26N2E-9.4b	332	91	15	-	-	-
49	Eau Claire	Stephenson County 26N6E-9.8f2	316	107	8	7.19E-03	25.627	0.005
50	Eau Claire	McHenry County 44N5E-35.3g	313	122	8	1.35E-03	27.432	0.004
51	Eau Claire	Lee County 37N2E-10.2b	310	122	8	2.84E-03	26.690	0.004
52	Eau Claire	Ogle County 25N8E-33.4e	305	122	15	8.92E-03	25.546	0.016
53	*Eau Claire*	*Winnebago County 27N10E-29.1d*	229	122	8	8.34E-04	27.915	0.004
54	Eau Claire	Winnebago County 27N10E-29.1d	229	122	8	1.68E-03	27.213	0.004
55	Eau Claire	Winnebago County 28N10E-10.4b	178	122	8	2.64E-03	26.761	0.004
56	Eau Claire?	Bureau County 15N6E-34.4c	823	122	15	-	-	-
57	Eau Claire?	Cook County 41N10E-15.4h	421	122	15	3.16E-03	26.582	0.016

Max:	**28.922**	
Min:	**25.258**	
No. of samples:	**46**	
Average:	**27.163**	
Std dev:	**0.772**	
†Propagated uncert., e :		**0.838**

*   Derived from isopach data of Willman et al. (1975)

**   Permemeablity calculated with formation thickness and kinematic viscosity of 1.1×10^{-6} m^2/s from well test (T = 16.8°C, P = 5.8 MPa)

†   Propageted uncertainty e accounts for the relative uncertainty in horizontal permeability k_h due to formation thickness. Propagated uncertainty ~

$$e = \sqrt{\sum_{1}^{N} l(nk_h \text{ uncert.})}$$

TABLE A.4.3: Selected well data reproduced from Slack and Darden (1991) for horizontal hydraulic permeability of the Tuscaloosa Marine Shale – Gordo/Coker equivalent formation in Mississippi.

No.	Direction	Formation	Location	**T (°C)	Depth (ft)	ft/day	m/s	k_h, m^2	ln(k_h)
1	Horizontal	TMS-Gord	Calhoun County	27	1,887	51.0	1.80E-04	1.76E-11	-24.765
2	Horizontal	TMS-Gord	Calhoun County	27	1,897	37.0	1.31E-04	1.27E-11	-25.086
3	Horizontal	TMS-Gord	Kemper County	26	1718	38.0	1.34E-04	1.31E-11	-25.060
4	Horizontal	TMS-Gord	Lee County	21	669	41.0	1.45E-04	1.41E-11	-24.984
5	Horizontal	TMS-Gord	Lee County	20	586	13.0	4.59E-05	4.48E-12	-26.132
6	Horizontal	TMS-Gord	Lee County	20	590	13.0	4.59E-05	4.48E-12	-26.132
7	Horizontal	TMS-Gord	Lee County	20	630	15.0	5.29E-05	5.17E-12	-25.989
8	Horizontal	TMS-Gord	Lee County	20	562	11.0	3.88E-05	3.79E-12	-26.299
9	Horizontal	TMS-Gord	Lee County	20	526	3.0	1.06E-05	1.03E-12	-27.599
10	Horizontal	TMS-Gord	Lee County	20	541	77.0	2.72E-04	2.65E-11	-24.353
11	Horizontal	TMS-Gord	Lowndes County	20	609	25.0	8.82E-05	8.61E-12	-25.478
12	Horizontal	TMS-Gord	Lowndes County	20	632	58.0	2.05E-04	2.00E-11	-24.637
13	Horizontal	TMS-Gord	Lowndes County	22	863	50.0	1.76E-04	1.72E-11	-24.785
14	Horizontal	TMS-Gord	Lowndes County	20	498	50.0	1.76E-04	1.72E-11	-24.785
15	Horizontal	TMS-Gord	Lowndes County	21	705	25.0	8.82E-05	8.61E-12	-25.478
16	Horizontal	TMS-Gord	Lowndes County	20	570	38.0	1.34E-04	1.31E-11	-25.060
17	Horizontal	TMS-Gord	Lowndes County	20	556	57.0	2.01E-04	1.96E-11	-24.654
18	Horizontal	TMS-Gord	Monroe County	18	179	90.0	3.18E-04	3.10E-11	-24.197
19	Horizontal	TMS-Gord	Monroe County	20	444	150.0	5.29E-04	5.17E-11	-23.687
20	Horizontal	TMS-Gord	Noxubee County	26	1724	19.0	6.70E-05	6.54E-12	-25.753
21	Horizontal	TMS-Gord	Noxubee County	25	1533	87.0	3.07E-04	3.00E-11	-24.231
22	Horizontal	TMS-Gord	Okitbbeha County	25	1430	84.0	2.96E-04	2.89E-11	-24.266
23	Horizontal	TMS-Gord	Okitbbeha County	25	1460	77.0	2.72E-04	2.65E-11	-24.353
24	Horizontal	TMS-Gord	Okitbbeha County	25	1500	89.0	3.14E-04	3.06E-11	-24.209
25	Horizontal	TMS-Gord	Okitbbeha County	24	1376	42.0	1.48E-04	1.45E-11	-24.959
26	Horizontal	TMS-Gord	Okitbbeha County	25	1441	101.0	3.56E-04	3.48E-11	-24.082
27	Horizontal	TMS-Gord	Pontotoc County	25	1575	6.0	2.12E-05	2.07E-12	-26.905
28	Horizontal	TMS-Gord	Tishomingo County	19	370	11.0	3.88E-05	3.79E-12	-26.299
29	Horizontal	TMS-Gord	Tishomingo County	19	407	5.0	1.76E-05	1.72E-12	-27.088
30	Horizontal	TMS-Gord	Tishomingo County	19	256	2.0	7.06E-06	6.89E-13	-28.004
31	Horizontal	TMS-Cokr	Lowndes County	24	1284	82	2.89E-04	2.82E-11	-24.290
32	Horizontal	TMS-Cokr	Lowndes County	24	1306	39	1.38E-04	1.34E-11	-25.034
33	Horizontal	TMS-Cokr	Noxubee County	27	1832	93	3.28E-04	3.20E-11	-24.165
			Min:	18.1	179.0	2.0	7.06E-06	6.89E-13	-28.00
			Max:	27.1	1897.0	150.0	5.29E-04	5.17E-11	-23.69
			No. of sample :	33.0	33.0	33.0	33.0	33.0	33.00
			Average :	22.3	974.4	47.8	1.69E-04	1.65E-11	-25.24
			Std Dev. :	2.86	547.71	35.77	1.26E-04	1.23E-11	1.08

Temperature:	22°C
Pressure:	1 atm
*Kinematic viscosity (m^2/s):	9.6E-07
Dynamic viscosity (kg/m-s):	9.54E-04
Density (kg/m^3):	9.98E+02

*   Based on the average temperatue of the well data readings, assuming the properties of water at atmospheric pressure using the NIST webbook database

**   Temperature estimated assuming a surface tempertature of 17.2°C with a normal temperature gradient of 5.21 x 10-3 °C/ft

APPENDIX B

ASSUMPTIONS AND CONSTRAINTS TO THE INTEGRATED ANALYTICAL MODEL

ASSUMPTIONS AND CONSTRAINTS TO THE INTEGRATED ANALYTICAL MODEL

Fluid flow within this study's idealized reservoir and caprock representation employed several simplifying assumptions to their governing equations to make initial estimates for CO_2 leakage under a range of reservoir and fracture geometric conditions. Categorically described below are some important simplifying assumptions.

B.1 RESERVOIR PRESSURE

The fundamental governing equation for radial fluid flow in this conceptual porous medium is a nonlinear partial-differential equation, where parameters: permeability (k), viscosity (μ), porosity (ϕ_m), and compressibility (c_t) have implicit pressure dependence (Lee et al. 2003; Dake 1978).

$$\frac{1}{r}\frac{\partial}{\partial r}\left(r\frac{\partial p}{\partial r}\right) = \left(\phi_m \frac{c_t \mu}{k}\right)\frac{\partial p}{\partial t}$$

(B.1)

To find analytical solutions to equation (B.1) that represent pressure distribution within the reservoir, the aforementioned parameters were linearize to reduce their pressure dependence with several assumptions:

x)   Injection well is fully penetrating the reservoir to ensure radial flow

xi)   Darcy's law is valid within reservoir, implying smooth laminar-type flow

xii)   Reservoir is homogeneous and isotropic with constant permeability, k

xiii) Isothermal conditions

xiv)   Fluid viscosity, μ, and compressibility, c_t, are constant

xv)   Negligible gravity effects on the reservoir fluid

xvi)   Effective permeability varies with saturation, but not pressure

xvii) Small pressure and saturation gradient terms

xviii) Negligible capillary pressure

The general flow equation B.1 is a partial differential equation for pressure, and is second order with respect to space and first order with respect to time for a cylindrical reservoir. In order to solve equation B.1, two boundary conditions (outer and inner) with respect to radius and one initial condition for time are needed. The particular initial and boundary conditions used in this study apply to a pseudo-steady state solution.

A pseudo-steady state solution is a condition that is applicable to a reservoir which has been subjected to a constant injection of $scCO_2$, where after a long time, the effect of the outer boundary condition is felt. This situation is depicted in Figure B.1 where the $scCO_2$ displaces the brine in the reservoir to a point where the resident brine acts as a "brick wall" preventing flow into the radial cell (Dake 1978).

This boundary was assumed to be the maximum extent of the CO_2 plume, $r = r_{max}$, after which Darcy flow is zero (Lee et al. 2003):

$$q = Q_{in} \, \alpha \left(\frac{\partial p}{\partial r} \right)_{r_{max}} = 0$$

(B.2)

The second (inner) boundary condition is a constant-rate injection, where flow at the wellbore radius ($r = r_w$) follows Darcy's law (Lee et al. 2003)

$$q = Q_{in} = \left(\frac{kA}{\mu} \frac{\partial p}{\partial r} \right)_{r_w} \rightarrow \left(r \frac{\partial p}{\partial r} \right)_{r_w} = \frac{-Q_{in}\mu}{2\pi kb}$$

(B.3)
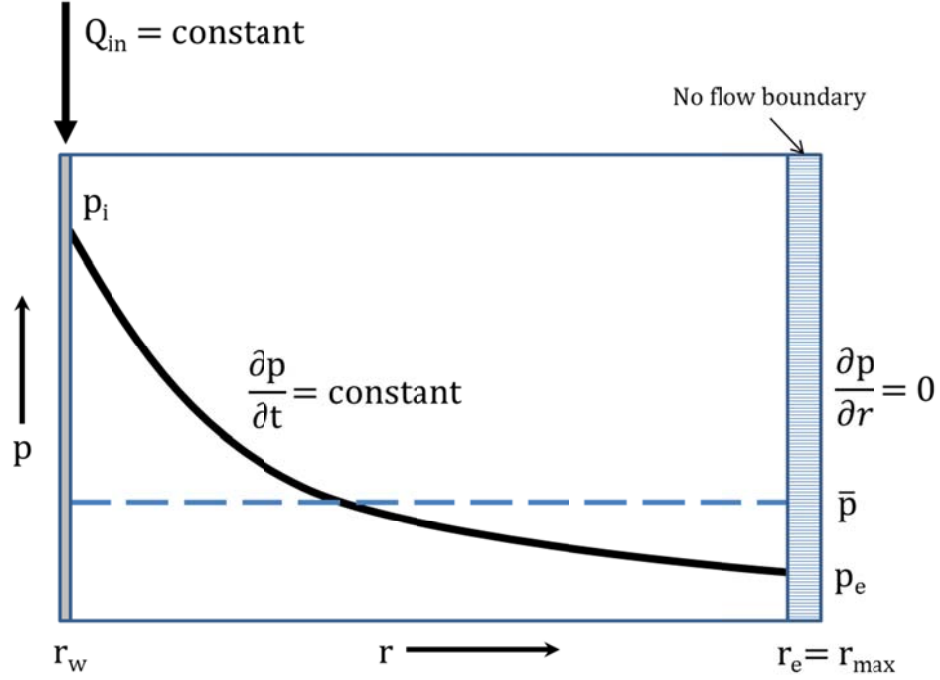
FIGURE B.1: Depiction of the pressure profile in a reservoir under pseudo-steady state conditions with average pressure ($\bar{p}$) pressure applicable to the reservoir extent (re) assumed to be the extent of the sCO$_2$ plume (r_{max})

Given no flow outer boundaries, a constant injection rate will give make the pressure within the radial cell depicted in Figure B.1 buildup in such a way that the change in pressure over all r ($r_w \rightarrow r_{max}$) and t is constant (Dake 1978)

$$\frac{\partial p}{\partial t} = \frac{-Q_{in}}{c_t \pi r_{max}^2 b \phi_m}$$
(B.4)

The initial condition of the pressure is assumed to be uniform and constant throughout the reservoir at time t = 0

$$p(r,0) = p_i$$
(B.5)

and is represented by the hydrostatic pressure discussed in section 3.4.2.

269

Taking the initial and boundary conditions aforementioned and substituting into equation B.1 yields an integrated analytical expression for the reservoir pressure with a single fluid phase:

$$p_r - p_i = \frac{-Q_{in}\mu}{2\pi kb} \ln\left[\frac{r}{r_w} - \frac{r^2}{2r_{max}^2}\right] \tag{B.6}$$

this represents the buildup of pressure over a distance r in the reservoir up to the boundary extent ($r_e = r_{max}$) depicted in Figure B.1.

In our simulations, we are interested in an average reservoir pressure over the entire volume of influence of the injected scCO$_2$, not just at the well. Volumetric average pressure can be determined by:

$$\overline{p_1}(r) = \frac{\int_{r_w}^{r_e = r_{max}} p\,dV}{\int_{r_w}^{r_{max}} dV} \tag{B.7}$$

with

$$dV = 2\pi rb\phi_m dr$$

The $\overline{p_1}(r)$ in equation B.7 represents the pseudo-steady state pressure buildup of equation B.6. When B.6 is substituted into equation B.7 and integrated from the well radius to the predicted extent of the scCO$_2$ plume, the result is (Dake 1978):

$$\overline{p_1}(r) - p_i = \frac{-Q_{in}\mu}{2\pi kb} \ln\left[\frac{r_{max}}{r_w} - \frac{3}{4}\right] \tag{B.8}$$

which represents volumetric average pressure with only one fluid phase. However, Lee et al. (2003) and Lee and Wattenbarger (1996) show that solutions to the general fluid flow equation (B.1) for single phase fluid flow also apply to multiphase flow with the inclusion of total mobility (λ_t) and a fluid phase saturation weighted system compressibility (c_t):

$$\lambda_t = \lambda_w + \lambda_g = \frac{k_w}{\mu_w} + \frac{k_g}{\mu_g} \qquad (B.9)$$

$$c_t = s_w c_w + s_g c_g + c_f \qquad (B.10)$$

where s_w, s_g, represent the water and gas saturation fractions in the reservoir, respectively; with c_g, c_w, c_f representing gas, water and rock formation compressibility. Therefore, the pseudo-steady state average pressure (B.8) can be re-written to account for the brine and scCO$_2$ in the reservoir:

$$\overline{p_1} - p_i = \frac{-Q_{in}}{2\pi\lambda_t b} \ln\left[\frac{r_{max}}{r_w} - \frac{3}{4}\right] \qquad (B.11)$$

The compressibility of the scCO$_2$ that contributes to the overall system compressibility in equation (B.10) was held constant throughout the reservoir under the assumptions stated earlier but its value used to evaluate (B.10) was approximated by:

$$c_g \approx \frac{1}{\overline{p_1}} \qquad (B.12)$$

where scCO$_2$ compressibility is approximately equal to the inverse of the average reservoir pressure. This approximation is shown to be valid in the temperature and pressure regime where most CCS activity occurs (Lee et al. 2003; Griffith et al. 2011; NETL 2009; Rodosta et al. 2010).

When there is an instantaneous or constant-rate injection into a well, it creates a pressure disturbance into the reservoir that extends beyond to front of the injected fluid. The distance that the pressure disturbance travels in the reservoir, over which it has a significant impact on the reservoir pressure, is called the radius of investigation r_{inv}, and the maximum effect of the injection on the reservoir at r_{inv} is felt at time t_{max}

$$t_{\max} = \frac{\phi_m \mu c_t r_{inv}^2}{k} = \frac{\phi_m c_t r_{inv}^2}{\lambda_t} \qquad (B.13)$$

According to Lee 1982, equation B.13 is derived under the conditions of an infinite acting reservoir, but serves as a constraint on the statistically conceptualized cases. The volumetric average pressure, equation B.11, is only applicable after t_{max}, when the boundaries of the reservoir start affecting the system's pressure. The effective size of the conceptualized system is limited to the predicted $scCO_2$ plume extent, r_{max}, where up to that distance in the reservoir, an average pressure is sought. Therefore the time required for CO_2 injection to be applicable to a pseudo-steady state solution is after the investigated radius at r_{max}:

$$t > t_{\max} > \frac{\phi_m c_t r_{\max}^2}{\lambda_t} \qquad (B.14)$$

B.2 MODEL CONSTRAINTS

In the Generalized Sensitivty Analysis, 10,000 output realizations were "pruned" by decision rules that reflected the theoretical constraints of the CO_2 model. The remaining model outputs were then separated into three classes: those with less than 100%, 10%, and 1%CO_2 loss, along with the inputs associated with these classified losses.

Model outputs were pruned by a series of IF-ELSE decision rules to address:

CO_2 plume extent constraints:

$$
\begin{aligned}
&\mathbf{IF} \quad \Gamma = \frac{2\pi\Delta\rho g \lambda_w k b_{res}^2}{Q_{in}} \leq 0.5 \\
&\quad \mathbf{THEN} \quad r_{\max} = \sqrt{\frac{M Q_{in} t}{\pi b_{res} \phi_m (1 - s_{wr})}} \\
&\mathbf{ELSE} \quad r_{\max} = 0
\end{aligned}
\qquad (B.15)
$$

pressure distribution constraints:

$$\textbf{IF} \quad r_{max} > r_w \, \textbf{AND} \left[\frac{r_{max}}{r_w} - \frac{3}{4} \right] < 0$$

$$\textbf{IF} \quad \overline{p_1}(r,t) < 90\% \, p_{frac}$$

$$\textbf{IF} \quad \overline{p_1}(r,t) - p_2 > p_{ce} \qquad \text{(B.16)}$$

$$\textbf{THEN} \quad \frac{\Delta p}{b_{cap}} = \frac{\overline{p_1} - p_2}{b_{cap}} - \rho_{CO_2} g$$

$$\textbf{ELSE} \quad \frac{\Delta p}{b_{cap}} = 0$$

and steady – state time constraint:

$$\textbf{IF} \quad t > \frac{\phi_m c_t r_{max}^2}{\lambda_t}$$

$$\textbf{THEN} \quad r_{max} = \sqrt{\frac{M Q_{in} t}{\pi b_{res} \phi_m (1 - s_{wr})}} \qquad \text{(B.17)}$$

$$\textbf{ELSE} \quad r_{max} = 0$$

Equation B.16 shows the upper and lower limit was placed on the pressure 'build up' at the injection well and within the reservoir, $\overline{p_1}$. Pressure at the well and in the reservoir could not exceed 90% of the estimated fracture pressure p_{frac}, an operational limit for the injection zone around wells utilizing geological sequestration (EPA, 2011). A lower limit to transport of scCO$_2$ across the caprock was that the reservoir pressure buildup $\left(\overline{p_1}(r,t) - p_2 \right)$ had to exceed the predicted capillary entry pressure $p_{ce} = 2\gamma / e$ at the caprock-reservoir interface. Surface tension γ data was drawn from experimental studies. The reservoir fracture pressures simulated in the Monte Carlo methodology (Table 4.2) were estimated using fracture pressure gradients G_f compiled from various regions across the U.S considered for CO$_2$ saline sequestration (EPA, 2011).

B.3   PERCOLATION THEORY AND CRITICAL FRACTURE DENSITY ESTIMATION

Percolation theory when applied to flow and transport in fractured media, depicts the situation where flow is concentrated into a sparse population of elements – such as microfractures and faults, in an otherwise impermeable matrix (Bour and Davy 1997). Percolation theory is a statistical approach that links global physical properties (connectivity, permeability, etc.) to an average measure of its geometrical properties.

The geometrical properties considered in this study are the fracture aperture and density, which are applied to a conceptually 'well-connected' fracture network within the caprock. In percolation theory, fracture density is correlated to network 'connectivity'. Fracture connectivity is described by a dimensionless percolation parameter p_p, which is independent of local geometry and depends the size of system L. There exists a crtical number of fractures in the system N_c, below which the system is on average not connected, while above it N_c is connected by an infinite cluster that spans the whole system (Bour and Davy 1997).

In Chapter 3, the fractures were considered to have constant length l, where the critical percolation parmater p_{pc} described the value at which N_c could be determined:

$$p_{pc} = 5.6 = N_c l^2 / L \qquad (B.18)$$

where system size was a function of CO_2 plume radius $L = 2r_{max}$. In Chapter 3, $l = b_{cap}$ – the caprock thickness, and r_{max} are fixed based on the case study modeled in Class et al (2009). In Chapter 4, the caprock thickness b_{cap} is not fixed but is varies uniformly between reported limits given in Chapter 2 (Griffith et al 2011). The critical number of fractures in the system N_c was now described with a Pareto (power law) distribution:

$$N_c = \alpha_c(L) \cdot l^{-a} \qquad (B.19)$$

where α_c is a constant of proportionality that reflects the fracture density at the critical percolation threshold p_{pc}, and a is the power law exponent.

$$p_{pc} = \int_{l_{min}}^{l_{max}} \frac{N_c(l,L)l^2}{L^2} dl \qquad (B.20)$$

where $N_c(l,L)\ dl$ is the critical number of fractures – which is now a function of l and L, having a length in the range $[l,l+dl]$. A power law distribution intrinsically has no characteristic length scale, except at it endmost limits (Bour and Davy 1997). In our system, the only relevant scale was the system size, which constituted the limit difference between "small" and "large" fractures, where small fractures were those with lengths l less than L (Bour and Davy 1997). The percolation threshold was then the sum of two terms describing "small" and "large" fractures.

$$p_{pc} = \int_{l_{min}}^{L} \frac{N_c(l,L)l^2}{L^2} dl + \int_{L}^{l_{max}} N_c(l,L) dl \qquad (B.21)$$

where the terms in expression B.21 reflect the ensemble contribution of small and large fractures in the fracture network, respectively. Based on the combination of B.17 and B.15:

$$p_{pc} = \int_{l_{min}}^{L} \frac{\alpha_c(L)l^{2-a}}{L^2} dl + \int_{L}^{l_{max}} \alpha_c(L)l^{-a} dl = 5.6 \qquad (B.22)$$

that has a solution of:

$$p_{pc} = \frac{\alpha_c}{L^2}\left[\frac{1}{a-3} - \frac{l_{max}^{3-a}}{a-3}\right] = 5.6 \qquad (B.23)$$

when $a \neq 3$, and when $L \geq l_{max}$, and a solution of:

$$p_{pc} = \alpha_c \left[\frac{1}{a-3} \cdot \frac{1}{L^2} + \left(\frac{1}{3-a} + \frac{1}{a-1} \right) L^{1-a} + \frac{1}{1-a} l_{max}^{1-a} \right] = 5.6 \qquad \text{(B.24)}$$

when $a \neq 3$, and $L < l_{max}$.

For $a = 3$, and $L \geq l_{max}$, the solution is:

$$p_{pc} = \alpha_c \left[\frac{1}{L^2} \ln(l_{max}) \right] = 5.6 \qquad \text{(B.25)}$$

wherefore if $L < l_{max}$:

$$p_{pc} = \alpha_c \left[\frac{1}{L^2} \ln(L) + \left(\frac{1}{a-1} \right) L^{-2} + \frac{1}{1-a} l_{max}^{1-a} \right] = 5.6 \qquad \text{(B.26)}$$

The solutions presented above, equations B.23-B.26, were adapted from Zhang et al. (2010), where equation B18 was normalized by l_{min} and l_{max} represented strata bound fractures that are equivalent to simulated caprock thickness.

In the Monte Carlo method, random input variables a, l_{max}, and those that determined L, were used to calculate α_c, which in turn determined N_c (Bour and Davy 1997, Bonnet et al. 2001; Zhang et al. 2010):

$$N_c = \frac{\alpha_c}{1-a} \left(l_{max}^{1-a} - 1 \right) \qquad \text{(B.27)}$$

which generated the total amount of fractures present within each system realization of the MC case experiments at percolation. Fracture density was calculated using equation B.27 divided by CO_2 resesvoir radius ($N_c/2r_{max}$).

References

Bour, O. and Davy, P., 1997. Connectivity of random fault networks following a power law fault length distribution. Water Resources Research, 33(7): 1567-1583.

Class, H. et al., 2009. A benchmark study on problems related to CO2 storage in geologic formations. COMPUTATIONAL GEOSCIENCES, 13(4): 409-434.

Dake, L.P., 1978. Fundamentals of reservoir engineering. Developments in petroleum science. Elsevier Scientific Publishing Company, Amsterdam, The Netherlands.

EPA, 2011. Draft Underground Injection Control (UIC) Program Class VI Well Site Characterization Guidance for Owners and Operators. 4606M, Office of Water, Environmental Protection Agency.

Griffith, C.A., Dzombak, D.A. and Lowry, G.V., 2011. Physical and chemical characteristics of potential seal strata in regions considered for demonstrating geological saline CO_2 sequestration. Environmental Earth Sciences, 64(4): 925-948.

Lee, J. and Wattenbarger, R.A., 1996. Gas reservoir engineering. SPE Textbook Series. Society of Petroleum Engineers, Richardson, TX.

NETL, 2009. Best Practices for: Monitoring, Verification, and Accounting of CO2 Stored in Deep Geologic Formations, National Energy Technology Laboratory

Rodosta, T. et al., 2011. US Department of Energy's Regional Carbon Sequestration Partnership Initiative: Update on Validation and Development Phases. Energy Procedia, 4(0): 3457-3464.

Zhang, Y.Q., Oldenburg, C.M. and Finsterle, S., 2010. Percolation-theory and fuzzy rule-based probability estimation of fault leakage at geologic carbon sequestration sites. Environmental Earth Sciences, 59(7): 1447-1459.

APPENDIX C

DIRECT AND IMPORTANCE SAMPLING PROCEDURE FOR MONTE CARLO METHOD

DIRECT AND IMPORTANCE SAMPLING PROCEDURE FOR MONTE CARLO METHOD

C.1. DIRECT MONTE CARLO PROCEDURE

The Monte Carlo (MC) sampling technique applied in each case used uniform random sampling across specified ranges for the parameters governing the probability density functions (PDFs) of each independent and identically distributed (iid) model input parameter for the CO_2 loss model. Each case had ten thousand (10,000) random realizations generated for each iid model input parameter, using a random seed number of 2011 to sample the uncertainty space.

The fracture aperture and density are key parameters examined in this study and apart from these two parameters, all other uncertain parameters examined in Cases 3 and 4 were modeled with uniform-law distribution. The uniform law was chosen in order to give an unbiased (equiprobable) maximum range to the resulting uncertainty in the set of fracture and reservoir parameters, given that data for each parameter was imported from various sources. As such, the results of the MC simulations do not reflect the characteristics of any one site but may be representative of the realistic bounds of the general population of parameters that can influence CO_2 transport and fracture properties for potential CCS projects.

Field studies have shown apertures and conductive fractures to be appropriately modeled with a power law (aka Pareto) distribution [e.g. *e ~ Power(a,b)*]. Initially, the parameters: *a* – the value of the exponent and *b* – the minimum aperture size are not known in this case but are assumed to uniformly vary between reported ranges (see Table 4.1 and 4.2).

The critical fracture density (N_c/L) for each MC realization was derived from the combination of power law distribution of number of fractures N_c along the line segment length of L (Guerriero et al 2011,2010).

$$\frac{N_c}{L} \sim \frac{Pareto(a,b)}{2r_{max}} \qquad \text{(C.1)}$$

where the number of fractures in the system are uniformly varied between reported parameter minimum a and maximum b ranges of Table 1 – given the expressions in Appendix B.3, and the line segment length is calculated from the r_{max} equation (4.11).

C.1.1 PRELIMINARY SENSITIVTY ANALYSIS

Before conducting the Monte Carlo simulations in Chapter 4, a sensitivity study was conducted to determine which *iid* input parameters governing the CO_2 loss equations could be ignored in the simulation of a more uncertain environment.

The sensitivity study utilized a 'Tornado' diagram that graphically represented the parametric analysis of CO_2 loss based on the minimum and maximum values for the *iid* parameters listed in Table 4.2 that fall within the validity of the analytical models. For the graph, the minimum value for the reservoir pressure (p_i) listed in Table 4.2 was estimated using the hydraulic gradient, 1.05×10^4 Pa m^{-1}(0.46 psi ft^{-1}) and a caprock depth (2,870 m) and thickness (5 m) of Chapter 2. Likewise on Table 4.2, the maximum reservoir pressure is estimated by multiplying the maximum fracture pressure gradient of 1.81×10^4 Pa m^{-1} (e.g 0.8 psi/ft) by the maximum reservoir depth, 3,476 m, and taking 90% of that value to represent the highest operating pressure applicable to CO_2 sequestration activities. The top caprock pressure is estimated in similar manner to the reservoir pressure, but using only the constant hydrostatic gradient for both the minimum and maximum values.

Figure C.1 depicts the results of the sensitivity analysis, with demarcations at the 10% and 1% CO_2 loss to indicate the parameters whose variance affects the CO_2 loss above these thresholds. The reference percent CO_2 loss in Figure C.1 from which the parameters' variance are compared, was calculated from Chapter 3's case study with e = 10^{-7} m, N/L=0.28 m^{-1}.

Examination of Figure C.1 revealed that uncertainty in fracture aperture, fracture density, and injection time had the biggest impact to the output CO_2 loss of the system. The variance within the fracture aperture parameter space had the largest positive impact, with uncertainty in the CO_2 fluid properties and residual water saturation fraction having the least impact to the CO_2 loss. Therefore, under the conservative assumptions listed in Appendix B for CO_2 transport, the effect of a 'warm' or 'cold' basin on the CO_2 fluid properties has minimal impact to CO_2 loss and was subsequently held constant for the MC simulations.
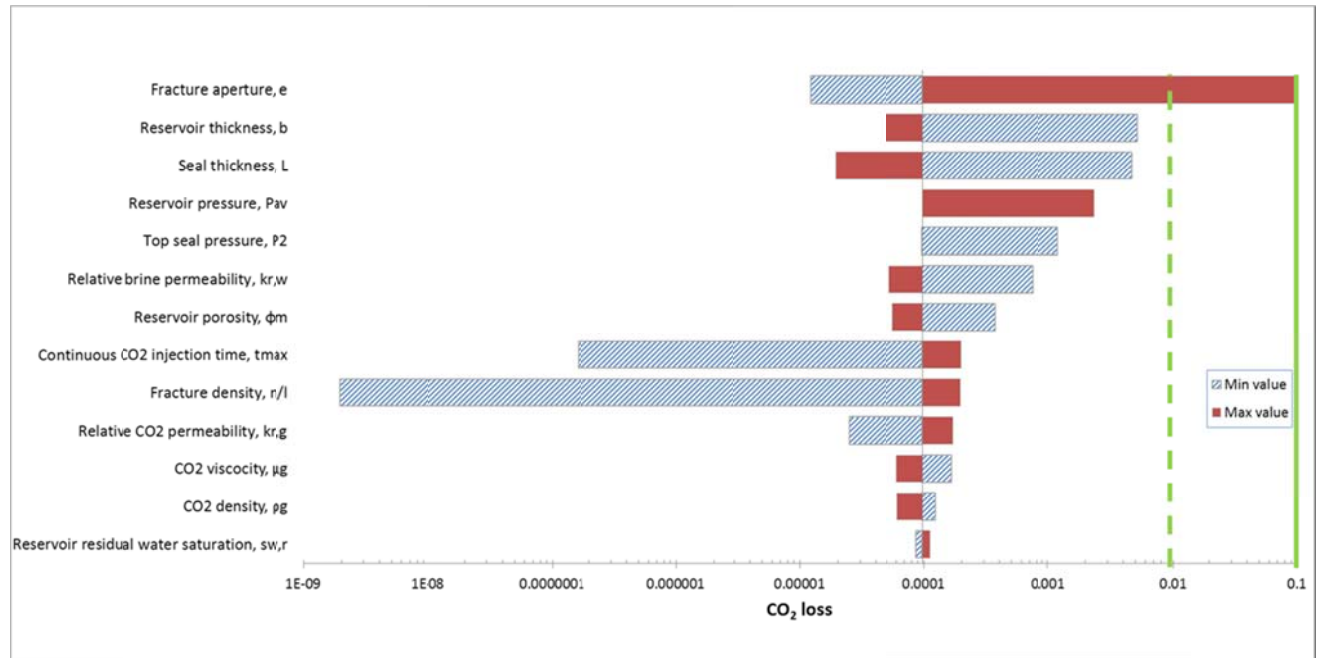
FIGURE C.1: Tornado diagram for independent input parameters within the validity of intergrated CO_2 loss analytical model and CCS performance goals.

C.1.2 INVERSE TRANSFORMATION METHOD

Ayyub and McCuen (2011) describe this as a simple and direct method. A random numer u is first generated in the range [0,1] where u $u \in U[0,1]$, with U[0,1] is a continuous uniform probability distribution. Then a generated continuous random variable (r.v.) X is determined as follows:

$$x = F_X^{-1}(u)$$
(C.2)

where F_X^{-1} is the inverse of the cumulative distribution function (CDF) of X. Because $F_X(x)$ is in the range [0,1], a unique value for x is obtained in each simulation realization for every model input r.v with an identified probability density function (PDF).

C.2 IMPORTANCE SAMPLING FOR MONTE CARLO

In simple a Monte Carlo simulation the sample values for an input variables X_i are drawn from the 'target' distribution f_X. Importance sampling introduces a 'design' distribution $g(\cdot)$ that emphasizes a particular feauture of the 'target' distribution. Importance sampling (I-S) is particularly effective when seeking samples from the 'target' distribution f_X that occur as rare events, or when it is impractical to generate samples from the target distribution (Hesterberg 1995;1988). Importance sampling is the process by which one can evaluate a particular parameter space, feature, or behavior – defined by a given distribution, through using one or more alternate 'design' distribution(s). By increasing the design frequency of 'important' events, it is possible to accureately estimate the frequency or expected magnitude of those events using fewer Monte Carlo replications. Importance sampling has been used in many fields to estimate small probabilities, particularly in economic or reliability studies of large and complex systems (Helton et al. 2006).

Importance sampling method is classically designed as a variance-reduction technique for Monte Carlo integration – the estimation of an intergral or equivalently the expected values of a random variable.

$$\mu = E_f[Y(X)] = \int Y(x)f(x)dx = \int \frac{Y(x)f(x)}{g(x)}g(x)dx \qquad \text{(C.3)}$$

where the expected value μ for a specified output function $Y(x)$ is calculated from r.v's drawn from distribution g. The outputs $Y(x)$ of particular interest in this study were CO_2 fractional loss ξ_{CO2}, fracture permeablility k_f, fracture porosity ϕ_f, fracture density N/L, fracture aperture e, CO_2 plume extent r_{max}, average reservoir pressure $\overline{p_1}$, and capillary entry pressure p_{ce}. In importance sampling, the outputs are corrected by weight functions that counteract the sampling bias introduced by using $g(\cdot)$. Three approaches to estimating the expected values from equation C.3 are described below. The first is the integration estimate, which is a weighted average:

$$\widehat{\mu}_{\text{int}} = \frac{1}{n}\sum_{i=1}^{n}Y(X_i) = \frac{1}{n}\sum_{i=1}^{n}\frac{Y(X_i)f(X_i)}{g(X_i)} \qquad \text{(C.4)}$$

where "int" signifies integration estimate with the weight function represented by:

$$W(x) = \frac{f(x)}{g(x)} \qquad \text{(C.5)}$$

and is based on the likelihood ratio between the 'target' and 'design' distribution. The weight function applies to every realization x_i of the output variable $Y(X_i)$ but the sum is not 1. However, the weights have an expected value of 1 but a nonzero variance (Hammersley and Handscomb 1964; Hesterberg 1995). In equation C.4, if $g(x) > 0$ when $Y(x)f(x) \neq 0$, the

estimate is unbiased and is asymptotically normally distributed with a normalized variance

$$\sigma_{\text{int}}^2 = \text{var}_g\left[Y(x) \cdot W(x)\right].$$

The second approach is the application of a ratio estimate. The ratio estimate is obtained by normalizing the weights of equation C.5, represented by factor:

$$V_{ratio,i} = \frac{W_i}{\sum_{i=1}^n W_i} \tag{C.6}$$

where then the expected value and variance are now:

$$\widehat{\mu}_{ratio} = \sum_{i=1}^n V_{ratio} Y(X_i) \tag{C.7}$$

$$\sigma_{ratio}^2 = \text{var}_g\left[Y(x)W(x) - \mu_{ratio}W(x)\right] \tag{C.8}$$

and are consistent iff $g(x) > 0$ whenever $f(x) > 0$.

The third approach is the use of a regression estimate. In the ratio estimate, all weights are multiplied by the same factor. The regession estimate improves on the ratio estimate in that its factor assigns greater weight to realizations with larger values of W and lesser weight to realizations with smaller W.

$$V_{reg,i} = W_i \frac{1 + \beta(W_i - \overline{W})}{n} \tag{C.9}$$

with components: $\beta = (1 - \overline{W})/\widehat{\sigma}_W^2$ and $\widehat{\sigma}_W^2 = \sum_{i=1}^n (W_i - \overline{W})^2$ yielding:

$$\widehat{\mu}_{reg} = \sum_{i=1}^n V_{reg,i} Q(X_i) = \overline{Y} - \widehat{\beta}(\overline{W} - 1) \tag{C.10}$$

Stratified defensive mixture 'design' distributions should be easy and fast to generate and should have good statistical properties. The general form for an importance sampling mixture distribution is:

$$g_{IS}(x) = \sum_{k=1}^{K} \lambda_{IS,k} g_k(x)$$ (C.11)

where $\sum \lambda_{IS,k} = 1$, $\lambda_k > 0$, and is unbiased when $g(x) > 0$ and $Y(x)f(x) \neq 0$. The choice forms for $g_k(x)$, and their associated parameters, are not necessarily known *a priori*. They are typically based on user intuition into the problem addressed, but in practice are based on preliminary calculations to make $Y(X_i)f(X_i)/g(X_i)$ more constatant (Hesterberg 1988).

In our application, the design distributions use the same PDF type as the target distributions assigned to the input variables. The parameters (and hyper-parameters) defining the design PDFs are taken from the resulting range from Case 1 Monte Carlo simulation – our 'preliminary' calculation. Case 2 and 3 had stratified realizations that applied:

$$g_{IS}(x) = \lambda_{IS} g_1(x) + (1 - \lambda_{IS}) g_2(x)$$ (C.12)

where $\lambda_{IS} = 0.1$ and $g_{IS}(x)$ components defined as:

$$g_2(x) = U(a^*, b^*)$$ (C.13)

$$g_1 = f(x) = U(a, b)$$ (C.14)

The term 'defensive' refers to the use of $f(\cdot)$ as one component of the mixture distribution to bound W.

$$W(x) = \frac{f(x)}{g(x)} \leq \frac{f(x)}{\lambda_{IS} f(x)} = \frac{1}{\lambda_{IS}} \tag{C.15}$$

Case 2 and 3 were 'stratified' in that $(1-\lambda_{IS}) \cdot n$ total realizations were attributed to design distributions $g_k(\cdot)$, and $(\lambda_{IS}) \cdot n$ realizations were assigned to the target distributions $f(\cdot)$.

TABLE C.1: Squared standard-deviation formulas with and without stratification for mixture distributions under various estimators used for Importance Sampling (Hesterberg 1995).

Method	Unstratified	Statified
Integration	$\dfrac{1}{n(n-1)} \sum_{i=1}^{n} (Y_i^{IS} - \overline{Y}^{IS})^2$	$\dfrac{1}{n(n-k)} \sum_{k=1}^{K} \sum_{i=1}^{n_k} (Y_{k_i}^{IS*})^2$
Ratio	$\dfrac{1}{n(n-1)} \sum_{i=1}^{n} (Y_i^{IS} - \widehat{\mu}_{ratio}\overline{W})^2$	$\dfrac{1}{n(n-k)} \sum_{k=1}^{K} \sum_{i=1}^{n_k} (Y_{k_i}^{IS*} - \widehat{\mu}_{ratio}W_{k_i}^*)^2$
Regression	$\dfrac{1}{n(n-1)} \sum_{i=1}^{n} (Y_i^{IS} - \widehat{\beta}W_i - \overline{Y} + \widehat{\beta}\overline{W})^2$	$\dfrac{1}{n(n-k-1)} \sum_{k=1}^{K} \sum_{i=1}^{n_k} (Y_{k_i}^{IS*} - \widehat{\beta}W_{k_i}^*)^2$

NOTE: $Y_i^{IS} = Y(X_i)f(X_i)/g(X_i)$ where for stratified methods, exactly n_k observations are generated from distribution g_k, $k = 1,2,...,K$, where $Y_{k_i}^{IS}$ is the ith observation from distribution k. $Y_{k_i}^{IS*} = Y_{k_i}^{IS} - \overline{Y}_k^{IS}$ with $\overline{Y}_k^{IS} = n_k^{-1} \sum_{i=1}^{n} Y_{k_i}^{IS}$; $W_{k_i} = f(x)/g_k(x)$ and $W_{k_i}^*, \overline{W}_k$ are similarly defined.

The estimated variances (square standard deviations) with and without stratification in Table C.1 may be untrustworthy, even for large n, because the distributions of W and Y^{IS} may be skewed. This is a common problem in rare event simulation, but there are three diagnostic indicators to test reliability of standard deviations in Table C.1:

1. $\overline{W} \sim 1$

2. $\dfrac{(\sum W_i)^2}{\sum (W_i^2)} \sim \text{large}$

3. $\sum (\cdots)^2 \sim \text{dominated by large } n$

In addition, it is also useful to exmain a histogram of the logathrims of the largest weights. Estimates will often be poor if the largest weight ratios are much greater than others applied to the parameters examined (Gelman et al. 2000).

Maximum likelihood and expontential tilting are other estimates, not listed in Table C.1, that can be used in importance sampling (Hesterberg 1995,1988). Each type of estimate used for importance sampling has its drawbacks; and, in general, there is no standard method for reliably estimating the accuracy of an importance sampling estimate (Gelman et al. 2000). For the application of simulating rare events in this study, the integration estimate was chosen because: 1) it was developed from target PDFs, 2) gave unbiased results, and 3) had been shown to be a more robust way for estimating small probabilities, as compared to the other estimates mentioned (Hesterberg 1995).

References

Ayyub, B.M., McCuen, R.H., 2011. Probability, Statistics, and Reliability for Engineers and Scientists. Third Edition. Taylor and Francis Group, LLC, Boca Raton.

Hammersley, J.M., and Handscomb, D.C., 1964. Monte Carlo Methods. Methuen & Co., London, and John Wiley & Sons, New York.

Helton, J.C., Johnson, J.D., Sallaberry, C.J. , Storlie, C.B., 2006. Survey of sampling-based methods for uncertainty and sensitivity analysis. Reliability Engineering and System Safety, 91: 1175–1209.

Hesterberg T.C., 1988. Advances in Importance Sampling. PhD, Department of Statistics, Stanford University, Stanford California.

Hesterberg T.C., 1995. Average Importance Sampling and Defensive Mixture Distributions. Technometrics, 37(2):185-194.

Gelman A., Carlin, J.B., Stern, H.S., Rubin, D.B., 2000. Bayesian Data Analysis. Chapman & Hall/CRC, Boca Raton.

APPENDIX D

HISTOGRAM AND KERNEL DENSITY ESTIMATION ALGORITHM

ALOGRITHM TO CALCULATE HISTOGRAM AND GAUSSIAN KERNEL DENSITIES

Histogram:

- Plot the x-axis range for the Log_{10} transform of either fracture permeability k_f or fracture porosity ϕ_f from minimum to maximum

- Calculate bin width spacing, h, using the total amount, N_{total}, of desired bins:

$$\frac{x_{max} - x_{min}}{N_{total} + 1}$$

- Calcluate bin value frequency of simulated data using frequency function in Excel

- Plot frequency vs. bin value

Gaussian Kernel density estimation (KDE):

- Plot the x-axis range for the Log_{10} transform of either fracture permeability k_f or fracture porosity ϕ_f from minimum to maximum

- Calculate standard deviation (Appendix E), upper quartile (Q3), lower quartile (Q1) and hence the inter-quartile range (IQR) of the data

- Calculate optimum bin width spacing, h_{opt}, using descriptive statistics and total amount of simulated data n for each variable:

$$h_{opt} = 0.9 \cdot \min\left(\sigma, \frac{IQR}{1.34}\right) n^{-\frac{1}{5}}$$

- Calculate kernel density estimator for each selected point on the x-axis of histogram using:

$$\widehat{f}(x,h) = \frac{1}{nh_{opt}} \sum_{i=1}^{n} NORMSDIST\left(\frac{x - x_i}{h_{opt}}\right)$$

where x is the selected x-axis bin value from histogram; x_i is k_f or ϕ_f data point from $x_1,...,x_n$; NORMSDIST the standard Normal probability mass density function in Microsoft Excel®; and $\widehat{f}(x,h)$ = a curve representing a univariate estimation for the sum of n Gaussian "bumps" at each bin value point on graph.

The algorithm for the KDE was adapted from Thompson (2001, 2006). The shape of fhat is critically dependent on the choice of h. In its application for this study, h was constant. The method presented for determining h_{opt} represents a straightforward way of producing an optimum bin width, given that n was relatively large. The kernel estimate, when calculated with an appropriate value of h, gives a good estimate of the population density function without making assumption of the distribution underlying the data. Figure D.1 and Figure D.2 illustrate the generated histograms and KDE curves for fracture permeability and porosity.

References

Thompson, M, 2001. AMC Technical Brief: Representing data distributions with Kernel Density Estimates. Analytical Methods Committee, Royal Society of Chemistry, AMCTB(4): 1-2.

Thompson, M, 2006. AMC Technical Brief: Representing data distributions with Kernel Density Estimates. Analytical Methods Committee, Royal Society of Chemistry, AMCTB(4): 1-2.
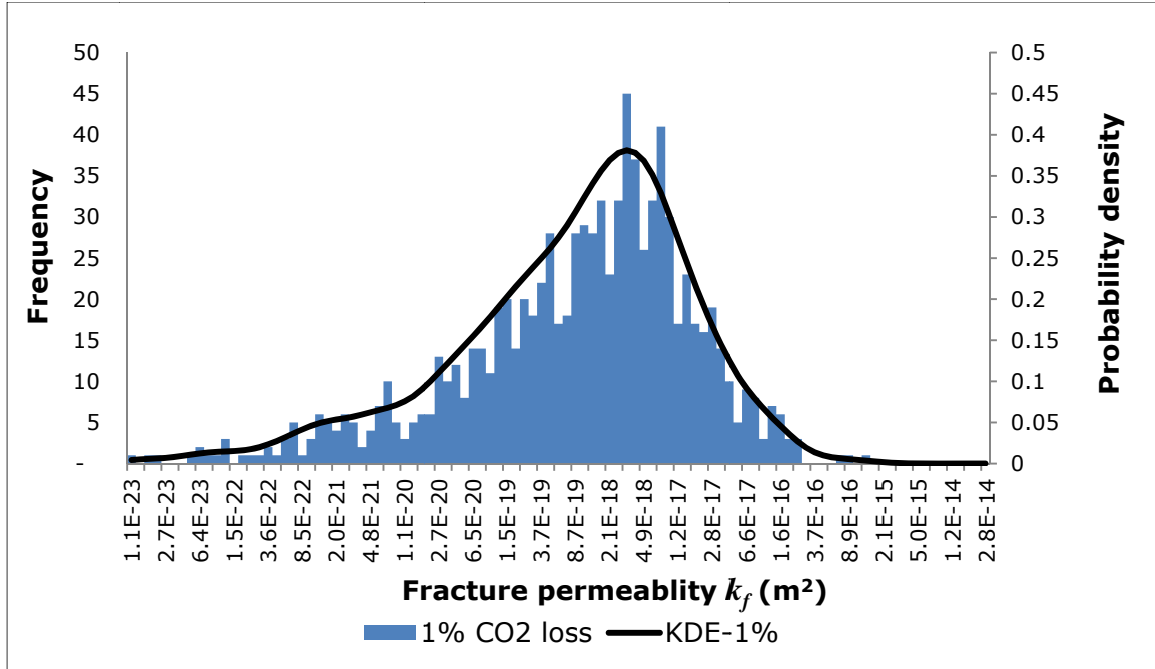
FIGURE D.1: Historgram and Gaussian kernel density estimation for 1% CO2 classified loss results for fracture permeability in Case 2.
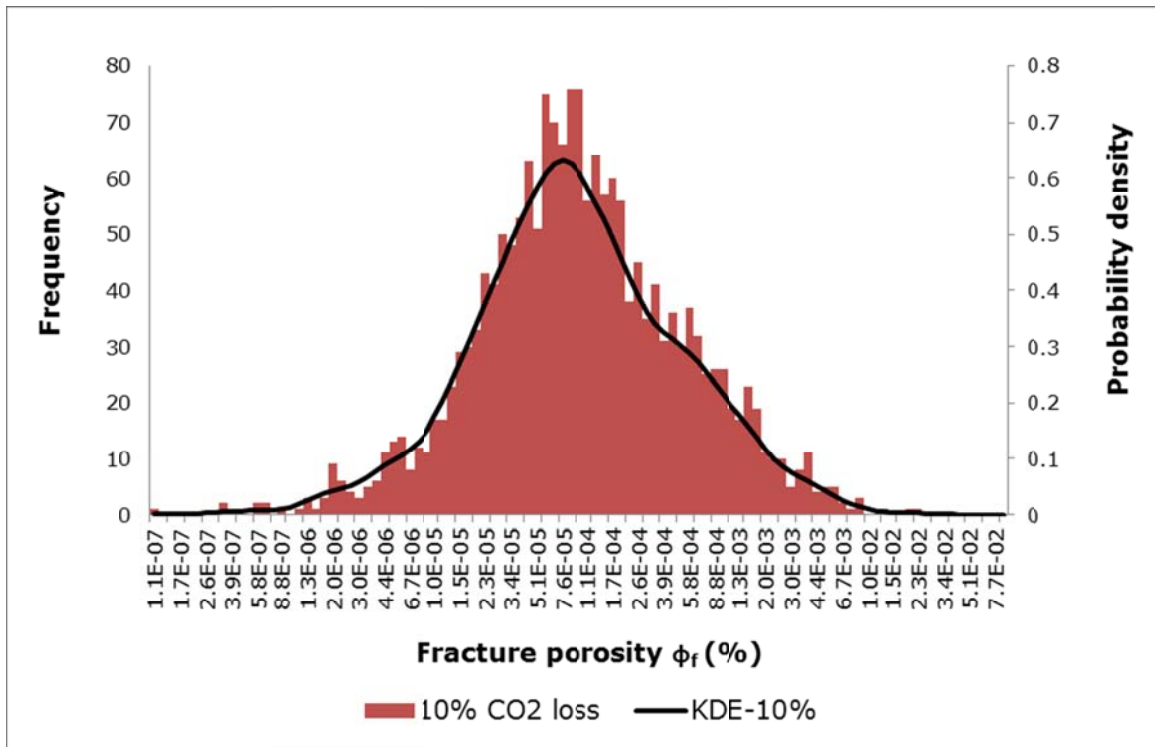
FIGURE D.2: Historgram and Gaussian kernel density estimation for 10% CO2 classified loss results for fracture porosity in Case 2.

APPENDIX E

DESCRIPTIVE STATISTICS TABLES FOR MONTE CARLO CASE SIMULATIONS

TABLE E.1:   Case 1 resulting descriptive statistics

| Statistic | Fracture aperture PDF parameters | | | | Fracture aperture, e (m) | | Fracture length PDF parameters | | | | Fracture density, N_c/L (m^{-1}) | | Fracture porosity Φ_f (%) | | Fracture permeability, k_f (m^2) | |
| | a | | b | | | | a | | b | | | | | | | |
System CO$_2$ loss constraint:	10%	1%	10%	1%	10%	1%	10%	1%	10%	1%	10%	1%	10%	1%	10%	1%
Min :	1.55	1.57	1.0E-07	1.0E-07	2.8E-07	2.8E-07	0.58	0.62	30.48	82.79	0.16	0.16	1.0E-04	1.0E-04	1.3E-19	1.3E-19
Max :	2.45	2.45	4.2E-05	1.1E-05	4.6E-05	1.5E-05	2.79	2.79	345.52	345.52	205.14	205.14	3.9E-02	6.5E-03	1.5E-15	4.8E-17
Median :	1.98	1.97	1.1E-06	6.8E-07	1.6E-06	9.0E-07	1.45	1.34	186.78	221.78	9.53	8.26	1.1E-03	6.2E-04	1.7E-18	8.7E-19
Mean :	1.97	1.96	4.2E-06	2.3E-06	5.1E-06	3.1E-06	1.38	1.36	191.19	226.90	43.73	41.16	4.5E-03	1.7E-03	1.1E-16	5.6E-18
Stdev:	0.32	0.30	9.6E-06	3.5E-06	1.1E-05	4.7E-06	0.69	0.69	101.76	88.94	65.94	71.70	8.9E-03	2.4E-03	3.4E-16	1.5E-17
C_v :	0.16	0.16	2.29	1.51	2.06	1.54	0.50	0.51	0.53	0.39	1.51	1.74	1.96	1.46	3.13	2.67
10th percentile :	1.57	1.63	2.0E-07	1.3E-07	3.8E-07	3.6E-07	0.66	0.68	68.37	113.85	0.19	0.19	1.5E-04	1.1E-04	1.7E-19	1.7E-19
90th percentile :	2.41	2.42	5.9E-06	5.2E-06	8.6E-06	6.4E-06	2.23	2.19	322.70	327.55	151.39	146.87	7.2E-03	5.9E-03	2.3E-16	7.1E-18
$\hat{p}$:	0.45	0.24	0.45	0.24	0.45	0.24	0.45	0.24	0.45	0.24	0.45	0.24	0.45	0.24	0.45	0.24
n :	19	10	19	10	19	10	19	10	19	10	19	10	19	10	19	10
Unclassified n :	9,557	9,557	9,557	9,557	9,557	9,557	9,557	9,557	9,557	9,557	9,557	9,557	9,557	9,557	9,557	9,557

TABLE E.1: Cont'd

Statistic	CO_2 plume extent, r_{max} (m)		Capillary entry pressure p_{ce}(Pa)		Mobility ratio, M (-)	
System CO_2 loss constraint:	10%	1%	10%	1%	10%	1%
Min :	59	169	1.5E+03	3.4E+03	0.42	0.42
Max :	1,842	1,842	2.4E+05	2.4E+05	7.89	7.89
Median :	542	490	4.3E+04	9.3E+04	1.00	0.95
Mean :	680	764	7.4E+04	9.9E+04	1.59	1.78
Stdev:	529	619	7.8E+04	8.6E+04	1.68	2.21
C_v :	0.78	0.81	1.04	0.87	1.06	1.24
10th percentile :	168	182	8.2E+03	1.5E+04	0.48	0.46
90th percentile :	1,455	1,513	2.0E+05	2.2E+05	2.32	2.57
$\hat{p}$:	0.45	0.24	0.45	0.24	0.45	0.24
n :	19	10	19	10	19	10
Unclassified n :	9,557	9,557	9,557	9,557	9,557	9,557

TABLE E.2:   Case 2 resulting descriptive statistics

| Statistic | Fracture aperture PDF parameters | | | | Fracture aperture, e (m) | | Fracture length PDF parameters | | | | Fracture density N_c/L (m^{-1}) | | Fracture porosity Φ_f (%) | | Fracture permeability, k_f (m^2) | |
	a		b				a		b							
System CO$_2$ loss constraint:	10%	1%	10%	1%	10%	1%	10%	1%	10%	1%	10%	1%	10%	1%	10%	1%
Min :	1.55	1.55	1.0E-07	1.0E-07	4.4E-09	4.4E-09	0.53	0.53	30.75	34.03	5.5E-04	5.5E-04	1.1E-07	1.1E-07	1.1E-23	1.1E-23
Max :	2.46	2.46	4.2E-05	4.2E-05	5.8E-05	1.6E-05	2.88	2.88	348.47	348.32	263.96	88.46	2.1E-02	5.0E-03	7.2E-15	1.1E-15
Median :	2.02	2.03	7.0E-06	3.5E-06	4.6E-07	2.4E-07	1.24	1.18	222.58	222.45	0.09	0.07	8.9E-05	4.4E-05	9.4E-18	1.4E-18
Mean :	2.02	2.02	1.0E-05	6.4E-06	8.7E-07	5.0E-07	1.36	1.32	215.79	216.67	1.34	1.10	3.7E-04	1.5E-04	7.5E-17	1.2E-17
*†Stdev:	0.26	0.26	9.9E-06	7.4E-06	1.9E-06	9.4E-07	0.59	0.57	83.93	84.05	8.01	5.16	1.0E-03	3.5E-04	3.2E-16	5.6E-17
C_v :	0.13	0.13	0.96	1.14	2.21	1.86	0.43	0.43	0.39	0.39	5.99	4.70	2.82	2.26	4.31	4.70
10th percentile :	1.65	1.65	9.7E-07	5.8E-07	7.9E-08	4.4E-08	0.67	0.67	97.38	99.55	0.011	0.009	1.4E-05	6.5E-06	9.2E-20	1.4E-20
90th percentile :	2.38	2.38	2.6E-05	1.7E-05	1.9E-06	1.2E-06	2.24	2.20	323.95	325.99	1.88	1.61	8.7E-04	3.9E-04	1.4E-16	2.2E-17
$\hat{p}$:	0.56	0.28	0.56	0.28	0.56	0.28	0.56	0.28	0.56	0.28	0.56	0.28	0.56	0.28	0.56	0.28
n :	1,830	907	1,830	907	1,830	907	1,830	907	1,830	907	1,830	907	1,830	907	1,830	907
Unclassified n :	9,504	9,504	9,504	9,504	9,504	9,504	9,504	9,504	9,504	9,504	9,504	9,504	9,504	9,504	9,504	9,504

*Standard deviation did not improve for all variables for the reasons stated in Appendix C.2.

†Standard deviation approximated as unstratified population since only 1-2 MC realizations gave values under the orginal PDF in the stratified importance-sampling scheme.

TABLE E.2: Cont'd

Statistic	CO$_2$ plume extent, r$_{max}$ (m)		‡Capillary entry pressure p$_{ce}$(Pa)		‡Mobility ratio, M (-)	
System CO$_2$ loss constraint:	10%	1%	10%	1%	10%	1%
Min :	0	0	8.0E+02	1.4E+03	2.6E-05	2.6E-05
Max :	3,541	1,308	7.0E+05	7.0E+05	12.88	3.82
Median :	11	11	9.1E+03	1.8E+04	0.04	0.04
Mean :	29	23	2.7E+04	4.5E+04	0.09	0.08
Stdev:	133	59	5.9E+04	7.9E+04	0.38	0.19
C$_v$:	4.66	2.63	2.19	1.77	4.08	2.44
10th percentile :	4	3	2.6E+03	4.2E+03	0.01	0.01
90th percentile :	44	44	6.0E+04	1.0E+05	0.15	0.15
$\hat{p}$:	0.56	0.28	0.56	0.28	0.56	0.28
n :	1,830	907	1,830	907	1830	907
Unclassified n :	9,504	9,504	9,504	9,504	9,504	9,504

‡Not subjected to weight function probability correction of importance-sampling scheme

TABLE E.3: Case 3 resulting descriptive statistics

Statistic	Fracture aperture PDF parameters				Fracture aperture, e (m)		Fracture length PDF parameters				Fracture density, N_c/L (m^{-1})		Fracture porosity Φ_f (%)		Fracture permeability, k_f (m^2)	
	a		b				a		b							
	10%	1%	10%	1%	10%	1%	10%	1%	10%	1%	10%	1%	10%	1%	10%	1%
System CO$_2$ loss constraint:	10%	1%	10%	1%	10%	1%	10%	1%	10%	1%	10%	1%	10%	1%	10%	1%
Min :	1.55	1.58	1.0E-07	1.0E-07	3.8E-09	3.8E-09	0.55	0.59	100	100	0.27	0.27	4.8E-06	4.8E-06	9.6E-23	9.6E-23
Max :	2.45	2.45	1.2E-06	6.5E-07	9.6E-08	3.6E-08	2.85	2.69	100	100	33.70	24.20	8.3E-04	4.4E-04	1.3E-19	1.4E-20
Median :	2.00	2.04	4.7E-07	2.5E-07	2.6E-08	1.1E-08	1.15	1.19	100	100	0.56	0.69	4.6E-05	2.4E-05	2.6E-20	3.7E-21
Mean :	1.99	2.01	5.2E-07	2.7E-07	2.7E-08	1.3E-08	1.22	1.22	100	100	2.06	1.62	8.5E-05	4.3E-05	3.9E-20	4.7E-21
†Stdev:	0.28	0.28	3.1E-07	1.5E-07	1.9E-08	7.2E-09	0.51	0.46	-	-	4.98	3.78	1.2E-04	7.0E-05	3.9E-20	4.3E-21
C_v :	0.14	0.14	0.59	0.56	0.70	0.56	0.42	0.38	-	-	2.41	2.33	1.43	1.63	1.00	0.91
10th percentile :	1.62	1.61	1.4E-07	1.1E-07	7.3E-09	5.5E-09	0.66	0.67	100	100	0.29	0.29	1.7E-05	8.0E-06	1.0E-21	2.8E-22
90th percentile :	2.38	2.39	9.8E-07	5.0E-07	5.1E-08	2.2E-08	1.94	1.61	100	100	3.65	2.40	1.6E-04	7.1E-05	1.0E-19	1.2E-20
$\hat{p}$:	0.41	0.15	0.41	0.15	0.41	0.15	0.41	0.15	-	-	0.41	0.15	0.41	0.15	0.41	0.15
n :	121	44	121	44	121	44	121	44	121	44	121	44	121	44	121	44
Unclassified n :	9,961	9,961	9,961	9,961	9,961	9,961	9,961	9,961	9,961	9,961	9,961	9,961	9,961	9,961	9,961	9,961

†Standard deviation approximated as unstratified population since only 1-2 MC realizations gave values under the orginal PDF in the stratified importance-sampling scheme.

TABLE E.3: Cont'd

Statistic	CO$_2$ plume extent, r_{max} (m)		‡Capillary entry pressure p_{ce}(Pa)		‡Mobility ratio, M (-)	
System CO$_2$ loss constraint:	10%	1%	10%	1%	10%	1%
Min :	36	36	5.6E+04	1.2E+05	0.03	0.03
Max :	232	76	7.0E+05	7.0E+05	0.17	0.06
Median :	40	40	1.3E+05	2.6E+05	0.03	0.03
Mean :	47	45	1.9E+05	3.1E+05	0.04	0.03
Stdev:	22	11	1.4E+05	1.5E+05	0.02	0.01
C$_v$:	0.46	0.25	0.76	0.50	0.46	0.25
10th percentile :	37	37	6.7E+04	1.5E+05	0.03	0.03
90th percentile :	64	61	3.9E+05	5.5E+05	0.05	0.05
$\hat{p}$:	0.41	0.15	0.41	0.15	0.41	0.15
n :	121	44	121	44	121	44
Unclassified n :	9,961	9,961	9,961	9,961	9,961	9,961

‡Not subjected to weight function probability correction of importance-sampling scheme

APPENDIX F

SPEARMAN RANK CORRELATION COEFFICIENT MATRICES

TABLE F.1

CASE 1 CORRELATION COEFFICIENTS BETWEEN SELECTED RESERVOIR AND CAPROCK FRACTURE PROPERTIES

TABLE F.1: Case 1 correlation coefficients between selected reservoir and caprock fracture properties

Model parameter	Fracture aperture			Fracture density			Fracture porosity			Fracture permeability		
System CO$_2$ loss constraint:	100%	10%	1%	100%	10%	1%	100%	10%	1%	100%	10%	1%
Fracture aperture	1.00	1.00	1.00									
Fracture density	-0.41	-0.78	-0.98	1.00	1.00	1.00						
Fracture porosity	0.02	-0.36	-0.81	0.72	0.82	0.88	1.00	1.00	1.00			
Fracture permeability	0.56	0.80	0.79	-0.27	-0.30	-0.67	0.42	0.22	-0.43	1.00	1.00	1.00
Aperture Pareto PDF: exponent	0.28	0.19	0.24	-0.10	-0.30	-0.28	0.00	-0.31	-0.47	0.13	-0.03	-0.04
Aperture Pareto PDF: min. length	0.65	0.96	0.92	-0.66	-0.76	-0.86	-0.01	-0.40	-0.69	0.88	0.76	0.86
Fracture length Pareto PDF: exponent	-0.25	-0.51	-0.77	0.82	0.82	0.84	0.78	0.74	0.89	0.05	-0.01	-0.35
Caprock thickness/ Fracture length Pareto PDF: min. length	-0.24	0.12	0.28	-0.29	-0.20	-0.21	-0.34	-0.30	-0.09	-0.08	0.11	0.56
CO$_2$% Loss	0.50	0.42	0.37	-0.06	0.06	-0.26	0.48	0.51	0.12	0.77	0.75	0.54
CO$_2$ injection rate	-0.23	-0.42	-0.37	0.35	0.41	0.42	0.39	0.38	0.65	0.03	-0.11	-0.21
Injection time	-0.44	-0.58	-0.59	0.39	0.41	0.66	-0.06	0.20	0.56	-0.60	-0.48	-0.41
CO$_2$ gas saturation	-0.08	0.05	-0.32	-0.09	-0.07	0.28	-0.21	-0.10	-0.08	-0.24	-0.09	-0.26
Relative CO$_2$ permeability	-0.12	0.29	0.30	-0.08	-0.18	-0.31	-0.12	-0.01	-0.39	-0.09	0.30	0.20
Reservoir water saturation	0.08	-0.05	0.32	0.09	0.07	-0.28	0.21	0.10	0.08	0.24	0.09	0.26
Reservoir residual water saturation	0.11	0.09	0.02	-0.12	-0.15	-0.07	0.02	-0.26	-0.13	0.13	-0.03	0.07
Relative brine permeability	0.08	0.27	0.55	-0.08	-0.07	-0.53	0.06	0.02	-0.50	0.19	0.25	0.54
Reservoir thickness	0.07	0.29	-0.12	0.09	-0.03	0.04	0.31	0.18	-0.28	0.36	0.36	-0.39
Reservoir porosity	-0.09	0.04	-0.49	-0.17	0.00	0.54	0.00	0.06	0.56	0.29	0.10	-0.16
Reservoir permabilty	-0.22	-0.24	-0.70	0.01	0.12	0.64	0.06	0.19	0.65	0.08	-0.16	-0.81
Fracture pressure gradient	0.07	0.39	0.09	-0.07	-0.26	-0.07	0.05	-0.07	-0.39	0.04	0.25	0.10
Capillary entry pressure	-0.63	-1.00	-1.00	0.68	0.80	0.98	0.02	0.39	0.81	-0.87	-0.78	-0.79
Pressure gradient, Δp/L-pg	0.11	-0.26	-0.02	0.32	0.21	0.08	0.22	0.07	0.25	-0.16	-0.22	0.12
Bouyancy Factor	-0.05	0.25	-0.22	-0.11	-0.17	0.14	0.01	0.01	-0.12	0.20	0.19	-0.42
Reseroir extent	-0.42	-0.73	-0.56	0.45	0.48	0.59	-0.01	0.24	0.66	-0.65	-0.56	-0.58

Left row-group labels: CAPROCK FRACTURE PROPERTIES AND CO$_2$% LOSS CORRELATIONS (rows Fracture aperture through CO$_2$% Loss); RESERVOIR PROPERTIES AND CO$_2$ INJECTION CORRELATIONS (rows CO$_2$ injection rate through Reseroir extent).

TABLE F.1: Cont'd

	Model parameter	Aperture Pareto PDF: exponent			Aperture Pareto PDF: min. length			Fracture length Pareto PDF: exponent			Caprock thickness/ Fracture length Pareto PDF: min. length			CO$_2$% Loss		
	System CO$_2$ loss constraint:	100%	10%	1%	100%	10%	1%	100%	10%	1%	100%	10%	1%	100%	10%	1%
CAPROCK FRACTURE PROPERTIES AND CO$_2$% LOSS CORRELATIONS	Fracture aperture															
	Fracture density															
	Fracture porosity															
	Fracture permeability															
	Aperture Pareto PDF: exponent	**1.00**	**1.00**	**1.00**												
	Aperture Pareto PDF: min. length	0.16	0.29	0.36	**1.00**	**1.00**	**1.00**									
	Fracture length Pareto PDF: exponent	-0.12	-0.39	-0.50	-0.31	-0.51	-0.67	**1.00**	**1.00**	**1.00**						
	Caprock thickness/ Fracture length Pareto PDF: min. length	-0.19	-0.18	-0.53	0.08	0.15	0.22	-0.08	0.18	0.07	**1.00**	**1.00**	**1.00**			
	CO$_2$% Loss	0.04	-0.23	-0.52	0.61	0.38	0.37	0.06	0.06	0.01	-0.03	-0.30	0.25	**1.00**	**1.00**	**1.00**
RESERVOIR PROPERTIES AND CO$_2$ INJECTION CORRELATIONS	CO$_2$ injection rate	-0.01	-0.04	-0.08	-0.14	-0.38	-0.19	0.39	0.43	0.38	0.13	0.25	-0.13	0.06	-0.05	0.27
	Injection time	-0.08	-0.02	0.16	-0.63	-0.47	-0.33	-0.06	0.03	0.37	0.11	-0.23	-0.39	-0.15	-0.11	-0.04
	CO$_2$ gas saturation	0.23	0.13	0.42	-0.11	0.07	-0.20	-0.15	-0.12	-0.05	0.01	-0.21	-0.07	-0.25	-0.19	-0.82
	Relative CO$_2$ permeability	-0.17	-0.16	-0.31	-0.09	0.19	0.15	-0.05	0.04	-0.04	0.04	0.25	0.39	-0.21	0.08	0.08
	Reservoir water saturation	-0.23	-0.13	-0.42	0.11	-0.07	0.20	0.21	0.12	0.05	-0.01	0.21	0.07	0.25	0.19	0.82
	Reservoir residual water saturation	0.13	-0.11	-0.21	0.16	0.12	-0.01	0.02	-0.12	-0.33	0.13	0.29	0.30	0.01	-0.09	-0.04
	Relative brine permeability	0.04	-0.05	0.32	0.21	0.25	0.63	0.06	-0.02	-0.54	-0.14	0.02	0.25	-0.06	-0.06	-0.19
	Reservoir thickness	0.31	0.34	0.60	0.17	0.21	-0.18	0.18	0.04	-0.12	-0.01	0.00	-0.26	0.21	0.27	-0.65
	Reservoir porosity	-0.02	0.02	-0.14	0.31	0.08	-0.29	0.01	0.24	0.45	0.21	0.41	0.32	0.10	-0.17	-0.10
	Reservoir permabilty	-0.23	-0.23	-0.15	0.01	-0.38	-0.77	0.12	0.30	0.53	-0.07	0.05	-0.56	-0.01	-0.15	-0.05
	Fracture pressure gradient	-0.09	0.02	0.42	0.04	0.31	0.14	0.05	-0.24	-0.31	-0.04	-0.10	0.01	0.10	0.16	-0.33
	Capillary entry pressure	-0.13	-0.20	-0.24	-0.98	-0.96	-0.92	0.34	0.54	0.77	-0.09	-0.13	-0.28	-0.61	-0.40	-0.37
	Pressure gradient, Δp/L-pg	0.05	0.04	-0.07	-0.21	-0.11	0.18	0.11	-0.11	-0.07	-0.23	-0.41	-0.37	0.07	0.12	0.54
	Bouyancy Factor	0.05	0.13	0.30	0.14	0.10	-0.37	0.00	0.02	0.15	-0.11	0.03	-0.12	0.00	0.02	-0.60
	Reseroir extent	-0.17	-0.24	-0.28	-0.72	-0.70	-0.53	0.12	0.21	0.43	0.13	-0.10	-0.33	-0.15	-0.11	0.25

TABLE F.1: Cont'd

Model parameter	CO₂ injection rate			Injection time			CO₂ gas saturation			Relative CO₂ permeability			Reservoir water saturation		
System CO₂ loss constraint:	100%	10%	1%	100%	10%	1%	100%	10%	1%	100%	10%	1%	100%	10%	1%
CAPROCK FRACTURE PROPERTIES AND CO₂% LOSS CORRELATIONS															
Fracture aperture															
Fracture density															
Fracture porosity															
Fracture permeability															
Aperture Pareto PDF: exponent															
Aperture Pareto PDF: min. length															
Fracture length Pareto PDF: exponent															
Caprock thickness/ Fracture length Pareto PDF: min. length															
CO₂% Loss															
RESERVOIR PROPERTIES AND CO₂ INJECTION CORRELATIONS															
CO₂ injection rate	1.00	1.00	1.00												
Injection time	0.19	0.43	0.61	1.00	1.00	1.00									
CO₂ gas saturation	-0.21	-0.37	-0.26	0.26	-0.04	0.22	1.00	1.00	1.00						
Relative CO₂ permeability	-0.25	-0.26	-0.52	-0.25	-0.53	-0.45	-0.08	-0.05	-0.25	1.00	1.00	1.00			
Reservoir water saturation	0.21	0.37	0.26	-0.26	0.04	-0.22	-1.00	-1.00	-1.00	0.08	0.05	0.25	1.00	1.00	1.00
Reservoir residual water saturation	0.17	0.04	-0.10	-0.19	-0.04	-0.12	0.01	0.10	0.41	-0.27	-0.44	-0.30	-0.01	-0.10	-0.41
Relative brine permeability	-0.23	-0.19	-0.27	-0.23	-0.20	-0.35	0.19	0.31	0.43	0.06	0.17	-0.07	-0.19	-0.31	-0.43
Reservoir thickness	0.28	0.04	-0.27	-0.18	-0.19	0.13	0.04	-0.04	0.35	0.04	0.35	0.14	0.05	0.04	-0.35
Reservoir porosity	0.00	0.42	0.72	-0.12	0.05	0.55	0.20	0.36	0.26	0.20	-0.06	-0.35	-0.03	-0.36	-0.26
Reservoir permabilty	0.01	0.36	0.47	-0.14	-0.07	0.39	0.26	0.03	-0.27	0.26	0.22	-0.27	0.22	-0.03	0.27
Fracture pressure gradient	-0.12	-0.44	-0.53	0.03	-0.08	0.20	-0.01	0.42	0.58	-0.01	0.25	-0.01	-0.23	-0.42	-0.58
Capillary entry pressure	0.72	0.42	0.37	0.65	0.56	0.59	0.09	-0.08	0.32	0.07	-0.28	-0.30	-0.09	0.08	-0.32
Pressure gradient, Δp/L-ρg	0.34	0.16	0.44	0.35	0.58	0.45	0.01	-0.16	-0.20	-0.49	-0.68	-0.47	-0.01	0.16	0.20
Bouyancy Factor	-0.29	-0.25	-0.35	-0.31	-0.44	-0.14	0.00	0.22	0.19	0.35	0.53	0.25	0.00	-0.22	-0.19
Reseroir extent	0.36	0.60	0.70	0.82	0.77	0.70	0.01	-0.47	-0.32	-0.10	-0.30	-0.21	-0.01	0.47	0.32

Model parameter	Reservoir residual water saturation			Relative brine permeability			Reservoir thickness			Reservoir porosity			Reservoir permeability		
System CO_2 loss constraint:	100%	10%	1%	100%	10%	1%	100%	10%	1%	100%	10%	1%	100%	10%	1%
CAPROCK FRACTURE PROPERTIES AND CO₂% LOSS CORRELATIONS															
Fracture aperture															
Fracture density															
Fracture porosity															
Fracture permeability															
Aperture Pareto PDF: exponent															
Aperture Pareto PDF: min. length															
Fracture length Pareto PDF: exponent															
Caprock thickness/ Fracture length Pareto PDF: min. length															
CO₂% Loss															
RESERVOIR PROPERTIES AND CO₂ INJECTION CORRELATIONS															
CO₂ injection rate															
Injection time															
CO₂ gas saturation															
Relative CO₂ permeability															
Reservoir water saturation															
Reservoir residual water saturation	**1.00**	**1.00**	**1.00**												
Relative brine permeability	-0.09	-0.09	0.43	**1.00**	**1.00**	**1.00**									
Reservoir thickness	0.07	-0.23	-0.42	-0.08	-0.11	-0.26	**1.00**	**1.00**	**1.00**						
Reservoir porosity	0.12	0.12	0.20	0.00	0.02	-0.07	-0.06	0.12	-0.09	**1.00**	**1.00**	**1.00**			
Reservoir permabilty	-0.09	-0.13	-0.36	-0.34	-0.36	-0.79	0.18	0.22	0.16	0.23	0.37	0.10	**1.00**	**1.00**	**1.00**
Fracture pressure gradient	0.17	0.07	0.16	-0.11	0.01	0.13	0.21	0.56	0.54	-0.09	0.08	-0.14	-0.03	0.19	-0.41
Capillary entry pressure	-0.16	-0.10	-0.02	-0.21	-0.28	-0.55	-0.15	-0.29	0.12	-0.32	-0.05	0.49	-0.02	0.23	0.70
Pressure gradient, Δp/L-ρg	0.14	0.20	0.26	0.02	-0.07	0.05	-0.35	-0.58	-0.65	-0.31	-0.32	0.05	-0.66	-0.52	0.07
Bouyancy Factor	-0.13	-0.29	-0.48	-0.17	-0.15	-0.41	0.63	0.73	0.88	0.13	0.24	-0.15	0.71	0.57	0.30
Reseroir extent	-0.15	-0.10	-0.20	-0.49	-0.45	-0.65	-0.21	-0.26	-0.07	-0.32	-0.16	0.37	0.01	0.21	0.76

TABLE F.1: Cont'd

Model parameter	Fracture pressure gradient			Capillary entry pressure			Pressure gradient, Δp/L-ρg			Bouyancy Factor			CO₂ plume extent, r_{max}		
System CO₂ loss constraint:	100%	10%	1%	100%	10%	1%	100%	10%	1%	100%	10%	1%	100%	10%	1%
CAPROCK FRACTURE PROPERTIES AND CO₂% LOSS CORRELATIONS															
Fracture aperture															
Fracture density															
Fracture porosity															
Fracture permeability															
Aperture Pareto PDF: exponent															
Aperture Pareto PDF: min. length															
Fracture length Pareto PDF: exponent															
Caprock thickness/ Fracture length Pareto PDF: min. length															
CO₂% Loss															
RESERVOIR PROPERTIES AND CO₂ INJECTION CORRELATIONS															
CO₂ injection rate															
Injection time															
CO₂ gas saturation															
Relative CO₂ permeability															
Reservoir water saturation															
Reservoir residual water saturation															
Relative brine permeability															
Reservoir thickness															
Reservoir porosity															
Reservoir permabilty															
Fracture pressure gradient	**1.00**	**1.00**	**1.00**												
Capillary entry pressure	-0.05	-0.41	-0.09	**1.00**	**1.00**	**1.00**									
Pressure gradient, Δp/L-ρg	0.00	-0.45	-0.18	0.23	0.27	0.02	**1.00**	**1.00**	**1.00**						
Bouyancy Factor	0.17	0.63	0.30	-0.14	-0.25	0.22	-0.84	-0.87	-0.83	**1.00**	**1.00**	**1.00**			
Reseroir extent	-0.02	-0.40	-0.33	0.72	0.72	0.56	0.34	0.47	0.37	-0.29	-0.41	-0.14	**1.00**	**1.00**	**1.00**

TABLE F.2

CASE 2 CORRELATION COEFFICIENTS BETWEEN SELECTED
RESERVOIR AND CAPROCK FRACTURE PROPERTIES

TABLE F.2: Case 2 correlation coefficients between selected reservoir and caprock fracture properties

Model parameter	Fracture aperture			Fracture density			Fracture porosity			Fracture permeability		
System CO$_2$ loss constraint:	100%	10%	1%	100%	10%	1%	100%	10%	1%	100%	10%	1%
CAPROCK FRACTURE PROPERTIES AND CO$_2$% LOSS CORRELATIONS												
Fracture aperture	1.00	1.00	1.00									
Fracture density	-0.18	-0.41	-0.46	1.00	1.00	1.00						
Fracture porosity	0.11	0.09	0.09	0.83	0.79	0.77	1.00	1.00	1.00			
Fracture permeability	0.47	0.77	0.79	0.13	-0.06	-0.16	0.62	0.51	0.46	1.00	1.00	1.00
Aperture Pareto PDF: exponent	-0.07	-0.10	-0.07	-0.04	-0.03	-0.07	-0.03	-0.03	-0.04	-0.02	0.00	0.03
Aperture Pareto PDF: min. length	0.50	0.82	0.83	-0.45	-0.55	-0.60	0.04	-0.01	-0.03	0.72	0.79	0.81
Fracture length Pareto PDF: exponent	-0.22	-0.37	-0.37	0.72	0.71	0.69	0.66	0.66	0.65	0.20	0.10	0.07
Caprock thickness/ Fracture length Pareto PDF: min. length	0.02	0.10	0.16	-0.39	-0.38	-0.42	-0.33	-0.31	-0.33	-0.10	-0.01	0.05
CO$_2$% Loss	0.36	0.55	0.55	0.23	0.12	0.04	0.62	0.55	0.52	0.82	0.79	0.77
RESERVOIR PROPERTIES AND CO$_2$ INJECTION CORRELATIONS												
CO$_2$ injection rate	-0.06	-0.09	-0.11	0.12	0.14	0.13	0.11	0.12	0.10	0.03	0.02	0.00
Injection time	-0.16	-0.36	-0.45	0.06	0.13	0.20	-0.06	-0.08	-0.08	-0.23	-0.35	-0.41
CO$_2$ gas saturation	0.01	0.03	0.01	0.01	0.01	0.01	0.00	0.02	0.02	-0.01	0.01	0.01
Relative CO$_2$ permeability	-0.07	-0.16	-0.13	0.05	0.10	0.11	-0.01	0.03	0.04	-0.10	-0.10	-0.10
Reservoir water saturation	-0.01	-0.03	-0.01	-0.01	-0.01	-0.01	0.00	-0.02	-0.02	0.01	-0.01	-0.01
Reservoir residual water saturation	-0.03	-0.03	-0.01	0.00	0.02	0.03	-0.02	0.00	0.01	-0.03	-0.03	-0.02
Relative brine permeability	0.08	0.14	0.14	-0.06	-0.08	-0.07	0.02	0.01	0.04	0.14	0.13	0.17
Reservoir thickness	-0.07	-0.04	-0.06	-0.15	-0.14	-0.15	-0.09	-0.08	-0.09	0.06	0.09	0.08
Reservoir porosity	0.06	0.15	0.15	-0.05	-0.07	-0.10	0.02	0.03	0.01	0.11	0.16	0.16
Reservoir permabilty	-0.04	-0.03	-0.03	-0.01	-0.01	0.00	0.02	-0.01	0.00	-0.01	0.00	0.00
Fracture pressure gradient	-0.04	-0.05	-0.03	-0.07	-0.08	-0.12	-0.05	-0.06	-0.10	0.00	0.02	0.02
Capillary entry pressure	-0.53	-0.86	-0.88	0.49	0.57	0.62	-0.03	0.02	0.03	-0.76	-0.82	-0.84
Pressure gradient, Δp/L-pg	0.22	0.27	0.23	0.28	0.27	0.29	0.22	0.21	0.23	0.02	-0.02	-0.05
Bouyancy Factor	-0.06	0.01	0.00	-0.18	-0.20	-0.20	-0.14	-0.13	-0.13	0.01	0.07	0.08
Reseroir extent	-0.20	-0.46	-0.51	0.20	0.28	0.33	0.02	0.01	-0.01	-0.28	-0.42	-0.49

TABLE F.2: Cont'd

Model parameter	Aperture Pareto PDF: exponent			Aperture Pareto PDF: min. length			Fracture length Pareto PDF: exponent			Caprock thickness/ Fracture length Pareto PDF: min. length			CO₂% Loss		
System CO₂ loss constraint:	100%	10%	1%	100%	10%	1%	100%	10%	1%	100%	10%	1%	100%	10%	1%
CAPROCK FRACTURE PROPERTIES AND CO₂% LOSS CORRELATIONS															
Fracture aperture															
Fracture density															
Fracture porosity															
Fracture permeability															
Aperture Pareto PDF: exponent	1.00	1.00	1.00												
Aperture Pareto PDF: min. length	0.04	0.03	0.07	1.00	1.00	1.00									
Fracture length Pareto PDF: exponent	0.03	0.06	0.03	-0.25	-0.28	-0.29	1.00	1.00	1.00						
Caprock thickness/ Fracture length Pareto PDF: min. length	-0.01	0.00	0.03	0.14	0.18	0.24	0.00	0.01	-0.02	1.00	1.00	1.00			
CO₂% Loss	0.01	0.01	0.04	0.53	0.55	0.56	0.12	0.08	0.07	-0.08	-0.01	0.02	1.00	1.00	1.00
RESERVOIR PROPERTIES AND CO₂ INJECTION CORRELATIONS															
CO₂ injection rate	-0.03	0.00	-0.01	-0.04	-0.06	-0.05	0.11	0.03	0.03	0.01	0.01	0.00	0.04	0.01	0.00
Injection time	0.01	-0.01	0.00	-0.21	-0.33	-0.38	-0.06	-0.09	-0.03	0.03	0.01	-0.04	0.12	0.05	0.02
CO₂ gas saturation	0.02	0.01	0.02	0.00	0.01	0.00	-0.01	0.01	0.04	0.00	0.02	0.04	-0.02	0.01	0.03
Relative CO₂ permeability	0.04	0.03	0.01	-0.10	-0.12	-0.12	-0.04	0.02	0.03	-0.01	-0.02	-0.04	0.06	0.08	0.09
Reservoir water saturation	-0.02	-0.01	-0.02	0.00	-0.01	0.00	0.00	-0.01	-0.04	0.00	-0.02	-0.04	0.02	-0.01	-0.03
Reservoir residual water saturation	-0.02	-0.02	0.02	-0.04	-0.03	-0.04	-0.02	0.00	-0.01	0.03	0.00	-0.01	-0.02	0.00	0.00
Relative brine permeability	-0.02	0.01	0.02	0.14	0.13	0.16	0.02	0.02	0.04	-0.03	0.00	0.01	-0.05	-0.04	0.01
Reservoir thickness	0.01	0.02	0.04	0.14	0.15	0.14	0.02	0.02	0.03	-0.03	-0.04	-0.03	-0.08	-0.04	-0.05
Reservoir porosity	-0.03	-0.05	-0.01	0.11	0.14	0.14	0.03	0.02	0.00	-0.04	-0.02	-0.03	-0.05	0.01	-0.01
Reservoir permabilty	-0.03	-0.05	-0.07	-0.01	-0.01	0.00	0.02	0.00	0.00	0.01	0.01	0.02	-0.03	-0.02	0.01
Fracture pressure gradient	0.00	0.00	-0.01	0.03	0.05	0.07	-0.05	-0.01	-0.04	0.00	-0.02	-0.01	-0.01	0.00	-0.03
Capillary entry pressure	-0.01	-0.03	-0.06	-0.94	-0.96	-0.96	0.27	0.30	0.31	-0.15	-0.19	-0.24	-0.55	-0.56	-0.58
Pressure gradient, Δp/L-ρg	-0.25	-0.29	-0.31	-0.14	-0.15	-0.20	-0.17	-0.18	-0.16	-0.27	-0.25	-0.24	0.06	0.01	-0.02
Bouyancy Factor	0.00	-0.01	0.00	0.10	0.15	0.15	0.03	-0.01	0.00	-0.03	-0.04	-0.01	-0.10	-0.04	-0.02
Reseroir extent	0.02	0.00	0.00	-0.33	-0.45	-0.49	-0.13	-0.06	-0.03	0.06	0.03	-0.01	0.20	0.09	0.04

TABLE F.2: Cont'd

Model parameter	CO₂ injection rate			Injection time			CO₂ gas saturation			Relative CO₂ permeability			Reservoir water saturation		
System CO₂ loss constraint:	100%	10%	1%	100%	10%	1%	100%	10%	1%	100%	10%	1%	100%	10%	1%
CAPROCK FRACTURE PROPERTIES AND CO₂ % LOSS CORRELATIONS															
Fracture aperture															
Fracture density															
Fracture porosity															
Fracture permeability															
Aperture Pareto PDF: exponent															
Aperture Pareto PDF: min. length															
Fracture length Pareto PDF: exponent															
Caprock thickness/ Fracture length Pareto PDF: min. length															
CO₂ % Loss															
RESERVOIR PROPERTIES AND CO₂ INJECTION CORRELATIONS															
CO₂ injection rate	1.00	1.00	1.00												
Injection time	0.00	0.00	0.03	1.00	1.00	1.00									
CO₂ gas saturation	0.00	0.03	0.04	0.01	0.02	0.06	1.00	1.00	1.00						
Relative CO₂ permeability	0.00	0.00	-0.02	-0.03	-0.03	-0.06	0.00	-0.03	-0.01	1.00	1.00	1.00			
Reservoir water saturation	0.00	-0.03	-0.04	-0.01	-0.02	-0.06	-1.00	-1.00	-1.00	0.00	0.03	0.01	1.00	1.00	1.00
Reservoir residual water saturation	0.02	0.03	0.01	-0.03	-0.01	0.00	-0.01	-0.02	0.01	-0.01	-0.03	-0.02	0.01	0.02	-0.01
Relative brine permeability	0.03	-0.01	-0.03	0.03	0.05	0.04	0.03	0.05	0.07	0.00	-0.01	0.01	-0.03	-0.05	-0.07
Reservoir thickness	0.09	0.11	0.15	0.04	0.02	0.02	0.04	0.02	0.03	0.04	0.03	0.02	-0.03	-0.02	-0.03
Reservoir porosity	-0.01	0.00	0.02	0.02	0.00	-0.02	0.03	0.01	0.06	0.03	0.03	-0.02	-0.01	-0.01	-0.06
Reservoir permabilty	0.06	0.10	0.06	0.01	-0.02	0.00	-0.02	-0.03	-0.04	-0.02	0.00	0.02	0.04	0.03	0.04
Fracture pressure gradient	0.02	0.02	0.02	-0.02	-0.02	-0.03	0.01	0.06	0.07	0.01	0.02	0.00	-0.01	-0.06	-0.07
Capillary entry pressure	0.35	0.06	0.06	0.23	0.35	0.41	0.01	-0.01	-0.01	0.10	0.13	0.12	-0.01	0.01	0.01
Pressure gradient, Δp/L-pg	0.02	-0.02	-0.04	-0.11	-0.11	-0.11	0.08	0.07	0.04	-0.11	-0.12	-0.07	-0.08	-0.07	-0.04
Bouyancy Factor	-0.29	-0.41	-0.40	0.03	-0.01	0.00	0.01	-0.02	-0.03	0.01	0.02	0.02	-0.01	0.02	0.03
Reseroir extent	0.38	0.36	0.34	0.61	0.66	0.70	-0.01	0.01	0.03	0.30	0.30	0.28	0.01	-0.01	-0.03

TABLE F.2: Cont'd

Model parameter	Reservoir residual water saturation			Relative brine permeability			Reservoir thickness			Reservoir porosity			Reservoir permeability		
System CO₂ loss constraint:	100%	10%	1%	100%	10%	1%	100%	10%	1%	100%	10%	1%	100%	10%	1%
CAPROCK FRACTURE PROPERTIES AND CO₂% LOSS CORRELATIONS															
Fracture aperture															
Fracture density															
Fracture porosity															
Fracture permeability															
Aperture Pareto PDF: exponent															
Aperture Pareto PDF: min. length															
Fracture length Pareto PDF: exponent															
Caprock thickness/ Fracture length Pareto PDF: min. length															
CO₂% Loss															
RESERVOIR PROPERTIES AND CO₂ INJECTION CORRELATIONS															
CO₂ injection rate															
Injection time															
CO₂ gas saturation															
Relative CO₂ permeability															
Reservoir water saturation															
Reservoir residual water saturation	**1.00**	**1.00**	**1.00**												
Relative brine permeability	0.01	-0.01	0.01	**1.00**	**1.00**	**1.00**									
Reservoir thickness	0.01	0.03	0.02	-0.04	-0.05	-0.05	**1.00**	**1.00**	**1.00**						
Reservoir porosity	-0.03	-0.03	0.00	-0.01	-0.02	0.00	-0.02	0.00	-0.05	**1.00**	**1.00**	**1.00**			
Reservoir permabilty	0.00	0.03	0.02	0.00	0.00	0.01	-0.04	-0.03	-0.04	0.02	0.01	0.00	**1.00**	**1.00**	**1.00**
Fracture pressure gradient	0.03	0.02	0.05	0.01	0.00	0.02	0.02	0.05	0.09	0.00	0.01	0.03	0.00	0.03	0.05
Capillary entry pressure	0.03	0.03	0.03	*-0.15*	*-0.14*	*-0.16*	*-0.14*	*-0.15*	*-0.14*	*-0.11*	*-0.15*	*-0.16*	0.00	-0.01	-0.01
Pressure gradient, Δp/L-pg	-0.03	-0.03	-0.01	-0.02	-0.02	-0.06	**-0.47**	**-0.47**	**-0.51**	0.01	0.00	0.02	*-0.21*	*-0.17*	*-0.17*
Bouyancy Factor	0.00	0.03	0.01	-0.05	-0.04	-0.03	**0.59**	**0.58**	**0.56**	-0.01	0.00	-0.05	**0.51**	**0.49**	**0.51**
Reseroir extent	0.03	0.05	0.05	*-0.31*	*-0.27*	*-0.26*	*-0.16*	*-0.14*	*-0.13*	*-0.26*	*-0.25*	*-0.27*	0.06	0.05	0.06

310

TABLE F.2: Cont'd

Model parameter	Fracture pressure gradient			Capillary entry pressure			Pressure gradient, Δp/L-ρg			Bouyancy Factor			CO₂ plume extent, r_max		
System CO₂ loss constraint:	100%	10%	1%	100%	10%	1%	100%	10%	1%	100%	10%	1%	100%	10%	1%
CAPROCK FRACTURE PROPERTIES AND CO₂% LOSS CORRELATIONS															
Fracture aperture															
Fracture density															
Fracture porosity															
Fracture permeability															
Aperture Pareto PDF: exponent															
Aperture Pareto PDF: min. length															
Fracture length Pareto PDF: exponent															
Caprock thickness/ Fracture length Pareto PDF: min. length															
CO₂% Loss															
RESERVOIR PROPERTIES AND CO₂ INJECTION CORRELATIONS															
CO₂ injection rate															
Injection time															
CO₂ gas saturation															
Relative CO₂ permeability															
Reservoir water saturation															
Reservoir residual water saturation															
Relative brine permeability															
Reservoir thickness															
Reservoir porosity															
Reservoir permabilty															
Fracture pressure gradient	**1.00**	**1.00**	**1.00**												
Capillary entry pressure	-0.04	-0.05	-0.08	**1.00**	**1.00**	**1.00**									
Pressure gradient, Δp/L-ρg	*-0.22*	*-0.24*	*-0.27*	*0.15*	*0.15*	*0.18*	**1.00**	**1.00**	**1.00**						
Bouyancy Factor	-0.01	0.03	0.07	*-0.12*	*-0.16*	*-0.16*	**-0.50**	**-0.46**	**-0.47**	**1.00**	**1.00**	**1.00**			
Reseroir extent	-0.01	-0.03	-0.05	*0.35*	**0.48**	**0.52**	0.02	0.00	0.02	*-0.29*	*-0.29*	*-0.27*	**1.00**	**1.00**	**1.00**

311

TABLE F.3

CASE 3 CORRELATION COEFFICIENTS BETWEEN SELECTED RESERVOIR AND CAPROCK FRACTURE PROPERTIES

TABLE F.3: Case 3 correlation coefficients between selected reservoir and caprock fracture properties

Model parameter	Fracture aperture			Fracture density			Fracture porosity			Fracture permeability		
System CO_2 loss constraint:	100%	10%	1%	100%	10%	1%	100%	10%	1%	100%	10%	1%
CAPROCK FRACTURE PROPERTIES AND CO2% LOSS CORRELATIONS												
Fracture aperture	1.00	1.00	1.00									
Fracture density	-0.31	-0.40	-0.31	1.00	1.00	1.00						
Fracture porosity	0.06	0.18	0.25	0.72	0.72	0.76	1.00	1.00	1.00			
Fracture permeability	0.46	0.77	0.69	0.04	0.06	0.23	0.65	0.66	0.77	1.00	1.00	1.00
Aperture Pareto PDF: exponent	-0.11	-0.29	-0.25	-0.16	-0.17	-0.27	-0.06	-0.15	-0.21	-0.02	-0.18	-0.13
Aperture Pareto PDF: min. length	0.54	0.81	0.66	-0.44	-0.42	-0.27	0.16	0.14	0.23	0.76	0.69	0.57
Fracture length Pareto PDF: exponent	-0.37	-0.52	-0.36	0.93	0.93	0.96	0.69	0.65	0.75	0.04	0.00	0.24
Caprock thickness/ Fracture length Pareto PDF: min. length	-	-	-	-	-	-	-	-	-	-	-	-
CO_2% Loss	0.46	0.77	0.69	0.04	0.06	0.23	0.65	0.66	0.77	1.00	1.00	1.00
RESERVOIR PROPERTIES AND CO2 INJECTION CORRELATIONS												
CO_2 injection rate	-	-	-	-	-	-	-	-	-	-	-	-
Injection time	-	-	-	-	-	-	-	-	-	-	-	-
CO_2 gas saturation	-	-	-	-	-	-	-	-	-	-	-	-
Relative CO_2 permeability	-	-	-	-	-	-	-	-	-	-	-	-
Reservoir water saturation	-	-	-	-	-	-	-	-	-	-	-	-
Reservoir residual water saturation	-	-	-	-	-	-	-	-	-	-	-	-
Relative brine permeability	-	-	-	-	-	-	-	-	-	-	-	-
Reservoir thickness	-	-	-	-	-	-	-	-	-	-	-	-
Reservoir porosity	-	-	-	-	-	-	-	-	-	-	-	-
Reservoir permabilty	-	-	-	-	-	-	-	-	-	-	-	-
Fracture pressure gradient	-	-	-	-	-	-	-	-	-	-	-	-
Capillary entry pressure	-0.59	-0.93	-0.93	0.49	0.44	0.33	-0.15	-0.19	-0.29	-0.79	-0.82	-0.75
Pressure gradient, $\Delta p/L-\rho g$	0.29	0.47	0.40	-0.34	-0.34	-0.30	-0.26	-0.22	-0.25	0.00	0.09	-0.05
Bouyancy Factor	-	-	-	-	-	-	-	-	-	-	-	-
Reseroir extent	-	-	-	-	-	-	-	-	-	-	-	-

TABLE F.3: Cont'd

Model parameter	Aperture Pareto PDF: exponent			Aperture Pareto PDF: min. length			Fracture length Pareto PDF: exponent			Caprock thickness/ Fracture length Pareto PDF: min. length			CO_2% Loss		
System CO_2 loss constraint:	100%	10%	1%	100%	10%	1%	100%	10%	1%	100%	10%	1%	100%	10%	1%
CAPROCK FRACTURE PROPERTIES AND CO2% LOSS CORRELATIONS															
Fracture aperture															
Fracture density															
Fracture porosity															
Fracture permeability															
Aperture Pareto PDF: exponent	**1.00**	**1.00**	**1.00**												
Aperture Pareto PDF: min. length	0.06	-0.01	*0.18*	**1.00**	**1.00**	**1.00**									
Fracture length Pareto PDF: exponent	0.03	0.03	-0.08	-0.41	-0.43	*-0.22*	**1.00**	**1.00**	**1.00**						
Caprock thickness/ Fracture length Pareto PDF: min. length	-	-	-	-	-	-	-	-	-	**-**	**-**	**-**			
CO2% Loss	-0.02	*-0.18*	*-0.13*	**0.76**	**0.69**	**0.57**	0.04	0.00	*0.24*	-	-	-	**1.00**	**1.00**	**1.00**
RESERVOIR PROPERTIES AND CO2 INJECTION CORRELATIONS															
CO2 injection rate	-	-	-	-	-	-	-	-	-	-	-	-	-	-	-
Injection time	-	-	-	-	-	-	-	-	-	-	-	-	-	-	-
CO2 gas saturation	-	-	-	-	-	-	-	-	-	-	-	-	-	-	-
Relative CO2 permeability	-	-	-	-	-	-	-	-	-	-	-	-	-	-	-
Reservoir water saturation	-	-	-	-	-	-	-	-	-	-	-	-	-	-	-
Reservoir residual water saturation	-	-	-	-	-	-	-	-	-	-	-	-	-	-	-
Relative brine permeability	-	-	-	-	-	-	-	-	-	-	-	-	-	-	-
Reservoir thickness	-	-	-	-	-	-	-	-	-	-	-	-	-	-	-
Reservoir porosity	-	-	-	-	-	-	-	-	-	-	-	-	-	-	-
Reservoir permabilty	-	-	-	-	-	-	-	-	-	-	-	-	-	-	-
Fracture pressure gradient	-	-	-	-	-	-	-	-	-	-	-	-	-	-	-
Capillary entry pressure	-0.03	0.07	-0.01	**-0.93**	**-0.86**	**-0.76**	**0.47**	**0.46**	*0.29*	-	-	-	**-0.79**	**-0.82**	**-0.75**
Pressure gradient, Δp/L-pg	**-0.72**	**-0.73**	**-0.74**	*0.11*	*0.18*	-0.07	**-0.55**	**-0.57**	**-0.50**	-	-	-	0.00	0.09	-0.05
Bouyancy Factor	-	-	-	-	-	-	-	-	-	-	-	-	-	-	-
Reseroir extent	-	-	-	-	-	-	-	-	-	-	-	-	-	-	-

314